An Investigation of the Role of the P2X7 Purinoceptor in the Pathogenesis of Diabetic Nephropathy

John William Roy Booth

December 2013

A thesis submitted to University College London in fulfilment of the requirement for the degree of Doctor of Philosophy

This work is kindly supported by a joint training fellowship from the MRC and Kidney Research UK

I, John William Roy Booth, confirm that the work presented in this thesis is my own. Where information has been derived from other sources, I confirm that this has been indicated in the thesis.

Signed _[redacted]_ Date _____15/12/2013_____

Abstract

P2X7 is a member of the P2X purine receptor family and functions as an ATP-gated non-selective cation channel. Expression is greatest in cells of the immune system where it plays a key role in the orchestration of IL1β maturation and release. Diabetic nephropathy (DN) is traditionally considered a 'metabolic' disease, but is increasingly recognized to have an important inflammatory component. The work in this thesis tests the hypothesis that P2X7 contributes to the pathogenesis of DN and, in particular, the development of renal inflammation in this disease.

P2X7 expression was examined by immunohistochemistry in human kidney biopsy tissue; glomerular expression was identified in a subset of patients with early clinical DN. P2X7 expression was also upregulated at 12 weeks in glomeruli of rodents with both type 1 and type 2 diabetes. After induction of diabetes with low dose STZ, GSK P2X7 KO mice exhibited a marked reduction in glomerular macrophage infiltration compared to WT, without impact on albuminuria or serum creatinine. A trend towards protection against induction of diabetes was also apparent in GSK KO mice; this protection was more pronounced in the Pfizer P2X7 KO strain and accompanied by reduced islet macrophage infiltration and preservation of β-cell mass.

The mechanism linking P2X7 and glomerular macrophage infiltration was explored *in vitro.* A selective P2X7 antagonist, A438079, partially abrogated hyperglycaemia-induced secretion of the macrophage chemokine, MCP-1, from primary human mesangial cells (pHMC). MCP-1 secretion was enhanced by the ATP-hydrolysing agent, apyrase, as well as by application of 5-BDBD, a selective P2X4 antagonist, suggesting chemokine secretion from pHMCs may be modulated by multiple competing purinoceptor signals.

In summary, P2X7 is upregulated at an early time-point in rodent diabetic glomeruli, and contributes to both glomerular and pancreatic inflammation in murine experimental disease. Comparable upregulation of P2X7 in glomeruli observed in human DN bodes well for future translational studies.

Acknowledgements

I am very grateful to the Medical Research Council and Kidney Research UK for jointly awarding my Clinical Training Fellowship, enabling me to carry out this research project.

I am also grateful for the guidance and support of my supervisors, Drs Jill Norman and Frederick Tam and Professor Robert Unwin, without whom this project would not have been possible.

I would also like to thank the following individuals who trained and supported me during this work: Mrs Gurjeet Bhangal (immunohistochemistry), Miss Jenny Smith and Dr Stephen McAdoo (animal techniques), Dr Claire Turner and Dr Richard Fish (P2X7 expertise), Dr Reiko Hewitt (animal husbandry and genotyping), Dr John McDaid (ELISAs), Dr Patricia DeWinter (qPCR), Dr Simona Deplano (Western blotting), Dr Min Jeong Kim (cell culture), Professor Roger Mason (diabetes models and project license) and Prof Charles Pusey (diabetes models and project license).

Dr Tim Johnson and Dr Ling-Hong Huang (Sheffield Kidney Institute) kindly provided protocols and practical advice for the uninephrectomised rat model of DN. I am very grateful to AstraZeneca for providing the selective P2X7 antagonist AZ11657312 for use in the consequent rat model experiment. GSK and Pfizer P2X7 KO mice were kind gifts from GlaxoSmithKline and Pfizer respectively. Dr Edward Debnam (UCL) kindly provided kidney tissue from GK rats and age-matched Wistar controls. Mrs Lorraine Lawrence performed paraffin-wax embedding and sectioning of formalin-fixed tissue. Professor Moin Saleem (University of Bristol) kindly provided the conditionally

immortalised podocyte line, while Dr Xiong Ruan provided the transformed human mesangial cell line.

Finally, I am very grateful to my wife, Ophelia, for her unstinting support and understanding, recognising that laboratory science refuses to respect conventional working hours.

Table of Contents

Part 2. Diabetic Nephropathy

Part 3. Hypothesis and aims

CHAPTER 2 - MATERIALS AND METHODS

List of Tables

CHAPTER 4 - INVESTIGATING THE ROLE OF P2X7 IN THE INDUCTION OF MURINE DIABETES USING STREPTOZOTOCIN

CHAPTER 5 - INVESTIGATING THE ROLE OF P2X7 IN THE DEVELOPMENT OF MURINE DIABETIC NEPHROPATHY USING STREPTOZOTOCIN

CHAPTER 6 - INVESTIGATING THE ROLE OF P2X7 IN DIABETIC NEPHROPATHY USING A UNINEPHRECTOMISED DIABETIC RAT MODEL

List of Figures

CHAPTER 1 - INTRODUCTION

CHAPTER 2 - MATERIALS AND METHODS

CHAPTER 3 - EXPRESSION OF P2X7 IN HUMAN DIABETIC NEPHROPATHY

CHAPTER 4 - INVESTIGATING THE ROLE OF P2X7 IN THE INDUCTION OF MURINE DIABETES USING STREPTOZOTOCIN

Abbreviations

5-BDBD	5-(3-bromophenyl)-1,3-dihydro-2*H*-benzofuro[3,2-*e*]-1,4-diazepin-2-one
A438079	3-[[5-(2,3-dichlorophenyl)-1*H*-tetrazol-1-yl]methyl]pyridine hydrochloride
A740003	*N*-[1-[[(Cyanoamino)(5-quinolinylamino)methylene]amino]-2,2-dimethylpropyl]-3,4-dimethoxybenzeneacetamide
αSMA	Alpha-smooth muscle actin
ADP	Adenosine diphosphate
ADPKD	Autosomal dominant polycystic kidney disease
ARPKD	Autosomal recessive polycystic kidney disease
APS	Ammonium persulphate
ATP	Adenosine triphosphate
BCA	Biocinchonic acid
BG	Blood glucose
BSA	Bovine serum albumin
BzATP	3'-O-(4-benzoylbenzoyl)-adenosine triphosphate
cAMP	Cyclic adensosine monophosphate
CKD	Chronic kidney disease
CTGF	Connective tissue growth factor
CTP	Cytidine triphosphate

DAB	3,3'-diaminobenzidine
DMSO	Dimethylsulfoxide
DN	Diabetic nephropathy
ECM	Extracellular matrix
ELISA	Enzyme-linked immunosorbent assay
EMT	Epithelial-mesenchymal transition
ERK	Extracellular signal-related kinase
ESAM	Endothelial cell-selective adhesion molecule
ESRD	End-stage renal disease
FBS	Foetal bovine serum
GBM	Glomerular basement membrane
GFR	Glomerular filtration rate
GLP-1	Glucagon-like peptide 1
GK	Goto-Kakasaki
H+E	Haematoxylin and eosin
(p)HMC	(Primary) human mesangial cell
HRP	Horse radish peroxidase
HPBCD	2-hydroxypropyl-beta-cyclodextrin
HPRT	Hypoxanthine phosphoribosyltransferase
IFNγ	Interferon gamma
IMCD	Inner-medullary collecting duct
IP	Intra-peritoneal

IV	Intravenous
KO	Knock-out
LPS	Lipopolysaccharide
MAPK	Mitogen-activated protein kinases
MC	Mesangial cell
MCP-1	Macrophage chemoattractant protein - 1
MTS	(3-(4,5-dimethylthiazol-2-yl)-5-carboxymethoxyphenyl)-2-(4-sulfophenyl)-2H-tetrazolium)
NDI	Nephrogenic diabetes insipidus
NMHHC-IIA	Non-muscle myosin heavy chain-IIA
NOD	Non-obese diabetic (mouse)
NTN	Nephrotoxic nephritis
oATP	Oxidised ATP
OCT	Optimal cutting temperature
PARP	Poly-(ADP-ribose) polymerase
PAS	Periodic acid-Schiff
PBS	Phosphate-buffered saline
PCR	Polymerase chain reaction
PFA	Paraformaldehyde
PLP	Periodate-lysine-paraformaldehyde (fixative)
PMSF	Phenylmethanesulfonylfluoride

qPCR	Quantitative polymerase chain reaction
RAAS	Renin-angiotensin-aldosterone system
RNA	Ribonucleic acid
ROS	Reactive oxygen species
RPL13a	Ribosomal protein L13a
SC	Subcutaneous
SDHA	Succinate dehydrogenase complex, subunit A
SDS	Sodium lauryl sulphate
STZ	Streptozotocin
TBM	Thin basement membrane
TEMED	N,N,N',N' tertramethylethylenediamine
TGFβ	Transforming growth factor beta
TMB	3,3',5,5' - tetramethylbenzidine
TNFα	Tumour necrosis factor alpha
uACR	Urinary albumin : creatinine ratio
UNx	Uninephrectomy
uPCR	Urinary protein : creatinine ratio
UUO	Unilateral ureteric obstruction
VEGF	Vasoactive endothelial growth factor
WT	Wild-type
WT-1	Wilms tumour 1 antigen

YWHAZ	Tyrosine 3-monooxygenase/tryptophan 5-monooxygenase activation protein, zeta polypeptide

CHAPTER 1

Introduction

Part 1. Purinoceptor Signalling in the Kidney

1.1 Overview

Since the first observation in 1970 that adenosine triphosphate (ATP) may be released from nerve terminals in the gut and function as a neurotransmitter, receptors for extracellular nucleotides have been identified on almost every cell type within the body (Burnstock et al., 1970, Burnstock, 2006). Broadly, these are divided into P (for purine) 1 receptors that recognise adenosine, and P2 receptors that recognise ATP and related di- and tri-phosphate nucleotides. P2 receptors are further subdivided into P2Y, which are metabotropic G protein-coupled receptors, and P2X, which function as non-selective cation channels (Figure 1.1) (Abbracchio et al., 2006, Khakh and North, 2006). Seven P2X receptors (P2X1-7) and eight P2Y receptors (P2Y1, 2, 4, 6 and 11-14) are currently recognised (Abbracchio et al., 2006, Khakh and North, 2006). P2X receptors are trimeric channels with the potential for further complexity through heteromeric subunit assemblies between some family members (North, 2002). Each receptor can be characterised pharmacologically by its preference for certain endogenous and synthetic ligands.

Both P2 receptor classes may couple to a wide range of intracellular second messenger systems with activation frequently provoking a rise in cytosolic calcium: through mobilisation of intracellular stores in the case of P2Y receptors, by direct calcium influx through P2X channels or via influx through voltage-gated calcium channels activated by cell depolarisation (Abbracchio

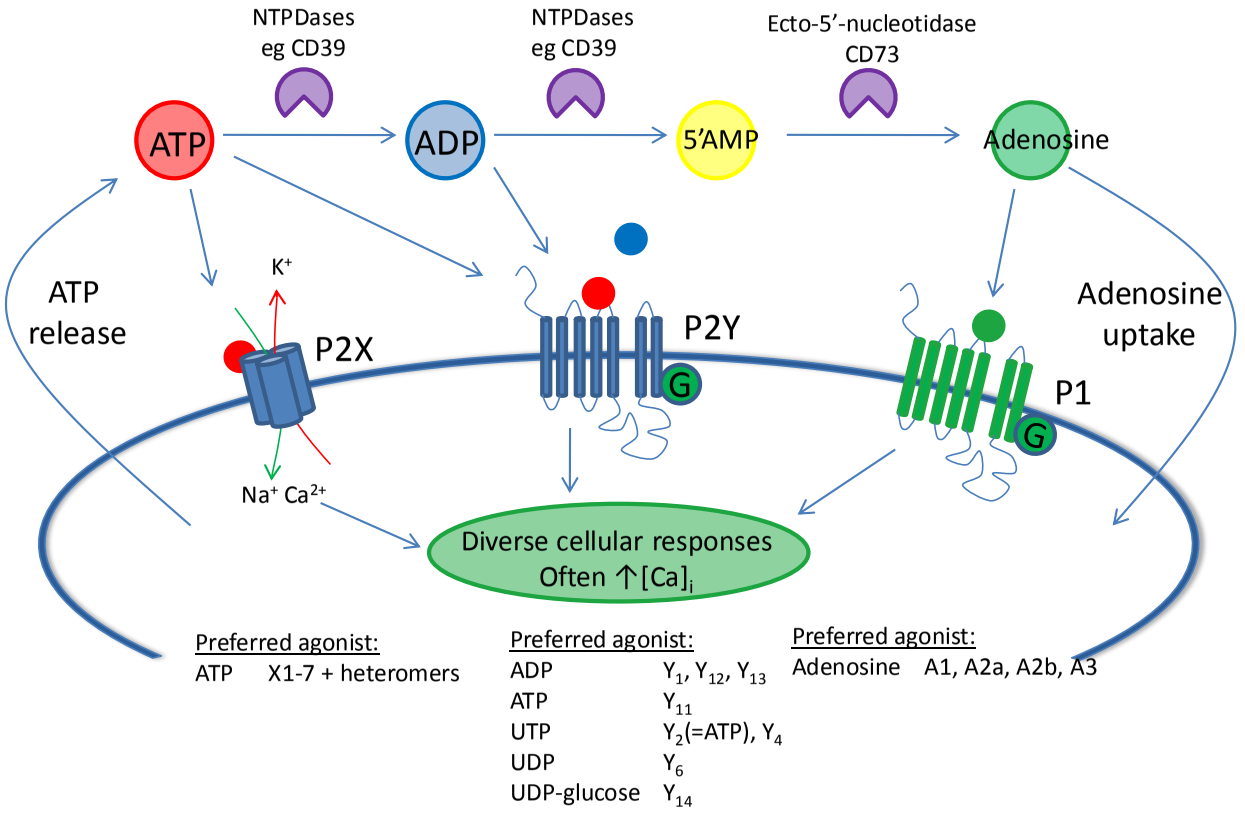

Figure 1.1 The autocrine / paracrine purinoceptor system. ATP release into the extracellular space is triggered by a range of stimuli including cellular stretch, trauma, or agonist binding. Ectonucleotidases located on the plasma membrane catalyse sequential hydrolysis of ATP to ADP, 5'AMP and adenosine. P1 receptors recognize adenosine while P2 receptors bind di- and tri-phosphate nucleotide molecules. P2X receptors are non-selective cation channels with 3 protein subunits which may form homo- or heteromeric arrangements; all bind ATP. P2Y receptors are 7 transmembrane-spanning domain G-protein-coupled receptors; agonist preferences span adenosine and uracil di- and tri-nucleotides. NTPDase: ectonucleoside triphosphate diphosphohydrolase.

et al., 2006, Khakh and North, 2006). Signalling through different P2 receptors may exert disparate and even antagonistic effects on cellular function (Solini et al., 2005).

ATP is secreted in renal tubular fluid with concentrations measured at around 200nM in the proximal tubule (Vekaria et al., 2006). Any renal cell may be provoked to release ATP under conditions such as mechanical stimulation or osmotic stress, fluid flow or agonist stimulation, while red cells, platelets, and damaged or dying cells also represent important sources of nucleotide release (Praetorius and Leipziger, 2009a). P2 receptors are expressed differentially throughout the kidney and purinoceptor signalling appears to have important roles in water and sodium transport, control of the renal microcirculation, and in autoregulatory responses (Turner et al., 2003, Unwin et al., 2003). In addition, ectonucleotidases can modulate agonist availability and the pattern of receptor activation in the local microenvironment (Shirley et al., 2009).

From these observations it is reasonable to speculate that the P2 purinoceptor system may function as a subtle autocrine or paracrine feedback system, integrating signals based on the local patterns of secretion, release and degradation of nucleotides. Moreover, it is becoming increasingly apparent that deleterious signals transduced via P2 receptors may contribute to disease within the kidney. One receptor which has generated particular interest in this setting is P2X7.

1.2 The P2X7 receptor

In the initial classification of P2 receptors, an additional class designated the 'P2Z' receptor was included, recognised by its requirement for a high

concentration of extracellular ATP for channel activation and ability to form transmembrane aqueous pores permitting passage of solutes up to 900 Da, typically culminating in cell death (Pizzo et al., 1992). Subsequent discovery and cloning of a receptor with 40% sequence homology to the existing six P2X receptors and pharmacological profile compatible with P2Z led to rechristening as P2X7 (Surprenant et al., 1996). As for the other P2X receptors, P2X7 displays preference for the endogenous agonist ATP, with brief stimulation leading to a rapid transient current due to non-densitizing monovalent and divalent cation conductance (Wiley et al., 2011). Repeated receptor stimulation, however, leads to a more slowly developing secondary permeability pathway transmitting larger cations such as N-methyl-D-glucamine and dyes including ethidium bromide (Surprenant et al., 1996, Wiley et al., 2011). This 'large pore' pathway is functionally dependent on the long intracellular carboxyl-domain of P2X7, which differentiates it structurally from other members of the P2X family (Figure 1.2A).

1.2.1 Receptor structure and channel properties

P2X receptors consist of 3 subunits, each comprising two transmembrane domains, an extracellular loop and intracellular N- and C- termini. P2X7 is thought to be homomeric, and while it can often be co-precipitated and co-isolated with P2X4 from cell extracts, this does not appear to represent true heteromer formation (Antonio et al., 2011). Recent elucidation of the crystal structure of zebrafish P2X4, which shares functional similarities with P2X7 including the capacity for large pore formation, has shed light on structure-function relationships across the P2X family (Kawate et al., 2009). Individual subunits of the homomeric P2X4 receptor resemble a dolphin with the extracellular domain forming the 'head' and 'body' and transmembrane helices the 'flukes' (Figure 1.2B). The TM2 domains line the aqueous permeation pathway with rotation of subunits on agonist binding

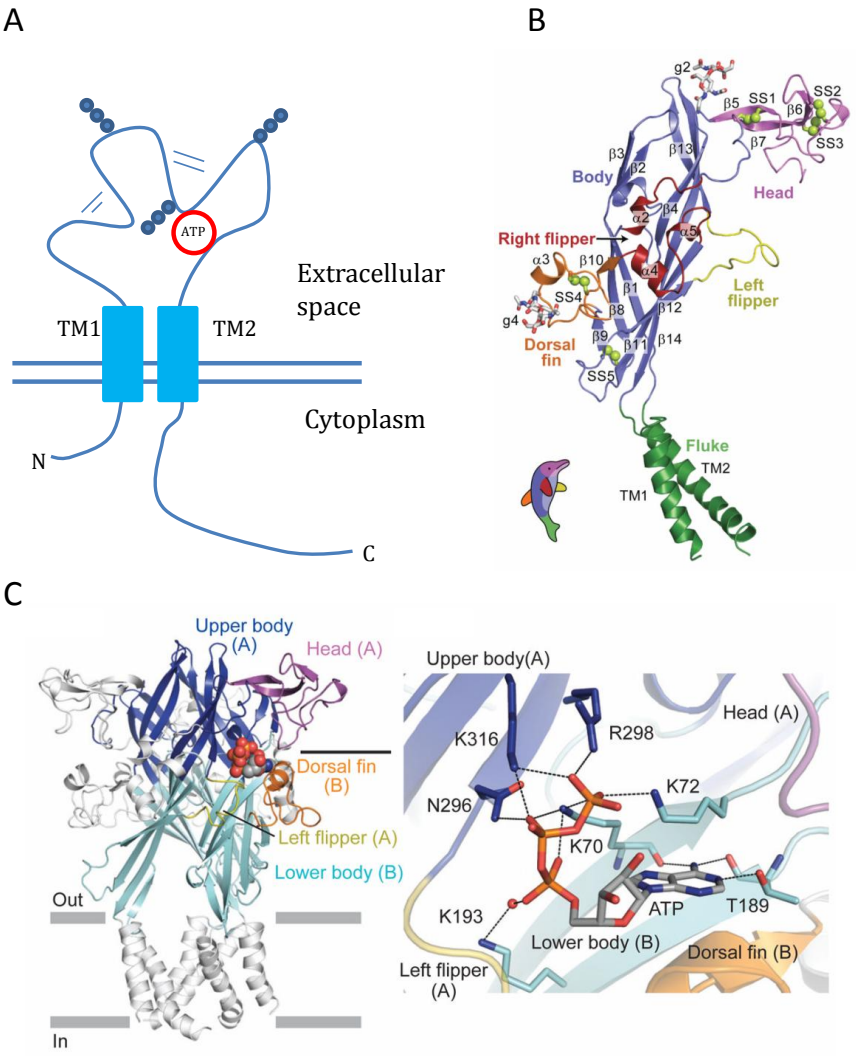

Figure 1.2 Transmembrane topography and subunit structure of the P2X7 receptor. A: The P2X7 receptor consists of three subunits, each comprising two transmembrane domains, intracellular N- and C-termini, and a hydrophilic extracellular loop including an ATP binding-pocket created by the interaction between neighbouring subunits. The position of putative disulphide bridges (=) and N-linked glycosyl chains (blue circles) are marked. B: Extracellular subunit structure of the related P2X4 receptor, as delineated by X-ray crystallography, which shows resemblance to a dolphin emerging from the cell membrane. C: A more topographically accurate representation of the ATP binding site of P2X4; ATP is shown in sphere configuration, and the right-hand pane shows a close-up of the pertinent molecular interations. TM: transmembrane; N: N-terminus; C: C-terminus. Part A adapted from Wesselius et al., 2007. Parts B and C reproduced by permission from Macmillan Publishers Limited: Nature, Kawate et al. 2009, copyright 2009 (A) and Nature, Hattori et al. 2012, copyright 2012 (B).

conjectured to realign these domains vertically to open the channel. Three ATP binding sites are thought to be located in the grooves between subunits.

Mathematical modelling of P2X7 receptor gating has led to a suggested scheme for receptor function: binding of a single ATP molecule induces receptor asymmetry and discourages binding of a second ATP molecule; binding of a second ATP molecule at higher concentration triggers opening of the 'small pore' cationic conductance; binding of a third molecule leads to further pore enlargement (permitting conductance of larger cations such as NMDG) and triggers activity of the associated 'large pore' conductance (Yan et al., 2010, Pelegrin, 2011). Studies demonstrating dissociation of the small cationic and large solute currents, for instance after mutating the C-terminus of the channel, suggest that the receptor itself does not form the large pore (Wiley et al., 2011).

The C-terminal domain of P2X7, which is 120-200 amino acids longer than the other P2X receptors, appears to be critical for large pore formation, interaction with adaptor proteins and receptor trafficking (Roger et al., 2010). Interaction with the recently discovered protein pannexin-1 (panx-1) appears to underlie, at least in some cell types, the large pore conductance: panx-1 and P2X7 co-immunoprecipitated in HEK293 cells demonstrating their structural association, while siRNA knockdown or panx-1 channel inhibition with carbenoxolone abolished P2X7-dependent dye uptake but not small cation currents in HEK293 cells and human and murine macrophages (Pelegrin and Surprenant, 2006, Pelegrin and Surprenant, 2009).

P2X7 can also be linked to other pore-forming pathways as demonstrated by: i) the existence of separate pathways for cationic and anionic dye conductance in mouse macrophages (panx-1 is permeable only to cationic dyes); ii) the existence of a MAPK-dependent dye uptake pathway independent of IL1β release or cytolytic pore formation; iii) and the finding

that colchicine can block P2X2- and P2X7-dependent dye uptake without affecting small cation conductance (panx-1 is not involved in the formation of P2X2-associated large pores) (Donnelly-Roberts et al., 2004, Schachter et al., 2008, Pelegrin, 2011, Marques-da-Silva et al., 2011).

1.2.2 Tissue distribution

P2X7 expression varies considerably from tissue to tissue with the highest constitutive levels found in cells of the immune system, consistent with its well-defined role in inflammatory cytokine processing and release (see below). Within this system, highest expression is found in macrophages, followed by dendritic cells, monocytes, NK cells, and B and T lymphocytes, although there is some inter-species variability in this rank order (Gu et al., 2000, Wiley et al., 2011). Neutrophils express minimal cell surface receptors but display abundant intracellular protein, as do all haemopoietic cells (Gu et al., 2000).

Within the kidney and renal tract, P2X7 is expressed in cultured mesangial cells and has been demonstrated at low levels in distal tubular epithelium in human kidney biopsy tissue (Harada et al., 2000, Solini et al., 2007, Gauer et al., 2007). P2X7 is also expressed in other renal interstitial or infiltrating cell types including fibroblasts and tissue macrophages (Ponnusamy et al., 2011). In common with several other epithelial tissues including vaginal and uterine epithelium, alveolar epithelial cells and stratified squamous skin epithelial cells, P2X7 is also expressed in urothelial cells lining the ureter and bladder (Groschel-Stewart et al., 1999, Bardini et al., 2000, Lee et al., 2000, Mishra, 2013). The function of P2X7 in epithelia is not fully understood, although it appears to contribute to regulation of surfactant production in alveoli, and

may contribute to mechanisms of epithelial turnover or pathogen defence (Wiley et al., 2011, Mishra, 2013).

In other tissues, P2X7 has been identified in microglia and astrocytes within the brain as well as spinal neurons where it has been implicated in nociceptive signalling (Wiley et al., 2011, Burnstock, 2013). In bone, P2X7 is found in both osteoblasts (of mesenchymal origin) and osteoclasts (derived from cells of haematopoietic lineage) and appears to have an important physiological role in the mechanotransduction of skeletal loading to new bone formation (Li et al., 2005).

1.2.3 Agonist and antagonists (Table 1.1)

P2X7 activation requires a high concentration of extracellular ATP (EC_{50} >80-100μM), one feature which distinguishes it from the other P2X receptors (North, 2002, Wiley et al., 2011). The ATP analogue BzATP is 10-30 times more potent than ATP (EC50 7μM) but lacks specificity, exerting stimulatory effects at other P2X receptors, as well as acting as an antagonist of P2Y receptors (North, 2002). ATPγS and ADP are essentially inactive at the channel in the resting state (Donnelly-Roberts and Jarvis, 2007). P2X7 activity is potentiated by reducing the extracellular concentration of calcium or magnesium, possibly through allosteric effects (Michel et al., 1999, Wiley et al., 2011). This phenomenon has bearing on P2X7 activation in the distal nephron, where tubular calcium and magnesium concentrations are reduced due to proximal reabsorption.

A recent study examining P2X7 agonist and antagonist responses using whole-cell patch clamp recordings in HEK 293 cells, suggests that intermediate activation states of P2X7 have altered nucleotide selectivity

(Browne and North, 2013). 'Tethering' of BzATP to P2X7, with consequent persistent membrane current, was achieved by coincident exposure to ultraviolet radiation. Both ADP and CTP stimulated membrane currents when applied to receptors with pre-'tethered' BzATP, while the same agonists proved ineffective when applied to receptors in the resting state. This finding suggests that our current schema for P2 receptor pharamacological responses likely underestimates the true complexity of receptor-agonist interactions in *in vivo* biological systems.

The endogenous human cathelicidin-derived peptide LL37, produced predominantly by neutrophils and endothelial cells, also displays activity at the P2X7 receptor, and is capable of stimulating IL1β release from LPS-primed monocytes in an ATP-independent fashion (Elssner et al., 2004). Mouse P2X7 can also be activated by ATP-independent ADP-ribosylation, an NAD-dependent process, although the physiological relevance to human P2X7 is questionable, as humans do not possess the requisite ADP-ribosyl–transferase (ART-2) enzyme (Seman et al., 2003).

A variety of compounds with inhibitory activity at P2X7 have been employed in pre-clinical studies. Oxidised ATP (oATP; 2',3' dialdehyde ATP) irreversibly inhibits receptor function, displaying highest potency at the human P2X7 receptor, but also inhibiting other P2X receptors including P2X1 and P2X2, rendering it unsuitable for *in vivo* human use (Hibell et al., 2001, North, 2002). The Ca^{2+}/calmodulin-dependent protein kinase II (CamKII) inhibitor, KN62, exhibits inhibitory activity at P2X7 but with significant inter-species differences in efficacy (King, 2007). The polysulphonic dye Brilliant blue G (BBG) is an effective antagonist at the rat P2X7 receptor but stains proteins (leading to visible cutaneous discolouration when used *in vivo*.)

High throughput *in vitro* screening of small molecule inhibitors using cation flux and pore formation assays has led to the identification of several new

	Agonists	**EC-50**
Nucleotides	ATP BzATP Potentiated by: $\downarrow[Ca^{2+}]_{EC}$ $\downarrow[Mg^{2+}]_{EC}$ $\downarrow[Na^{+}]_{EC}$ $\downarrow[Cl^{-}]_{EC}$	>80-100μM 7μM
Non-nucleotide	LL-37	
Alternative activation	ADP-ribosylation	
	Antagonists	**IC-50**
Ions	Ca^{2+} Mg^{2+} Zn^{2+} Cu^{2+} H^{+}	2900μM 500μM 11μM 0.5μM 0.4μM (≈pH 6.1)
Generic P2X antagonists	Suramin PPADS Brilliant Blue G Oxidised ATP	>300μM (R); 3μM (H) 50μM 10nM (R); 200nM (H) 25μM (R); 3μM (H)
Organic cations	Calmidazolium KN-62	10nM (R) 30nM (H)
Novel small molecule inhibitors	Cyclic imides eg AZ11645373 Disubstituted tetrazoles eg A438079 Cyanoguanidines eg A740003	10-90nM (H) 100nM (R); 300nM (H) 18nM (R); 40nM (H)
Other	17β-oestradiol Monoclonal αP2X7 Ab Decanvanadate ($H_2V_{10}O_{28}^{-4}$)	

Table 1.1 P2X7 receptor agonists and antagonists. The list of novel small molecule inhibitors is not exhaustive. Collated from Michel et al. 1999, Hibell et al. 2001, North et al. 2002 and Donnelly-Roberts and Jarvis, 2007. R: rat; H: human; EC: extracellular

classes of selective P2X7 antagonists; for example, A438079, a disubstituted tetrazole compound which acts as a reversible inhibitor of P2X7 with IC50 of 100nM and 300nM at rat and human P2X7 receptors, respectively, displays minimal activity at other P2 receptors (Donnelly-Roberts and Jarvis, 2007). The cyanoguanidine, A740003, shows similar properties.(Honore et al., 2006) Selective P2X7 antagonists from several pharmacological classes have been successfully used in phase I and II clinical trials with a favourable adverse effect profile (Arulkumaran et al., 2011).

1.2.4 Genetic polymorphisms and splice variants

Human P2X7 is located at 12q24 and comprises 13 exons (Buell et al., 1998). Multiple splice isoforms exist with the full-length receptor designated P2X7A and further variants labelled B-J (reviewed recently in (Sluyter and Stokes, 2011)). P2X7B lacks the C-terminal domain and consequently is unable to form the large pores characterstic of P2X7A and instead appears to stimulate trophic changes (Adinolfi et al., 2010). A and B are expressed at comparable levels at the mRNA level in those tissues which have been surveyed, and expression of P2X7B *potentiates* P2X7A responses when the two are coexpressed (Adinolfi et al., 2010). The truncated P2X7J receptor has been found at high levels in malignant cervical tissue and forms heteromeric non-functional receptors with P2X7A which may interfere with apoptotic functions (Sluyter and Stokes, 2011).

Multiple single nucleotide polymorphisms (SNPs) of the *P2RX7* gene have been characterised, and can lead to both gain or loss of function effects (Sluyter et al., 2004). rs3751143 (Glu496Ala) is the best studied and leads to loss of function, with deficits in pore formation and dye uptake, reduced IL1β maturation and impaired killing of intracellular pathogens by macrophages

(Gu et al., 2001, Sluyter et al., 2004, Lees et al., 2010). Numerous clinical correlative studies have linked rs3751143 with an increased susceptibility to Mycobacterium tuberculosis, presumably due to defects in bacterial killing by macrophages (Sluyter and Stokes, 2011). A different SNP, rs591874, has been associated with an increased ambulatory blood pressure; the effect of this polymorphism on receptor function has not been investigated, although the lack of association between rs3751143 and blood pressure suggests rs591874 does not result in loss of function (Palomino-Doza et al., 2008).

1.3 Cellular roles of P2X7

1.3.1 IL1β and IL18 maturation

Activation of P2X7 receptors in macrophages primed by exogenous bacterial peptides (eg. LPS) or TNFα leads to massive secretion of the leaderless inflammatory cytokines IL1β and IL18 (Ferrari et al., 1997, Solle et al., 2001, Franchi et al., 2009). This effect is dependent on the Nacht Domain-, Leucine-Rich Repeat-, and PYD-Containing Protein-3 (NLRP3) inflammasome for upstream signal integration and subsequent caspase-1 activation leading to maturation of pre-formed pro-IL1β (Ferrari et al., 2006). In the absence of a second signal, stimulation with LPS leads to cytosolic accumulation of pro-IL1β but only very muted release of mature peptide. Tissue damage, whether due to infection or 'sterile' injury, and additional non-lytic pathways lead to ATP exposure in the extracellular space, P2X7 binding and pro-IL1β processing and release; P2X7 hence appears to function as a 'damage sensor' transducing tissue injury to a local inflammatory response (Figure 1.3) (Di Virgilio, 2007, McDonald et al., 2010).

Both potassium efflux and large pore formation appear to be important in the mechanism for IL1β maturation (Ferrari et al., 1997, Ferrari et al., 2006). P2X7 may also play a role in disgorgement of IL1β-laden microvesicles upon entering the extracellular space, as vesicle exposure to ATP precipitates membrane breakdown (Bianco et al., 2005).

1.3.2 Cell death

Prolonged stimulation of cells with ATP frequently leads to cell death and P2X7 is a key mediator of this process (Di Virgilio et al., 1998). Depending on cell type and context, P2X7 activation can initiate cell death by either colloid-osmotic lysis or apoptosis. The former mechanism appears to stem from the propensity of P2X7 to form large membrane pores on prolonged agonist stimulation, leading to gross cell membrane disruption. Receptor activation can also, however, lead to the full spectrum of apoptotic changes including nuclear fragmentation, membrane blebbing, cell shrinkage and apoptotic body formation which may putatively relate either to downstream effects of the small pore conductance or caspase-1 activation after shorter periods of receptor stimulation (Chow et al., 1997, Di Virgilio et al., 1998).

Inter-species differences also impact on the cytotoxicity of P2X7; human P2X7 has lower affinity for ATP than rat, and consequently human macrophages are more susceptible to apoptosis than colloid-osmotic lysis after ATP stimulation, in contrast to their rat counterparts (Rassendren et al., 1997, Di Virgilio et al., 1998). Brief ATP stimulation of HEK293 cells stably transfected with P2X7 can lead to rapid alterations in cell morphology typically associated with apoptosis (eg. membrane blebbing, phosphatidylserine exposure and microvesicle release) which are then reversible with washing out of agonist, a process termed ‘pseudoapoptosis’,

which presumably represents an early but non-committed stage in the P2X7-dependent cell death pathway (Mackenzie et al., 2005).

1.3.3 Cellular proliferation

While diffuse or prolonged P2X7 stimulation culminates in cell death, P2X7 activation has also been linked to cell growth and proliferation in certain contexts. HEK293 cells stably transfected with P2X7 have a higher basal mitochondrial potential, intra-mitochondrial calcium levels and cellular ATP stores and are able to grow in serum-free conditions (Adinolfi et al., 2005).

P2X7-mediated responses also appear important in proliferation of T-lymphocytes and microglial cells (Baricordi et al., 1999, Bianco et al., 2006). P2X7 activation appears to able to modulate key components of aerobic glycolysis within the cell, potentially underlying the increased replicative vitality of P2X7 over-expressing cells (Amoroso et al., 2012). Of note, P2X7 is over-expressed in several human cancers while tumours induced *in vivo* using P2X7-transfected cell lines have accelerated growth as well as denser vascular networks and elevated amounts of secreted vaso-active endothelial growth factor (VEGF) (Adinolfi et al., 2012).

1.3.4 Phospholipid signalling

Numerous lipid derivatives, including diacylglycerol, arachadonic acid and phosphatidic acid, act as important secondary messengers in cellular signal transduction. P2X7 has been demonstrated to activate the phospholipase D pathway in macrophages and lymphocytes as well as certain epithelial cell types; this response requires a rise in intracellular calcium but cannot be

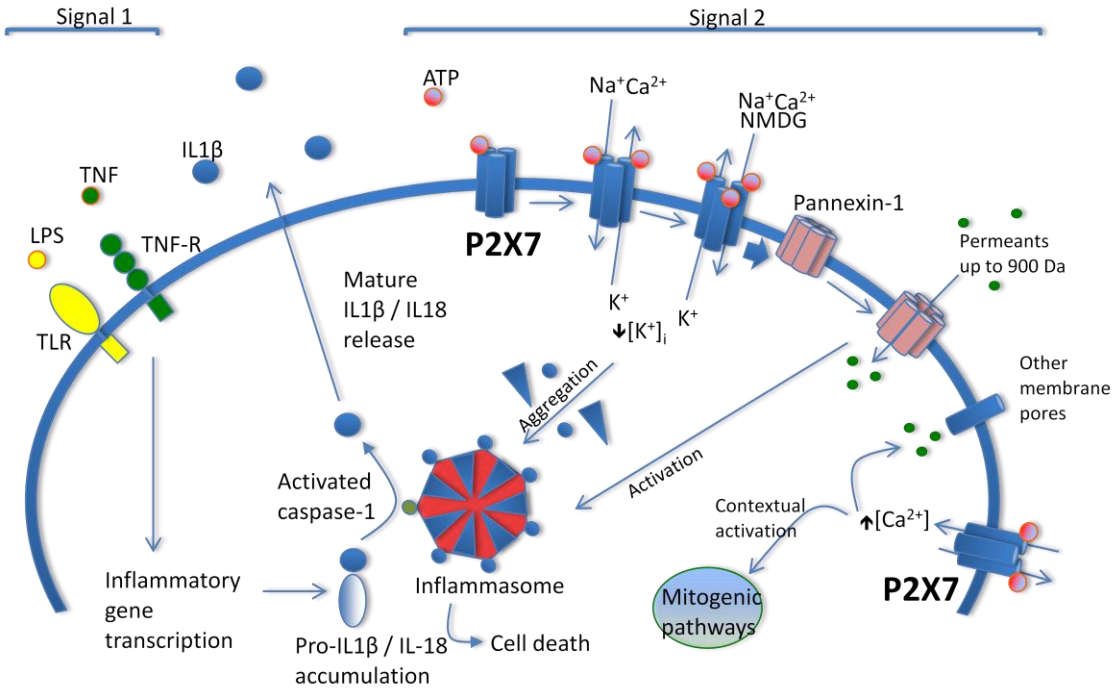

Figure 1.3 Model of P2X7 receptor participation in inflammatory responses. Release of mature IL1β from macrophages first requires a cellular priming signal, delivered either via toll-like receptors in the case of microbial infection, or inflammatory cytokine receptors (eg. TNF-R) in sterile inflammation, leading to inflammatory gene transcription and accumulation of pro-IL1β ('Signal 1'). Pericellular ATP ligates the P2X7 receptor, leading to inorganic cation transit when double-bound, progressing to pore dilatation and a high conductance state when all three binding sites are occupied. The resultant fall in intracellular potassium is required for assembly of the NLRP3 inflammasome, the central caspase-1 activating platform. Fully-bound P2X7 triggers opening of large diameter membrane pores including the pannexin-1 hemichannel. This event, through uncertain mechanisms, precipitates final activation of caspase-1 on the inflammasome, rapid maturation and release of IL1β and the related cytokine IL18 and ultimately, cell death. ('Signal 2'). Elevations of cytosolic calcium in the absence of large membrane pore opening, presumably associated with the double ATP-bound state, are hypothesised to underlie apparently paradoxical mitogenic responses to P2X7 activation seen in other contexts (eg. tumour growth). LPS: lipopolysaccharide; TNF: tumour necrosis factor, TLR: Toll-like receptor; TNF-R: tumour necrosis factor receptor; NMDG: N-methyl D-glucamine. From Booth et al. 2012.

replicated by calcium ionophores or mobilisation of intracellular calcium stores (el-Moatassim and Dubyak, 1992, Gargett et al., 1996, Pochet et al., 2003, Garcia-Marcos et al., 2006). Activation of phospholipase A2 after P2X7 stimulation has also been demonstrated in both monocytes and submandibular epithelial cells and appears to be a requisite step for lysosome exocytosis and final release of IL1β (Alzola et al., 1998, Andrei et al., 2004).

1.3.5 Phagocytosis

Recent work has established a role for the P2X7 receptor in phagocytosis of non-opsonised particles, bacteria and apoptotic bodies (Wiley et al., 2011). P2X7 is closely associated with non-muscle myosin heavy chain-IIA (NMMHC-IIA) in its resting state and it is this protein interaction that appears to mediate receptor-led phagocytosis; ATP binding and receptor activation leads to dissociation of NMMHC-IIA and attenuates phagocytosis (Gu et al., 2009, Gu et al., 2010, Gu et al., 2011). Phagocytosis can also be inhbited by BzATP, P2X7 ectodomain and selective antagonists of the P2X7 receptor including A438079, suggesting a dissociation between this role and classical receptor activity (Gu et al., 2010). P2X7-deficient peritoneal macrophages do not show inhibition of phagocytosis by ATP while stable expression of P2X7 in HEK293 cells confers the ability to phagocytose apoptotic cells (Gu et al., 2011). P2X7 thus appears to act as a scavenger receptor while bound to NMHHC-IIA in the resting state, switching to more classical pro-inflammatory activation states in the present of ATP.

1.4 P2 receptors in renal health and disease

Autocrine / paracrine P2 purinoceptor signalling contributes to several physiological mechanisms in the kidney including microcirculatory autoregulation, tubuloglomerular feedback and urinary concentration. Given these physiological roles of P2 receptors, together with the ubiquity of P2 receptor expression, it is not surprising that deleterious signals transduced via P2 receptors or interruption of normal purinoceptor signalling may contribute to disease within the kidney.

Renal diseases where P2 receptor pathways contribute signficantly to pathogenesis are discussed below, with reference to corresponding physiological roles where appropriate.

1.4.1 Glomerulonephritis

Inflammatory glomerular disease is common, potentially treatable, and is a major contributor to end-stage kidney disease (Byrne et al., 2010). Current treatment regimens depend on non-specific immunosuppression, often corticosteroid-based, and are associated with significant morbidity (Tam, 2006). Interest in identifying more specific treatment targets has led to examination of P2 signalling as a candidate pathogenic mechanism with a major focus on the P2X7 receptor.

A key role for P2X7 in glomerulonephritis has been suggested in experiments using the rodent nephrotoxic nephritis (NTN) model. This model uses injection of anti-glomerular basement membrane nephrotoxic serum to induce a lesion that histologically resembles human crescentic glomerulonephritis (McAdoo et al., 2010). A 3-fold upregulation of

glomerular P2X7 mRNA is seen by day 4 in rat NTN, correlating with the onset of significant proteinuria and peak macrophage infiltration (Turner et al., 2007b). Receptor upregulation, as assessed by immunostaining, is also seen by 24 hours in a mouse model of accelerated NTN, co-localising with caspase-3, a marker of apoptosis (Turner et al., 2007b).

Disease induced in Glaxo P2X7 KO mice showed reduced glomerular thrombosis, reduced proteinuria, and improved renal function at day 8 compared to WT animals (Taylor et al., 2009). This was associated with almost complete suppression of monocyte chemoattractant protein 1 (MCP-1) measured in urine and reduced glomerular macrophage infiltration. The selective P2X7 antagonist, A438079, also led to attenuation of disease in rat NTN when used at a dose of 300μmol/kg body weight twice daily (Taylor et al., 2009).

Glomerular and, to a lesser extent, tubular immunostaining for P2X7 has been observed in human renal tissue from patients with lupus nephritis, the hallmark of which is glomerular inflammation (Turner et al., 2007b). Orally-active and well-tolerated selective antagonists exist for human P2X7, but have yet to be tested in renal disease (Keystone et al., 2011, Arulkumaran et al., 2011).

The P2Y1 receptor, best characterised as a mediator of ADP-induced platelet aggregation, has also been studied in the murine NTN model (Leon et al., 1999, Hohenstein et al., 2007). The disease is attenuated and mortality is reduced in the P2Y1 KO mouse compared with WT, with a reduction in glomerular and peritubular capillary rarefaction (Hohenstein et al., 2007). The absence of differences in bleeding time and glomerular and peritubular capillary platelet aggregation between P2Y1 KO and WT mice, suggests that this may be a platelet-independent effect, while differences observed in

endothelial proliferative activity may implicate P2Y1-mediated endothelial dysregulation as a component of disease pathogenesis in this model.

The purinergic axis has also been studied in the anti-Thy-1 rat model of mesangial proliferative glomerulonephritis (Rost et al., 2002). Injection of a monoclonal anti-thymocyte antibody cross-reacting with a Thy-1 like antigen on mesangial cells results in initial complement-dependent mesangiolysis, followed by mesangial cell proliferation, exuberant ECM production and, contrary to human mesangial proliferative diseases, ultimate recovery and restoration of normal glomerular architecture (Bagchus et al., 1986, Hugo et al., 1997). The non-selective P2 receptor inhibitor pyridoxalphosphate-6-azophenyl-2',4',-disulfonic acid (PPADS), administered twice daily at a dose of 15-60 mg/kg body weight, led to a selective reduction in mesangial cell proliferation, maximal at day 5, with no effect on initial mesangial cell injury or inflammatory infiltrate (Rost et al., 2002). P2Y2 receptor upregulation was observed in a mesangial pattern by immunostaining. These findings support a role for nucleotide-dependent mesangial cell proliferation in this form of nephritis, and complement *in vitro* studies showing proliferation of cultured mesangial cells in response to P2Y activation (Schulze-Lohoff et al., 1992, Harada et al., 2000). Further studies employing subtype-selective P2 receptor antagonists are required to realise any potential therapeutic benefit, particularly since P2X-mediated responses may be predicted to contribute to the inciting inflammatory insult.

1.4.2 Fibrosis and chronic kidney disease

The paracrine P2 receptor system is of proven importance in coordinating several physiological responses within the kidney: P2X1 activation in the glomerular afferent arteriole is pivotal for normal autoregulation of renal

microcirculatory blood flow, while regulation of GFR by tubuloglomerular feedback depends, at least in part, on ATP release and P2 receptor-mediated signalling for transmission of the spreading calcium wave within the juxtaglomerular apparatus that culminates in afferent arteriolar vasoconstriction (Ren et al., 2004, Peti-Peterdi, 2006, Toma et al., 2008, Osmond and Inscho, 2010, Sipos et al., 2010). This importance of renal P2 signalling in health, together with the ubiquity of P2 receptor expression, and their ability to transduce mitogenic and apoptotic responses in resident renal cells have led to the candidacy of these receptors in the pathogenesis of chronic renal diseases such as diabetic nephropathy (Turner et al., 2003, Harada et al., 2000). A growing recognition that immune responses play a pivotal role in the perpetuation of these classically 'non-inflammatory' kidney diseases has directed attention to the part played by innate immunity, and particularly the pro-inflammatory P2X7 receptor (Navarro-Gonzalez and Mora-Fernandez, 2008, Vilaysane et al., 2010).

1.4.2.i Diabetic nephropathy

Diabetic nephropathy is characterised by excessive deposition of ECM proteins in the glomerular basement membrane, mesangium and tubulointerstitium, and is typified clinically by albuminuria and progressive loss of renal function (Mason and Wahab, 2003). While all resident glomerular cells contribute to glomerulosclerosis, mesangial cells are the main effector of ECM accumulation in response to the hyperglycaemic milieu (Qian et al., 2008). P2 receptors of both P2Y and P2X subclasses are expressed on mesangial cells and appear to exert opposite effects on cell turnover, with P2Y stimulating proliferation and P2X provoking apoptosis and necrosis (Harada et al., 2000, Rost et al., 2002, Solini et al., 2007). P2X7 is expressed at low levels on mesangial cells, but it can be upregulated by TNFα (Harada et al., 2000).

Rat mesangial cells exposed to a high glucose environment secrete increased amounts of ATP that appear to enhance ECM production via a TGFβ-dependent mechanism in an autocrine/paracrine fashion (Solini et al., 2005). This response is replicated by the addition of 3'-O-(4-benzoylbenzoyl)-ATP (BzATP), a P2X7 receptor agonist, and blocked by oxidised ATP (oATP), an antagonist (although neither compound is highly selective for P2X7), suggesting P2X7 receptor involvement. Addition of UTP, a P2Y2 and P2Y4 agonist, leads to reduced ECM protein expression in this model, although the recent finding that UTP can act as an agonist at intermediately-activated P2X7 receptors complicates the interpretation of this (Solini et al., 2005, Browne and North, 2013). Experiments in human fibroblasts also implicate P2X7 in diabetic cytopathy, since P2X7 activity is markedly enhanced in cells grown in high glucose media or obtained from a diabetic donor (Solini et al., 2000, Solini et al., 2004). This is accompanied by rearrangement of P2X7 into ring-like structures at the periphery of the cell, and apoptosis when high concentrations of ATP (5mM) are applied (Solini et al., 2000).

Minimal P2X7 expression can be detected immunohistochemically in the kidneys of normal rats, but the receptor is clearly upregulated by 6 weeks in the streptozotocin (STZ) model of type 1 diabetes (Vonend et al., 2004). Co-labelling with cell-specific markers and immuno-electron microscopy both suggest predominant podocytic expression (Vonend et al., 2004). BzATP has been shown to augment glucose uptake into rat podocytes cultured in hyperglycaemic conditions, potentially priming the development of the podocytopathy which contributes to disease initiation (Reddy et al., 2008, Karczewska et al., 2011).

The *P2X4* gene is very close to *P2X7* on human chromosome 12. The P2X4 receptor shares physical properties with P2X7, including the potential for large membrane pore formation and a response to stimulation by BzATP. It is

expressed at significantly higher levels in mesangial cells than P2X7, and recent data suggest that P2X4 may be the dominant receptor mediating ATP-induced apoptosis in human mesangial cells, a role previously attributed to P2X7 (Solini et al., 2007). Neither receptor has been studied in *in vivo* models of diabetic nephropathy, a prequisite step to determine whether either is functionally important in disease pathogenesis.

1.4.2.ii Tubulointerstitial fibrosis

Rodent unilateral ureteric obstruction (UUO) is a widely used model of tubulointerstitial fibrosis and progressive kidney disease; it is characterised by mononuclear cell infiltration, fibroblast differentiation and proliferation, increased ECM deposition, and tubular atrophy (Klahr, 2001, Goncalves et al., 2006). Induction of disease in P2X7 KO mice leads to an attenuated phenotype, with less fibrosis and collagen deposition, reduced macrophage infiltration, reduced surface TGFβ staining, and a greatly diminished population of medullary interstitial myofibroblasts at day 14 (Goncalves et al., 2006). Similar benefits have been seen with P2X7 deletion in models of inflammatory fibrosing disease in other organ systems, including bleomycin-induced lung fibrosis (Riteau et al., 2010). It is interesting to note that *in vitro* P2X7 receptors appear to mediate direct renal epithelial cell-fibroblast crosstalk under conditions of tubular damage, with necrotic tubular cells promoting fibroblast cell death by a P2X7-dependent mechanism (Ponnusamy et al., 2011).

1.4.3 Polycystic kidney disease

Parenchymal cyst formation is common to several human renal diseases, the most common being autosomal dominant polycystic kidney disease (ADPKD). While the fundamental genetic defects underlying ADPKD are well defined (mutations in *PKD1* and *PKD2* encoding polycystin-1 and polycystin-2, respectively) the pathogenic mechanisms promoting cyst formation and expansion remain less clear (Yoder, 2007, Torres and Harris, 2009). Cyst-lining epithelial cells are unable to maintain planar polarity; they express an abnormal secretory phenotype promoting fluid retention and display increased rates of proliferation and apoptosis (Torres and Harris, 2009). Knowledge that ATP is concentrated within the lumen of ADPKD cysts and can couple to chloride secretion via rises in intracellular calcium or cAMP, as well as trigger both proliferative and apoptotic pathways through P2 receptor activation, has made the P2 system attractive for study in renal cystic disease (Mangoo-Karim et al., 1989, Wilson et al., 1999, Communi et al., 2000, Schwiebert et al., 2002).

Madin-Darby canine kidney (MDCK) cells grown in a three-dimensional collagen matrix proliferate and form microcysts when exposed to the cAMP-forming adenylate cyclase stimulant, forskolin (Mangoo-Karim et al., 1989). The ectonucleotidase, apyrase, suppresses cyst growth when added to such cultures, demonstrating an ATP-dependence for cystogenesis in this model (Turner et al., 2007a). Cyst growth can also be retarded with the addition of non-selective P2 receptor antagonists, including reactive blue 2 (RB2) and suramin, although cyst growth in this model cannot be augmented by the addition of exogenous ATP. The pattern of antagonist responses suggest primacy of P2Y receptors in promoting cyst growth, but the lack of selective agents means that the specific P2 receptor dependence remains unclear (Turner et al., 2007a). Addition of ATP drives growth of cysts formed from enriched principal-like MDCK cells (with intercalated-like cells eliminated),

demonstrating clear ATP dependence for cAMP-mediated cyst formation in this subpopulation of cells (Buchholz et al., 2011).

The role of P2X7 in cystogenesis has also been examined *in vitro* using cell cultures derived from the *cpk/cpk* mouse model of autosomal recessive polycystic kidney disease (ARPKD). P2X7 is expressed in renal collecting ducts of the *cpk/cpk* mouse as they undergo fulminant cystogenesis, and the receptor can also be detected in human fetal ARPKD tissue (Hillman et al., 2002, Hillman et al., 2004). The P2X7 agonist, BzATP, caused a reduction in cyst number, but not in cyst size, when added to cultures derived from dissociated *cpk/cpk* kidneys (Hillman et al., 2004). The greater potency of BzATP over ATP in inhibiting cyst formation, together with the antagonising effect of oATP, was taken to support a role for P2X7 in this setting. However, an absence of classical downstream effects of P2X7 (eg. caspase activation), together with an appreciation that BzATP is also an antagonist at P2Y1 and P2Y4 receptors, raises the possibility that P2Y-mediated signalling may also underlie these findings (ie. P2Y responses *promoting* cyst growth).

More recently, the role of P2X7 in cystogenesis has been tested in a zebrafish model of polycystic kidney disease generated by *pkd2* knock-down with morpholinos. Here, exposure of zebrafish to the P2X7 antagonist oATP, together with the more selective antagonist A438079, and *P2X7* knock-down using morpholinos, significantly *reduced* the frequency of the cystic phenotype. A reduction was seen in phosphorylated extracellular signal-related kinase (phospho-ERK) activity and cell proliferation in pronephric kidneys suggests that P2X7 may couple to deleterious mitogenic signalling in this setting (Chang et al., 2011).

All renal epithelial cells, with the exception of intercalcated cells, possess a primary cilium capable of transducing a flow response manifest as an intracellular calcium transient (Praetorius and Spring, 2001, Torres and

Harris, 2009). Polycystin-1 and -2 localise to the primary cilium and participate in mechanotransduction, making impaired ciliary function an important candidate pathogenic mechanism in ADPKD (Nauli et al., 2003, Yoder, 2007). Autocrine/paracrine purinoceptor signals amplify the flow-mediated calcium response with ATP release seemingly dependent on the presence of the primary cilium (Jensen et al., 2007, Praetorius and Leipziger, 2009b). The flow-mediated rise in intracellular calcium is impaired in ADPKD epithelial cells, and flow-induced ATP release is reduced in parallel, despite cells maintaining normal sensitivity to exogenous nucleotides and displaying enhanced resting and hypotonicity-induced ATP release (Xu et al., 2009). Loss of normal cilia-dependent flow responses in the tubules of patients with ADPKD is conjectured to contribute to cyst development by promoting dysregulated proliferation and dedifferentiation; whether blunted ATP release is a bystander or contributor to this process remains to be determined. The link between these findings of disturbed flow-sensitive ATP release, intracellular calcium signalling and pathological cystogenesis is currently unclear (Calvet, 2002).

1.4.4 Disorders of water transport and hypertension

While arginine vasopressin (AVP) has a primary role in the regulation of water transport in the collecting duct, other autocrine and paracrine factors, including purinoceptor signals, are important modulators. P2Y2 has received particular attention: stimulation of P2Y2 in the microperfused rat inner medullary collecting duct (IMCD) antagonises AVP-induced water permeability**;** in immortalised mouse collecting duct cells, P2Y2 activation leads to internalisation of aquaporin 2, and in rat IMCD suspensions P2Y2 stimulation triggers release of prostaglandin E2 (PGE_2), which is another modulator of collecting duct function (Kishore et al., 1995, Welch et al., 2003, Wildman et al., 2009a, Wildman et al., 2009b). P2Y2 expression is increased in the inner medulla of dehydrated rats and P2Y2 KO mice display enhanced

urinary concentration capacity, together with increased expression of the machinery for water conservation, including aquaporin 2 (Kishore et al., 2005, Zhang et al., 2008).

The potential pathophysiological correlate of these findings has been examined in rat models of lithium-induced nephrogenic diabetes insipidus (NDI), and in the diuresis of post-obstructive uropathy, both conditions involving PGE2-mediated water diuresis (Zhang et al., 2009, Zhang et al., 2010). In the former study, enriched IMCDs from rats in which NDI had been induced with lithium were stimulated *ex vivo* with nucleotides, and PGE2 release measured. PGE2 release was enhanced by 50-130% on exposure to nucleotides compared with control preparations (Zhang et al., 2009). Interestingly, and in contrast to control animals, IMCDs from lithium-fed rats responded to ADP, ATPγS, and UTP, suggesting a role for P2Y6 and/or P2Y1 in promoting PGE2 release, in addition to P2Y2. RT-PCR revealed significant upregulation of P2Y4 receptor mRNA in lithium-fed rats, while P2Y6 remained unchanged, and P2Y2 expression diminished (but was still the most abundant P2Y receptor). Similar analysis in the post-obstructive uropathy model revealed upregulation of P2Y2 and P2Y6 mRNA without a change in P2Y4 (Zhang et al., 2010). In this setting, nucleotide responses in *ex vivo* IMCDs were suggestive of predominant P2Y2 involvement. The contribution of P2X receptors, which may also influence water transport, were not examined (Wildman et al., 2009b). While these studies suggest an important role for P2 receptor signalling in diseases of water transport, complementary studies with KO mice or selective antagonists will be needed to realise future therapeutic benefit.

Purinoceptors have also been implicated in the aetiology of hypertension and consequent renal damage. Polymorphic variation in P2X7, P2X4 and P2Y2 have been associated with essential hypertension (Palomino-Doza et al., 2008, Wang et al., 2010). Both P2Y2 and P2X4 have been shown to regulate

function of the ENaC sodium channel in the distal nephron and KO mouse models of both receptors display a hypertensive phenotype (Yamamoto et al., 2006, Rieg et al., 2007, Pochynyuk et al., 2008, Wildman et al., 2008).

Upregulation of the P2X7 receptor has been shown in the glomerulus of hypertensive renin-overexpressing rats at 12 weeks of age, although the cellular location was not defined and the functional significance is unexplored (Vonend et al., 2004). The P2X7 antagonist, Brilliant Blue G, has been shown to ameliorate hypertension, renal macrophage infiltration, albuminuria, and renal fibrosis when administered *in vivo* to Dahl rats rendered hypertensive through a high salt diet; a reduction in albuminuria and macrophage infiltration was also reported with the highly selective P2X7 antagonist, A438079, in the same study (Ji et al., 2011). ATP levels are increased in the renal interstitial fluid of rats with angiotensin II-induced hypertension, and both clopidogrel (a selective P2Y12 antagonist), administered orally in drinking water at 20mg/kg daily, and pyridoxalphosphate-6-azophenyl-2',4'-disulfonic acid (PPADS; a non-selective P2 receptor blocker), administered IP at a dose of 20mg daily, led to reduced phenotypic mesangial cell activation, afferent arteriolar wall thickness, macrophage infiltration, and renal cell proliferation in the early stages of this model (Graciano et al., 2008).

Autoregulation of renal blood flow is dependent on local purinoceptor signalling and is disrupted in hypertensive nephropathy, leading to increased transmitted capillary pressures (Loutzenhiser et al., 2006). Attenuated afferent arteriolar vasoconstrictor responses to P2X1 stimulation have been documented in angiotensin II hypertensive rats fed a high salt diet, and are thought to underlie this phenomenon (Inscho et al., 2011).

1.5 Conclusion - purinoceptor signalling

A growing body of evidence supports the view that ATP and related nucleotides, once recognised only in their capacity for cellular energy transfer, perform a crucial role as autocrine and paracrine stimuli when present within the extracellular space. Through the diverse repertoire of P2 receptors, nucleotide signals appear to conduct a wide range of physiological responses within the kidney, and participate in the pathogenesis of numerous and disparate renal diseases. Dissecting the role of individual P2 receptors in renal disease has proved difficult to date, because ligands may activate multiple receptors and selective antagonists exist for only a small number of receptors. However, the impact that clopidogrel (a P2Y12 antagonist and anti-platelet agent) has had in cardiovascular medicine illustrates the potential therapeutic benefit to be reaped from continuing efforts to modulate the activity of this finely balanced system, with the ultimate goal of manipulating P2 signalling to ameliorate human renal disease (Yusuf et al., 2001).

Part 2. Diabetic nephropathy

1.6 Overview

Diabetic nephropathy (DN) is the commonest cause of chronic kidney disease (CKD) and end-stage renal disease (ESRD) worldwide, with an enormous projected increase in the burden of disease as the prevalence of diabetes continues to increase (Byrne et al., 2010, USRDS, 2012). Renal disease may be consequent to both type 1 and type 2 diabetes mellitus. Type 1 diabetes is an auto-immune disorder, often presenting in childhood or adolescence, characterized by cellular and humoral auto-immune destruction of pancreatic β-cells, leading to rapidly progressive insulin deficiency, weight loss and severe hyperglycaemia requiring immediate insulin replacement therapy. Type 2 diabetes, on the other hand, typically affects older individuals and co-segregates with other features of the so-called 'metabolic syndrome', including obesity, hypertension and hyperlipidaemia. The appearance of hyperglycaemia is initially attributable to peripheral insulin resistance, which overwhelms compensatory increases in pancreatic insulin secretion, although secondary β-cell degeneration and hypoinsulinaemia frequently develop as the disease progresses.

1.7 Clinical manifestations

The diabetic state pre-disposes to both 'macro-vascular' (such as coronary and cerebral vascular disease) and 'micro-vascular' end-organ complications, the latter group comprising nephropathy, neuropathy and retinopathy, the incidence of which increases with disease duration. Renal hyperfiltration, due to disruption of normal glomerular haemodynamics, with a consequent increase in glomerular filtration rate (GFR), is common in early diabetes and

precedes overt evidence of renal damage. Clinical renal disease classically follows a gradual progression through low-grade albuminuria ('microalbuminuria') indicative of early glomerulopathy, to overt proteinuria and finally loss of GFR, culminating ultimately in ESRD. This progression is not absolute, however, and as many as 50% of patients may present with loss of GFR in the absence of significant proteinuria, likely, in part, attributable to the widespread use of renin-angiotensin system (RAS) inhibition as first-line anti-hypertensive therapy (Halimi, 2012).

1.8 Histopathological features of DN

The renal histopathological findings of nephropathy due to type 1 or type 2 diabetes are essentially indistinguishable and have thus been considered together in recent classifications (Tervaert et al., 2010). Early hyperfiltration is typically accompanied by glomerular enlargement which may translate to an increase in renal size of up to 15% (Feehally et al., 2007). Increased production and deposition of ECM proteins within the glomerulus initially manifests as glomerular basement membrane (GBM) thickening, best identified on electron microscopy, and increases with duration of disease (Perrin et al., 2006). Expansion of the supporting mesangial areas with ECM is the archetypal glomerular lesion of DN and is best appreciated on periodic acid-Schiff (PAS) or silver stains. Mesangial expansion is typically diffuse but mesangiolysis and focal exuberance may produce a nodular pattern (Kimmelstiel-Wilson lesions). Increasing mesangial area correlates with worsening albuminuria, suggesting it represents a key structural-functional correlate in progressive disease (Fioretto et al., 1995). A high proportion of globally sclerosed glomeruli are observed in advanced DN with ESRD.

Other histological features include arteriolar hyalinosis, classically of the efferent arteriole, and thickening of tubular basement membranes due to ECM deposition, analagous to those of the glomerulus. Interstitial fibrosis and tubular atrophy progresses in parallel to glomerular disease and represents an important predictor of outcome (Okada et al., 2012).

1.9 Cellular and molecular mechanisms in DN

While hyperglycaemia represents the core clinical and diagnostic abnormality in diabetes, the consequent haemodynamic and metabolic perturbations which summate to produce renal injury are complex. All resident renal cell types are affected and contribute to development of disease. Abnormalities in podocyte architecture with subsequent cell death and detachment are observed early in disease, and the local, aberrant, podocyte response to GBM denudation may drive the onset of GBM thickening and albuminuria (Gnudi, 2012). Mesangial cells are chief effectors of the progressive glomerulosclerosis observed in DN, while tubular cell injury may lead directly to interstitial fibrosis through epithelial-mesenchymal transition (EMT), or indirectly through deleterious cross-talk with other interstitial cell types. Once renal disease is established, many mechanisms of progressive injury are shared with non-diabetic CKD, including secondary hypertensive injury, activation of the renal-angiotension-aldosterone system (RAAS) and proteinuria-induced tubular toxicity (Gnudi, 2012, Forbes and Cooper, 2013).

The breadth of pathogenic mechanisms involved in DN is summarised in Figure 1.4. Initiators of cellular injury include increased glucose translocation into cells with subsequent deleterious channeling down polyol and hexosamine pathways; haemodynamic or stretch-related injury due to glomerular hypertension; and interaction with abnormally glycated proteins. Subsequent accumulation of reactive oxygen species (ROS) within the cytosol

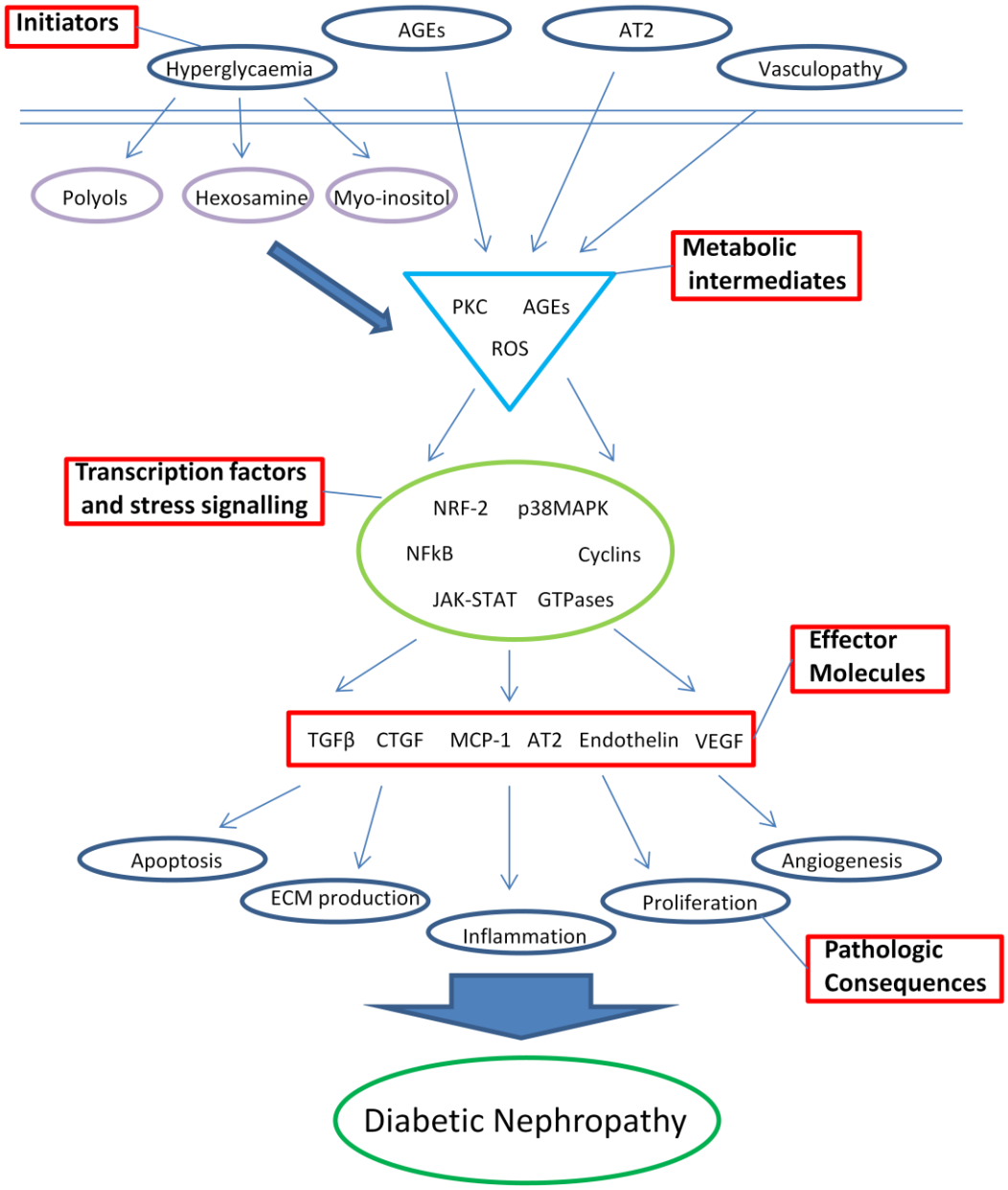

Figure 1.4 Overview of pathogenic mechanisms in DN illustrating the breadth of pathways operating in parallel. Although the schematic shows a linear flow of events, multiple opportunities exist for cross-talk, and positive and negative feedback between pathways. Optimal therapy for human disease is likely to involve interventions targeted at multiple points in this process to overcome the substantial biological redundancy. Adapted from Gnudi, 2012 and Kanwar et al, 2013. AGEs: advanced glycation end-products; AT2: angiotensin-II; PKC: protein kinase C; ROS: reactive oxygen species; NRF-2: nuclear factor (erythroid-derived 2)-like 2; MAPK: mitogen-associated protein kinase; JAK-STAT: Janus kinases – signal transducer and activator of transcription; TGFβ: transforming growth factor beta; MCP-1: monocyte chemoattractant factor-1; CTGF: connective tissue growth factor; VEGF: vasoactive endothelial growth factor.

triggers multiple stress-activated signalling pathways and activation of protein kinase C, an important intermediary event. Among the host of downstream signalling pathways and cytokines regulated by this response, transforming growth factor-β (TGFβ) and connective tissue growth factor (CTGF; induced by TGFβ) have cardinal roles in conducting ECM production, vasoactive endothelial growth factor (VEGF) is critical to disturbance of local blood flow and vascular permeability, angiotensin-II (AT2) provokes glomerular hypertension in addition to direct fibrogenic effects, and inflammatory cytokine release engages innate immune mechanisms in renal injury (Kanwar et al., 2011, Gnudi, 2012).

Despite increasing knowledge of the pathways and interactions involved in the development of DN, clinical treatments remain limited to central strategies of good glycaemic and blood pressure control and RAAS blockade. Although these approaches are successful in prolonging renal survival in a proportion of patients, the fact that many patients continue to progress to ESRD despite this emphasises the need to develop novel approaches to treatment.

1.10 Inflammation in DN

While DN has traditionally been regarded as a corollary of the cardiovascular and metabolic disturbances contingent on the diabetic state, it has become increasingly evident over the last 20 years that immune mechanisms play a key role in initiation and progression of disease. Persistent low grade activation of innate immune pathways occurs within renal cells as a consequence of aberrant intracellular metabolism, generation of reactive oxygen species (ROS), exposure to advanced glycation end-products (AGEs) and haemodynamic stress, resulting in elaboration of pro-inflammatory

cytokines, recruitment of circulating inflammatory cells and ultimately an amplification loop of tissue injury driving fibrosis and nephron loss. This inflammatory facet of DN represents an important potential opportunity for clinical intervention and has been the subject of intensive research. Several recent in-depth reviews have synthesised the current experimental evidence in this area (Navarro-Gonzalez and Mora-Fernandez, 2008, Rivero et al., 2009, Navarro-Gonzalez et al., 2011, Lim and Tesch, 2012, Wada and Makino, 2013).

1.10.1Inflammatory factors

The immune network comprises a wide array of secreted and cell surface molecules, acting via specific cell surface receptors to transduce signals that are often tissue- and context-specific (Navarro-Gonzalez et al., 2011). The repertoire of immune cells is similarly complex with increasing recognition of multiple states of activation and, in the case of monocytes and macrophages, a plasticity allowing a change in phenotype over time (Geissmann et al., 2010). The tools of cell biology have allowed for in-depth study of individual mediators in the context of DN, often by examining the consequences of selectively interfering with their function, allowing a gradual outline to develop of the full complexity of interactions (Figure 1.5).

1.10.1.i Inflammatory cytokines

The cytokines interleukin-1 (IL1), interleukin-18 (IL18), interleukin-6 (IL6) and tumour necrosis factor-α (TNFα) have received the most attention in the study of inflammation and DN. Incubation of peritoneal macrophages with GBM from STZ diabetic rats enhances secretion of IL-1 and TNFα, and levels

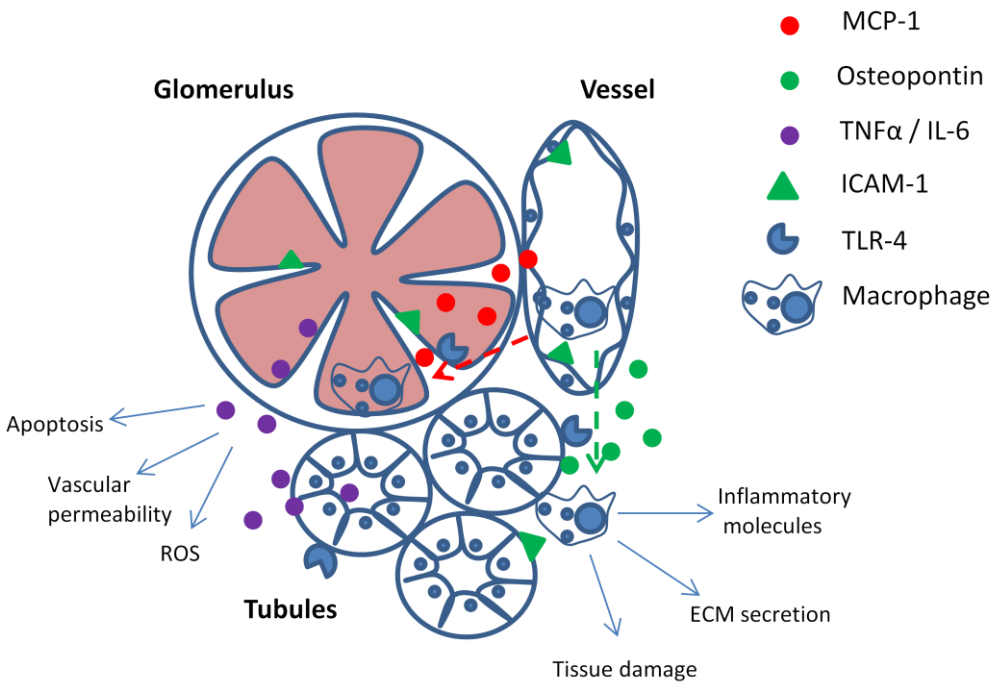

Figure 1.5. Schematic of central innate inflammatory mechanisms in DN. Local production of chemokines, adhesion molecules and inflammatory cytokines are upregulated in the hyperglycaemic state. Macrophages are the main infiltrating inflammatory cell type in both the glomerular and tubulointerstitial compartments where they contribute to tissue damage, ECM secretion and amplification of the inflammatory cascade.

of IL-1, IL-6 and TNFα mRNA increase in the renal cortex with time in the same model (Hasegawa et al., 1991, Navarro et al., 2006). In addition, all intrinsic renal cell types, including podocytes, mesangial cells, endothelial cells, tubular cells and fibroblasts are capable of synthesizing and secreting inflammatory cytokines (Rivero et al., 2009).

Both IL1 and the related leaderless peptide IL18, induce upregulation of leukocyte adhesion molecules including intercellular adhesion molecule-1 (ICAM-1) and E-cadherin, contributing to the influx of inflammatory cells into the diabetic kidney, as well as increasing local production of other cytokines (Park et al., 2000, Stuyt et al., 2003). IL-1 can directly induce proliferation and secretion of matrix proteins from mesangial cells, contributing to glomerulosclerosis (Melcion et al., 1982). IL-1 has also been demonstrated to act synergistically with TNFα to stimulate production of vasoactive eicosanoids such as prostoglandin E2 (PGE2) and phospholipase A2 (PLA2) from rat mesangial cells, increasing vascular endothelial cell permeability *in vitro*, and potentially contributing to intraglomerular haemodynamic abnormalities (Pfeilschifter et al., 1989, Royall et al., 1989, Navarro-Gonzalez et al., 2011). IL-18 is predominantly secreted from tubular cells and has been shown to have an important role in the pathogenesis of acute ischaemic nephropathy in mice (Melnikov et al., 2001). It can also act to increase the susceptibility of endothelial cells to TNFα-induced apoptosis (Marino and Cardier, 2003). Serum and urinary IL-18 is elevated in patients with type 2 diabetes and correlates with albuminuria both at baseline and during follow-up (Nakamura et al., 2005).

A survey of IL6 mRNA in the diabetic kidney using *in situ* hybridisation has revealed expression in mesangial cells and glomerular epithelial cells as well as tubular and infiltrating cells; most cells in the vicinity of areas of mesangial proliferation stain strongly for IL-6 mRNA (Suzuki et al., 1995). In this study, IL-6 expression also correlated well with the degree of interstitial injury. IL-6

has been implicated in pathways governing mesangial proliferation, ECM protein synthesis and endothelial permeability, all relevant to pathogenesis of DN (Lim and Tesch, 2012). Serum IL-6 levels increase in the course of DN and are highest in those with overt proteinuria (Shikano et al., 2000).

TNFα is an important, largely macrophage-derived, soluble cytokine with pleiotropic inflammatory and immunostimulatory effects (Wajant et al., 2003). Its importance in the pathogenesis of inflammatory diseases such as rheumatoid arthritis and inflammatory bowel disease has been underlined by the efficacy of anti-TNFα monoclonal antibodies such as Infliximab in these conditions (Wada and Makino, 2013). TNFα expression increases in the renal cortex of diabetic rats, and serum and urine levels increase in humans with DN (Moriwaki et al., 2003, Navarro et al., 2006). Infliximab has been shown to reduce albuminuria in the STZ rat model of diabetes although the mechanism has not been further explored (Moriwaki et al., 2007). Potential toxic effects of TNFα include a contribution to leukocyte influx, stimulation of local production of ROS, effects on endothelial permeability and induction of apoptosis (Lim and Tesch, 2012).

1.10.1.ii Cell adhesion molecules and chemokines

Cell adhesion molecules play an important role in determining the location of leukocyte adherence to the vasculature and subsequent tissue infiltration, and may be upregulated by inflammatory cytokines such as TNFα (Navarro-Gonzalez et al., 2011). Similarly, chemokines produce molecular gradients towards which leukocytes are attracted in order to concentrate immune cells at a site of tissue injury. Hence both classes of molecule have been investigated for their importance to the inflammatory state in DN.

ICAM-1 is an an endothelial glycoprotein which binds leukocytes via the ligand LFA-1 (Lim and Tesch, 2012). ICAM-1 levels are upregulated in renal tissue in rat models of DN and correlate with infiltration of mononuclear cells which can be prevented by administration of an anti-ICAM-1 monoclonal antibody (Sugimoto et al., 1997). Both type 1 (STZ) and type 2 (*db/db*) DN mouse models are attenuated when induced in mice genetically deficient in ICAM-1 (Okada et al., 2003, Chow et al., 2005). Analysis of serum ICAM-1 levels in serum samples from patients in the Diabetes Control and Complications Trial (DCCT) demonstrated an increased risk of progressive nephropathy in those patients with ICAM-1 levels in the highest tertile; these patients also had an increased relative risk (RR 1.67) of developing new sustained microalbuminuria compared to patients in the lowest tertile (Lin et al., 2008).

Levels of vascular cell adhesion protein-1 (VCAM-1), another important mediator of tissue-leukocyte interactions, are also increased in both human DN (predominantly on tubular epithelial cells) and rodent DN (predominantly venular endothelial cells and infiltrating leukocytes in the KKAy mouse model) and plasma levels of soluble VCAM-1 appear to correlate with albuminuria in hypertensive type 2 diabetics (Seron et al., 1991, Ina et al., 1999, Rubio-Guerra et al., 2009). Other adhesion molecules which have been linked to the pathogenesis of DN include endothelial cell-selective adhesion molecule (ESAM), which appears to have an important role in regulation of endothelial protein permeability, and E-selectin (Navarro-Gonzalez et al., 2011).

Monocyte chemoattractant protein-1 (MCP-1), an important chemoattractant factor for monocytes and macrophages, is the best studied chemokine in DN and has an important functional role in disease (discussed in section 1.7.2.a). Other chemokines which have been linked to renal injury, albeit less robustly, include CX3CL1 (fractalkine) and CCL5 (RANTES) (Navarro-Gonzalez et al.,

2011). CX3CL1 is upregulated in the kidneys of STZ-treated rats and this increase can be suppressed by angiotensin converting enzyme (ACE) inhibition (Kikuchi et al., 2004). Although the functional role of CX3CL1 has not been directly tested in animal models of DN, an inhibitory monoclonal antibody to this molecule has been shown to attenuate renal injury in a mouse model of bovine serum overload proteinuria, although this was accompanied by only a modest and non-significant reduction in leukocyte infiltration (Donadelli et al., 2003). CCL5 is upregulated in the kidneys of patients with type 2 diabetes and nephropathy, predominantly in the tubules (as detected by *in situ* hybridisation and immunhistochemistry) with more prominent expression in those with interstitial cell infiltration and fibrosis (Mezzano et al., 2004).

1.10.1.iii Pattern recognition receptors

Both exogenous pathogen-derived molecules (pathogen-associated molecular patterns; PAMPs) and endogenous damage-associated molecules (danger-associated molecular patterns; DAMPs) are capable of directly acitvating innate immune mechanisms through interaction with cell membrane or cytosolic pattern recognition receptors (PRRs). DAMP-PRR interactions are now recognised as important initiators and perpetuators of tissue inflammation and injury in a range of non-infective kidney diseases (Rosin and Okusa, 2011).

The cell membrane PRR, toll-like receptor (TLR) 4, is upregulated in proximal tubules and peritubular capillaries in human DN, and expression can be induced by hyperglycaemia in cultured human proximal tubular epithelial cells (PTECs) (Lin et al., 2012). Albuminuria and serum creatinine are both reduced in uninphrectomised STZ-diabetic TLR-4 KO mice compared to WT,

with reduced cortical macrophage infiltration and MCP-1 expression. The TLR-4 antagonist, CRX-526, is also effective in attenuating DN and inflammation in STZ-diabetic eNOS KO mice in the absence of an effect on BG or blood pressure (Lin et al., 2013). The related PRR, TLR-2, is also upregulated in the kidney of STZ-diabetic rats, although corresponding upregulation could not be demonstration in kidney biopsy specimens from patients with advanced DN (Li et al., 2010, Lin et al., 2012).

1.10.2 Inflammatory cells

1.10.2.i Macrophages

Macrophages are resident phagocytes derived from circulating mononuclear cells which have been recruited to the tissue compartment. Specialised for phagocytosis, macrophages play an important role in tissue maintenance and remodelling as well as host defence against micro-organisms, antigen presentation and local cytokine secretion (Gordon, 2002, Geissmann et al., 2010).Macrophages are also recognised as important orchestrators and effectors of tissue injury in a range of non-infective human inflammatory diseases, including those of the kidney (Nelson et al., 2012).

It is increasingly recognised that macrophages retain a significant degree of plasticity allowing for phenotypic sub-differentiation according to the context of the local prevailing cytokine environment. Although now generally regarded as an oversimplification, the concept of classically activated pro-inflammatory 'M1' macrophages differentiating under the influence of IFNγ and alternatively activated 'M2' macrophages, directed primarily by the TH2 cytokines IL-4 and IL-13, represents a useful conceptual dichotomy (Gordon and Martinez, 2010, Sica and Mantovani, 2012).

Macrophages are present in both the interstitial inflammatory infiltrate observed in human DN and also glomeruli where peak infiltration has been reported in association with moderate degrees of glomerulosclerosis (Bohle et al., 1991). Interstitial macrophage accumulation correlates strongly with clinical and histological parameters including serum creatinine, proteinuria and degree of interstitial fibrosis (Nguyen et al., 2006, Yonemoto et al., 2006).

P- and E-selectin, leukocyte adhesion molecules involved in the recruitment and transmigration of monocytes to the periphery, are upregulated in both glomerular and interstitial capillaries in patients with DN (Hirata et al., 1998). The important macrophage recruitment factor MCP-1 is upregulated in tubules and interstitial cells but not glomeruli of patients with DN as detected by *in situ* hybridisation, while urinary MCP-1 secretion increases with worsening clinical disease and correlates well with both the number of interstitial macrophages and clinical markers of disease progression (Wada et al., 2000, Tam et al., 2009). Tubulo-interstitial expression of another macrophage attractant factor, osteopontin, is also enhanced in DN and correlates with tubulo-interstitial fibrosis (Junaid and Amara, 2004). Experimental data describing the activation state of macrophages accumulating within the human diabetic kidney is scarce, although an increase in cells displaying active phosphorylated p38 MAPK in human diabetic kidney has been described, particularly within interstitial macrophages and myofibroblasts (Adhikary et al., 2004).

In the STZ mouse model of type 1 diabetes, most glomerular and interstitial leukocytes recruited into the kidney are macrophages and an increase can be detected as early as 2 weeks (Chow et al., 2004b). Glomerular macrophage number correlates with indices of glomerular injury including renal function, albuminuria, glomerular hypertrophy and type IV collagen deposition, while interstitial macrophages also correlate with scores of tubular atrophy,

interstitial type IV collagen and alpha-smooth muscle actin (αSMA;Chow et al., 2004b). In this study, macrophages were frequently observed in proximity to proliferating interstitial fibroblasts suggesting deleterious cross-talk between the two cell types promoting interstitial fibrosis. Although significant renal macrophage accrual occurs later in the *db/db* type 2 diabetes mouse model (4-6 months of age), similar correlation with markers of renal function and ECM deposition has been observed (Chow et al., 2004a).

While macrophage infiltration correlates closely with markers of disease and tissue injury, it has been debated whether their presence is truly injurious or in fact reactive to tissue damage, in which case they may have a beneficial role such as phagocytosis of cellular debris. This debate has been informed by functional studies of macrophages in animal models. Induction of diabetes with STZ in mice genetically deficient in MCP-1 leads to diminished macrophage infiltration in both glomerular and interstitial compartments, reduced macrophage activation (as assessed by iNOS and sialoadhesin expression) and amelioration of albuminuria, glomerular hypertrophy and cellularity and interstitial fibrosis (Chow et al., 2006). Similar findings have also been reported in an MCP-1 deficient strain of *db/db* mouse where reduced renal macrophage infiltration and protection from renal injury was observed compared to control animals despite a lack of effect on development of obesity, diabetes or macrophage infiltration into adipose tissue (Chow et al., 2007). Beneficial effects have been reported in both type 1 and type 2 diabetes disease models using antagonists of CCR2, the receptor for MCP-1 (Awad et al., 2011, Sayyed et al., 2011). Interestingly, while adoptive transfer of monocytes to diabetic CCR2 KO mice induces renal injury (where previously it was ameliorated) and leads to increased macrophage accumulation in the kidneys, this is true whether the transferred monocytes are CCR2 +/+ or CCR2 -/-, suggesting that this receptor may predominantly control monocyte mobilisation from the bone marrow rather than tissue infiltration (Awad et al., 2011). Induction of diabetes with STZ in

osteopontin KO mice also reduces macrophage infiltration and interstitial fibrosis but not markers of glomerular injury, suggesting greater relevance of this chemokine to the tubulointerstitial compartment (Nagao et al., 2012).

Treatment of *db/db* mice for 6 weeks with a neutralising anti-c-fms (the receptor for colony stimulating factor-1) monoclonal antibody after the establishment of albuminuria (from 12 weeks) did not affect progression of albuminuria, but did attenuate tubular damage and markers of renal fibrosis in conjunction with the predicted reduction in macrophage accumulation (Lim et al., 2009). This is consistent with the hypothesis that progression of established human DN is accelerated by recurrent episodes of macrophage-dependent inflammation and acute kidney injury (Kelly and Dominguez, 2010). Adoptive transfer of M2 macrophages, polarised with IL-4 and IL-13, to mice subsequently made diabetic with STZ, reduced the development of tubular atrophy and interstitial fibrosis as well as attenuating pancreatic injury, suggesting this macrophage phenotype may exert a protective effect at least in early disease (Zheng et al., 2011).

1.10.2.ii Lymphocytes

Although less prominent than macrophage infiltration, accumulation of lymphocytes, predominantly T cells, within the diabetic kidney is well recognised (Wu et al., 2011). A minor component of the glomerular and interstitial leukocytic infiltrate in rodent models of both type 1 and type 2 DN is comprised of T cells, while an early T cell infiltrate in the juxtaglomerular apparatus has been reported in human type 1 diabetes (Moriya et al., 2004, Chow et al., 2004a, Chow et al., 2006). A recent study has reported a marked increase in the number of CD4, CD8 and CD20+ cells within the renal interstitium of patients with type 2 DN, with the numbers of

CD4 and CD20+ cells correlating with proteinuria (Moon et al., 2012). The proportion of circulating activated T lymphocytes is increased in diabetic patients with sub-nephrotic proteinuria compared to those with non-proteinuric disease (Bending et al., 1988). T cells have been proven to play an important role in animal models of other 'non-immunological' renal disease such as ischaemia-reperfusion injury (Rabb et al., 2000).

There is no clear evidence for classical antigen-dependent T cell activation in DN although the exposure of previously hidden epitopes due to renal damage or production of neoantigens due to protein modification has been hypothesised as a mechanism of immune activation (Lim and Tesch, 2012). CD4+ cells express receptors for AGEs which can directly stimulate the production of IFNγ, contributing both to local tissue inflammation and oxidative stress as well as macrophage activation (Imani et al., 1993, Lim and Tesch, 2012).

The functional importance of lymphocytes in experimental DN has been tested by inducing diabetes with STZ in *Rag1* deficient mice, which do not produce mature T or B lymphocytes (Lim et al., 2010). In this study lymphocyte deficiency prevented the development of albuminuria and partially protected against podocyte loss, while indices of interstitial injury, macrophage number and renal function were not affected. Selective depletion of regulatory T cells (Tregs) with a monoclonal antibody to CD25 enhanced insulin resistance in the uninephrectomised *db/db* mouse model and worsened parameters of DN including albuminuria and glomerular hyperfiltration (Eller et al., 2011). Adoptive transfer of CD4+FoxP3+ Tregs from healthy donor animals had the opposite effect, strengthening the evidence that this subset of cells exert a beneficial effect, although the direct effects on renal injury and indirect effects due to changes in insulin resistance could not be separated in this study. While circulating immune complexes and glomerular deposition of IgG may be detected in DN, a direct

role for B lymphocytes in disease pathogenesis has not been proven (Lim and Tesch, 2012).

1.11 Rodent models of diabetes and DN

Animal models of human disease represent an important tool for study of natural history, molecular mechanisms of disease pathogenesis, and development and testing of novel therapeutic agents. Characteristics of ideal models include replication of most aspects of human disease, wide availability, ease of reproduction and cost-effectiveness (Alpers and Hudkins, 2011). The latter considerations have led to rodents, and in particular mice and rats, being the most frequently used species for disease modeling in biomedical research.

While acute disease can frequently be modeled in animals over a similar time-frame to the human illness, slowly-evolving diseases such as DN represent a greater challenge. Many established models of DN require aging of animals, often to >1 year to achieve full expression of renal lesions, and these are frequently variable and incomplete (Brosius et al., 2009). While genetic, pharmacological or surgical manipulations can compress the time-line of disease this is often at the expense of elements of the full disease phenotype, or superimposition of a second injurious process, limiting the translational relevance of subsequent findings. Additional modifying factors, such as the genetic background or the age of the animal, also impact significantly on disease expression.

The difficulties in establishing robust and reproducible models of DN led to the creation of the Animal Models of Diabetic Complications Consortium (AMDDC; www.diacomp.org), a network of researchers collaborating to identify and characterize new models of disease, standardize assessment and

reporting of disease metrics and share data on phenotyping and validation. This group has published criteria for validation of new disease models, providing a clear description of the desirable features of a model faithful to the human disease (Table 1.2).

No model identified to date encapsulates all features of the AMDCC validation criteria and hence model selection is often dictated by local availability, experience and time-constraints as well as the planned application. Hence, interpretation of data must be in the context of the recognized limitations of the chosen model.

1.11.1 Mouse models

Mouse models of human disease are attractive due to the relative ease with which the effects of genomic manipulation, such as global or tissue-specific gene inactivation, can be tested on disease evolution. Moreover, a strategy of ingressing important pro-diabetic mutations onto mice with nephropathy-susceptible genetic backgrounds has rapidly expanded the repertoire of disease models (Alpers and Hudkins, 2011).

Limitations when compared to rat models include their smaller size, meaning smaller quantities of blood, urine or tissue available for analysis, and greater physiological differences from humans, often limiting studies of novel pharmacological agents (Huang et al., 2011). With respect to the current project, mouse, rat and human P2X7 receptors display important pharamacological and operational differences which bear relevance to interpretation and translation of experimental findings; for instance, BzATP is 10-fold more potent to activate human and rat P2X7 receptors, compared to mouse (Donnelly-Roberts et al., 2009).

Core critera for assessment of a new disease model

Assessment domain	Desirable level
GFR	50% decline over life-time of animals
Albuminuria	10-fold increase compared with controls of same age, gender and genetic background
Pathological features -Mesangium -Arterioles -GBM - Tubulointerstitial fibrosis	 Advanced expansion +/- nodular sclerosis Any degree of hyalinosis >50% thickening over baseline Present

Additional criteria in the presence of lesions of advanced disease

Assessment domain	
Mesangial matrix	- Quantification, ideally by morphometric analysis - Analysis of mesangiolysis and microaneurysms on appropriately stained sections
Exclusion of immune complexes	IHC for IgG, IgM and IgA on frozen sections
Arteriolar hyalinosis	Identification of hyalinosis in either afferent or efferent vessels using silver methenamine or PAS stains
GBM thickening	Quantification with electron microscopy
Podocyte loss	Detection and morphometric quantification on appropriately stained sections
Macrophage infiltration (optional)	Detection by Mac-2 IHC
Lipid deposition (optional)	Detection by oil Red O staining

Table 1.2 Validation criteria for animal models of DN as set out by the American Diabetes Complications Consortium (www.diacomp.org). IHC: Immunohistochemistry

1.11.1.i Effect of genetic background on disease expression

Many different inbred mouse strains are available for experimental use and genetic background has an important modifying effect on disease expression. C57BL/6 mice are widely used due to the frequent availability of genetically-engineered mutants on this background together with the fact they breed well and have a low frequency of spontaneous tumours (Breyer et al., 2005). However, this strain appears particularly resistant to the development of glomerulosclerosis, whether due to hyperglycaemia or reduction of renal mass (Zheng et al., 1998, Ma and Fogo, 2003). This is despite displaying relative susceptibility to the induction of hyperglycaemia with STZ and also to the metabolic complications of a high fat diet (West et al., 1992, Gurley et al., 2006).

The DBA/2 mouse strain, however, appears to be more susceptible to the development of diabetic renal injury (Doi et al., 1989, Gurley et al., 2006). This is further reflected in the strain dependence of the *db/db* type 2 diabetes mouse model where the commonly used and susceptible C57BLKS background, which shares 84% of its alleles with C57BL/6 and 16% with DBA/2, shows more severe disease than animals on a pure C57BL/6 background (Breyer et al., 2005).

Other important strain effects are discussed with relation to the individual models below.

1.11.1.ii Effect of age on disease expression

While development of diabetic renal injury in mice is clearly time-dependent, there is also evidence that inducing disease in older animals may promote a

more severe disease phenotype. Induction of diabetes with repetitive low dose STZ in 18 month-old female C57BL/6 mice (a resistant sex and strain) produces a severe disease phenotype with marked glomerular, tubulointerstitial and vascular disease, and 10-fold higher albuminuria than 5 month old comparator animals (Wu et al., 2010a). In this study, oxidative stress, markers of endoplasmic reticulum stress and inflammatory cytokines were all upregulated in the kidneys of aged non-diabetic mice while marked increases in these parameters were observed in aged diabetic animals along with the appearance of diffuse interstitial macrophage infiltration. This apparent synergism between aging and diabetes may hence provide a useful tool to accelerate the development of experimental renal injury (Zheng et al., 2003, Wu et al., 2010a).

1.12 Individual mouse models of DN

Numerous mouse models of DN have been described, consequent to both type 1 and type 2 diabetes. The most commonly used models are discussed below, with emphasis on their individual stengths and weaknesses (Table 1.3).

1.12.1 Type 1 diabetes models

1.12.1.i Streptozotocin-induced DN

STZ is an antibiotic derived from *Streptomycetes achromogenes* used to induce a phenotype of type 1 diabetes in experimental animals (Szkudelski, 2001). Taken up into pancreatic β-cells via the GLUT-2 receptor, it causes alkylation of DNA, overstimulation of poly-(ADP-ribose) polymerase (PARP) in an attempt to repair DNA, depletion of NAD+ and ATP and ultimately

Mouse models	Strengths	Weaknesses
Type 1 diabetes		
High dose STZ	'Pure' hyperglycaemic insult Simple and low cost	STZ causes off-target nephrotoxicity Carcinogen
Repetitive low dose STZ	Minimal off-target nephrotoxicity Early renal macrophage infiltration	Milder disease than high dose STZ C57BL/6 relatively resistant to DN
Akit a mouse	Spontaneous diabetes 'Pure' hyperglycaemic injury with no off-target effects	Minimal interstitial disease Glomerular IgA deposition common
NOD mouse	Spontaneous diabetes Insulinitis closely models human type 1 disease	DN very slow to develop (> 1 year) Insulin treatment often necessary
eNOS KO mouse	Accelerates DN due to both type 1 (eg STZ) and type 2 (eg *db/db*) diabetes Advanced glomerulopathy (nodular sclerosis)	Mechanism of early podocytopathy unclear Prominent hypertension Tubulointerstitial disease often mild or even ameliorated
OVE26 mouse	Marked albuminuria and glomerulosclerosis on FVB background No need for exogenous insulin	Albuminuria markedly reduced on C57BL/6 and DBA/2 backgrounds
Type 2 diabetes		
High fat diet	Simple and low cost Recapitulates human metabolic syndrome	Mild hyperglycaemia and consequently mild DN Renal lipid accumulation common
Db/db mouse	Spontaneous diabetes Obese but not hypertensive Advanced DN with eNOS KO strain	Tubulointerstitial disease mild C57BL/6 relatively resistant to DN

Table 1.3 Mouse models of diabetic nephropathy. NOD: Non-obese diabetic; eNOS: Endothelial nitric oxide synthase

cellular necrosis and death (Lenzen, 2008). STZ also inhibits β-cell O-GlcNAcase, the protein responsible for export of O-linked N-acetylglucosamine (O-GlcNAc) from the cell, leading to irreversible O-glycosylation of proteins, which compounds cellular injury (Lee et al., 2006, Tesch and Allen, 2007).

Injection of STZ is followed by a tri-phasic metabolic response, with an initial early hyperglycaemic phase (c. 1 hour) due to inhibition of insulin secretion, followed by hypoglycaemia (4-8 hours) due to β-cell necrosis and fulminant release of insulin into the circulation (Lenzen, 2008). Complications of hypoglycaemia, such as seizures, can be prevented by ensuring animals have free access to oral sugar solutions during this phase. Permanent hyperglycaemia develops by 12-48 hours after β-cell degranulation and necrosis is complete (Lenzen, 2008).

STZ will potentially accumulate in any cell type expressing GLUT-2, activating the same injurious mechanisms elicited in β-cells. Off-target toxicity has been described in both liver and kidney, with the latter manifesting as proximal renal tubular injury and potentially confounding detection and assessment of metabolic kidney injury (Tay et al., 2005). These effects are particularly apparent when STZ is administered as one or two 'high dose' injections (eg. 100-200 mg/kg).

Repetitive low dose protocols (eg. 50mg/kg on five consecutive days) are also effective in inducing a diabetic phenotype, with initial milder β-cell injury followed by a secondary autoimmune insulinitis, not observed in the high-dose schedule, commencing at 5-6 days after the last injection (Like and Rossini, 1976). The inflammatory islet infiltrate comprises predominantly lymphocytes and macrophages and is not accompanied by circulating islet cell antibodies (Like et al., 1978). Achieved hyperglycaemia is comparable to that seen with high dose induction schedules while off-target toxicity is

typically diminished (Breyer et al., 2005). No direct podocyte injury is observed in the low dose model (Breyer et al., 2005). C57BL/6 and DBA/2 strains exhibit more robust and sustained hyperglycaemia than BALB/C, MRL/Mp and 129 SvEv strains (Gurley et al., 2006).

Albuminuria, seen variably from ~5 weeks post induction, is typically lower than with the high dose schedule, although this may in part reflect reduced STZ nephrotoxicity. The evolution of advanced DN lesions (mesangial expansion and nodule formation) occurs late (> 15 weeks), and also has a strong dependence on background genetic strain, with DBA/2 animals exhibiting the highest levels of albuminuria and greatest mesangial expansion on head-to-head testing (Gurley et al., 2006). Diabetes may require partial correction of hyperglycaemia with insulin to sustain mice for the requisite duration to induce histological changes of DN (Roxburgh et al., 2009).

1.12.1.ii Akita mouse

Originally identified as the result of a chance mutation in a C57BL/6 colony in Japan, Akita mice develop spontaneous type 1 diabetes by 3-4 weeks of age through β-cell loss in the absence of insulinitis (Yoshioka et al., 1997). The responsible *Ins2*^{C69Y} mutation disrupts a disulphide bond between insulin A and B chains, leading to misfolding, retention within the endoplasmic reticulum and β-cell proteotoxicity (Wang et al., 1999, Ron, 2002). While homozygote mice die in infancy, mice carrying a heterozygote mutation manifest a dominant phenotype, as expression of the mutant misfolded protein interrupts secretion of normal insulin expressed from the wild-type allele (Ron, 2002).

Blood glucose is similar or higher than that seen in the STZ model and the absence of off-target effects and non-metabolic nephrotoxicity potentially make it an attractive model for study of microvascular complications (Breyer et al., 2005, Gurley et al., 2010). When the phenotype of C57BL/6 Akita mice was compared directly to that of low dose STZ on the same genetic background, a similar, but more uniform, degree of mesangial expansion was observed in Akita mice and albumin excretion was higher (Gurley et al., 2010). Albuminuria is enhanced when the Akita mutation is imposed on a DBA/2 or 129/SvEv background, although mesangial expansion is only a feature of disease in C57BL/6 or 129/SvEv Akita mice (Gurley et al., 2010). Interstitial disease is not a feature and no study has reported changes of advanced DN such as mesangial nodule formation (Alpers and Hudkins, 2011). Akita mice have a propensity for glomerular IgA deposition by 20 weeks, complicating the interpretation of experimental interventions on mesangial expansion.

1.12.1.iii Non-obese Diabetic (NOD) mouse

First described in Japan in 1980, the NOD mouse exhibits a spontaneous diabetic phenotype present in 80% of female animals by 30 weeks of age (Makino et al., 1980). NOD mouse shares many important pathogenic and genetic features to human autoimmune type 1 diabetes including an exuberant insulinitis comprising antigen presenting cells, T cells and B cells, MHC-dependent and -independent genetic susceptibility, and development of anti-islet cell antibodies, meaning the model has been used extensively to study events underlying autoimmune β-cell injury (Atkinson and Leiter, 1999, Breyer et al., 2005, Thayer et al., 2010). Although they exhibit other extra-pancreatic phenotypic features (eg. deafness, complement abnormalities, T cell accumulation in peripheral lymphoid organs) target

organ damage can be assumed to arise from metabolic disturbance, as opposed to non-specific nephrotoxicity (Atkinson and Leiter, 1999).

NOD mice do develop features of early nephropathy including albuminuria, GBM thickening and mesangial expansion, albeit with some variability in the time of onset (Doi et al., 1990). The strain has been used successfully to demonstrate the effect of therapeutic interventions on histological and biochemical parameters of DN, although partial treatment of diabetes with insulin is needed to maintain animals for the requisite experimental time that may be in excess of 1 year (Zheng et al., 2002). Production of genetically-engineered congenic NOD stock with deletions or modifications to genes of interest in DN is feasible, but multiple genetic loci must be preserved in order to maintain development of diabetes and identification of suitable non-diabetic control mouse strains can be difficult (Breyer et al., 2005).

1.12.1.iv Endothelial Nitric Oxide Synthase (eNOS) knockout models

Endothelial dysfunction represents an early and important component of the glomerular injury in both type 1 and type 2 diabetes (Badal and Danesh, 2012). Nitric oxide (NO), produced locally by eNOS, is an important mediator of both vascular tone and vascular permeability, with inhibition or genetic deletion of eNOS leading to opening of interendothelial junctions and albumin leak in multiple murine microvascular beds (Predescu et al., 2005, Zhao et al., 2006). Endothelial NO availability is reduced in diabetes and polymorphisms in the human *NOS3* gene (encoding eNOS) have been demonstrated both to be functional, corresponding to lower measured levels of NO, and to predict development of advanced nephropathy in patients with both type 1 and type 2 diabetes (Tsukada et al., 1998, Zanchi et al., 2000, Du et al., 2001, Ezzidi et al., 2008, Brosius et al., 2009).

Induction of diabetes with a low dose STZ protocol in eNOS KO animals leads to 10 fold-higher albuminuria by week 20, increased mesangiolysis and thicker GBM on electron microscopy, compared to diabetic WT animals (Kanetsuna et al., 2007). Mesangial expansion is not increased compared to WT, tubulointerstitial pathology is mild, and blood pressure is elevated in eNOS KO animals (Kanetsuna et al., 2007). The phenotype is more severe with a higher dose STZ schedule: around 20-fold higher albuminuria by 5 months compared to WT, increased mesangial expansion and occasional mesangial nodular sclerotic changes (Nakagawa et al., 2007). Similar potentiating effects on albuminuria, mesangial expansion, glomerulosclerosis and mesangiolysis were seen in a study of the F1 cross between heterozygous 129S6/SvEvTac eNOS +/- mice and heterozygous C57BL/6J eNOS +/- mice carrying the Akita mutation, with eNOS -/- having more severe disease than +/- and, in turn, +/+ progeny (Wang et al., 2011). Of note, tubulointerstitial fibrosis, as assessed by Masson's trichrome staining, was ameliorated in eNOS KO Akita mice compared to eNOS WT animals (Chen et al., 2005).

A similar enhancement of renal pathologic changes by eNOS deficiency has also been observed in a model of type 2 diabetes, where eNOS +/- mice on a C57BL/6 background were backcrossed for 10 generations on to the nephropathy-sensitive C57BLKS/J strain and then crossed with *db/db* mice (Zhao et al., 2006). By 26 weeks, eNOS KO mice had dramatically more albuminuria, increased mesangial expansion and GBM thickness, early nodular sclerotic changes and, strikingly, a >50% reduction in GFR. Although, at face value, these changes appear more robust and severe than those observed with the low dose STZ model, this may in part be explained by the background genetic strains used in the relevant experiments (Brosius et al., 2009).

While genetic eNOS deficiency appears to overcome many of the shortcomings of traditional mouse models of DN, the precise mechanisms underlying the acceleration of renal pathology have not been clear. A recent study examining the effect of a VEGF receptor blocker, Vatalanib, after induction of diabetes with low dose STZ in eNOS KO mice, has shed some light on this (Yuen et al., 2012). In this study, Vatalanib, administered by daily oral gavage commencing 2 weeks after induction of diabetes, inhibited glomerular capillary enlargement in both eNOS KO and WT diabetic animals, but only attenuated albuminuria in WT mice. In eNOS KO animals an acute podocytopathy was evident by 2 weeks after diabetes induction, concomitant with onset of marked albuminuria, not apparent in WT animals and preventable with RAAS blockade. As podocytes do not express significant amounts of eNOS, this suggests that deleterious endothelial cell-podocyte crosstalk may in part explain the amplified diabetic phenotype observed in the absence of eNOS.

1.12.1.v OVE26 mice

OVE26 transgenic mice over-express calmodulin in pancreatic β-cells, leading to cell toxicity and a type 1 diabetic phenotype (Epstein et al., 1989). When expressed on an FVB background, OVE26 mice exhibit marked albuminuria, far in excess of that seen in any other diabetes mouse model, reaching levels 200-fold greater than control mice by 9 months (Zheng et al., 2004). This is accompanied by mesangial expansion, progressing to more global glomerulosclerosis, podocyte loss and mild tubulointerstitial fibrosis (Alpers and Hudkins, 2011). Mice can maintain body weight and survive for over a year without the need for exogenous insulin therapy (Zheng et al., 2004). The primary limitation of OVE26 mice is the marked strain-dependence of DN development: while OVE26 transgenic mice bred onto a C57BL/6 or DBA/2 background still develop marked hyperglycaemia, albuminuria and mesangial expansion are signficantly reduced (Xu et al., 2010). As a result, it

is challenging to ingress additional genetic mutations onto this model (Alpers and Hudkins, 2011).

1.12.2 Type 2 Diabetes Models

1.12.2.i High-fat diet

Feeding mice a high-fat diet has been used as an approach to model type 2 diabetes and the metabolic syndrome (Surwit et al., 1988, Panchal and Brown, 2011). High fat diet promotes obesity, dyslipidaemia, insulin resistance, impaired glucose tolerance and hypertension as well as end organ damage including cardiac hypertrophy and hepatic steatosis (Panchal and Brown, 2011). Hyperglycaemia is modest with random BG values of 8-14 mM by 12 weeks of feeding (West et al., 1992, Deji et al., 2009). Susceptibility to high fat diet shows strain-dependence with greatest success using C57BL/6 and AKR/J inbred genetic backgrounds (West et al., 1992).

Obese animals manifest a mild renal phenotype comprising albuminuria (3-4 fold higher than control animals), glomerular hypertrophy, mesangial expansion and irregular GBM thickening, together with interstitial macrophage accumulation (Deji et al., 2009). Of note, these abnormalities could be prevented by feeding a restricted volume high fat diet, matching body weight to low fat diet controls. Lipid accumulation in renal tissue is also observed, driven by accelerated local lipogenesis and depressed lipolysis, which may contribute to the development of kidney injury (Kume et al., 2007).

1.12.2.ii Db/db mouse

The *db/db* (db referring to diabetes) mouse was first described as a chance mutation in C57BLKS stock at the Jackson Laboratory in the 1960s and is a commonly used model of obese type 2 diabetes (Hummel et al., 1966). A point mutation in the gene encoding the hypothalamic leptin receptor leads to aberrant splicing and production of defective protein; transmitted by autosomal recessive inheritance, this leads to hypothalamic resistance to the adipocyte-derived satiety hormone leptin, with consequent hyperphagia and obesity (Tesch and Lim, 2011, Panchal and Brown, 2011). In C57BLKS mice, hyperglycaemia develops by 4 weeks, albuminuria may be observed by 8 weeks, and mesangial expansion by 12-16 weeks of age (Sharma et al., 2003). Subsequent β-cell degeneration means intermittent insulin administration is required to keep animals alive for longer periods (Tesch and Lim, 2011). Significant interstitial fibrosis is not a feature (Breyer et al., 2005).

Db/db mice on a C57BL/6 background have a lower incidence of diabetic-range hyperglycaemia and delayed onset of renal injury compared to C57BLKS. They also manifest β-cell hypertrophy rather than degeneration meaning maintenance insulin replacement is not required (Sharma et al., 2003, Chow et al., 2007). Nephropathy can be accelerated by uninephrectomy (Bower et al., 1980, Tesch and Lim, 2011). Male mice of both strains are more susceptible to diabetes than females (Tesch and Lim, 2011).

Ob/ob mice carry a mutation in the gene for leptin (as opposed to the receptor) which is transmitted by autosomal recessive inheritance (Panchal and Brown, 2011). While the overall phenotype of these animals is similar to *db/db*, renal disease is mild and mainly comprises diffuse and nodular lipohyaline glomerular changes, limiting their use for interventional studies (Sharma et al., 2003).

1.13 Rat models of DN

As with mice, rat models of both type 1 and type 2 diabetes have been used to study DN . The most commonly used models are discussed below, with emphasis on their individual stengths and weaknesses (Table 1.4).

1.13.1 Type 1 diabetes models

1.13.1.i Streptozotocin-induced DN

As with mice, STZ is commonly used to induce type 1 diabetes in rats through direct pancreatic β-cell toxicity (Tesch and Allen, 2007). Sprague-Dawley and Wistar are the most commonly used strains. The majority of animals develop diabetes after a single IV or IP dose and, unlike in the mouse, off-target acute kidney injury is minimal or absent (Junod et al., 1967). DNA damage and resultant proliferative responses do occur within the kidney, however, these have typically resolved by 3 weeks post-administration (Kraynak et al., 1995). It is generally felt advisable to wait for this 3 week window to elapse after STZ injection before beginning treatment with potential therapeutic agents.

Albuminuria may be observed from 2 weeks after diabetes induction increasing to 5-10 times control values by 24 weeks (Osicka et al., 2000, Kalantarinia et al., 2003). However, histological abnormalities are mild, even after prolonged hyperglycaemia, and are limited to modest mesangial expansion, interstitial fibrosis and deposition of ECM proteins (Sanai et al., 2000, Nakamura et al., 2007). Many investigators superimpose an additional insult to accelerate the development of nephropathy, such as uninephrectomy or hypertension (Kelly et al., 1998, Huang et al., 2009). A model has recently been described in which STZ diabetes is induced in a rat

Rat Models	Strengths	Weaknesses
Type 1 diabetes		
STZ	'Pure' hyperglycaemic injury Low cost DN can be accelerated by UNx or inducible hypertension	Mild renal phenotype Cataracts common Insulin treatment necessary
Obese Type 2 diabetes		
Zucker diabetic fatty rats	Spontaneous diabetes Recapitulates human metabolic syndrome	Dominant renal abnormality is hydronephrosis
OLETF rats	Spontaneous diabetes Recapitulates human metabolic syndrome	DN onset very slow (proteinuria 20 weeks, GBM thickening 40 weeks) Insulin treatment often required
Lean type 2 diabetes		
GK rats	Spontaneous diabetes Dyslipidaemic but not hypertensive Insulin treatment not required	DN onset very slow (mild albuminuria by 1 year, glomeruosclerosis at 2 years)

Table 1.4 Rat models of diabetic nephropathy. OLETF: Otsuka Long-Evans Tokushima fatty; GK: Goto-Kakasaki

harbouring the *Ren2* renin gene under the control of the cytochrome P4501a1 promoter. In this rat hypertension can be induced by the dietary administration of indole-3-carbinol (Conway et al., 2012). This permits hypertension to be induced after the onset of diabetes (as opposed to being present from the outset in non-conditional *Ren*2 transgenics) and titrated to the desired level, more closely modelling the biology of human disease.

1.13.2 Obese type 2 diabetes rat models

1.13.2.i Zucker diabetic fatty rats (ZDF/Drt-fa)

ZDF/Drt-*fa* rats develop spontaneous hyperglycaemia in the context of obesity and hyperlipidaemia driven by a mutation in the leptin receptor (Panchal and Brown, 2011). Outbred obese Zucker rats do not exhibit hyperglycaemia; the diabetic variant was identified as a chance mutant in a Zucker colony, transmitted in an autosomal dominant fashion, and selectively inbred for 16 generations (Clark et al., 1983, Vora et al., 1996). Obesity and increased body weight is apparent by 6 weeks of age while hyperglycaemia and hyperinsulinaemia manifests by 8-12 weeks together with hypercholesterolaemia and hypertriglyceridaemia (Vora et al., 1996). While albuminuria is increased by 6 weeks in obese animals compared to lean controls, and increases progressively thereafter, the dominant histopathological finding in animals with prolonged hyperglycaemia is of hydronephrosis, presumed to be of neurogenic origin, and complicating the interpretation of experimental findings (Vora et al., 1996).

1.13.2.ii Otsuka Long-Evans Tokushima Fatty (OLETF) Rats

OLETF rats display spontaneous hyperglycaemia in the context of mild obesity and were derived from a mutation in a colony of Long-Evans rats in Tokushima, Japan, in the early 1980s (Kawano et al., 1992). Rats exhibit hyperglycaemia at ~18 weeks of age, followed by hyperinsulinaemia and then pancreatic degeneration by 40 weeks of age, often requiring insulin replacement. Renal complications develop with time, with increased proteinuria by 20 weeks, mesangial expansion and GBM thickening apparent by 40 weeks, and glomerular nodular changes developing by 60-70 weeks (Kawano et al., 1992, Yagi et al., 1997). Compared to lean controls, animals exhibit hypertension from 10 weeks of age, which may contribute to the development of nephropathy (Yagi et al., 1997)

1.13.3 Lean type 2 diabetes rat models

1.13.3.i Goto-Kakizaki (GK) rat

The GK rat represents a model of lean type 2 diabetes and was produced by repeated inbreeding of Wistar rats selected through oral glucose tolerance testing (Goto et al., 1976). The mechanism of diabetes onset is consequently complex, including impairment in gestational β-cell neogenesis and abnormal β-cell differentiation (Panchal and Brown, 2011). Hyperglycaemia is evident by 4-6 weeks of age and supplemental insulin is not required for long-term maintenance as blood sugars remain only modestly elevated (<20mM). By 35 weeks, renal abnormalities are limited to glomerular hypertrophy and GBM thickening with no accompanying increase in albuminuria (Phillips et al., 2001). Interstitial macrophage infiltration is observed from 12 weeks, increasing up to 35 weeks, and an excess of glomerular macrophages is

present by 35 weeks (Phillips et al., 2001). An increase in type IV collagen and αSMA expression is observed by 1 year but glomerular sclerotic changes and tubulointerstitial fibrosis only appear after 2 years of diabetes (towards the end of the animal's life) (Sato et al., 2003).

1.14 Conclusions - diabetic nephropathy

Despite the panoply of molecules and pathways now identified as contributing to the pathogenesis of DN, there have been no major therapeutic advances in the last 10 years, and a substantial proportion of sufferers continue to progress to end-stage renal disease (ESRD). Recognition that innate immune mechanisms, classically associated with infective or inflammatory diseases, contribute to progression of DN, has presented a new avenue for investigation, and potentially the development of novel therapeutic agents. Any proposed anti-inflammatory or immuno-modulatory treatment for DN will, however, require careful target selection and thorough evaluation in pre-clinical disease models, to ensure both efficacy and specificity of action.

A number of animal models of DN have been discussed, resulting from both type 1 and type 2 diabetes. Common to all of these, with the possible exception of diabetic eNOS KO mice, is a mild renal phenotype, failing to recapitulate the features of advanced human DN. This is further complicated by differences in reported severity of renal disease between different strains, ages and sex of mice, increasing heterogeneity of published data and hindering replication of important findings. Ultimately, investigators should select a model of DN to test their specific research question by considering which features are most desirable eg. presence of associated hypertension or obesity, early robust albuminuria or interstitial disease, or presence of a well-developed inflammatory response.

Part 3. Hypothesis and aims

1.15 Hypothesis

The central research question addressed in this project is:

Does the P2X7 receptor contribute to the pathogenesis of diabetic nephropathy?

As reviewed above, circumstantial evidence already exists which connects P2X7 to DN, including upregulation of glomerular expression observed at an early timepoint in the STZ diabetic rat, and a potential contribution to ECM synthesis in rat MCs exposed to hyperglycaemia (Vonend et al., 2004, Solini et al., 2005). To date, no studies have directly explored the functional importance of P2X7 in development of DN. Given the established role of P2X7 in secretion of IL1β/IL18 from macrophages and its proven importance in the pathogenesis of inflammatory and fibrotic kidney diseases, a key aim of this project is to examine the contribution of P2X7 to renal inflammation in DN. An increasing body of evidence has linked activation of innate immune mechanisms to progressive kidney injury in diabetes, making interruption of these pathways an important focus for development of new therapies.

1.16 Experimental aims and rationale

The specific goals of the study are:

1) To examine the expression of P2X7 in human kidney biopsy tissue from patients with DN by immunohistochemistry and assess the relationship between expression and clinical parameters of disease.

2) To study the functional importance of P2X7 to DN by comparing renal outcomes and measures of renal inflammation in WT and GSK P2X7 KO mice made diabetic by repetitive low dose STZ injection.

3) To complement the murine study of genetic P2X7 deficiency by examining the effect of a selective P2X7 antagonist on the development of kidney disease in the uninephrectomised STZ rat model of DN.

4) To further investigate the potential mechanism by which P2X7 signalling may promote glomerular inflammation in DN, through *in vitro* studies of human glomerular cells exposed to hyperglycaemia.

In addition, a supplementary study has been conducted to specifically examine the role of P2X7 in the development of insulinitis and β-cell injury after STZ, by comparing pancreatic outcomes in WT and Pfizer P2X7 KO mice.

The low dose STZ mouse model of DN was selected for use on the following grounds:

1) The model is established and well characterised, and manifests an early and robust macrophage infiltrate, providing a good model for study of early inflammatory events in DN.

2) Although low dose STZ results in milder renal disease than a high dose induction schedule, it is associated with minimal bystander nephrotoxicity, a problem with high dose regimes.

3) STZ-induced diabetes offers the opportunity to look at the renal consequences of hyperglycaemia without confounding effects of hypertension, obesity and dyslipidaemia, common to most type 2 diabetes mouse models.

4) STZ can also be used to induce diabetes in rats, facilitating comparison between the mouse and rat models of DN used in this study.

CHAPTER 2

MATERIALS AND METHODS

2.1 General materials

All laboratory chemicals were purchased from Sigma-Aldrich (Poole, UK) unless otherwise specified. Tissue culture plasticware was manufactured by Corning (New York, USA), cell scrapers by Greiner (Frickenhausen, Germany) and scalpels by Swann-Morton (Sheffield, UK). Microcentrifuge tubes were supplied by Eppendorf (Hamburg, Germany). Specific materials and their source are described in the relevant sections below.

2.2 Animal husbandry

Mice and rats were maintained in a pathogen-free animal facility at Imperial College London (Hammersmith Hospital campus) in individually-ventilated cages with free access to water and standard laboratory diet. Maximum cage occupancy was five for mice and two for rats. All experimental animals were male. All animal procedures were licensed by the Home Office Science Unit: personal license 70/23327 and project licenses 70/7250 (Prof Roger Mason) and 70/7104 (Prof Charles Pusey).

2.3 Breeding of genetically modified mice

Two strains of P2X7 KO mice were used in experiments: one generated by GlaxoSmithKline (GSK; Harlow, UK) and the other by Pfizer (Groton, USA). Both were provided as kind gifts for use in this project. GSK KO mice were

bred in-house from heterozygote breeding pairs, with WT animals used as experimental controls. Pfizer KO mice were bred from homozygote KO breeding pairs and unrelated WT C57BL/6 animals were used as controls for experiments using these mice.

2.3.1 Background: Generation of GSK P2X7 KO mice

The GSK mouse was generated by targeted insertion of a *lacZ* gene at the beginning of exon 1 of the *P2RX7* gene (Sim et al., 2004, Chessell et al., 2005); (Figure 2.1A and B). To achieve this, the *P2X7R* gene was isolated from a genomic library obtained from 129/Sv mice, the 5' exons partially sequenced, and two fragments ligated into a neomycin-resistant 'knock out vector' plasmid. Homologous recombination of the resulting plasmid DNA into embryonic stem cells resulted in P2X7 gene disruption. Chimaeric mice were created by injection of transformed embryonic stem cells into C57BL/6 host embryos. These were subsequently crossed with C57BL/6 females to generate heterozygotes and then intercrossed to create healthy mutant offspring. Loss of channel function was confirmed by testing IL1β production from peritoneal macrophages in response to ATP and LPS, which was abolished in KO animals (Chessell et al., 2005).

2.3.2 Background: Generation of Pfizer P2X7 KO mice

The Pfizer mouse was generated by insertion of a neomycin resistance cassette into the *P2X7R* gene after the Arg^{505} codon (Solle et al., 2001); (Figure 2.1C). This insertion led to deletion of Cys^{506} to Pro^{532} in the long intracellular C-terminal region of the *P2X7R* gene product. Using methodology similar to that described for the GSK KO, a targeting vector (plasmid) was constructed and used for transformation of embryonic stem cells with the disrupted gene. Chimaeric mice derived from transformed

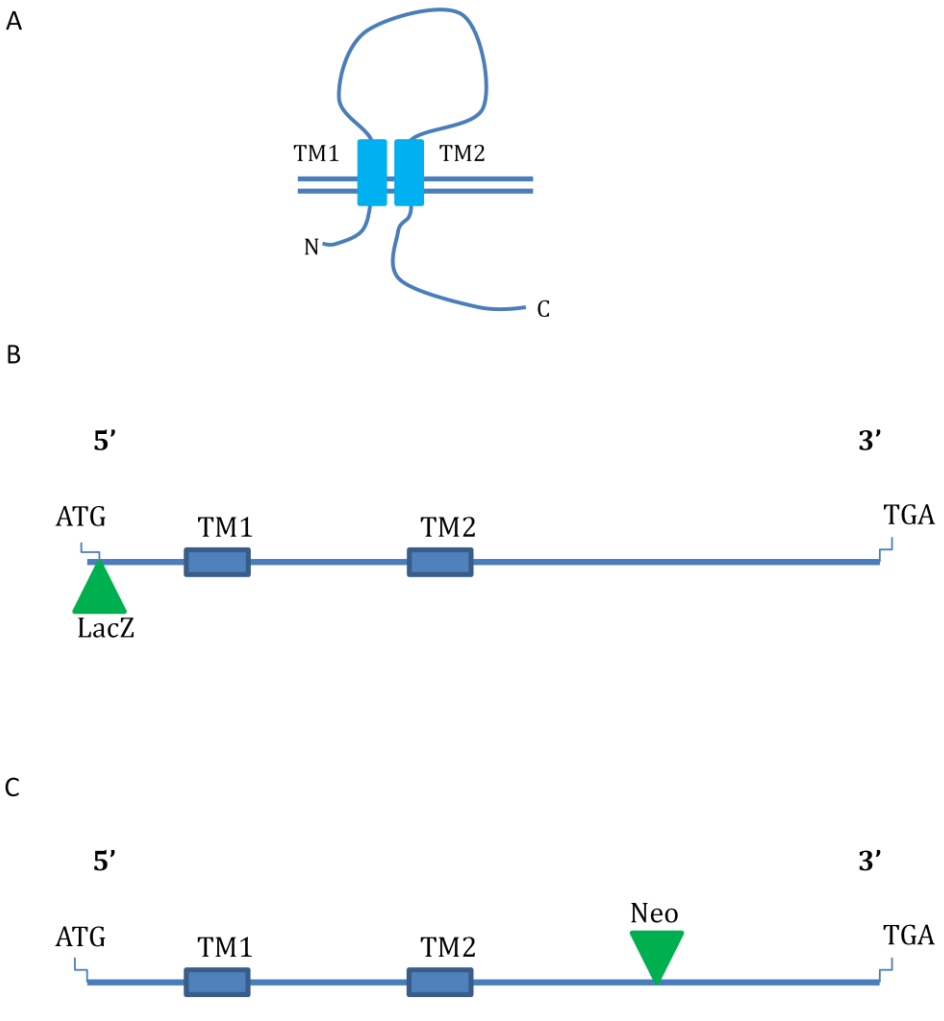

Figure 2.1 Generation of P2X7 receptor KO mice. A: Schematic diagram of P2X7 protein within the cell surface membrane demonstrating the relative positions of N-terminal (N), transmembrane (TM) and C-terminal (C) domains. B: Generation of the GSK P2X7 KO mouse. A *lacZ* gene (green triangle) was inserted after the initial ATG in exon 1. C: Generation of the Pfizer KO mouse. A neomycin (Neo) cassette (green triangle) was inserted in a 3' to 5' direction leading to deletion of nucleotides 1527 to 1607, corresponding to the intracellular C-terminal tail. Adapted from Sim et al ., 2004.

embryonic stem cells were subsequently mated with C57BL/6 mice. Northern blot analysis in bone marrow-derived mast cells confirmed absence of the transcript for P2X7 in KO animals, while Western blot of membrane preparations from KO macrophages suggested no intact or truncated forms of the receptor were expressed. Loss of channel function and biological activity were confirmed in macrophages by dye-uptake and cytokine release assays (Solle et al., 2001).

2.4 Genotyping of genetically-modified mice

All genetically-modified mice underwent confirmatory genotyping prior to use in experiments. This was achieved by extracting DNA from mouse tissue and performing PCR using oligonucleotide primers designed to discriminate between the native and disrupted forms of the *P2RX7* gene.

2.4.1 Extraction of DNA

Tissue for DNA extraction was collected by ear punching and DNA was extracted using the QIAamp DNA Mini and Blood Mini Kit (Qiagen, Crawley, UK). Tissue was lysed by incubating at 56^{o}C in a mixture of proprietary lysis buffer (buffer ATL) and proteinase K (600mAU/ml). Samples were vortexed intermittently and tissue lysis, as judged by disintegration of all visible tissue, was typically complete within 1-3 hours. Samples were then incubated in a further lysis buffer (buffer AL) for 10 minutes at 70^{o}C to enhance protein degradation before adding 100% ethanol to precipitate DNA. Samples (and any DNA pellet precipitated by addition of ethanol) were then transferred to the QIAamp Mini spin column before centrifugation wash steps with buffers AW1 and AW2. DNA was then eluted from the membrane of the spin column

in 200µl buffer AE by centrifuging at 6000 x *g* for 1 minute at room temperature.

2.4.2 PCR

PCR was used to amplify fragments of the *P2RX7* gene using primers designed to discriminate between WT and KO mice (Table 2.1). PCR was performed using the GoTaq HotStart Polymerase kit (Promega, Madison, USA). This system employs a high performance DNA polymerase bound to a proprietary antibody which blocks polymerase activity at temperatures <70^{o}C; this activity is restored on heating samples to 94^{o}C for the initial denaturation step. This system hence facilitates preparation of reactions at room temperatures and minimizes formation of non-specific products.

Each PCR reaction was assembled as follows:

5 x PCR buffer	5 µl
10mM dNTP mixture	0.1µl
25mM $MgCl_2$	1.5µl
10µM Primers (5' and 3')	1.25µl
Taq DNA polymerase	0.25µl
Distilled H_2O	9.4µl
Ear punch DNA	5µl
TOTAL	**25µl (per reaction)**

GSK KO	
WT Foward (5' to 3')	TGCCCATCTTCTGAACACC
WT Reverse (3' to 5')	CTTCCTCTTACTGTTTCCTCCC
KO Forward	TGCCCATCTTCTGAACACC
KO Reverse	GCAAGGCGATTAAGTTGGG
Pfizer KO	
WT Foward	TGGACTTCTCCGACCTGTCT
WT Reverse	TGGCATAGCACCTGTAAGCA
KO Forward	CTTGGGTGGAGAGGCTATTC
KO Reverse	AGGTGAGATGACAGGAGATC

Table 2.1 PCR primers used in genotyping of P2X7 KO mice.

The subsequent PCR thermal cycling program was:

1. 94°C for 5 mins	Activation of Taq DNA polymerase
2. 94°C for 1 min	Denaturation of DNA
3. 63°C for 1 min	Annealing of primers
4. 72°C for 1 min	Extension of PCR products
Cycling: repeat steps 2 to 4, 34 times	
5. 72°C for 10 mins	Final extension step
6. 4°C indefinitely	Holding step until sample collection

PCR products were stored at 4°C prior to gel electrophoresis.

2.4.3 Agarose Gel Electrophoresis

PCR products were analysed by electrophoresis on a 2% agarose gel. This technique allows separation of amplified DNA based on fragment size. The 2% gel was prepared by placing ultrapure agarose in TAE buffer (40mM Tris base, 20mM acetic acid, ImM EDTA, pH 8), microwaving for 2 minutes to solubilise and stirring for 5 minutes. Ethidium bromide (33µl/l) was added during cooling. Once cool, the gel was poured into a casting tray, a sample comb inserted and left to set for 60 minutes.

Once set, the gel was removed from the casting tray, combs were removed and the gel was transferred to an electrophoresis tank and covered with TAE buffer. PCR reaction products (15µl) were loaded into wells with a 100 base-pair resolution DNA ladder (New England Biolabs, Ipswich, USA) used as a

reference marker. Electrophoresis was performed at 150V for ~40 minutes. Ethidium bromide intercalates between DNA base pairs and fluoresces when exposed to ultraviolet light allowing visualisation of DNA bands of different sizes when the gel is viewed under these conditions.

Predicted band sizes for amplified DNA from wild-type and KO mice were:

GSK wild-type	568 bp
GSK KO heterozygote	568 bp and 393 bp
GSK KO homozygote	393 bp
Pfizer wild-type	280 bp
Pfizer KO heterozygote	280 bp and 363 bp
Pfizer KO homozygote	363 bp

Sample data is presented in Figure 2.2.

2.5 Induction of Type 1 diabetes in mice

Mice aged 8 months or older, either WT or KO, were randomly divided into two groups: Group A, treated with streptozotocin (STZ, 2-deoxy-2(3-(methyl-3-nitrosoureido)-d-glucopyranose) dissolved in 100mM sodium citrate buffer at pH 4.5; or Group B, treated with citrate buffer alone (all groups n=8; Figure 2.3). STZ was dissolved in citrate buffer at the point of use, and 50mg/kg was injected intraperitoneally (IP) on 5 consecutive days after a 4-6 hour fast (repetitive low-dose protocol; http://www.diacomp.org).

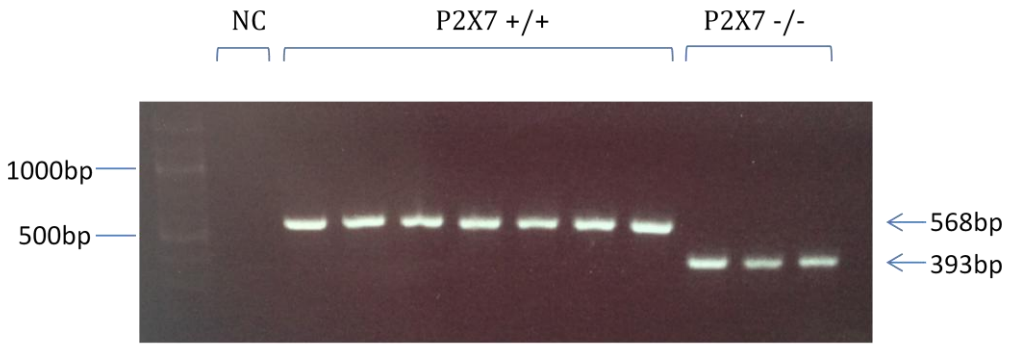

Figure 2.2 Example gel electropherogram for genotyping GSK P2X7 KO mice. PCR of ear punch DNA using primers specific for the P2X7 WT allele produced a single band of 568bp in homozygous animals. A single band of 393bp was seen in homozygous GSK P2X7 KO mice. NC: Negative control.

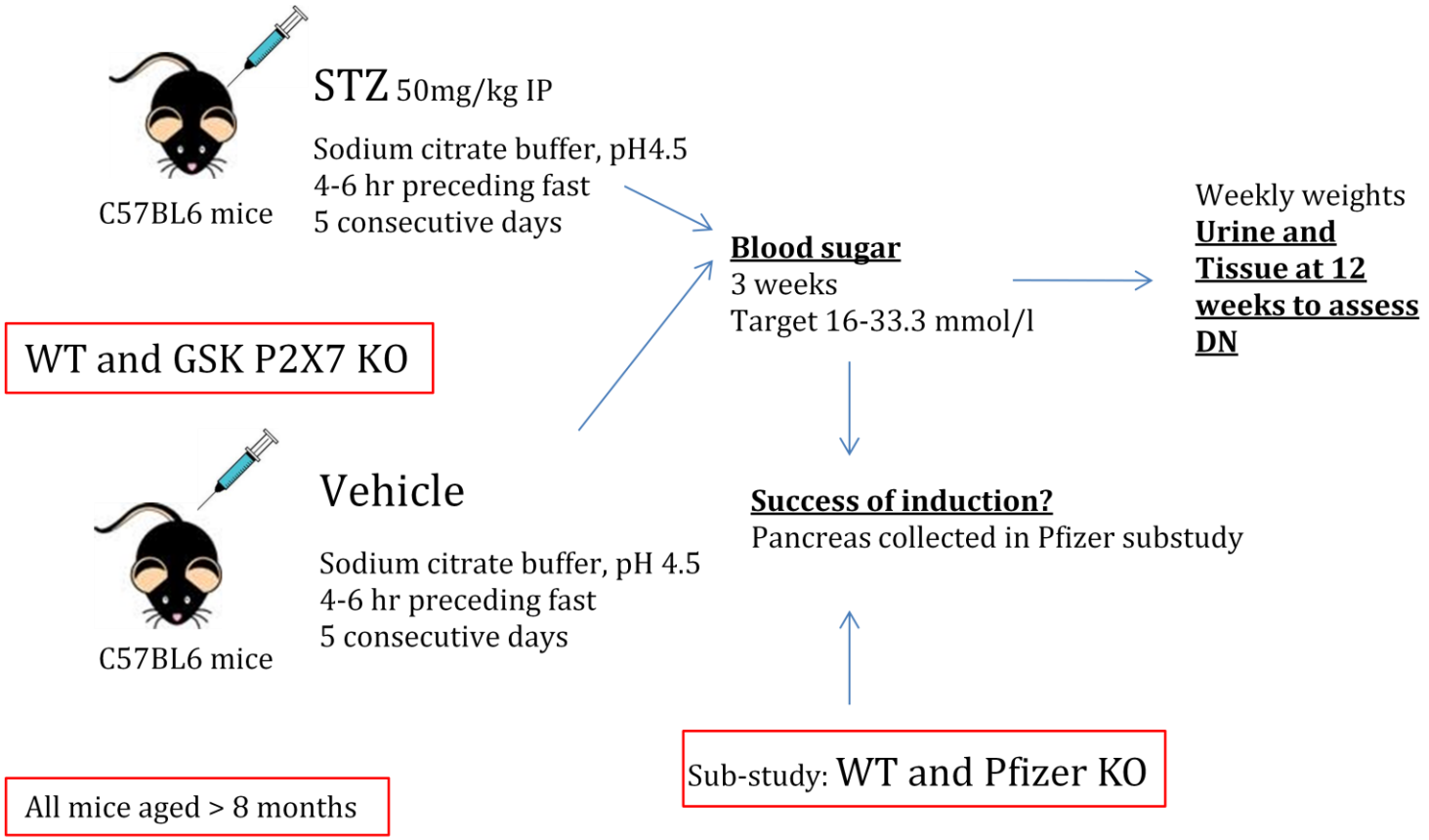

Figure 2.3 Schematic of experimental design for STZ-induced diabetes in the mouse

STZ is an antibiotic derived from *Streptomycetes achromogenes* used to induce a phenotype of type 1 diabetes in experimental animals (Szkudelski, 2001). Taken up into pancreatic beta cells via the GLUT-2 receptor, it causes alkylation of DNA and activation of poly-ADP ribosylation, processes which ultimately lead to irreversible cellular damage and necrosis. When administered as multiple low dose injections in the mouse this effect is augmented by a subsequent autoimmune 'insulinitis' with consequent destruction of pancreatic beta cells (Tesch and Allen, 2007).

Random blood glucose (BG) was measured at 3 weeks after the last injection. Mice were immobilised in a restrainer, a tail vein 'prick' performed with a 23 gauge needle and a OneTouch glucometer (Lifescan, Milpitas, USA) used for glucose measurement. A BG of greater than 16mmol/l was regarded as diabetic. WT and GSK KO mice with a BG of 16-33.3 mmol/l were subsequently maintained for a total of 12 weeks. BG was measured at 3 weekly intervals during the study, and animals with readings falling outside of the desired range were excluded. Urine was collected at baseline and week 12 and terminal collection of blood and kidney tissues was made at week 12.

A sub-study was conducted with WT and Pfizer KO mice to examine the susceptibility of this mutant strain to induction of diabetes with STZ. Animals were randomly divided into the following groups: WT, repetitive low dose STZ (n=8), WT, citrate buffer vehicle (n=4), Pfizer KO, repetitive low dose STZ (n=7) and Pfizer KO, citrate buffer vehicle (n=4). BG was measured at 3 weeks and pancreas tissue taken for immunohistochemistry at this time point.

2.6. Uninephrectomy, induction and maintenance of type 1 diabetes and administration of a selective P2X7 antagonist in rats

An initial pilot experiment (Experiment 1) was performed using Sprague Dawley rats (Charles River, Margate, UK). In this experiment, rats weighing 200-250g were randomly assigned either to group A, single intravenous (IV) injection with STZ (50mg/kg) in citrate buffer or B, citrate buffer alone (n=5/group), and followed for 21 weeks with periodic urine collections and terminal collection of blood and kidney tissue.

Subsequent experiments were performed using Wistar Han IGS rats (Charles River). An initial pilot experiment (Experiment 2) was performed to establish an effective dose of STZ for induction of diabetes. A further experiment (Experiment 3) was performed to establish the duration of diabetes required to provoke albuminuria (as the earliest sign of diabetic nephropathy) in animals which had undergone a uninephrectomy. In this experiment, rats weighing 200-250g underwent right uninephrectomy (UNx) followed by either A, single IV injection of STZ (40mg/kg) (n=6) or B, citrate buffer alone (n=4), one week later. Animals were followed for 16 weeks with urine collections made at baseline, weeks 4, 8, 12 and 16 and collection of blood and kidney tissue at week 16. In this experiment, the time of onset of robust albuminuria was established to be 8 weeks.

The main rat experiment (Experiment 4) was designed to test the effect of a highly selective P2X7 receptor antagonist (AZ11657312; AstraZeneca, Alderley Park, UK) on the evolution of DN in uninephrectomised diabetic animals. Right UNx was performed in rats weighing 200-250g and a single injection of IV STZ (40mg/kg) or vehicle was administered one week later. Antagonist or drug vehicle (see below) was administered IP twice-daily for 28 days starting from week 8. Animals were divided into 5 groups (n=8-9 per group) (Figure 2.4):

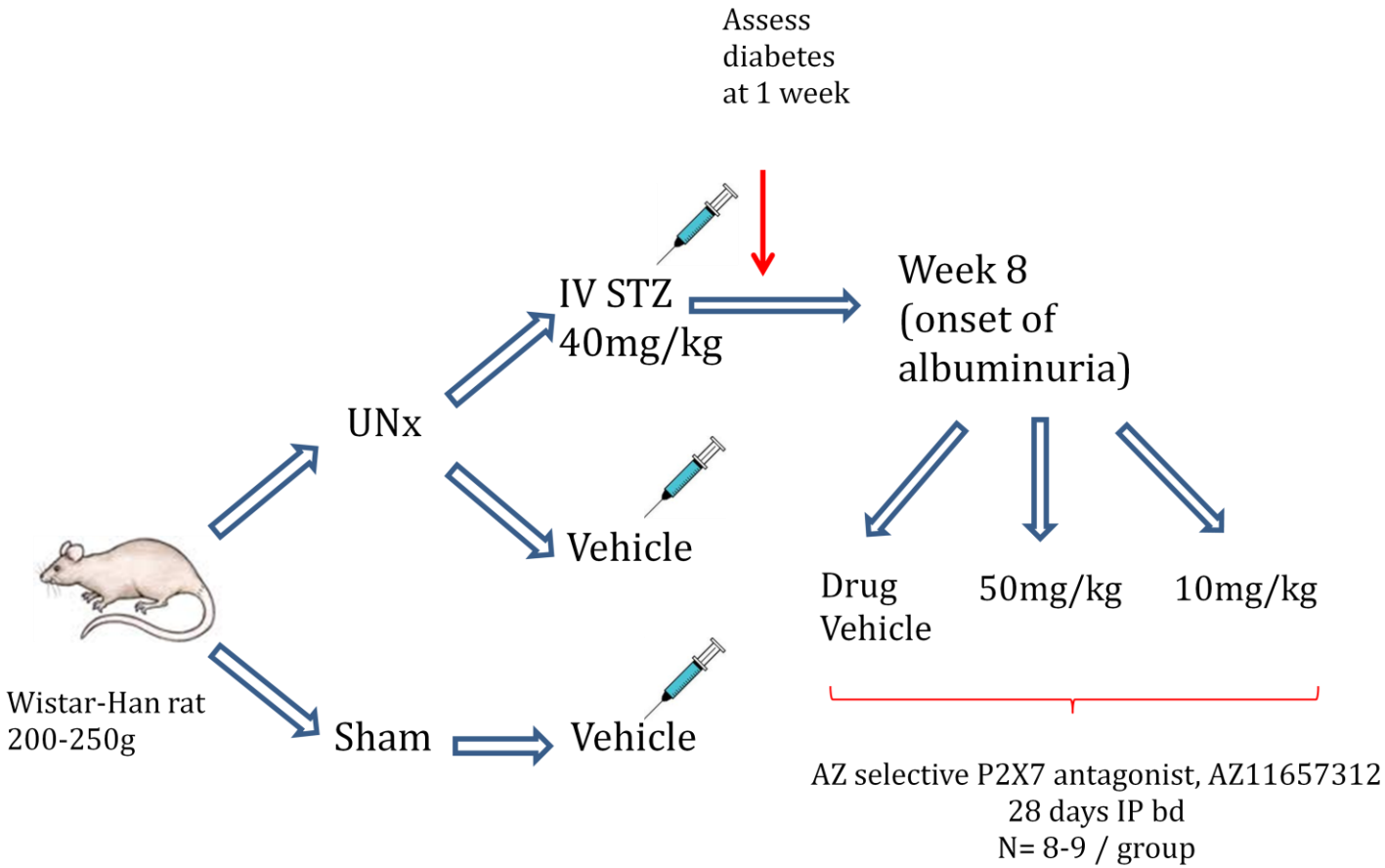

Figure 2.4 Schematic of experimental design for STZ-induced diabetes in the uninephrectomised rat

A: Sham UNx + IV citrate buffer

B: UNx + IV citrate buffer

C: UNx + IV STZ 40mg/kg + IP drug vehicle

D: UNx + IV STZ 40 mg/kg + IP AZ11657312 10mg/kg

E: UNx + IV STZ 40mg/kg + IP AZ11657312 50mg/kg

The doses of AZ11657312 chosen for study were based on previous published experience with the antagonist in the streptococcal cell wall model of inflammatory arthritis (Cruwys et al., 2007) and unpublished pharmacokinetic data supplied by AstraZeneca. Urine collections were made at baseline, week 4, 8 and 12. Terminal blood and kidney tissues were collected at week 12.

2.6.1 Right Uninephrectomy

Procedures were performed in a clean, purpose-built operating theatre in the animal facility. The right flank was shaved prior to anaesthetization with isofluorane. Once anaesthetised, a 1.5-2cm incision was made in the right flank and the subcutaneous tissue and the muscle layer divided using dissecting scissors. The right kidney was identified (lying deep to the liver in the retroperitoneal compartment) and manipulated through the flank incision. The capsule was divided and a cross-clamp placed over the vascular pedicle and ureter. A silk tie was used to ligate the vessels and ureter proximal to the clamp and the kidney removed. The clamp was subsequently removed and silk tie cut to a short length. The muscle layer was sutured closed using an absorbable stitch in a continuous pattern. 3-4 clips were applied to the skin (removed one week later). Animals undergoing sham nephrectomy were shaved and anaesthetized but underwent a flank incision only with the fully-functional kidney left *in situ*.

Animals received a single subcutaneous (sc) dose of buprenorphine analgesia (0.02mg/kg) at the end of the operation. Enrofloxacin (Baytril; Bayer, Leverkusen, Germany) was added to drinking water for 48 hours post-operatively as antibiotic prophylaxis against wound infection.

2.6.2 Induction and maintenance of type 1 diabetes

STZ was dissolved in 100mmol/l citrate buffer (pH 4.5) at the point of use. Animals were placed under light anaesthesia with isofluorane and STZ or vehicle injected intravenously (IV) via the dorsal penile vein. Water in drinking bottles was replaced with 10% sucrose for 48 hours after injection to combat the risk of early hypoglycaemia due to insulin release from injured beta cells.

Venous BG was checked at one week post-injection using a OneTouch glucometer (Lifescan). Light anaesthesia was induced with isofluorane and a tail vein 'prick' performed with a 23 gauge needle. Animals with a blood glucose of >33.3 mmol/l were administered slow-release sc insulin pellets (Linshin, Toronto, Canada) to prevent ketoacidosis and maintain weight. To do this, the animal's scruff was shaved and a 16 gauge needle used to make a small sc incision. A metal trocar was inserted through the incision into the sc space and 1/8 of a pellet pushed through the trocar with a stylet. The skin was pinched over the incision site for 1 minute after removal of the trocar to ensure contraction of the skin defect.

1/8 insulin pellet provides approximately 0.25 units insulin/day. BG was retested one week after insertion and a further 1/8 pellet inserted if persistently >33.3 mmol/l. This cycle was continued until BG had been

titrated to <33.3 mmol/l. Diabetic animals with BG in the desired range had repeat tests at two weekly intervals. Control animals were tested every 4 weeks.

2.6.3 Administration of highly selective P2X7 antagonist

AZ11657312 was dissolved in a vehicle of 5% DMSO/95% 2-hydroxypropyl-beta-cyclodextrin (HPBCD) solution. HPBCD was reconstituted as a 20% solution in distilled water. A 30mg/ml solution of drug was used for administration of high dose (50mg/kg) treatment with an approximate dose volume of 0.4 – 0.5 mls. A 6mg/ml solution was used to administer the low dose (10mg/kg) treatment ensuring dose volumes equivalent to the high dose injections. Injection volumes for vehicle-treated animals were calculated to ensure weight-based equivalence to both treatment groups.

Antagonist or vehicle injections were administered IP twice daily under light anesthesia using a 1ml syringe and 25 gauge needle.

2.6.4 GK rats

Kidney tissue from GK rats and age-matched Wistar controls was provided by Dr Edward Debnam (UCL, London). GK rat kidney tissue used for P2X7 immunohistochemistry was fixed overnight in neutral-buffered formalin, while tissue for gene expression analysis was stored in RNAlater prior to mRNA extraction.

2.7 Collection of biological specimens from mice and rats

2.7.1 Urine collection

Mice and rats were housed in individual metabolism cages for collection of urine samples. Mice were left in cages overnight while rats were kept in cages during daytime only. Due to significant polyuria in diabetic rats, urine collection containers were emptied midway through the collection period to prevent overflowing and ensure accurate measurement of urine volume.

At the end of the collection, total urine volume was measured and an aliquot centrifuged at 240 x *g* for 5 minutes to sediment macroscopic debris. Urine glucose was measured semi-quantitatively using reagent strips (IND Diagnostics, Delta, Canada) before aliquoting samples for storage at -80^{o}C.

2.7.2 Collection of terminal blood and tissue specimens

At the end of the study, animals were placed under isofluorane anaesthesia for collection of blood and tissues. Blood was obtained by cardiac puncture using a 1 ml syringe and 25 gauge needle. Tissues were dissected out after the animal had been culled by exsanguination.

For mice, the right kidney was divided longitudinally and one half kidney placed in neutral-buffered formalin together with specimens of liver, lung and spleen. Specimens were left in formalin fixative overnight before transfer to 70% ethanol, prior to paraffin embedding and sectioning. Remaining kidney tissue was divided and used as follows i) placed in RNAlater ii) snap-frozen in a cryovial in liquid nitrogen iii) placed in OCT embedding matrix

(Thermo Fisher Scientific, Loughborough, UK) on a cork disc and frozen by immersion in isopentane cooled in liquid nitrogen iv) placed in periodate-lysine-paraformaldehyde (PLP) fixative (see below). In the Pfizer KO substudy, a specimen of pancreas was obtained and fixed in neutral-buffered formalin.

For rats, the left (remaining) kidney was dissected out. A coronal mid-pole section was placed in neutral-buffered formalin together with a specimen of spleen. A neighbouring coronal section was placed in RNAlater. The upper pole was divided longitudinally with one half placed in PLP fixative. The lower pole was divided into 4 quarters, one of which was placed in OCT embedding matrix on a cork disc and snap frozen, and the other three quarters snap frozen in a cryovial.

Paraffin-embedded kidney tissue was cut at 4 μm thickness on a rotary microtome and stained with haematoxylin and eosin (H+E), periodic acid Schiff (PAS) or picrosirius red (sectioning and staining performed by Mrs L Lawrence, Department of Leukocyte Biology, Imperial College London).

2.7.2.i Preparation of PLP fixative

PLP fixative contains paraformaldehyde 1%, lysine 0.075M, sodium periodate 0.01M and phosphate buffer 0.037M. This fixative provides enhanced morphological preservation in comparison to frozen tissue, but facilitates use of some antibodies, in particular monoclonal preparations, which will not recognize their target epitope in formalin-fixed paraffin-embedded tissue.

A lysine stock solution of 0.2M lysine monohydrochloride and 0.1M disodium hydrogen orthophosphate was prepared and pH adjusted to 7.4 with concentrated HCl. 4% paraformaldehyde in distilled water was prepared by prolonged stirring at 60°C, with the addition of a few drops of 1M NaOH to clear the solution. On the morning of use, lysine and paraformaldehyde stock solutions were mixed in a ratio of 3 vols : 1 vol and sodium metaperiodate 0.214g/100mls was added. The solution was aliquoted and placed on ice, ready for tissue specimens to be placed in during retrieval.

Tissues were fixed in PLP for 4 hours at 4°C and then transferred to 7% sucrose in PBS overnight to dehydrate. The following morning, the tissue was removed from sucrose and placed in OCT embedding matrix on a cork disc and frozen by immersion in isopentane cooled in liquid nitrogen before storage at -80°C.

2.8 Serum and urine biochemical analysis

2.8.1 Measurement of urinary albumin excretion

Concentration of urinary albumin was measured in both rats and mice using a specific indirect 'sandwich' ELISA (Bethyl Laboratories, Montgomery, TX). (See Section 2.14 for detailed description of sandwich ELISAs and Table 2.5 for materials used in this protocol). All steps were performed at room temperature.

Urine specimens were thawed and allowed to equilibrate at room temperature. Samples were then mixed, centrifuged at 10,600 x *g* for 5 minutes and supernatant decanted to clean tubes. Typical dilutions required for measurement were 1:1000 for control samples and 1:100-1:1000 for STZ-

treated animals, depending on the timepoint of disease. Rat or mouse reference serum was serially diluted in sample diluent to produce a reference series ranging from 1.95 - 125 ng/ml in the rat and 7.8 - 500 ng/ml in the mouse, allowing a standard curve to be plotted (Figure 2.5A).

Mouse urinary albumin concentration values (transformed from ODs using the standard curve and expressed in mg/l) were divided by paired urinary creatinine (see below; expressed in mmol/l) yielding the urine albumin:creatinine ratio (uACR; mg/mmol creatinine). This manoeuvre corrects albumin levels for urine concentration allowing inter-animal comparison. Calculation of timed albumin excretion rates was not possible with mice due to inaccuracies in ascertainment of urine collection volume due to urine frequently bypassing the collection container.

Rat urinary albumin concentration values were normalized to the collection volume to provide an albumin excretion rate (expressed as μg/hr).

2.8.2 Measurement of urinary creatinine

Urinary creatinine was measured in both rats and mice using the Jaffe reaction. This works on the principle that addition of an alkaline picrate solution to creatinine yields a bright orange-red complex. Intensity of the colour as measured by spectrophotometry at 490nm corresponds to the concentration of creatinine in the sample.

Samples were diluted with distilled water prior to measurement. Control samples were diluted by a factor of 1:20 and samples from diabetic animals by 1:5. A solution of creatinine was serially diluted with distilled water to produce a reference series with concentration ranging from 0.03125 - 2

A

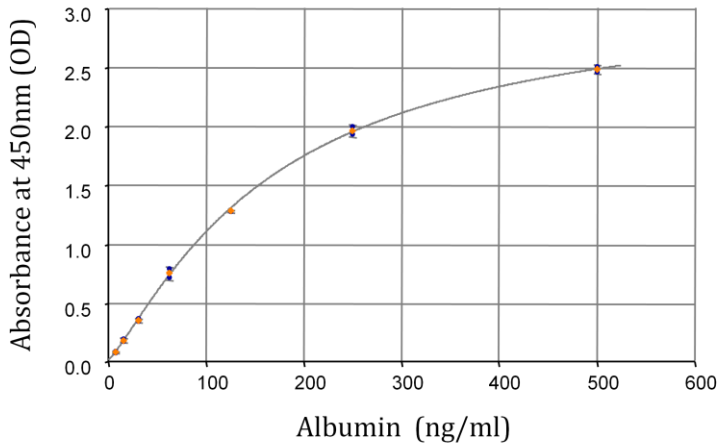

B

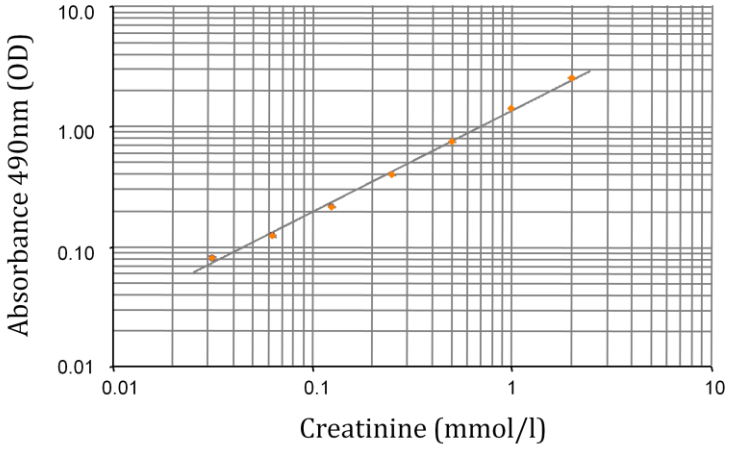

Figure 2.5. Sample standard curves used for quantification of mouse urinary albumin by ELISA (A) and urinary creatinine measurement (B). The standard curve used for urinary albumin measurement was created using a 4-variable non-parametric fit, while a logarithmic transformation of both axes was applied for plotting urinary creatinine. In both cases, the standard curve was used to transform OD measurements of samples to analyte concentration. Final concentration values were achieved by multiplying by the sample dilution factor.

mmol/l. Standard or sample (50µl) were added to each well of a 96 well plate. Each sample was measured in duplicate.

An alkaline picrate solution was prepared by adding 2.5ml of 1N sodium hydroxide to 12.5mls of picric acid, and 100µl of this solution added to each well. The plate was then incubated for 30 minutes at room temperature. The optical density (OD) of each well was determined using a plate reader (ELx800; BioTek, Potton, UK) at a wavelength of 490nm and ODs averaged for the two replicates. ODs were corrected for background absorbance by subtraction of the measured OD for a 'blank' sample (distilled water alone). A standard curve was created by plotting the log of the concentration of the standards against the log of the ODs (Figure 2.5B). Using this standard curve, ODs for sample wells could be transformed to creatinine concentration values. Results were then multiplied by sample dilution to achieve a final value.

2.8.3 Measurement of serum creatinine

Whole blood samples from animals were centrifuged at 240 x *g* for 5 minutes. The serum (supernatant after centrifugation) was collected and used for analysis. Creatinine was measured by the modified Jaffe reaction in an Olympus AU600 analyser (Olympus, Watford, UK) by the clinical biochemistry laboratory at the Hammersmith Hospital (London, UK)

2.9 Morphometric analysis of rodent kidney tissue

2.9.1 Measurement of glomerular size

Glomerular size was measured on PAS-stained sections. Working systematically from one corner of the tissue section, the first 30 glomeruli encountered were digitized using a scientific grade digital colour camera (Olympus, Tokyo, Japan) at x400 magnification. Subsequent image analysis was conducted using ImagePro software (Media Cybernetics, Bethesda, USA).

Measurements were calibrated by photographing and measuring an etched graticule of known diameter. The 'polygon' tool was then used to carefully outline and isolate each glomerular tuft and the surface area calculated. The mean value of 30 glomerular areas for each animal was calculated.

2.10 Quantification of tissue fibrosis

Tissue fibrosis in rodent kidney tissue was assessed on picrosirius red-stained sections, viewed under polarized light. Picrosirius red staining is highly specific for detection of fibrillar collagen when viewed under polarized light; type 1 collagen fibrils display a yellow-orange birefringence while type 3 collagen fibrils show green birefringence.(Junqueira et al., 1979)

For each section, 5 randomly selected cortical fields viewed under polarized light were photographed and digitized at x200 magnification. Blood vessels larger than neighboring tubules were systematically excluded from selected fields to prevent skewing of results due to collagen component of vessel walls. Using ImagePro, images were converted to grayscale, rendering

birefringent collagen fibrils light grey or white. The 'measurement' tool was used to highlight all picro-sirius red stained areas, pixel by pixel. The highlighted area could then be measured and expressed as a fraction of the area of the section:

$$\frac{\text{Area of picrosirius red staining}}{\text{Total area of section}}$$

The mean value for 5 cortical fields of view was calculated for each animal.

2.11 Immunohistochemistry in rodent and human tissue

2.11.1 General principles

Immunohistochemistry (IHC) is the process by which discrete protein epitopes in a tissue specimen are labelled using a specific antibody, and visualized using a secondary detection system with consequent colour reaction. IHC provides information on the location of protein expression in a tissue (eg glomerular vs tubular in kidney tissue) as well as the degree of expression.

IHC can be performed on tissue fixed in a variety of ways; different fixation methods may modify protein structure and alter antibody binding, meaning the optimal fixation protocol must be established for each antibody used. Formalin-fixed, paraffin-embedded tissue is frequently used for IHC as tissue architecture is preserved well with this fixation method. Formaldehyde preserves tissues by cross-linking amino groups in proteins with other

nearby nitrogen atoms in protein or DNA producing methylene bridges and other types of bridging links (Fox et al., 1985). These cross-links must usually be broken either by thermal or enzymatic means ('epitope retrieval') before primary antibody may be applied (Shi et al., 1991).

'Frozen sections' are not treated with fixative at the time of collection, preserving native protein structure and circumventing the need for epitope retrieval. Freshly harvested tissue is immersed in liquid-nitrogen cooled isopentane and then 'snap-frozen' in liquid nitrogen before storage at -80^{o}C. Once thawed and sectioned, the tissue is fixed for 5 - 10 minutes in a 'precipitating' (or 'denaturing') fixative (such as cooled 50:50 acetone:methanol) and left to air dry prior to staining. Precipitating fixatives act to dehydrate and reduce the solubility of protein molecules, as opposed to cross-linking proteins, and hence native epitopes are retained. Precipitating fixatives do not, however, preserve three-dimensional tissue structure and limit appreciation of native architecture.

Other fixative techniques have been developed in an effort to combine the benefits of formalin fixation (preservation of architecture) and frozen sectioning (preservation of epitope conformation). One example is periodate-lysine-paraformaldehyde (PLP) fixation (see section 2.6.2.a for method). Tissue is immersed in PLP fixative at the time of collection and snap-frozen and sections cut with a cryostat before air-drying. This technique extends the spectrum of antibody-epitope binding over formalin fixation (including some monoclonal antibodies) and tissue architecture preservation is superior to standard frozen sections.

2.11.2 Tissue sectioning and mounting

Paraffin wax embedding and sectioning of formalin-fixed animal tissues was performed by Mrs Lorraine Lawrence (Department of Leukocyte Biology, Imperial College London). Sections were cut on a rotary microtome to a thickness of 4μm.

Frozen and PLP-fixed animal tissue were sectioned using a cryostat. Sections (5μm thickness) were cut and collected onto poly-L-lysine coated slides. All sections were allowed to air-dry overnight before use. The following morning. frozen sections were immersed in 4^{o}C 50:50 acetone:methanol fixative for 10 minutes. PLP sections did not require this step.

Human renal biopsy specimens were paraffin sections retrieved from the histology archive at Hammersmith Hospital (approval was granted by the local research ethics committee).

2.11.3 Pretreatment of paraffin sections

Paraffin-embedded sections require removal of wax prior to performing IHC. Sections were placed in two sequential baths of xylene, before passage through graded ethanol concentrations and finally water. The latter steps serve to remove xylene and rehydrate the tissue.

Dewaxed sections subsequently underwent heat-induced epitope retrieval (HIER). Sections were placed in boiling 0.01M sodium citrate buffer (pH 6.0) and transferred to a 95^{o}C water bath for 20 minutes. Sections were then cooled under running water for 5 minutes before placing in PBS.

2.11.4 Blocking endogenous peroxidase activity and non-specific binding sites

All sections underwent steps to reduce false positive colour reactions either due to endogenous peroxidase activity or non-specific (epitope-independent) binding of antibody. A wax pen (Dako, Glostrup, Denmark) was used to encircle tissue sections on the slide to minimize 'run-off' when solutions were applied. The sections were covered with 0.3% hydrogen peroxide for 10 minutes before tapping off and washing three times in PBS. Depending on the primary antibody being employed a solution of either 10% dry powdered milk (Marvel; Premier Foods, St Albans, UK) or 20% normal goat serum (Dako) was applied for 30 minutes (See Table 2.2).

2.11.5 Primary antibody and controls

Primary antibodies were reconstituted and diluted as per the manufacturer's instructions. Blocking solution was tapped off the slide and a tissue used to carefully blot residual solution. Antibody at the appropriate dilution was then applied in sufficient volume to cover the section (typically 100-200µl) (Table 2.2). Slides were placed in a covered, humidified staining chamber to minimize evaporation and left to incubate for the appropriate duration.

For exploratory P2X7 IHC, negative controls comprised omission of primary antibody, addition of polyclonal normal rabbit immunoglobulin at an equivalent concentration to the primary antibody, and use of primary antibody pre-incubated with the cognate immunizing peptide at a 1:1 ratio. Omission of primary antibody was used for established IHC protocols (eg. CD68, insulin).

Target Protein (Species)	Blocking Solution	Primary antibody	Primary dilution (incubation)	Secondary antibody
P2X7 (H, M, R)	10% whole milk in PBS	APR-004 (Alomone, Jerusalem, Israel) Rabbit polyclonal	1:50 – 1:100 (1hr M,R; O/N H)	Dako Enivision HRP-linked Polymer Anti-rabbit
CD68 (H)	10% whole milk in PBS	Clone KP-1 (Dako) Mouse monoclonal	1:100 (1hr)	Dako Envision HRP-linked Polymer Anti-mouse
CD68 (R)	10% whole milk in PBS	Clone ED-1 (Serotec, Oxford, UK) Mouse monoclonal	1:200 (1hr)	Dako Envision HRP-linked Polymer Anti-mouse
CD68† (M)	20% goat serum in PBS	Clone FA-11 (Serotec) Rat monoclonal	1:200 (1hr)	Polink-1 HRP-linked Polymer (GBI, Mukilteo, USA) Anti-rat
Mac-2* (M)	Serum-free protein block (Dako)	Clone m3/38 (Cedarlane, Burlington, Canada)	1:100 (3hrs)	HRP-linked anti-rat antibody
Insulin (M)	10% whole milk in PBS	Ab63820 (Abcam, Cambridge, UK) Rabbit Polyclonal	1:400 (1hr)	Dako Enivision HRP-linked Polymer Anti-rabbit

Continued overleaf

Table 2.2 Antibodies used for immunohistochemistry. All IHC was performed on formalin-fixed paraffin-embedded sections, subjected to pretreatment with heat-induced epitope retrieval, unless otherwise specified. *Staining performed by C &C Lab Services Ltd. †Staining performed on PLP-fixed frozen sections. H: human; R: rat; M: mouse; O/N: overnight.

Continued from previous page

Target Protein (Species)	Blocking Solution	Primary antibody	Primary dilution (incubation)	Secondary antibody
Type 4 Collagen (M, R)	10% whole milk in PBS	Ab6586 (Abcam) Rabbit polyclonal	1:100 (O/N)	Dako Enivision HRP-linked Polymer Anti-rabbit
Glut-2 (M)	10% whole milk in PBS	Sc-9117 (Santa Cruz, Dallas, TX) Rabbit polyclonal	1:50 (O/N)	Dako Enivision HRP-linked Polymer Anti-rabbit
Ki-67 (M)	10% whole milk in PBS	Ab15580 (Abcam) Rabbit polyclonal	1:100 (1hr)	Dako Enivision HRP-linked Polymer Anti-rabbit
CD3 (M)	10% whole milk in PBS	Ab5690 (Abcam) Rabbit polyclonal	1:100 (O/N)	Dako Enivision HRP-linked Polymer Anti-rabbit

Table 2.2 Antibodies used for immunohistochemistry. All IHC was performed on formalin-fixed paraffin-embedded sections, subjected to pretreatment with heat-induced epitope retrieval, unless otherwise specified. *Staining performed by C &C Lab Services Ltd. †Staining performed on PLP-fixed frozen sections. H: human; R: rat; M: mouse; O/N: overnight.

2.11.6 Detection

A commercial secondary antibody detection system (EnVision, Dako) was used. The EnVision reagent consists of a peroxidase-conjugated polymer backbone which carries secondary antibody molecules raised in goat and directed against rabbit or mouse immunoglobulins. When applied to primary antibody-treated tissue, this complex will bind immunoglobulin adherent to the target epitope, permitting subsequent visualisation. The combination of several peroxidase molecules and several secondary antibody molecules on the same polymer increases detection sensitivity.

Primary antibody was tapped off and slides washed 3 times for 5 minutes in PBS. Sufficient EnVision reagent was then added to completely cover the tissue section and the slide placed in the humidified incubation chamber for 30 minutes. The reagent was then tapped off and a further 3 PBS washes performed. A 3,3'-diaminobenzidine (DAB) chromagen solution was prepared by mixing DAB+ chromagen with DAB+ substrate buffer in a ratio of 1:50. This was applied to tissue sections for 3-5 minutes depending on the primary antibody; oxidation of DAB by peroxidase / H_2O_2 yields a dark brown pigment signifying positive staining. The appropriate duration of DAB exposure was determined by comparison of staining intensity in positive and negative control sections. Reaction was terminated by placing slides in PBS.

Slides were then rinsed in water and counterstained by immersion for 30 seconds in 0.1% Harris haematoxylin (a nuclear stain). After rinsing, excess stain was removed by brief (<1 second) immersion in acid-alcohol solution (0.1% HCl in 70% EtOH). Sections were then dehydrated by sequential passage through ascending alcohol concentrations to xylene. Slides were then mounted with DPX (Distrene, Plasticiser, Xylene; VWR, Lutterworth, UK) and glass coverslips and allowed to dry before examination.

2.12 Quantification of immunostained tissue

2.12.1 Renal macrophages (CD68 staining)

Glomerular macrophage number was counted for 20 glomeruli in each section and the mean value obtained. The same starting point was used in each section and the first 20 randomly encountered glomeruli were included.

Interstitial macrophage number was counted for 5 randomly selected fields of view (x200 magnification) and the mean value obtained.

2.12.2 Islet macrophages (Mac-2 staining)

Macrophage infiltration in pancreatic islets was assessed using ImagePro. Islets were digitized at x400 magnification. Using ImagePro the image was scaled so that the entire islet could be seen on the screen. The 'polygon' tool was then used to carefully outline and isolate each islet allowing measurement of islet area. The isolated islet was then resized to 150-200% to allow precision when setting the colour threshold.

The 'measurement' tool was then used to carefully highlight all Mac-2-stained areas of the islet, pixel by pixel. This overlay was then saved as a 'template' to apply to subsequent islets. The highlighted, Mac-2-stained area was then measured and the fractional stained area calcuated. All islets present in the section (9.85 ± 4.44) were scored and the mean value taken.

2.12.3 Islet insulin

For each animal, islet insulin staining was assessed semi-quantitatively using the following scoring system:

1	=	<50% surface area stained
2	=	50-70%
3	=	70-90%
4	=	>90%

Very few islets had insulin staining reduced significantly below 50% hence the scoring system was adjusted to maximize sensitivity within the observed range. All islets within the section were scored and the mean value obtained.

2.12.4 Glomerular type 4 collagen

Type 4 collagen was assessed using ImagePro. Glomeruli were outlined and area measured and type 4 collagen calculated as percentage stained area per glomerular area (Figure 2.6). Fifteen glomeruli in each section were scored and the mean value taken (AMDCC protocols suggest averaging fifteen glomeruli when assessing mesangial expansion).

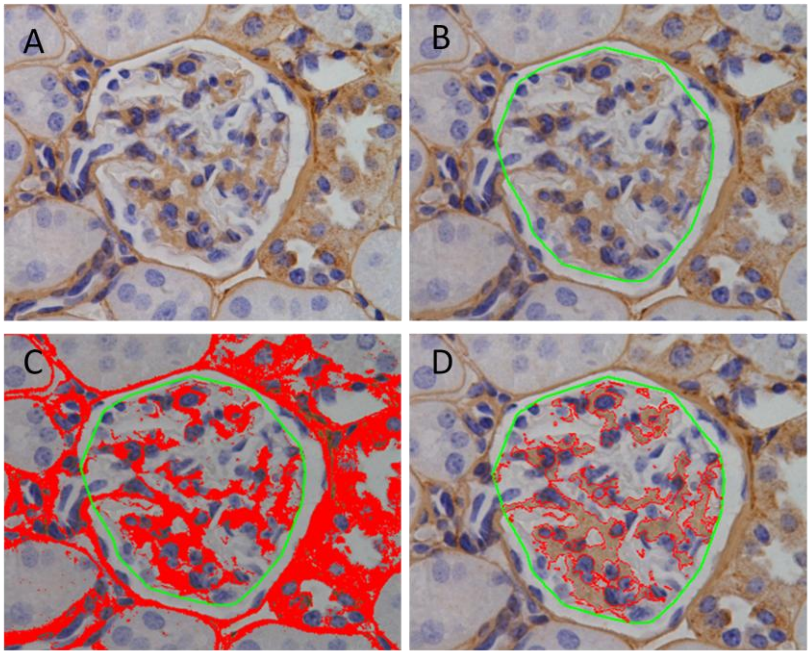

Figure 2.6 Measurement of glomerular area and quantification of immunohistochemical staining using ImagePro. A: Mouse glomerulus after performing specific immunohistochemistry for type IV collagen, labelled brown. B: Glomerular area was calculated by digitally outlining the glomerular tuft and measuring the enclosed area. The image analysis system was calibrated by photographing and measuring a graticule of known dimensions. C: Brown-stained areas of the glomerulus were selected pixel by pixel to highlight the area of interest within each glomerulus. D: The collagen-stained area within the glomerulus could then be measured and expressed as a fraction of the total glomerular area.

2.13 Quantitative PCR

2.13.1 General principles

The core principle of PCR is the specific detection and amplification of a chosen gene sequence. This is achieved through use of specific oligonucleotide primer pairs which can anneal to the region of interest when DNA is denatured, and DNA polymerase which synthesises new nucleotide chains based on these specificities. Repeating multiple cycles of DNA denaturing, primer annealing and new nucleotide synthesis permits exponential amplification of the region of interest. In classical 'end point' PCR techniques, the final product is typically visualized by electrophoresis on an agarose gel; as well as confirming presence or absence of the target gene, this allows confirmation of identity based on expected product length (compared to a standard nucleotide 'ladder') and assessment of specificity (absence of other, unanticipated, bands of different molecular weight).

End-point PCR is not suitable, however, for measurement of the relative abundance of a gene of interest in an experimental sample. Although the concentration of PCR product correlates well with the concentration of genetic starting material during the exponential phase of the PCR reaction, the final end-point product concentration does not. This is in part explained by the loss of efficiency which occurs towards the end of the PCR reaction due to reduced primer and free nucleotide concentrations, reduced primer annealing probability (as DNA strands are in excess by the latter stages, favouring strand reannealing) and reduced DNA polymerase activity.

Quantitative or 'real time' PCR (qPCR) has sought to overcome the limitations of the end-point method to allow accurate quantitation of gene expression in experimental samples. By using a fluorescent intercalating nucleic acid stain,

a PCR machine incorporating a sensitive fluorimeter can measure the increase in fluorescence intensity on a cycle-by-cycle basis. By selecting a threshold fluorescence intensity in the exponential amplification phase, the abundance of a gene of interest can be compared between experimental samples. Accurate comparison requires normalization of abundance to that of one or a number of 'housekeeping' genes, the expression of which is not regulated by the experimental conditions.

To attain good quality qPCR data requires careful attention to detail and quality control. RNA, once extracted, should be assayed both for purity (by spectrophotometry) and also integrity, as comparison of samples with different degrees of degradation will yield unreliable results. Conversion of RNA to cDNA should be efficient and ideally the PCR reaction should be performed on a rotary machine, to avoid the uneven heating and cooling in a plate based system. The highest accuracy is attained by measuring gene abundance relative to a standard series and normalizing expression to a panel of housekeeping genes which have been assayed for their stability under the prevailing experimental conditions (Vandesompele et al., 2002).

2.13.2 RNA extraction from whole kidney tissue

RNA was extracted from animal kidney tissue using the RNEasy Mini Kit (Qiagen). This kit employs columns containing selective RNA-binding silica membranes which enable RNA purification from tissue lysates. Rat or mouse kidney was stored at -20^{o}C in RNAlater RNA preservation solution after harvest. Samples were thawed and a 3mm^{3} piece of tissue dissected and placed into a microtube containing proprietary buffer RLT, a highly denaturing guanidine-thiocyanate-containing buffer supplemented with 2-mercaptoethanol. Microtubes were then placed in a TissueLyser bead mill

(Qiagen) and homogenized at 50Hz using 5mm steel beads for four 2-minute blocks.

Samples were then centrifuged at 10,600 x *g* for 3 minutes before removing the clear supernatant (lysate) and mixing with 1 volume of 70% ethanol to provide appropriate binding conditions for the RNA. This mixture was then transferred to an RNeasy spin column and centrifuged for 15 seconds at >8000 x g to enable RNA binding to the silica membrane. Successive centrifugation wash steps were then performed using proprietary buffers RW1 and RPE. A final centrifugation was performed (2 minutes at >8000 x g) to dry the membrane and ensure no carryover of ethanol during RNA elution. RNA was then eluted from the column by adding 50µl nuclease-free water directly to the membrane and centrifuging for 1 minute at >8000 x g. Samples were aliquoted for subsequent concentration and integrity testing and stored at -80^{o}C.

2.13.3 Measurement of RNA concentration and integrity

Once extracted, total RNA concentration and purity was measured using a microspectrophotomer (Nanodrop; Thermo Fisher Scientific). Absorbance at 260nm (A_{260}) correlates directly with RNA concentration in the sample and can be used to quantitate this. The ratio of readings at 260 and 280 nm (A_{260} / A_{280} ratio) provides a measure of RNA purity, with a ratio of 1.9-2.1 suggesting pure RNA. Lower values typically reflect protein contamination which absorbs in the UV spectrum. A_{260} / A_{280} ratios >1.8 were deemed acceptable for further analysis.

RNA integrity was assayed using a bioanalyzer (2100 Bioanalyzer; Agilent Technologies, Wokingham, UK). This uses chip-based technology incorporating a series of microchannels through which nucleic acid

fragments are separated based on size as they are driven through it electrophoretically. (Figure 2.7) As the various RNA species elute they pass a fluorescence detector which provides a read out of the peaks and troughs of fluorescence intensity, corresponding to the abundance of different sized fragments in the sample. By comparing the abundance of 18S and 28S ribosomal RNAs, an RNA integrity number (RIN) is generated.

The RNA gel matrix was was filtered and mixed with dye concentrate to produce a working gel-dye mix. This was then injected into the RNA chip to prime it ready for sample measurement. RNA marker was pipetted into all wells, followed by 1 µl of either ladder or sample RNA. The chip was then vortexed for 1 minute at 2400 rpm using a customised chip vortex (Agilent) before running immediately on the bioanalyser. RIN values of >7 were deemed acceptable for further analysis.

2.13.4 Synthesis of cDNA

Although measurement of gene expression using qPCR assesses the abundance of transcribed mRNA, RNA templates must first be converted into cDNA. This process requires a viral reverse transcriptase enzyme derived from viruses with an RNA genome (retroviruses) such as Avian myeloblastosis virus (AMV) or Moloney murine leukaemia virus (MMLV) which have an RNA-dependent DNA polymerase activity. Priming for this reaction can either be gene specific or using random oligonucleotides which bind to RNA throughout its length and give an unbiased, full representation of the RNAs expressed.

The Superscript VILO system (Invitrogen, Paisley, UK) was used. A 20µl reaction mixture was assembled comprising 4µl of 5x VILO reaction mix (containing random primers, $MgCl_2$ and dNTPs in a buffer formulation

A

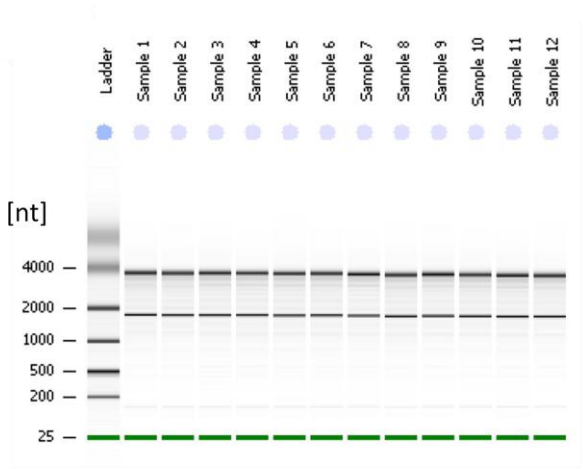

B

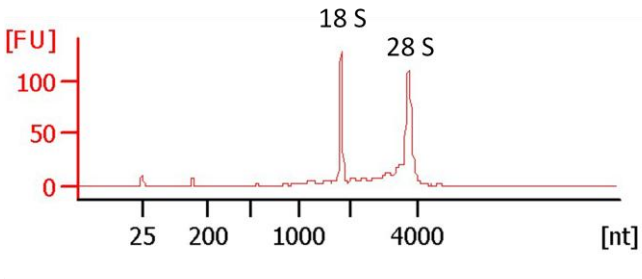

Figure 2.7 Assessment of RNA integrity using the bioanalyser. A: Example electopherogram produced by a set of RNA samples (1-12) extracted from mouse kidney tissue. The two prominent bands in the sample lanes represent 18S and 28S ribosomal RNA. If RNA has become degraded, the intensity of these bands diminish, and additional bands of smaller size are observed. B: Plot showing quantified intensity of bands from electropherogram with the peaks corresponding to 18S and 28S. Although simple measurement of the 28S:18S ratio provides some information on RNA integrity, use of additional data from signal measurements to construct regression models based on Bayesian learning produces a more accurate marker referred to as the RNA integrity number (RIN). A RIN of 10 represents fully intact RNA while 1 is completely degraded. In this example the RIN was 8.7. NT: nucleotide number; FU: fluorescence units.

optimized for qPCR), 2µl of 10x SuperScript enzyme mix and 1µg of purified RNA, with the remaining volume nuclease-free water. Samples were then incubated at room temperature for 10 minutes (primer annealing), 42°C for 60 minutes (cDNA synthesis), 85°C for 5 minutes (heat inactivation) before cooling to 4°C. Samples were then diluted 10 fold using a solution of yeast tRNA (10 µg/ml) before aliquoting and storing at -20°C. tRNA acts as a carrier to minimize adsorption of cDNA onto surfaces and cannot be amplified by PCR.

2.13.5 Preparation of cDNA standards

Although gene expression can be measured and expressed solely as an amount relative to the expression of one or more housekeeping genes, greater precision is obtained by measuring absolute copy number for each gene studied. To do this requires comparison between each unknown sample and a standard curve generated from samples containing known concentrations of cDNA. Six-point standard curves were generated with serial 10-fold dilutions from 10^7 to 10^2 molecules (Figure 2.8A and B).

To make standards for each gene, a quantitative PCR assay was performed using one sample measured in 6 replicates. Melt curves were inspected to assess specificity of priming and formation of primer-dimers; primer pairs were rejected if multiple peaks were apparent. (Figure 2.8C) Products were then pooled and added to blue 5x pre-mixed gel loading buffer before electrophoresing on a 2% agarose gel run at 80V for 30 minutes. Gels were inspected under UV light to confirm the presence of a solitary product band of the expected size as a further check of primer specificity.

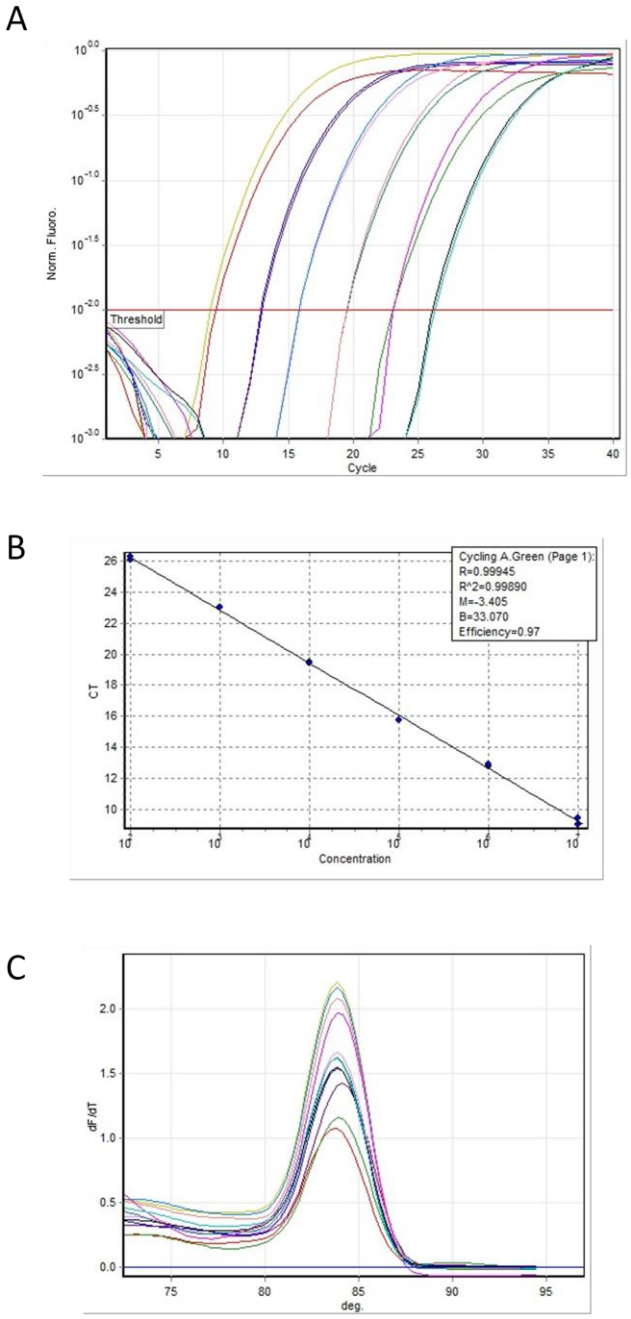

Figure 2.8 Quantitative PCR using the absolute quantitation method. A: Family of curves produced by performing qPCR on a series of standards generated by 10-fold serial dilutions from 10^7 to 10^2 molecules. Example shown is for rat ICAM-1. B: Consequent standard curve produced by plotting template copy number (DNA 'concentration'; x-axis) against cycle number at which fluorescence intensity threshold was reached (C_T; y-axis). The reaction efficiency can be calculated from the slope of the curve, in this case 0.97. C: Corresponding melt curves. The products of each reaction produce a single clean peak, implying a single reaction product and the absence of significant primer dimerisation.

cDNA was purified using the Geneclean spin kit (MPBiomedicals, Solon, USA). Gel bands were excised under UV light and melted at 55^{o}C in an aqueous suspension of silica matrix ('Spin Glassmilk'). DNA binds to silica in the presence of high concentrations of chaotropic salt, presumed to be due to chaotropic disruption of water structure around negatively-charged silica allowing cation bridge formation between the silica matrix and the phosphate backbone of DNA. Samples were then centrifuged inside a spin filter at 14000 x *g* to promote binding of silica-DNA to the membrane. After two centrifugation wash steps using a buffer containing 100mM NaCl and 50% EtOH ('Geneclean Spin wash solution'), DNA was eluted by lowering the salt concentration and rehydrating the silica matrix, breaking the attraction between matrix and DNA.

The concentration of purified DNA was measured using a Nanodrop microspectrophotomer. The number of DNA copies in 1 µl of solution could then be calculated using the following series of equations:

Mean molecular weight of amplicon = 660 x amplicon length (bp)

Where 660 is the mean MW of 1bp

$$\text{Number of copies of amplicon in 1ng} = \frac{6.02 \times 10^{23} \text{ (Avogadro's constant)} \quad x10^{9}}{\text{Molecular weight of amplicon}}$$

Number of copies in 1 µl = cDNA/uL x copies of amplicon/ng

cDNA was then sequentially diluted to a stock solution of 10^8 copies/2 µl (sample volume used in qPCR reactions) and a six-point standard curve prepared by serial 10-fold dilutions using tRNA 10µg/ml as diluent

2.13.6 Quantitative PCR reaction

Quantitative PCR was performed using the Sybr green fluorophore as a DNA intercalating agent. Sybr green dye binds double-stranded DNA non-selectively and, once bound, emits green light after excitation. Fluorescence levels hence increase as DNA product accumulates during the PCR reaction and can be monitored in real-time. By specifying a threshold detection level of fluorescence during the linear phase of amplification, absolute abundance of starting template can be assessed by comparison with reference samples used to create a standard curve.

10 µl reactions were prepared by adding 2 µl of cDNA to 5 µl of 2x Sensimix Sybr Green mastermix (containing heat-activated DNA polymerase, dNTPs, 6mM $MgCl_2$ and Sybr Green I dye; Bioline, London, UK), 2µl nuclease-free water and 0.5µl each of forward and reverse oligonucleotide primers, specific for the gene of interest (0.5µM concentration). Specific primers for each gene of interest are listed in Tables 2.3 and 2.4. PCR was performed using a Rotorgene 6000 cycler (Qiagen), a rotary qPCR system, using the following template PCR program:

Gene	Forward (5′ to 3′)	Reverse (3′ to 5′)
28S	AGCGACACTCGGACTTGC	CGAAGGACTCCACAGGTTTT
βactin	CTAAGGCCAACCGTGAAAAG	ACCAGAGGCATACAGGGACA
HPRT	TCCTCCTCAGACCGCTTTT	CCTGGTTCATCATCGCTAATC
YWHAZ	CTTCCTGCAGCCAGAAGC	GGTTTCCTCCAATCACTAGCC
ICAM-1	GCTACCATCACCGTGTATTCG	TGAGGTCCTTGCCTACTTGC
Fibronectin	CGGAGAGAGTGCCCCTACTA	CGATATTGGTGAATCGCAGA
IL1β	AGTTGACGGACCCCAAAAG	TTTGAAGCTGGATGCTCTCAT
Osteopontin	CCCGGTGAAAGTGACTGATT	TTCTTCAGAGGACACAGCATTC
MCP-1	CATCCACGTGTTGGCTCA	GATCATCTTGCTGGTGAATGAGT
TGFβ	TGGAGCAACATGTGGAACTC	GTCAGCAGCCGGTTACCA
COL1A1	CATGTTCAGCTTTGTGGACCT	GCAGCTGACTTCAGGGATGT
COL4A1	AGGTGTACCCGGCCCTAA	GGTTCTCCTTTGATGACATCGT
NLRP3	CCACAGTGTAACTTGCAGAAGC	GGTGTGTGAAGTTCTGGTTGG
ASC	GAGCAGCTGCAAACGACTAA	GTCCACAAAGTGTCCTGTTCTG
Caspase-1	CCCACTGCTGATAGGGTGAC	GCATAGGTACATAAGAATGAACTGGA

Table 2.3 Oligonucleotide primers for qPCR of mouse genes

Gene of Interest	Forward (5' to 3')	Reverse (3' to 5')
SDHA	CCCTGAGCATTGCAGAATC	CATTTGCCTTAATCGGAGGA
RPL13a	CCCTCCACCCTATGACAAGA	GGTACTTCCACCCGACCTC
HPRT	GACCGGTTCTGTCATGTCG	ACCTGGTTCATCATCACTAATCAC
YWHAZ	CTACCGCTACTTGGCTGAGG	TGTGACTGGTCCACAATTCC
ICAM-1	GCAGACCACTGTGCTTTGAG	TCCAGCTCCACTCGCTCT
P2X7	AAGAAGTGTGAGCCCATCGT	GCTCGTCCACAAAGGACAC
COL4A1	CCATGGTCAGGACTTGGGTA	AAGGGCATGGTGCTGAACT
Fibronectin	CAGCCCCTGATTGGAGTC	TGGGTGACACCTGAGTGAAC
IL1β	TGTGATGAAAGACGGCACAC	CTTCTTCTTTGGGTATTGTTTGG
Osteopontin	CGGTGAAAGTGGCTGAGTTT	GGCTACAGCATCTGAGTGTTTG
MCP-1	CGTGCTGTCTCAGCCAGAT	GGATCATCTTGCCAGTGAATG
TGFβ	CCTGGAAAGGGCTCAACAC	CAGTTCTTCTCTGTGGAGCTGA
COL1A1	CATGTTCAGCTTTGTGGACCT	GCAGCTGACTTCAGGGATGT

Table 2.4. Oligonucleotide primers for qPCR of rat genes

95°C for 10 mins (activation of DNA polymerase)

40 cycles of:

- 95°C for 10s (denaturation)
- 60°C for 15s (annealing)
- 72°C for 20s (extension)

Melt curve, rising from 72 to 95 °C by 1°C every 5s

Adequacy of the qPCR run was confirmed by inspecting standard curve linearity (accepting r^2 >0.99), reaction efficiency (ideally 0.9 – 1.1) and melt curve morphology (single peaks). RT negative samples and 'no template' samples (ie. tRNA diluent alone) were run as controls. Copy number was obtained by comparing the cycle number (C_T) at which a sample reached threshold fluorescence to the standard curve. Samples were run in duplicate and the mean copy number for each replicate pair calculated.

2.13.7 Calculation of final copy number in genes of interest

Copy number of any gene of interest measured in a sample requires correction for the abundance of a housekeeping gene which is not significantly regulated by the experimental conditions employed. Increased accuracy can be achieved by using more than one housekeeping gene for this normalization process.

Four housekeeping genes were measured in both rat (HPRT, SDHA, RPL13a and YWHAZ) and mouse (28S ribosomal RNA, βactin, HPRT and YWHAZ). Genorm software was used to measure the stability of each housekeeping gene under experimental conditions by determining the pairwise variation with all other control genes as the standard deviation of the logarithmically-

transformed expression ratios (Vandesompele et al., 2002). This process results in an 'M value' which expresses the average pairwise variation of a particular gene with all other control genes. This analysis works on the principle that expression level of two ideal internal control genes should be identical in all samples regardless of the experimental conditions imposed. Lower M values reflect increased stability and an arbitrary cut-off of 1.5 is frequently used to decide if a control gene displays adequate stability to be used for reference purposes.

Having selected stable control genes, the relative expression of each gene of interest compared to all stable housekeeping genes was calculated and the geometric mean computed. From this a 'normalisation factor' was determined for each individual sample, allowing the most accurate correction for control gene abundance and a final copy number was obtained by applying this factor to the raw copy number data.

2.14 ELISAs for cytokine analysis

2.14.1 General principles

Concentrations of cytokines (eg. MCP-1) in cell culture supernatants and urine were measured by specific capture or 'sandwich' ELISAs. The ELISA microplate technique was first described in 1971 by Engvall and Perlmann (Engvall and Perlmann, 1971). The general principle of all ELISAs is to detect and quantify a protein of interest by using a specific antibody coupled directly or indirectly to a signal-generating enzyme or fluorophore. In a standard 'indirect' ELISA, samples are incubated in a 96-well microplate allowing proteins to be adsorbed on the wall of the plate. A specific primary antibody is then applied, followed by a secondary enzyme-linked antibody. In

contrast, in a sandwich ELISA, the microplate is first coated with a target-specific 'capture' antibody meaning only the protein of interest is immobilized on the wall of the wells. This protein is then 'sandwiched' between the capture antibody and an enzyme-linked secondary antibody to facilitate detection (Figure 2.9). Sandwich ELISAs are particularly useful when assaying complex protein solutions (eg. urine) as they isolate immobilisation of the protein of interest thereby increasing assay sensitivity and specificity. Addition of enzyme substrate yields a colour reaction proportional to the concentration of bound antigen, allowing quantification when compared to a 'standard' dilution series of the target cytokine.

The steps below refer to the assay for human MCP-1 to exemplify the general principles of a sandwich ELISA. Specific details of the antibodies and solutions used for other assays can be found in Table 2.5. All steps were performed at room temperature.

2.14.2 Coating

An optically clear, high protein-binding capacity 96-well plate (Nunc 'Maxisorp', Thermo Fisher Scientific) was coated with 100µl of an affinity-purified mouse anti-human MCP-1 antibody (R+D Systems, Abingdon, UK) at a concentration of 2µg/ml diluted in PBS. The plate was covered with an adhesive strip (Appleton Woods, Birmingham, UK) and placed at 4^{o}C overnight to allow adsorption of antibody to the walls of the microplate. The following morning the contents of the plate were expelled and wells were washed 3 times with 0.05% Tween 20 in PBS (wash buffer) before blotting on a tissue to remove excess fluid.

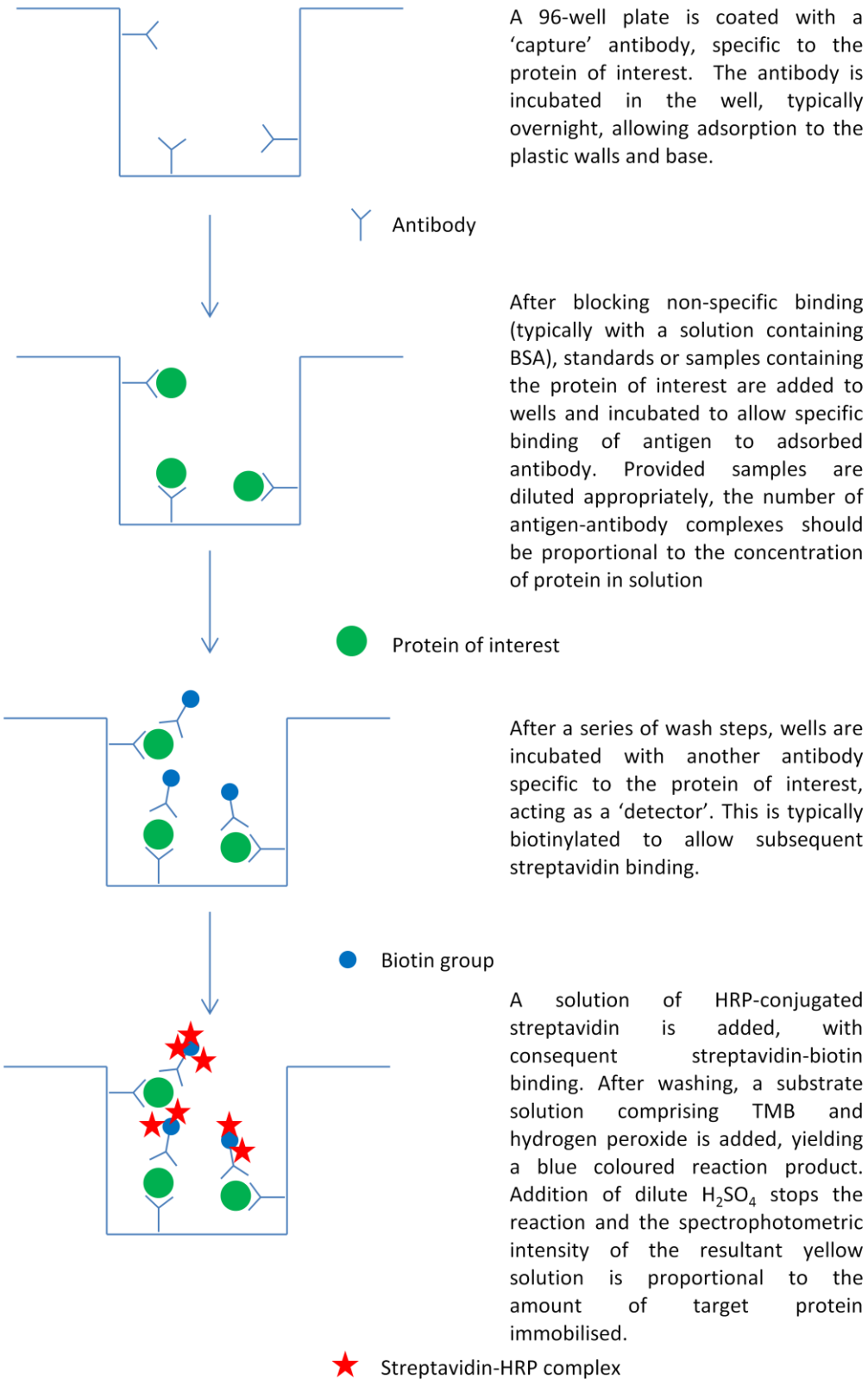

Figure 2.9 Basic schema of an indirect 'sandwich' ELISA.

Protein	Albumin (R)	Albumin (M)	IL1β (H)	MCP-1 (R)	MCP-1 (H)
ELISA kit	Rat albumin ELISA (Bethyl Labs, Montgomery USA)	Mouse albumin ELISA (Bethyl Labs)	Human IL-1β Duoset (R&D Systems)	OptEIA Rat MCP-1 ELISA set (BD Biosciences)	N/A
Standard	Rat reference serum	Mouse reference serum	Recombinant human IL1β	Recombinant rat MCP-1	Recombinant human MCP-1 (279-MC) R&D Systems
Capture Antibody	Sheep anti-rat albumin Ab (10µg/ml)	Goat anti-mouse albumin Ab (10µg/ml)	Mouse anti-human IL1β Ab (4µg/ml)	Anti-rat MCP-1 monoclonal Ab 1:250 dilution	Mouse anti-human IgG (MAB679) R&D Systems 2µg/ml
Detection Antibody	HRP-conjugated sheep anti-rat albumin Ab (0.13µg/ml)	HRP-conjugated goat anti-mouse albumin Ab (0.13µg/ml)	Biotinylated goat anti-human IL1β Ab (200ng/ml)	Biotinylated anti-rat monoclonal Ab 1:500 dilution	Goat anti-human IgG (BAF279) R&D Systems 100ng/ml
Wash Buffer	50 mM Tris, 0.14M NaCl, 0.05% Tween 20, pH 8.0	50 mM Tris, 0.14M NaCl, 0.05% Tween 20, pH 8.0	0.05% Tween 20 in PBS	0.05% Tween 20 in PBS	0.05% Tween 20 in PBS
Sample Diluent	50 mM Tris, 0.14 M NaCl, 1% BSA, 0.05% Tween 20	50 mM Tris, 0.14 M NaCl, 1% BSA, 0.05% Tween 20	1% BSA in PBS	10% FBS in PBS	0.1% BSA, 0.05% Tween 20 in TBS

Table 2.5. Constituents of ELISAs used for quantification of proteins of interest in human cell culture supernatants and rodent urine. R: rat; M: mouse; H: human.

2.14.3 Blocking and addition of samples

A blocking solution of 5% sucrose in PBS with 1% BSA was prepared and 300µl added to each well. The BSA acts to block non-specific protein binding sites on the surface of the plate.

While blocking, standard protein and cell culture supernatant samples for analysis were thawed, mixed and allowed to equilibrate at room temperature. A diluent solution of 0.1% BSA, 0.05% Tween 20 in PBS pH 7.3 was freshly prepared. Recombinant human MCP-1 (R+D Systems) was used to create a reference concentration series. From a stock concentration of 10 µg/ml, recombinant protein was diluted in diluent solution to form a 9-point standard series with concentration ranging from 9.76 - 2500 pg/ml. A 'blank' sample comprising diluent alone was also included.

The plate was inverted to remove blocking solution, washed 3 times with washing buffer and excess solution blotted. Reference standard or sample (100µl) was then added to each well in a pre-determined plate layout and the plate incubated for 2 hours at room temperature on a plate shaker. Each sample was measured in duplicate to decrease variability. For human MCP-1 measurement of cell culture supernatants no pre-dilution of samples was required.

2.14.4 Secondary antibody and detection

The plate was washed 3 times with washing buffer and excess solution removed. An affinity-purified biotinylated polyclonal goat anti-human MCP-1 antibody (100µl; R+D systems) at a concentration of 100ng/ml diluted in diluent solution was added to each well. This antibody has been validated by

the company for use as a detection antibody in conjunction with its partner capture antibody. The plate was then incubated for 2 hours before washing 3 times with washing buffer and blotting excess solution.

A streptavidin-HRP conjugate (100µl), diluted in PBS as per the manufacturer's instructions (typically 1:200), was then added to each well. Streptavidin binds with high affinity to biotin, bringing the HRP enzyme into close proximity with the secondary antibody, facilitating a subsequent detection step. The plate was incubated for 20 minutes before washing 3 times with wash buffer.

A solution of 3,3',5,5'-tetramethylbenzidine (TMB; Cambridge Bioscience, Cambridge, UK) and hydrogen peroxide, was prepared and 100 µl added to each well. TMB is colourless in solution in basal conditions but forms a blue product when oxidized by HRP in the presence of hydrogen peroxide, the colour intensity of which is proportional to the degree of HRP activity and, in turn, the amount of bound secondary antibody. The plate was incubated in the dark for approximately 10 minutes before stopping the reaction by adding 50 µl of 2N sulphuric acid. This final step yields a yellow colour change, proportionally identical in intensity to its blue counterpart.

2.14.5 Data capture and analysis

The plate was transferred to an ELx800 spectrophotometric microplate reader (Biotek, Winooski, USA) and the absorbance measured at 450nm. Adjusted absorbances were calculated by subtracting the background absorbance of the 'blank' sample.

A best-fit standard curve was generated from the absorbances of the recombinant MCP-1 reference series using 4 variable non-parametric regression modeling (Figure 2.10). Concentrations of MCP-1 in samples could then be calculated from the raw blank-subtracted absorbances using the resultant regression equation. A co-efficient of variance of <10% between sample replicates was accepted.

2.15 Western blotting

2.15.1 General principles

Western blotting provides a method by which specific proteins, and, to some degree, their relative abundance, can be detected in biological samples or solutions. Samples are homogenised using a cell or tissue lysis buffer and the total protein concentration measured. A known quantity of protein solution is then separated on a sodium lauryl sulphate (SDS) – polyacrylamide gel, typically in the presence of the denaturing agent 2-mercaptoethanol. The ladder of separated proteins is then transferred from the gel to a nitrocellulose membrane which can be probed with a primary antibody specific to the protein of interest. An enzyme-linked secondary antibody is then applied, followed by a substrate solution, the chemiluminescent reaction of which can be visualised using standard photographic methodology. The identity of the labeled bands can be confirmed by comparing the position with protein of a known molecular weight run in parallel.

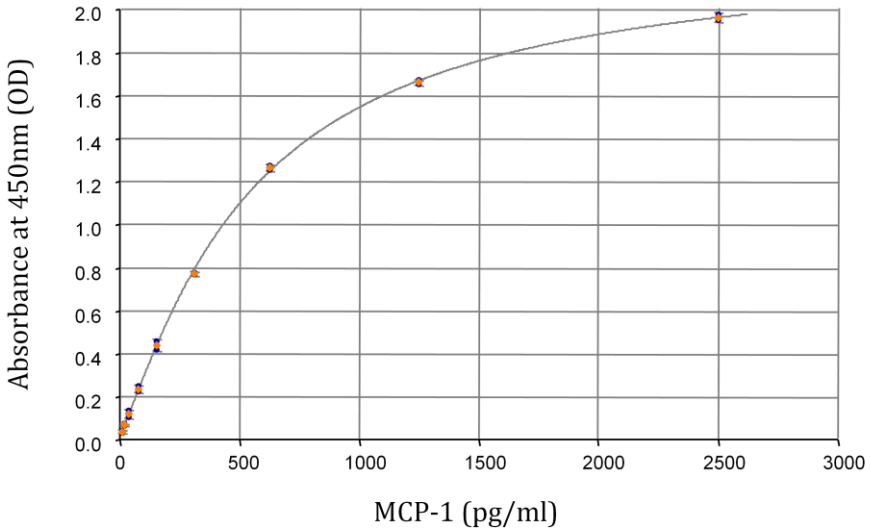

Figure 2.10 Sample standard curve used for quantification of human MCP-1 by ELISA. The standard curve was generated by 4-variable non-parametric data modelling and was used to transform OD measurements of unknown samples to analyte concentration. Final concentration values were achieved by multiplying by the sample dilution factor.

2.15.2 Protein extraction

All steps during harvest of proteins from cell culture monolayers were performed on ice. Cells were washed twice with ice-cold PBS before adding 100µl of a proprietary cell lysis buffer (Invitrogen; Constituents: 10mM Tris pH 7.4, 100mM NaCl, 1mM EDTA, 1mM EGTA, 1mM NaF, 20mM $Na_4P_2O_7$, 2mM Na_3VO_4, 1% Triton X-100, 10% glycerol, 0.1% SDS, 0.5% deoxycholate) supplemented with 1mM phenylmethanesulfonylfluoride (PMSF; a serine protease inhibitor) and protease inhibitor cocktail (P2714, Sigma). Monolayers were agitated for 2-3 minutes before scraping and collecting the lysate into microcentrifuge tubes.

Tubes were rested on ice for 30 minutes, vortexing at 10 minute intervals, to ensure complete lysis of cell membranes and solubilisation of proteins. The extract was then centrifuged at 18,000 x *g* for 10 minutes at 4°C to pellet insoluble cellular debris. Supernatant was transferred to a fresh microcentrifuge tube and stored at -80°C. A 6 µl aliquot of each sample was removed before freezing for quantification of total protein concentration.

2.15.3 Quantification of total protein concentration

Total protein concentration of lysates were quantified using the Pierce bicinchonic acid (BCA) assay. The cornerstone of this assay is the Biuret reaction, whereby protein in an alkaline medium reduces Cu^{2+} to Cu^{1+} and forms a coloured chelate complex. In the subsequent colour development reaction, biocinchonic acid reacts with the Cu^{1+} cation in a ratio of 2:1 to form an intense purple-coloured soluble reaction product. Spectophotometric absorbance at 562nm is linearly proportional to the total protein concentration within the solution.

BCA assay reagent A (biocinchonic acid and tartrate in an alkaline carbonate buffer) was mixed in a 50:1 ratio with reagent B (4% copper sulphate pentahydrate solution). A reference protein series (BSA) was prepared by diluting from a concentration of 1400 µg/ml down to 0.1 µg/ml in distilled water; lysis buffer was added to each reference solution in order to constitute 20% by volume. A 'blank' sample consisted of 20% lysis buffer in distilled water alone. Sample aliquots were thawed and diluted 1 in 5 in distilled water. Ten µl of sample or standard was then added to each well of a 96-well microplate followed by 200 µl of assay mixture. The plate was incubated for 30 minutes at 37^{o}C before cooling to room temperature and measuring the absorbance at 562nm on a plate reader.

A standard curve was created by linear regression of blank-subtracted absorbances for the reference protein series (Figure 2.11). Total protein concentrations of the samples could then be calculated using the consequent regression equation, and multiplying by the dilution factor (ie. x 5).

2.15.4 SDS-Polyacrylamide gels

Ten millilitres of 10% resolving gel was prepared by mixing the following constituents: 4 mls distilled water, 3.4 mls 30% acrylamide/methylene bisacrylamide solution (Protogel; National Diagnostics, Charlotte, USA), 2.5 mls 1.5M Tris-HCl (pH 8.8), 0.1 mls 10% SDS. Immediately before pouring, 0.1 mls of 10% ammonium persulfate (APS) and 4 µl 1% N,N,N',N' tertramethylethylenediamine (TEMED) were added to induce gel polymerization; APS decomposes to sulphate free-radicals, a process accelerated in the presence of TEMED, and these free radicals initiate gel polymerization. Ten % polyacrylamide gels are versatile and can resolve proteins in the range of 20-200 kDa; higher percentage gels have a smaller

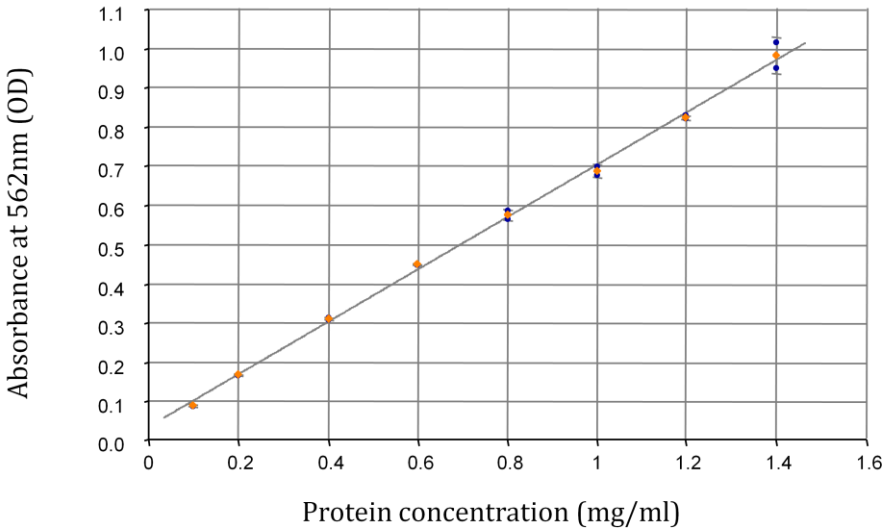

Figure 2.11 Sample standard curve used for quantification of protein concentration in cell culture lysates using the BCA assay. The standard curve was generated by linear regression and was used to transform OD measurements of unknown samples to analyte concentration. Final concentration values were achieved by multiplying by the sample dilution factor.

pore size and are hence better suited to resolving lower molecular weight proteins.

Gels were prepared and electrophoresis performed using the Mini-Protean II system (Biorad, Berkeley, USA). Two clean glass plates were apposed in a casting block, separated by 1.5mm diameter spacers. The resolving gel was poured between the plates and left for 20 minutes to set. Immediately after pouring, the gel was covered by a shallow depth of water-saturated butan-2-ol to exclude air and level the surface.

Five millilitres of 5% stacking gel were prepared by mixing the following components: 3.4 mls distilled water, 0.83 mls 30% acrylamide/methylene bisacrylamide solution, 0.63 mls 1.5M Tris-HCl (pH 6.8). Once polymerized, the stacking gel has a large pore size allowing proteins to concentrate rapidly at the stacking gel – resolving gel interface, allowing proteins to separate by size in the resolving gel. The butan-2-ol was poured off and the gel surface washed with distilled water before blotting dry. Immediately before pouring, 50µl APS and 5µl 1% TEMED were added to the stacking gel to catalyse polymerization. A 1.5mm, 10 well comb was carefully inserted into the stacking gel before leaving to set for 1 hour. The comb was then removed, excess gel carefully cleaned away with a needle and the casting block placed into the gel electrophoresis tank submerged in running buffer diluted from a 10x stock (50mM Tris pH 8.3, 500mM glycine, 0.2% SDS).

2.15.5 Sample preparation and electrophoresis

Samples were thawed and kept on ice. Samples containing 10-40 µg of protein were mixed with 7µl 5x sample buffer (constituents: 4% SDS, 20% glycerol, 10% 2-mercaptoethanol, 0.004% bromophenol blue and 0.125M

Tris HCl) and sufficient distilled water added to bring the sample buffer to its working dilution and maintain a constant volume across all samples (35µl). 2-mercaptoethanol acts, in tandem with sample heating, as a potent reducing agent, breaking disulphide bonds and linearising proteins so that subsequent electophoretic separation is governed by molecular weight alone.

Samples were then heated at 95^{o}C for 10 minutes before cooling rapidly on ice and centrifuging briefly to ensure the full volume could be recovered. A marker protein ladder mixture ('Full range rainbow marker'; GE healthcare, Amersham, UK) was reconstituted to the working dilution with distilled water and sample buffer. Negative controls consisted of sample buffer diluted with distilled water alone.

Samples and ladder were loaded onto the gel taking care not to cross-contaminate between lanes. The gel tank was connected to a power supply and the gel run at 80V for approximately 2.5 hours.

2.15.6 Transfer to nitrocellulose membrane

Adequate separation of proteins was confirmed by inspection of the coloured ladder markers before halting electrophoresis. The MiniProtean wet tank transfer system (Biorad) was used for transfer of proteins to nitrocellulose. The glass plates were removed from the casting block and immediately submerged in transfer buffer (48mM Tris, 39mM glycine, 0.037% SDS, 20% methanol). A sheet of nitrocellulose membrane with pore size 0.45µm (Hybond ECL; GE Healthcare) was cut to size and 'activated' by briefly submerging in methanol before soaking in transfer buffer. 4 sheets of filter paper, cut to the size of the gel, were also soaked in transfer buffer. The stacking gel was discarded and a 'sandwich' formed within the gel-holder

cassette comprising: 1 foam pad, 2 sheets of filter paper, nitrocellulose membrane, resolving gel, 2 sheets of filter paper, 1 foam pad. Any trapped air bubbles were removed by rolling with a plastic pipette.

The cassette was then inserted into the transfer tank adjacent to a cooling unit, the tank filled with transfer buffer, and a charge of 100 Volts applied for ~1 hour 10 minutes. The membrane was removed and transferred to wash buffer solution (0.1% Tween 20 in TBS; TBS/T). Adequate transfer of protein was confirmed by visual inspection of coloured ladder protein transfer and, if necessary, by reversible staining of protein with Ponceau S solution.

2.15.7 Blocking and antibody application

The membrane was transferred to a solution of 5% milk in TBS/T and placed on a rocker for 1 hour in order to block non-specific protein binding sites. The blocking solution was poured off and the membrane washed briefly with wash buffer before adding the relevant primary antibody diluted in 5% BSA in TBS/T and placing on a rocker for a variable period of time optimized for each antibody (see Table 2.6). The membrane was then washed 3 times for 5 minutes each in wash buffer before incubating with a species-specific HRP-linked secondary antibody diluted in 5% dry milk in TBS/T for 1 hour. The membrane was then washed 3 times for 5 minutes each in preparation for the detection step.

Target Protein (Species)	Blocking Solution	Primary antibody	Primary dilution	Secondary antibody
P2X7 (H)	5% Marvel milk in TBS/T	Ab109246 (Abcam) Rabbit monoclonal	1:2000 (O/N)	HRP-conjugated swine anti-rabbit (Dako)
P2X4 (H)	5% Marvel milk in TBS/T	APR-002 (Alomone) Rabbit polyclonal	1:300	HRP-conjugated swine anti-rabbit (Dako)
SV40 big T	5% Marvel milk in TBS/T	Ab16879 (Abcam)	1:80 (O/N)	HRP-conjugated donkey anti-goat (Santa Cruz)
Actin (H)	5% Marvel milk in TBS/T	A2066 Rabbit polyclonal	1:1000 (1hr)	HRP-conjugated swine anti-rabbit (Dako)
Acetylated tubulin (H)	5% Marvel milk in TBS/T	T7451 (Sigma) Mouse monoclonal	1:10000 (1 hr)	HRP-conjugated rabbit anti-mouse (Abcam)

Table 2.6. Antibodies used for Western blotting. H: human.

2.15.8 Chemiluminescence and signal detection

The chemiluminescence reaction was used for detection of bound antibody. The enhanced chemiluminescence kit (ECL; GE Healthcare) used in this step consists of two reagents: hydrogen peroxide and luminol. These were mixed in a 1:1 ratio prior to use and applied directly to the membrane lying on a cellophane sheet. The membrane was incubated in ECL medium for approximately 1 minute before gently tapping off and wrapping the membrane in the cellophane sheet. The membrane was placed in a photographic cassette and transferred to the dark room where it was exposed against x-ray film (Hyperfilm ECL; GE Healthcare) and developed using an automatic film processor (SRX-101A; Konica Minolta, Tokyo, Japan).

In the presence of an oxidising agent (produced by decomposition of hydrogen peroxide by HRP), luminol is converted to an excited state and chemiluminesces as this species decays. This chemiluminescence is proportional to the amount of HRP present, and consequently the abundance of target protein, and can be detected with great sensitivity using high performance x-ray film. After development of the exposed x-ray film, the target protein(s) can be seen as discrete bands and the identity confirmed by comparing the molecular weight with those of the marker ladder proteins. Relative abundance of protein between samples was assessed by visual comparison of band size and density and by densitometry using image analysis software (ImageJ, Bethesda, USA).

2.16 *In vitro* studies of human glomerular cells

2.16.1 Background

Transformed human mesangial cells (tHMCs) were kindly provided by Dr Xiong Ruan (UCL, UK) and their generation has been described previously (Sraer et al., 1996); in brief this line was created by taking human mesangial cells cultured from normal human kidney unsuitable for transplantation and immortalising them by transfection with the viral oncogene large T-SV40 and H-ras. The cells maintain many of the phenotypic characteristics of primary HMC including cytoplasmic projections, stellate shape and microvilli and express α-smooth muscle actin (αSMA), a protein present in HMC but absent in glomerular epithelial and endothelial cells.

Primary human mesangial cells (pHMCs) were purchased from Lonza (Lonza Biologics, Slough, UK).

A conditionally-immortalized human podocyte line was kindly provided by Prof Moin Saleem (University of Bristol, UK), and generation of their line has been described in detail (Saleem et al., 2002). The line was created by isolating podocytes from a nephrectomy specimen from a 3 year old child with reflux nephropathy and transfecting a temperature sensitive *SV40-T* gene. These cells proliferate at the 'permissive' temperature of 33^{o}C but transfer to 37^{o}C leads to growth arrest, differentiation and expression of mature podocyte markers including nephrin and podocin, together with morphological changes including development of fine processes and slit diaphragm-like structures rendering them a good model of mature human podocytes.

2.16.2 Maintenance of proliferating cultures

2.16.2.i Transformed human mesangial cells

tHMCs were cultured in a medium composed of RPMI 1640 supplemented with 4mmol/l D-glucose, 1% penicillin-streptomycin and 5% foetal calf serum (FCS). Cells were maintained in a humidified incubator at 37^{o}C with 5% CO_2. Medium was changed every 2-3 days and cells inspected daily using an inverted phase-contrast microscope. Cells were subcultured when 90-100% confluent.

2.16.2.ii Primary human mesangial cells

pHMCs were cultured in a proprietary basal medium (Lonza) supplemented with 5% FCS and gentamicin / amphotericin-B. Cells were maintained in a humidified incubator at 37^{o}C with 5% CO_2. Medium was changed every 2-3 days and cells inspected daily using an inverted phase-contrast microscope. Cells were subcultured when 90-100% confluent and cells used for experiments at passage 7-12.

2.16.2.iii Transformed human podocytes

Podocytes were cultured in a medium composed of RPMI 1640 supplemented with 4mmol/l D-glucose, 1% penicillin-streptomycin and 5% FCS. Cells were maintained in an incubator at 33^{o}C with 5% CO_2. Medium was changed every 2-3 days and cells inspected daily using an inverted phase-contrast microscope. Cells were subcultured when 90-100% confluent.

For experiments, cells were subcultured into plates with the appropriate number of wells at a seeding density of 0.5-2 x10^5 cells / ml. Plates were then transferred to a humidified incubator at 37^{o}C with 5% CO_2 to allow differentiation over a 14 day period, in growth medium as before. Cells were inspected daily to confirm their anticipated change in morphology and medium was changed every 2 days.

2.16.3 Subculture of cells and cell counting

For subculture of cells, medium was removed and cells washed with a small quantity of pre-warmed 0.05% trypsin-EDTA (Invitrogen). For 75cm^2 (T75) flasks, 1-2 mls of trypsin-EDTA was then added to cover the monolayer and the flask incubated at 37^{o}C for 3 minutes to allow cell detachment. The flask was then tapped firmly and cell detachment confirmed by microscopy. An excess of culture medium supplemented with 5% FCS was then added to the flask to inactivate the trypsin and a homogeneous cell suspension created by repeated pipetting against the base of the flask. The cell suspension was then divided into 3-5 T75 culture flasks and an appropriate volume of culture medium added. Cell adhesion was confirmed by microscopy after 24 hours.

When sub-culturing to multi-welled cell culture plates for experiments, cells were counted after detachment to ensure seeding at a consistent density within and between experiments. To do this, a 50 µl aliquot of homogeneous cell suspension was removed from the trypsinised suspension, and mixed with an equal volume of trypan blue. Trypan blue dye is taken up through the cell membrane of dead cells, staining them blue, but is not taken up into living cells. Ten µl of this mixture was then place on each of two graticules of a haemocytometer and covered with a cover slip before transferring to the

stage of a microscope for counting. The haemocytometer is constructed such that the volume of fluid captured between slide and coverslip overlying one large graticule square is known precisely (in this case 0.1 mm^3). By counting the number of cells overlying each large square (four per graticule over two graticules) and taking the mean, an estimate of the number of cells in solution was obtained. Cells stained with trypan blue were excluded from the count. The final cell concentration was obtained by correcting for dilution with trypan blue (multiplication factor of two). Cells were plated at a density of 0.5-2 $x10^5$ / ml depending on the cell type and experiment.

2.16.4 Freezing of cells for long-term storage and cell recovery

Cells were detached from their substrate using trypsin-EDTA as described above, and culture media used to neutralize enzymatic activity. Cell mixture was then transferred to a 15ml plastic tube and centrifuged at 1000 x *g* for five minutes. Medium was carefully aspirated off and the cell pellet resuspended in 1 – 1.5 mls of proprietary cell culture cryopreservation media (Recovery media; Life Technologies; contains 10% DMSO) before transferring to a cryovial. The cryovial was placed at -80°C in a polystyrene container overnight before moving to liquid nitrogen for long term storage.

When recovering cells, the cryovial was removed from liquid nitrogen and warmed in a 37°C water bath. When only a small ice pellet remained, the tube was transferred to the laminar flow hood. When fully thawed, the cell suspension was quickly pipetted into an appropriately sized flask containing pre-warmed culture medium, the contents mixed and transferred to a humidified incubator at the correct temperature for the cell-type in question. Culture media was changed after 24 hours in order to remove DMSO-containing cryopreservation media.

2.16.5 Confirmatory phenotyping of podocytes

Culture conditions used for podocytes during proliferation and differentiation differed from previous published protocols; cells were routinely cultured in a low glucose (4mM) basal medium without the addition of the insulin / transferrin / selenium (ITS) supplement. As such, the following tools were used to characterize the phenotype of the cells and confirm podocyte differentiation prior to use: assessment of cell morphology by phase-contrast microscopy; immunofluorescent cytostaining for nephrin and podocin expression; Western blot analysis of SV40 T-antigen expression.

2.16.6 Treatment of cells

The core cell culture model used to simulate the diabetic milieu was the same for all cell types (Figure 2.12). Experiments were performed after cells had been plated into multi-well plates and had reached >70% confluence. In the case of podocytes, cells had also undergone a 2 week period of differentiation at 37^{o}C.

Medium was removed and replaced in all cases with glucose-free RPMI 1640 supplemented with 4mM D-glucose with no serum. Unstimulated serum-free conditions were maintained for 24 hours to induce cell cycle synchronization and quiescence prior to treatment. All subsequent media used for experiments were serum-free.

Hyperglycaemic conditions were recreated by supplementing glucose-free RPMI 1640 with 30mM D-glucose, whereas 'normoglycaemic' media contained 4mM D-glucose. L-glucose, the metabolically inactive stereoisomer of D-glucose, was added to normoglycaemic media at a concentration of

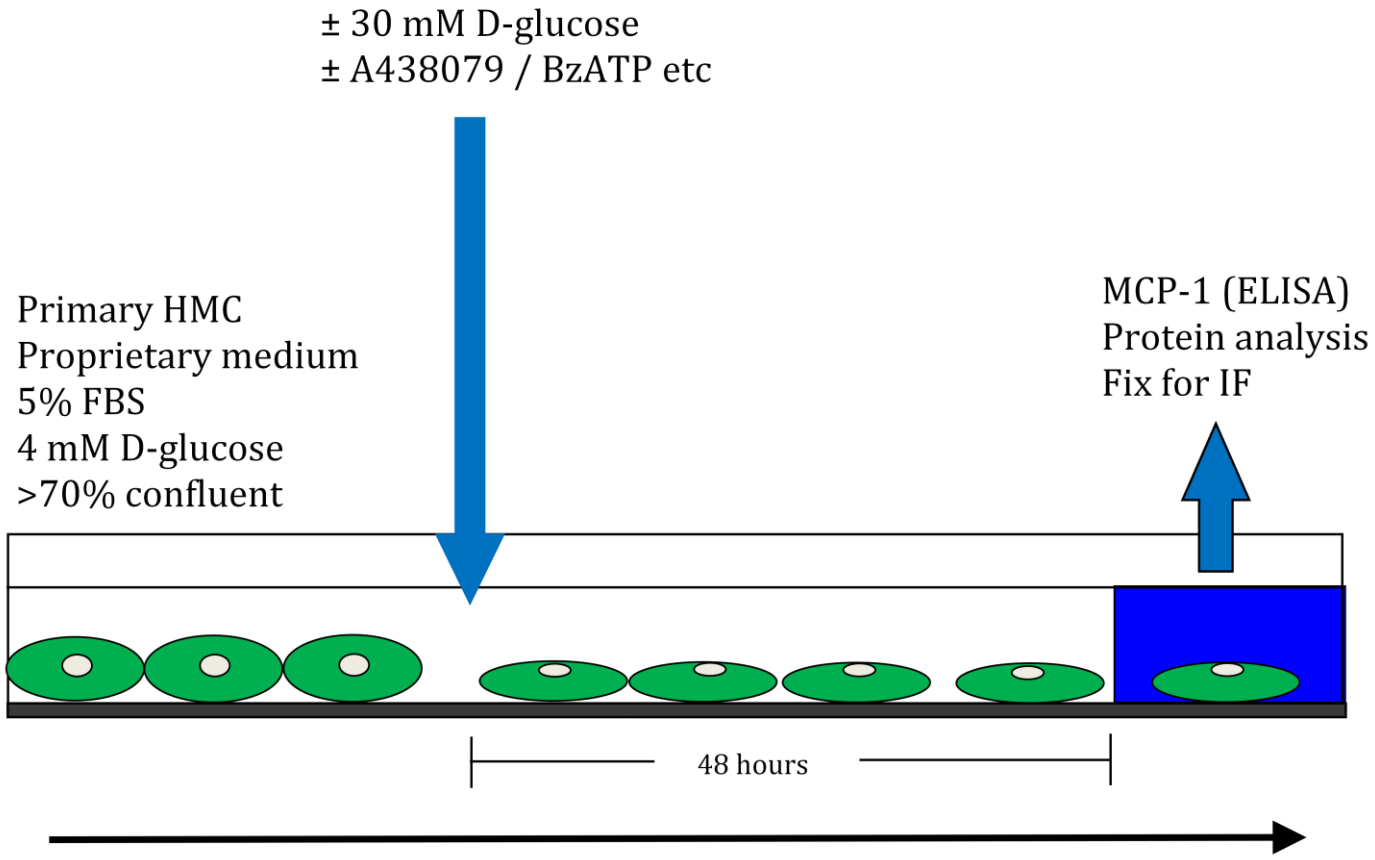

Figure 2.12 Basic schema of *in vitro* model used to assess the P2X7-dependence of hyperglycaemia-induced MCP-1 release from primary HMCs. The same protocol was employed for investigations in transformed HMCs and podocytes. IF: Immunofluorescence.

26mM to act as an osmotic control for hyperglycaemic media. Cells were maintained in these conditions for 48 hours without a medium change, before collection of supernatants for cytokine analysis or cell monolayer lysates for protein extraction.

The effects of a selective P2X7 antagonist, A438079 (Tocris Bioscience, Bristol, UK), a P2X7 agonist BzATP, a selective P2X4 antagonist, 5-BDBD (Tocris), a P2Y2 / P2Y4 agonist UTPγS (Tocris) and an ATP-hydrolyzing agent, apyrase, on MCP-1 production were tested both in the presence and absence of hyperglycaemia by supplementing normoglycaemic and hyperglycaemic media respectively with the appropriate reagent concentration. The effect of ATP on pHMC IL1β release was tested by growing cells for 48 hours in either normoglycaemic or hyperglycaemic conditions and then replacing the medium with identical fresh medium supplemented with 5mM ATP. Cells were stimulated for 30 minutes before collecting supernatants.

2.16.7 Cell viability assay

Viability of pHMCs cultured in the presence of small molecule receptor inhibitors was assessed using a 3-(4,5-dimethylthiazol-2-yl)-5-(3-carboxymethoxyphenyl)-2-(4-sulfophenyl)-2H-tetrazolium, inner salt (MTS) assay (CellTiter 96; Promega, Madison, USA). Viable and metabolically active cells reduce MTS to a coloured soluble formazan product, the absorbance of which at 490nm is directly proportional to the number of living cells present in the culture system. It can thus be employed to assess viability or proliferative responses to substances under test.

pHMCs were subcultured in a 96-well plate at a seeding density of 2 x 10^4/well. Cells were allowed to proliferate to >70% confluence before replacing medium with serum-free medium for 24 hours. This was then replaced with normoglycaemic RPMI 1640 supplemented with the appropriate concentrations of inhibitor or drug vehicle and cultures incubated at 37^{o}C for 48 hours.

Medium was then removed and replaced with 100µl of MTS reagent and the plate returned to the 37^{o}C incubator for 1-2 hours, checking regularly for appropriate maturation of the colour reaction. The spectrophotometric absorbances of each well at 490nm were then analysed using a plate reader, and cell viability assessed by comparing the relative absorption compared to cells grown in basal medium alone in the absence of inhibitor or drug vehicle.

2.16.8 Immunofluroescent cytostaining

Immunofluorescent labelling was used for the detection of P2X7 protein in pHMCs and nephrin and podocin in podocytes. The core principles of this technique are similar to those described for immunohistochemical analysis of tissue sections (Section 2.10): a specific primary antibody is applied to bind the protein of interest, before adding a species-specific anti-immunoglobulin secondary antibody, in this case coupled to a light-emitting fluorophore. Fluorescence microscopy can then be used to detect and visualise expression of the protein of interest.

2.16.8.i Culture of cells for immunofluorescence

Standard tissue culture plastic autofluoresces between 360 and 620nm, the excitation range for commonly used fluorescent dyes, and is hence not suitable for this application. Cells must therefore be grown on a glass surface to circumvent this. Glass coverslips were coated with poly-L-lysine to improve cell adherence, and sterilised by baking at 200^{O}C for 3 hours in an oven. Coverlips were then placed into the bottom of wells of a plastic 24-well plate before subculturing cells to the plate as normal. Once cell adhesion had occurred, further cell culture, experimental treatments and initial immunofluorescence protocol steps were performed with the cell-coated coverslips remaining inside the culture plate.

2.16.8.ii Cell fixation and permeabilisation

After completing experimental incubations, medium was removed and cells washed twice with PBS. A solution of 4% paraformaldehyde (PFA) in PBS was then added to wells, the plate covered and left for 5 minutes in the fume cupboard. PFA acts as a fixative to preserve cellular morphology during subsequent steps. PFA was then aspirated from wells and the cells washed a further 3 times with PBS.

To permit access of primary antibody to the intracellular compartment in addition to the exterior surface of the cell membrane, a permeabilisation step is required. To achieve this, 1ml 0.1% Triton x100 in PBS was added to cells and incubated for 10 minutes before washing twice with PBS. Triton is a detergent and has a non-selective disruptive effect on membrane lipid, producing holes through which antibody may pass.

2.16.8.iii Blocking and antibody application

Non-specific binding sites were blocked by incubation with 5% BSA in 0.1% Triton in PBS for 1 hour at room temperature. This was aspirated and the primary antibody or control (polyclonal IgG or diluent alone) applied for a duration optimised for each antibody (Table 2.7). Cells were then washed 3 times in PBS for 5 minutes each before incubating with a fluorochrome-conjugated secondary antibody diluted in 5% BSA in 0.1% Triton in PBS for 1 hour in the dark.

2.16.8.iv Mounting and microscopy

Cells were washed 3 times in PBS for 5 minutes each. One drop of mounting media with DAPI (a nuclear stain; Vector labs, Peterborough, UK) was placed on a microscope slide and the glass coverslip was carefully transferred on to it. Nail varnish was used to seal the edges of the coverslip ready for microscopy viewed through the appropriate narrow-band filter.

2.17 Statistical analysis

All values described in the text and figures are expressed as mean ± standard deviation. Statistical analysis was carried out by GraphPad Prism 6.02 (GraphPad Software, San Diego, CA). Numerical data comparing two groups were analyzed by the Student's *t*-test for parametric data and Mann-Whitney U test for non-parametric data. Categorical data comparing two groups were analysed with Fisher's exact test.

Data comparing more than two groups were analysed by one-way ANOVA with post-tests corrected by the Bonferroni method for multiple

Target Protein (Species)	Blocking Solution	Primary antibody	Primary dilution (Time)	Secondary antibody
P2X7 (H)	5% BSA Triton 0.1% in PBS	Ab109246 (Abcam) Rabbit monoclonal	1:200 (O/N)	Alexa 488-conjugated goat anti-rabbit (Invitrogen)
Nephrin (H)	5% BSA Triton 0.1% in PBS	SC19000 (Santa Cruz) Goat polyclonal	1:200 (O/N)	FITC-conjugated mouse anti-goat Ab (Sigma)
Podocin (H)	5% BSA Triton 0.1% in PBS	Ab65291 (Abcam) Rabbit polyclonal	1:200 (O/N)	Alexa 488-conjugated goat anti-rabbit (Invitrogen)

Table 2.7. Antibodies used for immunofluorescent labelling of cell monolayers. O/N: overnight; H: human.

comparisons for parametric data, and Kruskal-Wallis with Dunn's post-test for non-parametric data. Outlying values, clearly inconsistent with a population's distribution, were confirmed as such using the robust regression and outlier removal (ROUT) method (Graphpad Software), and excluded from subsequent analysis. Where oulying values have been excluded this is clearly described in the figures and/or text.

$P < 0.05$ was considered to be significant. *,** and ***, used in figures, denote p values of <0.05, <0.01 and <0.001 respectively. NS (not significant) denotes a p value >0.05.

CHAPTER 3

Expression of P2X7 in human diabetic nephropathy

3.1 Introduction

P2X7 is expressed at very low levels in rodent kidney under normal conditions (Turner et al., 2003). Upregulation in glomeruli has been demonstrated in the mouse model of nephrotoxic nephritis, where P2X7 has been shown to play an important role in pathogenesis of glomerular inflammation (Turner et al., 2007b, Taylor et al., 2009). Glomerular upregulation, predominantly within the podocyte, has also been shown in STZ-induced diabetes in the rat and ren-2 transgenic hypertensive rats, although the functional significance of these findings has not yet been tested (Vonend et al., 2004).

Few studies, however, have examined P2X7 expression within the human kidney. In this chapter, I have sought to examine the expression of P2X7 in human renal biopsy tissue using a specific and contemporary anti-P2X7 antibody, and, in particular, in renal tissue from patients with biopsy-proven DN, to test the hypothesis that P2X7 may be upregulated in human disease in a manner analogous to that seen in animal models.

3.2 Results

3.2.1 P2X7 is constitutively expressed in human renal tubular epithelium

Renal biopsy tissue from 4 patients with thin basement membrane (TBM) lesion was probed with a rabbit polyclonal antibody raised against an epitope in the C-terminal domain of P2X7 (Table 3.1 and Figure 3.1). TBM typically represents the carrier state for autosomal recessive Alport Syndrome, a hereditary nephropathy due to a mutation in basement membrane collagen, but which is only rarely associated with progressive renal impairment (Savige et al., 2013). TBM represents a benign lesion in the majority of patients, manifesting as isolated microscopic haematuria with normal renal function and normal renal architecture other than GBM thinning.

Glomerular immunoreactivity for P2X7 was observed in only 1 of 4 patients with TBM, while no P2X7-positive cells were identifiable in the interstitium in any biopsy (Figure 3.1A). Of note, the patient in whom glomerular P2X7 staining was apparent had a reduced eGFR, proteinuria (urinary PCR 33mg/mmol) and evidence of mild mesangial expansion, suggesting possible occult DN. Three of 4 patients had pronounced tubular staining which appeared morphologically to be restricted to distal tubules (Figure 3.1B).

Renal tissue from one patient with class IV proliferative lupus nephritis was also examined and showed focal glomerular staining for P2X7 (Figure 3.1C), corroborating published data (Turner et al., 2003).

Category	Age / Sex	DM type	Serum Creatinine (µmol/l)	eGFR (mls/min)	uPCR (mg/mmol)	% Fibrosis on biopsy	Mesangial Expansion	P2X7 Staining		
								Glomerulus	Tubules	Interstitium
TBM	65 / F	N/A	101	48	33	<5	Mild	+	+	-
	35 / M	N/A	104	76	6	0	None	-	+	-
	58 / M	N/A	57	>90	n	5	None	-	+	-
	33 / M	N/A	88	>90	n	0	None	-	-	-
DN (G-)	42 / F	2	339	13	2155	90	Severe	-	+	+
	54 / M	n	151	42	n	90	Severe	-	+	+
	52 / M	2	160	40	1500	60	Severe	-	+	+
	75 / M	2	405	13	n	80	Mild	-	+	+
	77 / M	n	440	11	n	30	Mild	-	-	+
	66 / M	2	102	63	240	15	Severe	-	+	-
	51 / M	2	78	90	90	5	Mild	-	+	+
	61 / M	2	88	76	80	30	Severe	-	+	+
	31 / F	1	131	41	n	10	Severe	-	+	+
	58 / M	2	126	51	100	15	Mild	-	+	-
	50 / M	2	322	17	654	75	Severe	-	+	+
	62 / M	2	310	18	1246	75	Severe	-	+	+
	67 / M	2	200	29	100	20	Mild	-	+	+
	50 / M	2	268	22	n	60	Severe	-	+	+
DN (G+)	51 / M	1	80	89	295	20	Mild	+	+	-
	67 / M	n	230	25	180	30	Mild	+	+	+
	69 / M	2	114	59	150	25	Mild	+	+	-
	59 / M	n	165	37	0	15	Mild	+	+	+
	63 / F	2	99	66	0	10	Mild	+	+	+
	55 / M	2	199	30	n	50	Mild	+	+	+
	59 / M	n	228	26	n	75	Mild	+	-	-
	72 / M	n	219	26	n	25	Mild	+	+	+
	70 / M	2	112	56	n	15	Mild	+	+	+
	67 / M	2	138	47	18	15	Mild	+	+	-
	77 / M	n	193	30	n	15	Mild	+	+	+
	51 / F	2	156	30	950	30	Severe	+	+	+
	35 / M	2	93	89	n	10	Mild	+	+	+
	56 / M	n	110	60	16	10	Severe	+	+	-
	66 / M	2	230	25	0	30	Severe	+	+	+
	57 / M	n	260	22	n	10	Mild	+	+	+

Table 3.1 Immunohistochemistry for P2X7 on human biopsy tissue: patient clinical data. G+: positive glomerular staining for P2X7; G-: negative glomerular staining for P2X7; n: data not available.

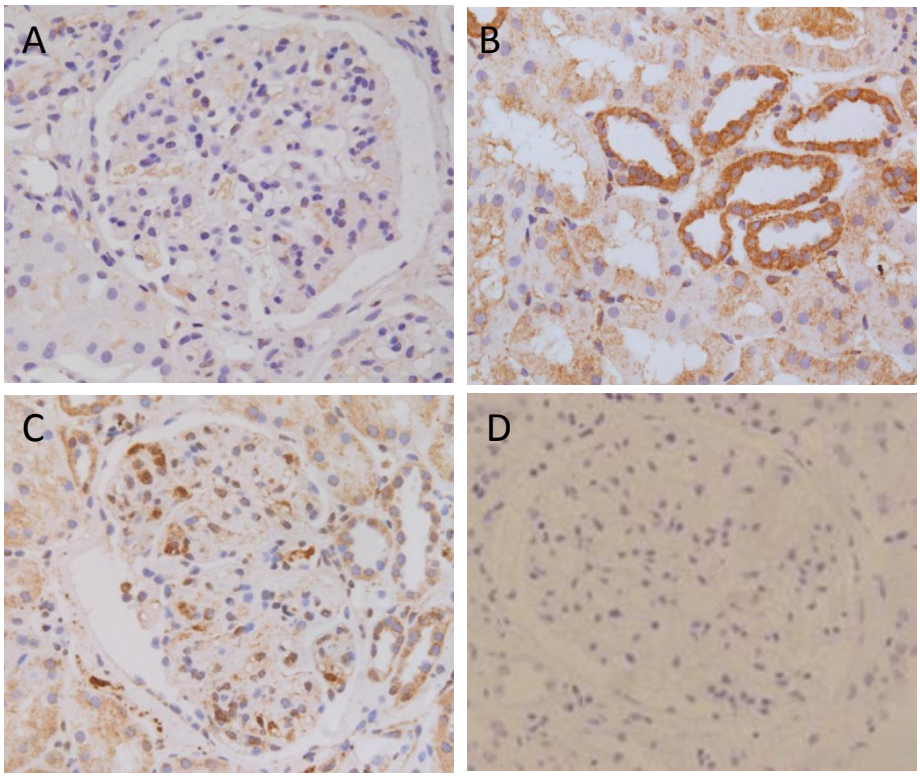

Figure 3.1. Immunohistochemistry for P2X7 in Thin Basement Membrane disease and Lupus Nephritis A: Typical appearance of a glomerulus from a patient with TBM lesion, with no appreciable P2X7 staining. B: Tubular appearance in TBM disease. Marked P2X7 expression (brown) was seen in a subset of tubular epithelial cells with characteristics of distal tubule (thin cuboidal epithelium with little brush border and open lumens), while minimal proximal tubular staining was seen. C: Glomerulus from a patient with class IV proliferative lupus nephritis. Numerous P2X7 positive cells were present, scattered focally within the glomerulus, consistent with a previous published report.(Turner et al., 2007b) D: Control with omission of primary antibody. (Magnification: x200)

3.2.2 P2X7 expression is upregulated in glomeruli and interstitial cells in a subset of patients with DN

Renal biopsy tissue from 30 patients with biopsy-confirmed DN, predominantly due to type 2 diabetes, was also examined for P2X7 expression (Table 3.1 and Figure 3.2). Twenty-seven of 30 patients showed evidence of distal tubular staining, in keeping with that observed in patients with TBM (Figure 3.2A). Glomerular immunoreactivity was present in 16/30 patients, either as granular circumferential deposits around capillary loops or more focally within the glomerulus (Figure 3.2B). The intensity of glomerular P2X7 staining frequently varied between glomeruli within the same biopsy. The majority of patients (23/30) had evidence of P2X7-positive cells within the interstitum, often in areas of established tubular atrophy where a significant number of infiltrating inflammatory cells were apparent (Figure 3.2C). Glomerular and interstitial P2X7 staining were not mutually exclusive, co-existing in 11/30 patients.

Immunohistochemistry for CD68, a macrophage marker, was performed on two patient biopsies, one with significant glomerular P2X7 immunoreactivity and the other with predominantly interstitial P2X7 expression, to compare the relative pattern and extent of staining (Figure 3.3). In both cases, P2X7 staining was substantially more widespread than CD68, suggesting that P2X7 expression is not explained solely by infiltration of P2X7-positive macrophages.

3.2.3 Glomerular P2X7 expression is a feature of early clinical DN

Clinical and histological makers of disease severity were compared between patients with or without evidence of appreciable glomerular or interstitial

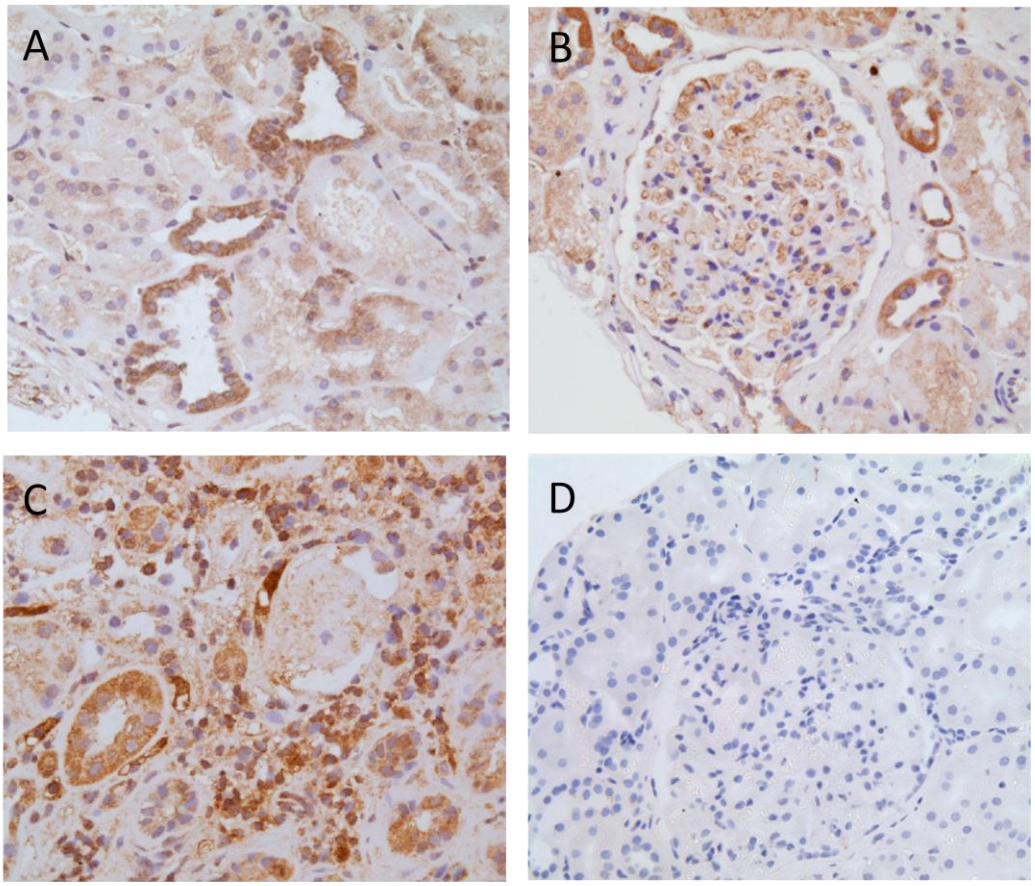

Figure 3.2 Immunohistochemistry for P2X7 in Diabetic Nephropathy. A: Typical appearance of tubules in DN. Distal tubular P2X7 expression was observed in 27 of 30 biopsies, in a pattern identical to patients with TBM. Minimal proximal tubular staining was seen. B: Glomerular P2X7 expression in DN. 16 of 30 patients had appreciable glomerular P2X7 expression. C: P2X7-positive interstitial cells in a patient with DN. Clusters of positively-stained cells were frequently observed in areas of tubular atrophy as part of a wider inflammatory infiltrate. D: DN biopsy tissue probed with P2X7 antibody after prior incubation with the specific immunising peptide in a 1:1 ratio. (x200 magnification)

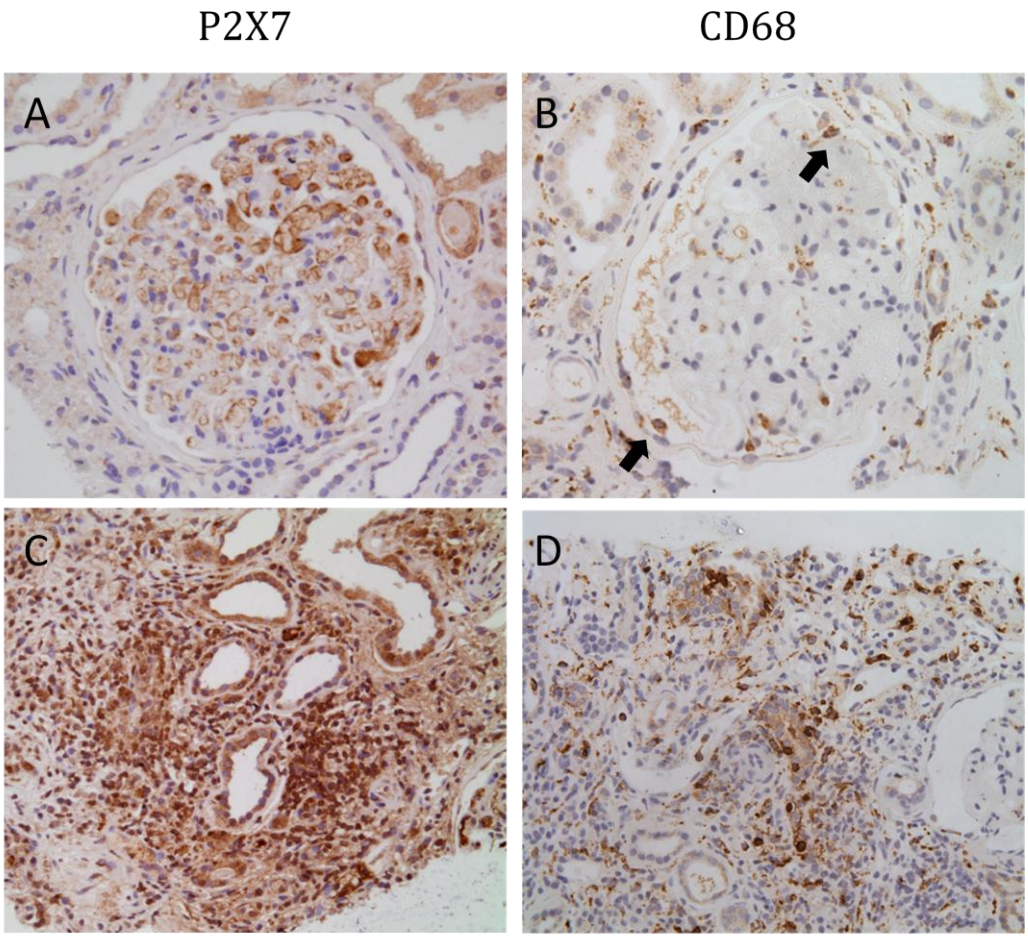

Figure 3.3 Comparison of P2X7 and CD68 Immunohistochemistry in Diabetic Nephropathy. A: Glomerulus from a patient with DN exhibiting significant P2X7 immunoreactivity. B: Glomerulus from the same patient as A stained for CD68. CD68 positive cells (arrows) are much more limited in distribution than P2X7. C: Tubulointerstitium of patient with DN exhibiting numerous P2X7-positive cells in a region of marked tubular atrophy. D: Biopsy from the same patient stained for CD68. CD68-positive cells are again much more limited in distribution than cells expressing P2X7, suggesting that P2X7 expression is not confined to macrophages within the interstitium. (A,B: Magnification x200; C,D: Magnification x100)

cell P2X7 staining. (Table 3.2 and Figure 3.4). A trend towards lower values of proteinuria, serum creatinine, and % interstitial fibrosis on biopsy was apparent in patients with positive glomerular immunoreactivity compared to those with absent glomerular staining (Figure 3.4A,C,E and G). The opposite trend was seen in those patients where interstitial P2X7-positive cells were present, with higher values of the same variables compared to those with absent interstitial staining, reaching statistical significance for serum creatinine (Figure 3.4B,D,F and H).

Six % of patients with positive glomerular P2X7 expression had a serum creatinine >250μmol/l compared to 43% of those without glomerular P2X7 staining. Similarly 11% of patients with glomerular P2X7 expression had a uPCR ≥300 mg/mmol, compared to 56% without, while 6% of patients with glomerular P2X7 staining had an interstitial fibrosis score of ≥50% compared to 50% of patients without.

3.3 Discussion

In this chapter, the expression of P2X7 within the human kidney has been examined by immunohistochemistry, employing an antibody specific to the intracellular C-terminal receptor domain. By this approach, near-ubiquitous constitutive expression of P2X7 in human distal tubule was observed, comparable to that found in both mice and rats (see Chapters 5 and 6). No appreciable glomerular expression was present in the majority of subjects with TBM, while P2X7-positive cells were found in both the glomerulus and interstitium in a subset of patients with DN.

Few studies have previously examined the expression of P2X7 in human kidney. In one study, a small number of nephrectomy specimens from

Glomerular staining	Positive	Negative	P value
% Type 2 DM	88.9% (n=9)	91.7% (n=12)	N/A
Creatinine (µmol/l)	164.1 ± 59.1 (n=16)	222.9 ± 122.3 (n=14)	0.098
eGFR (mls/min)	44.8 ± 22.6 (n=16)	37.6 ± 25.0 (n=14)	0.411
uPCR (mg/mmol)	194.8 ± 301.8 (n=9)	765.0 ± 735.9 (n=9)	**0.047**
% Fibrosis	24.1 ± 17.3 (n=16)	46.8 ± 31.8 (n=14)	0.063

Interstitial staining	Positive	Negative	P value
% Type 2 DM	93.8% (n=16)	80% (n=5)	N/A
Creatinine (µmol/l)	210.8 ± 100.6 (n=23)	128.3 ± 47.6 (n=7)	**0.042**
eGFR (mls/min)	36.9 ± 23.3 (n=23)	56.4 ± 19.0 (n=7)	**0.032**
uPCR (mg/mmol)	639.6 ± 710.9 (n=12)	160.5 ± 98.5 (n=6)	0.567
% Fibrosis	37.6 ± 28.3 (n=23)	25.0 ± 22.6 (n=7)	0.312

Table 3.2 Clinical disease parameters in patients with DN with or without appreciable P2X7-positive glomerular or interstitial cells. Glomerular and interstitial staining were not mutually exclusive, co-existing in 11/30 patients studied. Complete datasets were available for serum creatinine and eGFR; unattainable data for uPCR and diabetes category analyses are reflected in reduced n values. Statistically significant p values are shown in bold.

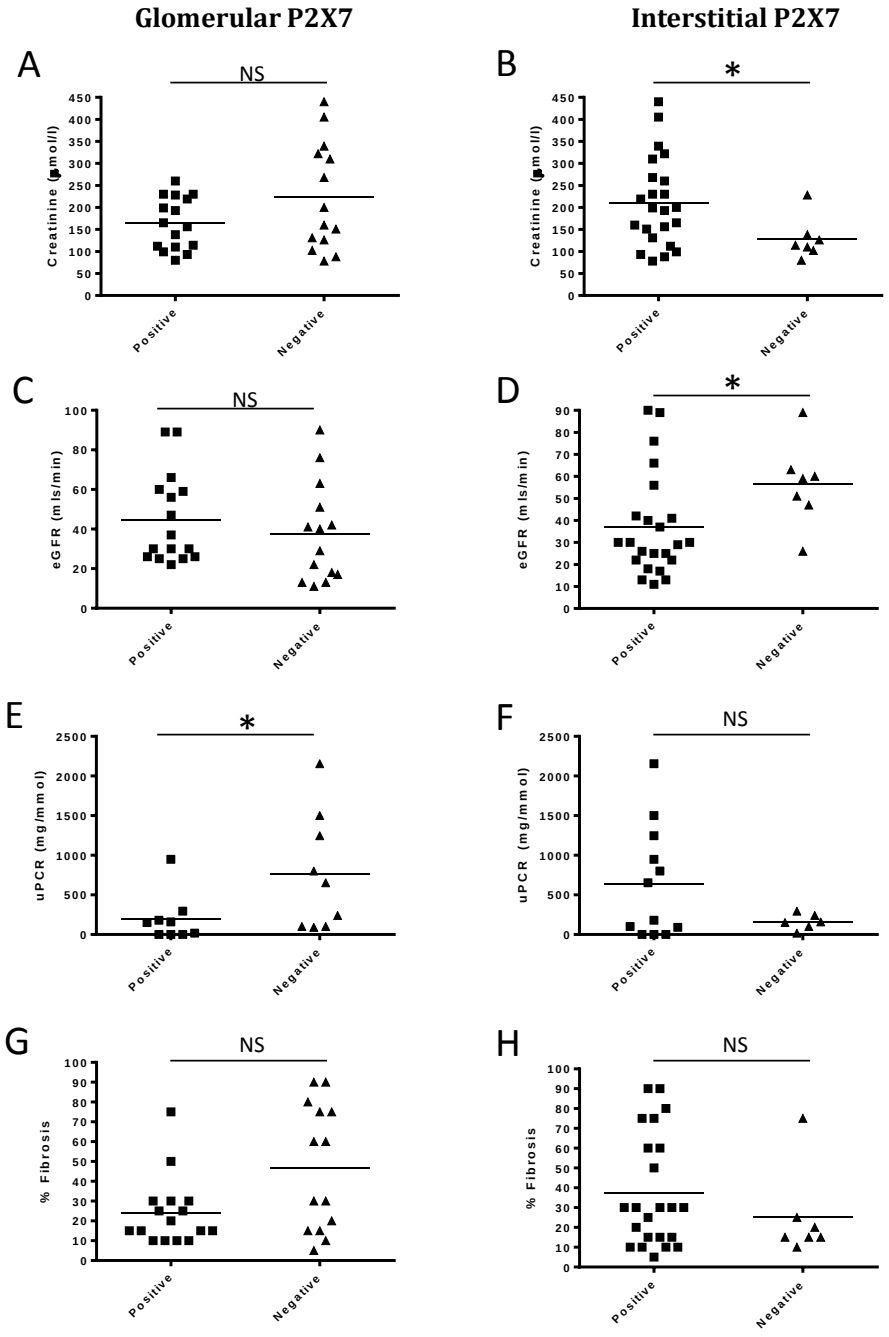

Figure 3.4 Clinical disease parameters in patients with DN with or without appreciable P2X7-positive glomerular or interstitial cells. A, C, E, G: Comparing patients with (positive) or without (negative) P2X7-positive glomerular cells. B, D, F, H: Comparing patients with or without P2X7-positive interstitial cells. A,B: Serum creatinine; C,D: eGFR; E,F: uPCR; G,H: % Interstitial fibrosis. . *: $p<0.05$; NS: Not significant.

patients with carcinoma and cadaver donor kidneys unsuitable for transplantation, were probed with an antibody raised against the C-terminal domain of P2X7 (a different antibody to that used in the current study), and 'very little immunoreactivity' was reportedly detectable in tubules or glomeruli (Turner et al., 2003). Nine patients with lupus nephritis (6 'proliferative' and 3 'membranous') were also examined with the same antibody and receptor protein expression was found in all patients, predominantly within glomeruli. P2X7 expression has also been demonstrated in human foetal ARPKD renal cyst epithelium (Hillman et al., 2002). Of note, P2X7 is highly expressed in a number of immune cells in humans, including the macrophage, capable of infiltrating the kidney during injury (North, 2002).

Another recent study has investigated the expression of P2X7 in kidney specimens from patients with type 2 diabetes (Solini et al., 2013). This study examined P2X7 expression in nephrectomy specimens from 6 patients with metabolic syndrome, DN and concomitant renal cancer, and 3 non-diabetic controls. A different antibody (Ab48871, Abcam) was used, recognising an 'internal region' of P2X7, and for which 'human kidney tissue' is stated on the datasheet as a positive control. Increased renal cortical and glomerular expression of P2X7 was observed, pictured in a focal distribution. No appreciable staining, either glomerular or tubular, was seen in the pictured control specimen.

In the present study, the finding that P2X7 is upregulated within the glomerulus of some patients with DN is consistent with published data examining expression during experimental diabetes in the rat (Vonend et al., 2004). The preponderance of glomerular staining in patients with early clinical DN also corresponds well with rodent experimental findings presented in this thesis, where glomerular expression is upregulated at an early time-point in rat models of DN due to both type 1 and 2 diabetes, and

also DN due to type 1 diabetes in the mouse (Chapters 5 and 6). Glomerular staining was typically granular and located circumferentially around capillary loops in patients with DN, as opposed to the more focal reactivity observed in proliferative lupus nephritis, although focal staining was also apparent in some diabetic subjects. Although the cell types expressing P2X7 have not been formally established, the widespread glomerular distribution compared to the relatively sparse presence of CD68+ macrophages, suggests expression in resident glomerular cells, presumably either capillary endothelial cells or podocytes. Examination of expression by immuno-gold electron microscopy in diabetic rats has suggested predominant podocytic expression in experimental disease (Vonend et al., 2004).

While patients with positive glomerular immunostaining for P2X7 had, as a group, earlier clinical DN than those without, this association was not entirely specific. Further work looking longitudinally at patients with or without glomerular P2X7 staining is required to determine whether this impacts on clinical outcomes.

In summary, P2X7 is expressed constitutively in human distal tubules and is upregulated in glomerular and interstitial compartments in a subset of patients with DN; as a group, patients with glomerular P2X7 expression have earlier clinical disease than those without. These immunohistochemical findings correspond well with those seen in rodent kidney during experimental diabetes and hence bode well for translation of findings from animal models to human disease.

CHAPTER 4

Investigating the role of P2X7 in the induction of murine diabetes using streptozotocin

4.1 Introduction

Streptozotocin (STZ) is commonly used to produce a phenotype of type 1 diabetes in experimental mice and rats. Taken up into pancreatic β-cells via the GLUT-2 receptor, STZ causes alkylation of DNA and subsequent cellular necrosis and death. Administration as a repetitive low dose regime in mice results in reduced renal bystander toxicity and also pancreatic injury, but the latter is augmented by a secondary auto-immune insulinitis with an inflammatory infiltrate comprising lymphocytes and macrophages, with similarities to that seen in human type 1 diabetes (Like et al., 1978, In't Veld, 2011). This model also has relevance to the pathogenesis of human type 2 diabetes, where initial hyperinsulinaemia and β-cell hypertrophy is succeeded by β-cell loss, with many patients consequently requiring treatment with exogenous insulin.

P2X7 has well-defined roles in inflammatory cytokine secretion from macrophages, and genetic deficiency or inhibition of the receptor in models of inflammatory disease often reduce accumulation of this cell type at the site of injury (Goncalves et al., 2006, Taylor et al., 2009). P2X7 is also expressed in T cells and has been implicated in proliferation and effector functions of these cells (Lang et al., 2010). P2X7 expression has been demonstrated in human pancreatic β-cells with upregulation observed in obese subjects and reduction of expression in patients with overt diabetes (Glas et al., 2009).

However, previous studies of the functional role of P2X7 in pathogenesis of diabetes in animal models have produced conflicting results (Glas et al., 2009, Lang et al., 2010, Chen et al., 2011).

I have sought to address the question of the role of P2X7 in β-cell injury by studying the effect of low dose STZ on diabetes induction in mice genetically lacking the P2X7 receptor. Two strains of P2X7 KO mouse with differing profiles of residual receptor expression (GSK and Pfizer) were examined, with pancreatic tissue available for analysis in the Pfizer mice.

4.2 Results

4.2.1 GSK KO mice show partial protection against STZ-induced pancreatic toxicity and a less severe disease course

Tail vein blood glucose (BG) was measured 3 weeks after the final injection of STZ and a non-fasting value of ≥16 mmol/l was considered diabetic. Physical and biochemical data at baseline and week 3 is summarised in Table 4.1. Early mortality (<3 weeks, before measurement of BG) was similar in WT STZ and KO STZ-injected animals (14.7% vs 10%; p=1.0). (Figure 4.1A) A higher proportion of WT STZ-injected animals developed diabetes than KO (83% vs 72%; p=0.47) (Figure 4.1B). BG was significantly higher in both STZ groups compared to their corresponding vehicle-injected controls, but only marginally higher in WT STZ animals compared to KO mice (WT 23.4 ± 8.4 vs KO 22.2 ± 7.3 mmol/l; p>0.05, Kruskal-Wallis with Dunn's post-test; Figure 4.1C). Glucometer readings were capped at 33.3 mmol/l, however, and 17% of WT STZ-injected animals had BG values >33.3 compared to 0% of the KO group (p=0.14; Figure 4.1D). A greater proportion of diabetic WT animals subsequently developed severe disease after the 3 week time-point, causing death or necessitating early culling (33% WT vs 15% KO; p=0.44), although a

	WT Vehicle	WT STZ	KO Vehicle	KO STZ
Age (m)	9.9 ± 1.9 (n=15)	10.0 ± 2.0 (n=34)	9.4 ± 1.2 (n=8)	9.9 ± 1.3 (n=20)
Baseline weight (g)	36.2 ± 3.7 (n=15)	36.3 ± 3.5 (n=34)	37.6 ± 4.8 (n=8)	36.4 ± 3.6 (n=20)
% Weight loss (Wk 0 to Wk3)†	1.3 ± 4.3 (n=13)	13.6 ± 7.0[a] (n=29)	2.0 ± 4.6 (n=8)	11.0 ± 3.9[b] (n=18)
Baseline BG*	8.0 ± 2.0 (n=13)	8.5 ± 1.7 (n=23)	8.5 ± 2.5 (n=8)	8.4 ± 1.7 (n=9)
Wk 3 BG†	8.3 ± 1.8 (n=13)	23.4 ± 8.4[a] (n=29)	8.5 ± 2.7 (n=8)	22.2 ± 7.3[b] (n=18)

Table 4.1 Summary of physical data for GSK P2X7 KO mouse diabetes induction experiment. [a] p<0.001 vs WT vehicle; [b] p<0.001 vs KO vehicle; * Baseline blood glucose was measured in only a subset of animals; † Reduced sample numbers reflect deaths prior to week 3 measurements. BG: Blood glucose.

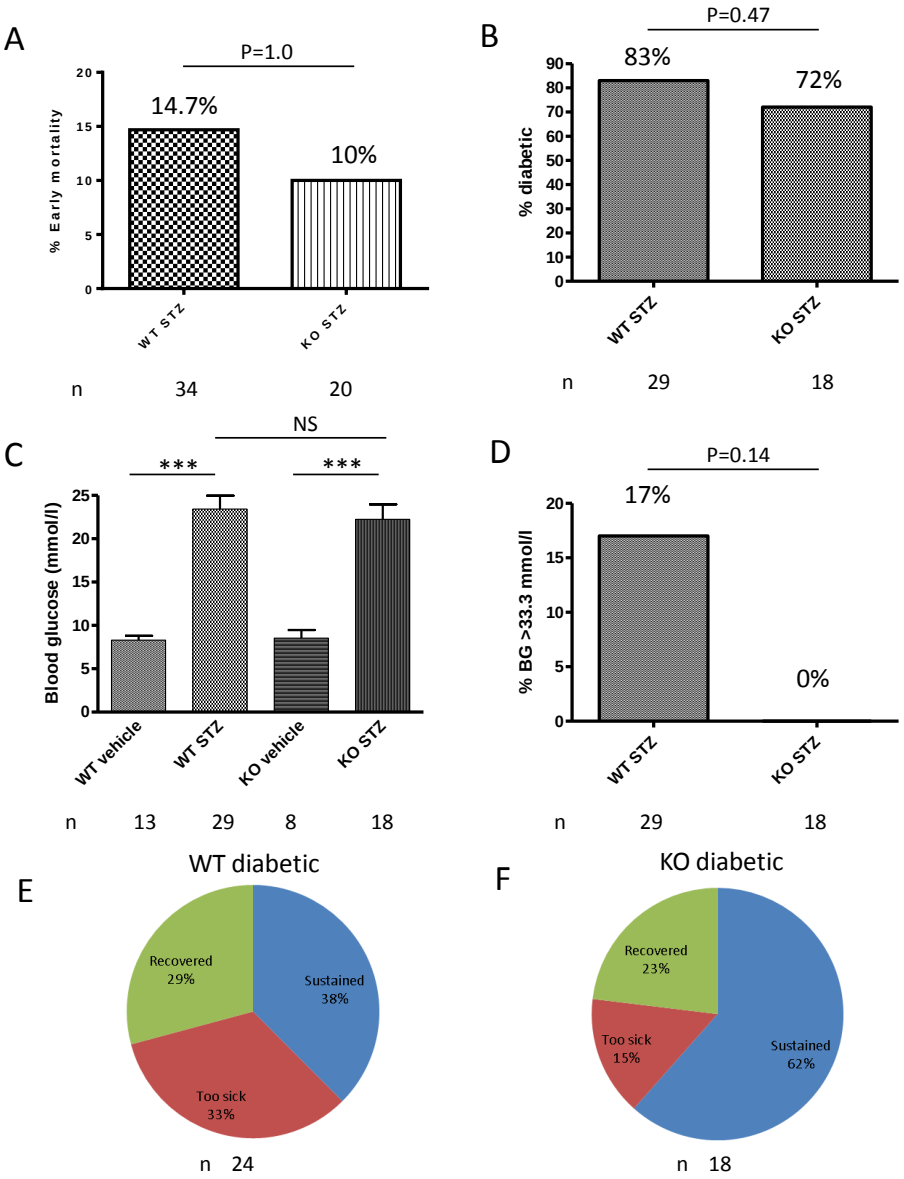

Figure 4.1 Induction of diabetes with STZ in C57BL/6 WT and GSK P2X7 KO mice. A: Early mortality (<3 weeks, prior to measurement of blood glucose). B: Percentage of WT and KO STZ-injected mice achieving a diabetic blood glucose (> 16 mmol/l) at 3 weeks, edited for death before 3 weeks. C: Blood glucose measured at 3 weeks. Although no significant difference was detected between WT and KO STZ-injected animals, blood glucose measurement was capped at 33.3 mmol/l, which may have masked the full effect. D: Percentage of WT and KO STZ-injected mice achieving a BG of >33.3 mmol/l (above range of glucometer) at 3 weeks. E,F: Proportion of animals diagnosed diabetic at 3 weeks which maintained sustained hyperglycaemia (16-33.3 mmol/l), became too sick (either dying or developing a BG >33.3 mmol/l) or spontaneously recovered to a BG <16 mmol/l). n: number of mice. ***: $p<0.001$; NS: Not significant.

correspondingly higher proportion of KO mice maintained a blood glucose in the target range (38% WT vs 62% KO; p=0.18) (Figure 4.1E,F). A similar proportion of both groups reverted to a non-diabetic BG on follow-up (29% WT vs 23% KO; p=1.0).

4.2.2 Pfizer KO mice show marked protection against STZ-induced pancreatic toxicity

Physical data at baseline and week 3 is summarised in Table 4.2. One animal from both STZ-injected groups died before the 3 week time point. Six out of seven (86%) WT STZ-injected mice achieved a diabetic BG compared to one out of six (17%) of KO STZ-injected animals (p=0.027; Figure 4.2A). BG was significantly higher in WT STZ than WT vehicle-injected animals (22.8 ± 7.0 vs 8.6 ± 1.0; $p<0.05$, Kruskal-Wallis with Dunn's post-test) but not so for KO STZ compared to KO vehicle-injected mice (14.1 ± 8.6 vs 8.5 ± 1.0; $p>0.05$) (Figure 4.2B). A trend towards reduced BG values was observed in KO STZ mice compared to WT STZ ($p>0.05$). Glucometer readings were again capped at 33.3 mmol/l and one out of seven (14%) WT mice had a BG in excess of this level compared to zero out of six STZ, obscuring the full magnitude of the difference between groups (Figure 4.2C).

To examine the possibility that P2X7 KO mice may be resistant to STZ-induced pancreatic damage due to reduced STZ uptake into β-cells, expression of GLUT-2 was assessed by specific immunohistochemistry (Figure 4.3). GLUT-2 staining was predominantly observed at the cell membrane in cells within the pancreatic islets, with no difference in the distribution between WT and KO mice.

	WT Vehicle	WT STZ	KO Vehicle	KO STZ
Age (m)	9.3 ± 1.3 (n=4)	9.5 ± 1.2 (n=8)	9.8 ± 0.5 (n=4)	9.6 ± 0.5 (n=7)
Baseline weight (g)	34.4 ± 2.1 (n=4)	32.9 ± 2.7 (n=8)	33.4 ± 4.3 (n=4)	31.8 ± 4.9 (n=7)
% Weight loss (Wk 0 to Wk 3)	-5.6 ± 2.4 (n=4)	1.9 ± 5.1[a] (n=7)	-1.0 ± 1.6 (n=4)	6.1 ± 5.4 (n=6)
Baseline BG	7.9 ± 1.2 (n=4)	8.7 ± 2.3 (n=8)	7.7 ± 0.4 (n=4)	8.2 ± 0.7 (n=7)
Wk 3 BG	8.6 ± 1.0 (n=4)	22.8 ± 7.0[b] (n=7)	8.5 ± 1.0 (n=4)	14.1 ± 8.6 (n=7)

Table 4.2 Summary of physical data for Pfizer P2X7 KO mouse diabetes induction experiment. [a] $p<0.05$ vs WT vehicle; [c] $p<0.01$ vs WT vehicle

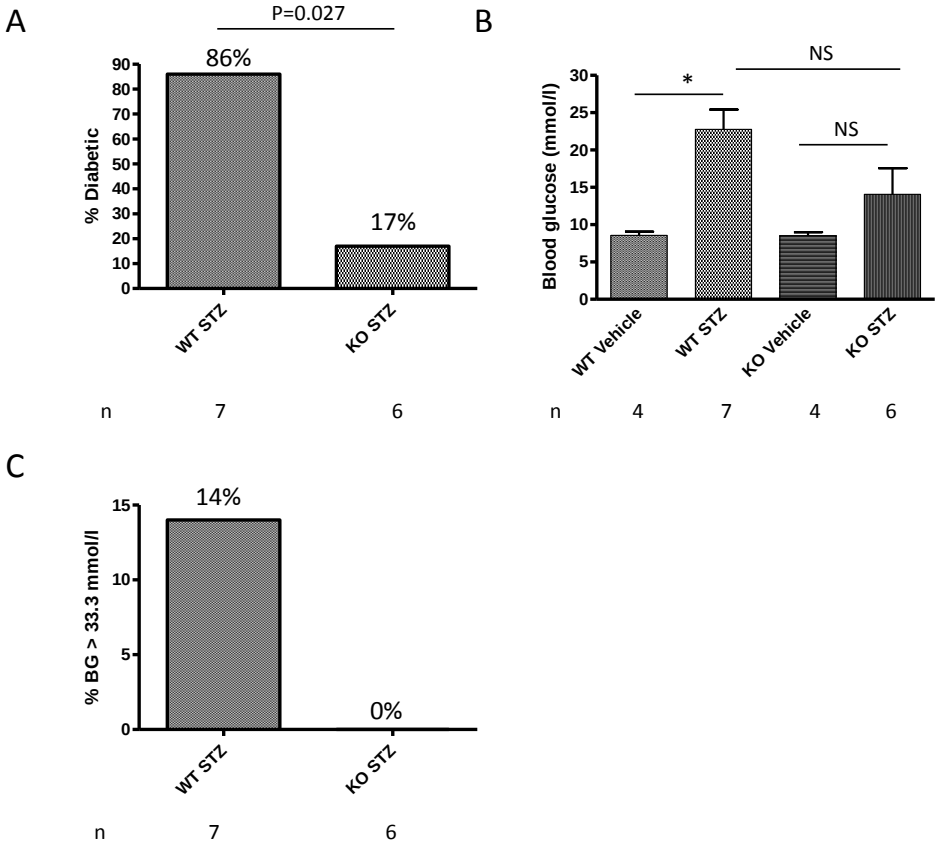

Figure 4.2 Induction of diabetes with STZ in C57BL/6 WT and Pfizer P2X7 KO mice. A: Percentage of WT and KO STZ-injected mice achieving a diabetic BG (>16 mmol/l) at 3 weeks, edited for death before 3 weeks. B: Blood glucose measured at 3 weeks. A trend towards lower BG was seen in the KO STZ group compared to WT STZ, and KO STZ BGs did not differ significantly from KO controls. Blood glucose measurement was capped at 33.3 mmol/l, which may have masked the full effect. C: Percentage of WT and KO STZ-injected mice achieving a BG of >33.3 mmol/l (above range of glucometer) at 3 weeks. . *: $p<0.05$; NS: Not significant.

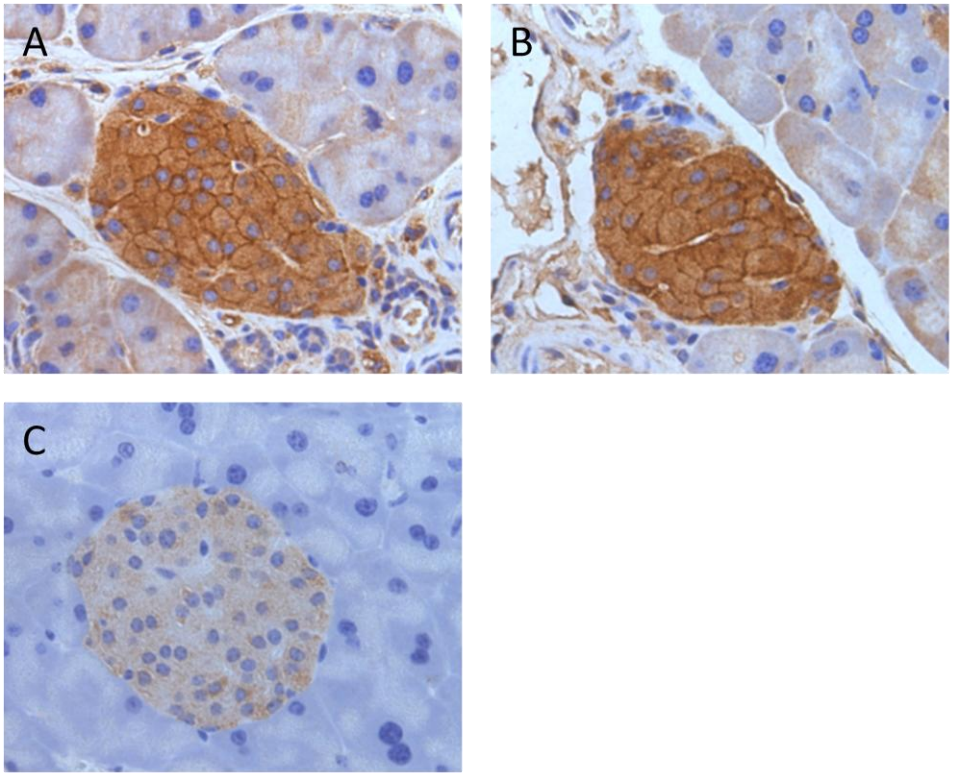

Figure 4.3 Immunohistochemistry for GLUT 2 in mouse pancreas. A: P2X7 WT islet. A cobblestone staining pattern was observed, reflecting predominant cell membrane localisation of GLUT 2. B: P2X7 Pfizer KO islet. The staining pattern was indistinguishable from WT tissue. C: WT islet with non-immune polyclonal IgG control staining.

4.2.3 Pfizer KO mice display preserved pancreatic islet architecture and beta cell density after STZ injection

No macroscopic abnormalities were apparent on light microscopy of islets from vehicle-injected KO mice compared to WT at 3 weeks post-injection (Figure 4.4A and C). Islets of WT STZ-injected mice appeared markedly abnormal with irregular outline, increased cellularity, early vacuolar degenerative change and rare central core necrosis (Figure 4.4B). Islets from KO STZ-injected mice more closely resembled normal architecture with minimal degenerative changes and only mild hypercellularity (Figure 4.4D).

Islet β-cell mass was assessed by specific immunohistochemistry for insulin (Figure 4.5). Islets from both WT and KO vehicle-injected animals showed uniform staining across the entire islet area (Figure 4.5A and C); a patchy reduction in the stained area was observed in WT STZ animals with a relatively preserved pattern in KO STZ mice, confirmed on semi-quantitative analysis of insulin-stained islet area (Figure 4.5B and D; WT STZ 2.52 ± 0.8 units vs KO STZ 3.34 ± 0.4; $p<0.05$). As expected, BG and insulin-stained area correlated well ($r^2= 0.75$, $p<0.001$).

4.2.4 P2X7 is expressed peripherally within the healthy mouse islet with central translocation after treatment with STZ

Expression of P2X7 within pancreatic islets was examined by specific immunohistochemistry (Figure 4.6). Islets from WT vehicle-injected mice showed peripheral decoration by P2X7-positive cells and minimal staining within the body of the islet (Figure 4.6A). Surrounding exocrine tissue displayed no staining. After STZ, the density of peripheral staining increased, with positive cells often layered 2 to 3 deep, with increased numbers of

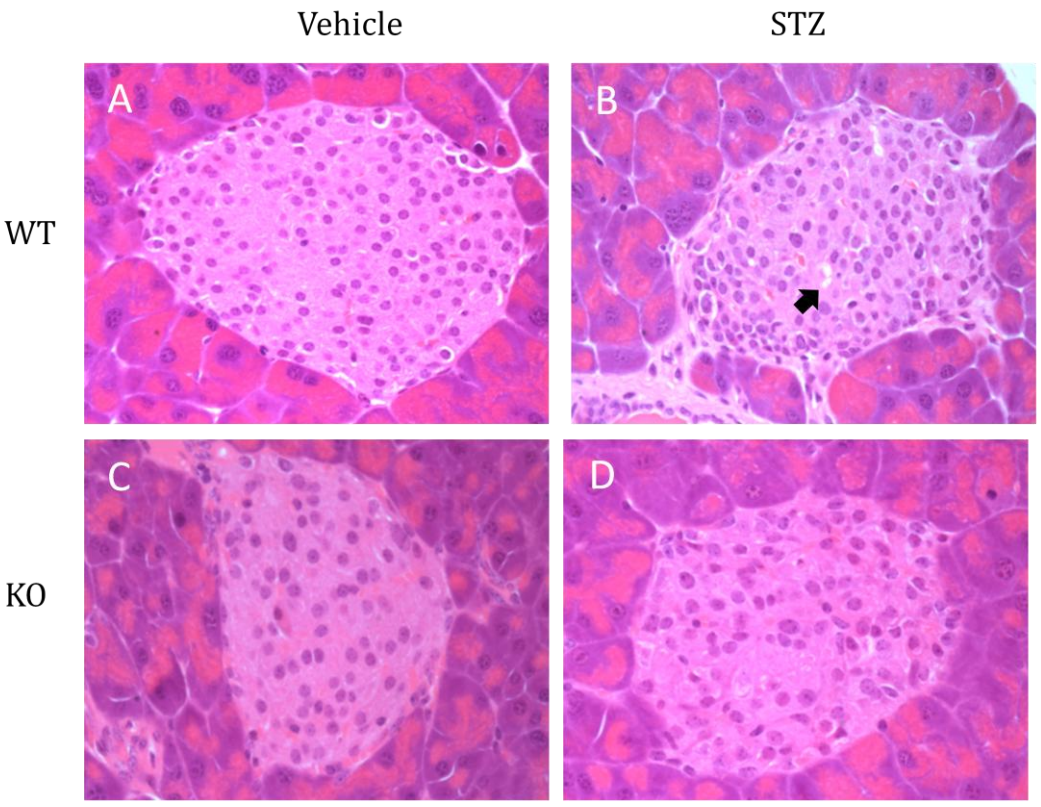

Figure 4.4 H+E stained sections of pancreatic tissue from WT and Pfizer P2X7 KO mice showing representative islets. A,C: Islets from both WT and KO vehicle treated control mice appeared uniform in architecture and cellularity. B: Islets from WT STZ mice showed evidence of early vacuolar degeneration (arrow) and a hypercellular appearance. D: Islets from KO STZ mice appeared largely protected from the abnormalities found in WT animals.

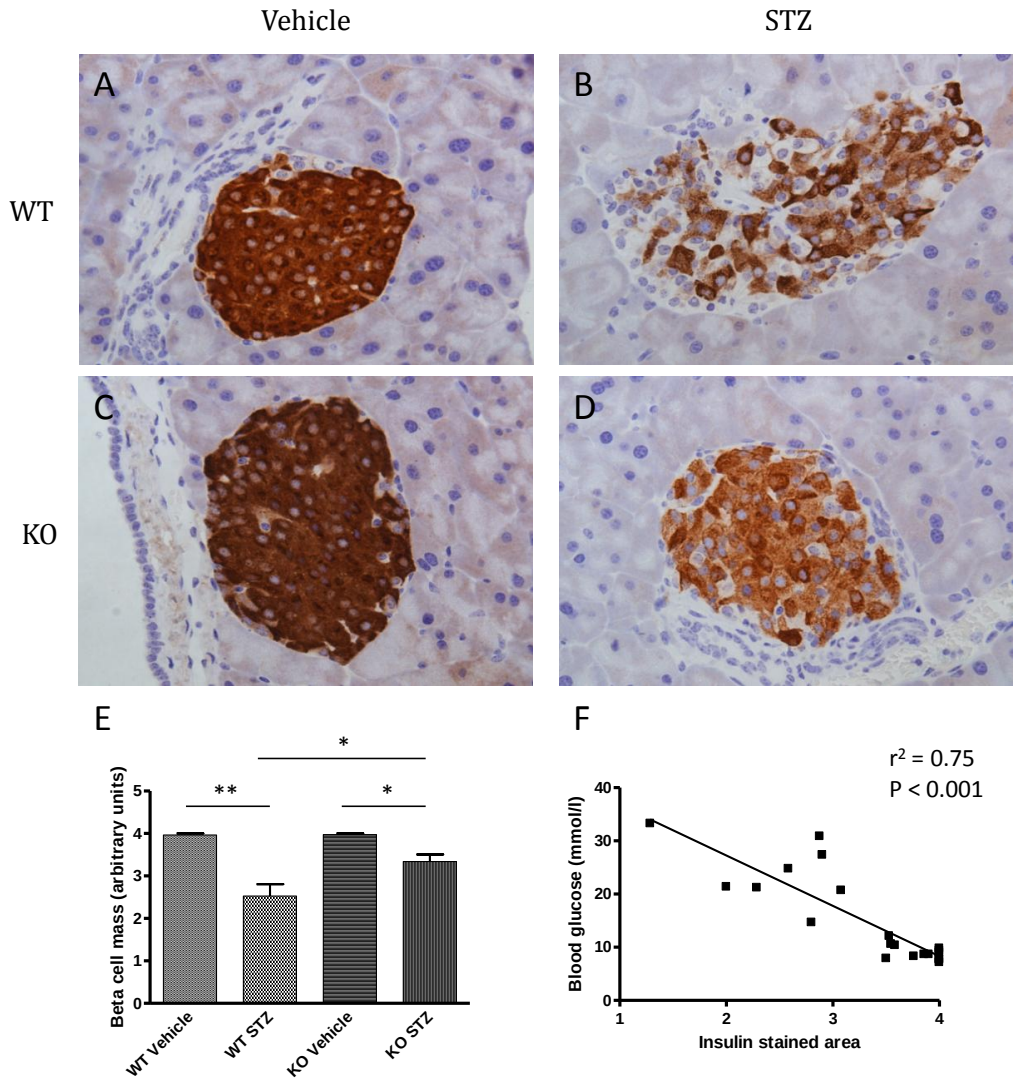

Figure 4.5 Analysis of beta cell mass in pancreatic tissue from WT and Pfizer P2X7 KO mice. A-D; Specific immunohistochemistry for insulin, delineating beta cells within pancreatic islets. A,C: Islets from both WT and KO control mice showing widespread staining across the islet; B: WT STZ-injected mice show reduced and discontinuous staining reflecting β-cell necrosis and loss. D: KO STZ-injected mice have relative preservation of pancreatic islet insulin staining. E: Quantification of beta cell mass by measurement of insulin-stained islet area (5 greatest, 0 least) confirming the qualitative findings. F: Scatter plot of blood glucose and insulin-stained area across all mice showing, as expected, these two parameters correlate well. *: $p<0.05$, **: $p<0.01$.

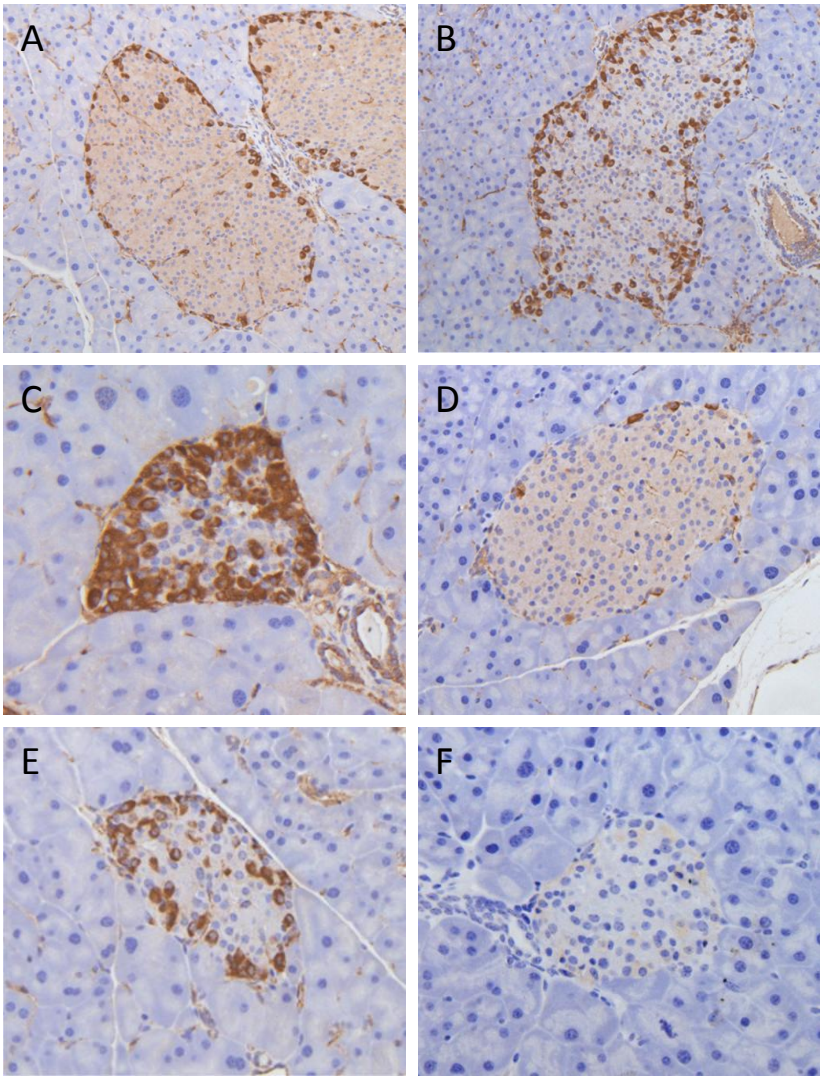

Figure 4.6 Immunohistochemistry for P2X7 in pancreatic islets from WT and Pfizer KO mice. A: Islet from WT vehicle treated mouse. The most peripheral layer of cells stained positive for P2X7 with occasional positive cells in the centre of islets. The peripheral location of P2X7-positive cells suggests they are α-cells. B: Typical appearance of islet from STZ-injected WT mouse. The number and depth of peripheral P2X7-positive cells was increased compared to WT with a greater number also observed in the centre of islets. C: An islet from an STZ-injected mouse with severe diabetes (BG >33.3 mmol/l at 3 weeks). The majority of cells in the islet stain positive for P2X7. D: Typical islet from KO vehicle treated mouse. A few peripheral cells stain positive, implying residual expression of receptor protein. E: Islet from KO STZ-injected mouse. The number of peripheral P2X7-positive cells is increased compared to control. F: Islet from WT STZ-injected mouse incubated with non-immune polyclonal rabbit immunoglobulin at an equivalent concentration to the primary antibody.

P2X7-positive cells within the centre of the gland (Figure 4.6B and C). These observations corroborate those in the NOD mouse model of type 1 diabetes, where co-localisation studies confirmed the P2X7-expressing cells to be α-cells (Coutinho-Silva et al., 2007). After STZ-induced β-cell damage and death, α-cells undergo compensatory proliferation, explaining the appearance of P2X7 positive cells within the core of the islet.

Sparse P2X7-positive cells were also observed around the periphery of islets in healthy P2X7 KO mice with an increase in number and density after STZ (Figure 4.6D and E). This staining is presumed to represent expression of a splice variant which escapes deletion and is consistent with published data where immunoblotting was performed on brain tissue from the Pfizer mouse using the same antibody (recognising the extracellular domain), and residual protein expression was observed (Sanchez-Nogueiro et al., 2005).

4.2.5 Islet macrophage infiltration after STZ is diminished in Pfizer KO mice

To further investigate the differences in cellularity between islets of WT and KO STZ-injected animals, specific immunohistochemistry for the macrophage antigen, Mac-2 (galectin-3), was performed. Mac-2 is a 32kD protein highly expressed on activated macrophages.(Ho and Springer, 1982) Significant macrophage accumulation was observed in islets from WT STZ-injected mice compared to vehicle-injected controls (mean fractional stained area: WT STZ 0.024 ± 0.004 vs WT Vehicle 0.009 ± 0.004 arbitrary units; $p<0.001$) (Figure 4.7). Macrophage infiltration was much reduced in islets from KO STZ mice compared to WT STZ (WT 0.024 ± 0.004 vs KO 0.013 ± 0.004; $p<0.001$).

Specific immunohistochemistry for the T cell marker, CD3, was also performed (Figure 4.8). No CD3-positive cells were present in islets from WT

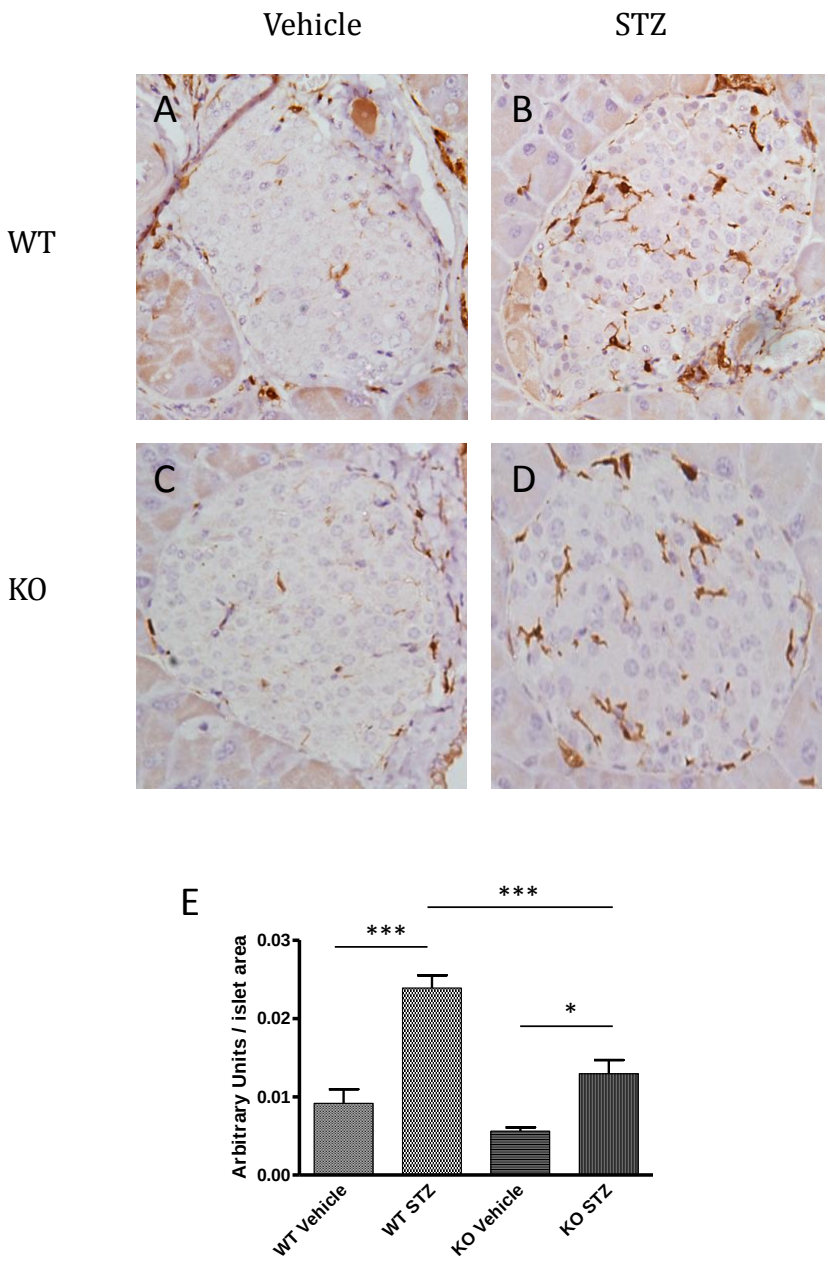

Figure 4.7 Macrophage accumulation in pancreatic islets from WT and Pfizer P2X7 KO mice. A-D; Specific immunohistochemistry for Mac-2, delineating macrophages within pancreatic islets. A,C: Islets from both WT and KO control mice showed minimal macrophage infiltration; B: WT STZ-injected mice displayed evidence of significant macrophage influx. D: KO STZ-injected mice had reduced macrophage infiltration compared to WT. E: Quantification of macrophage infiltration by image analysis, confirming this pattern of results. . *: $p<0.05$; ***: $p<0.001$.

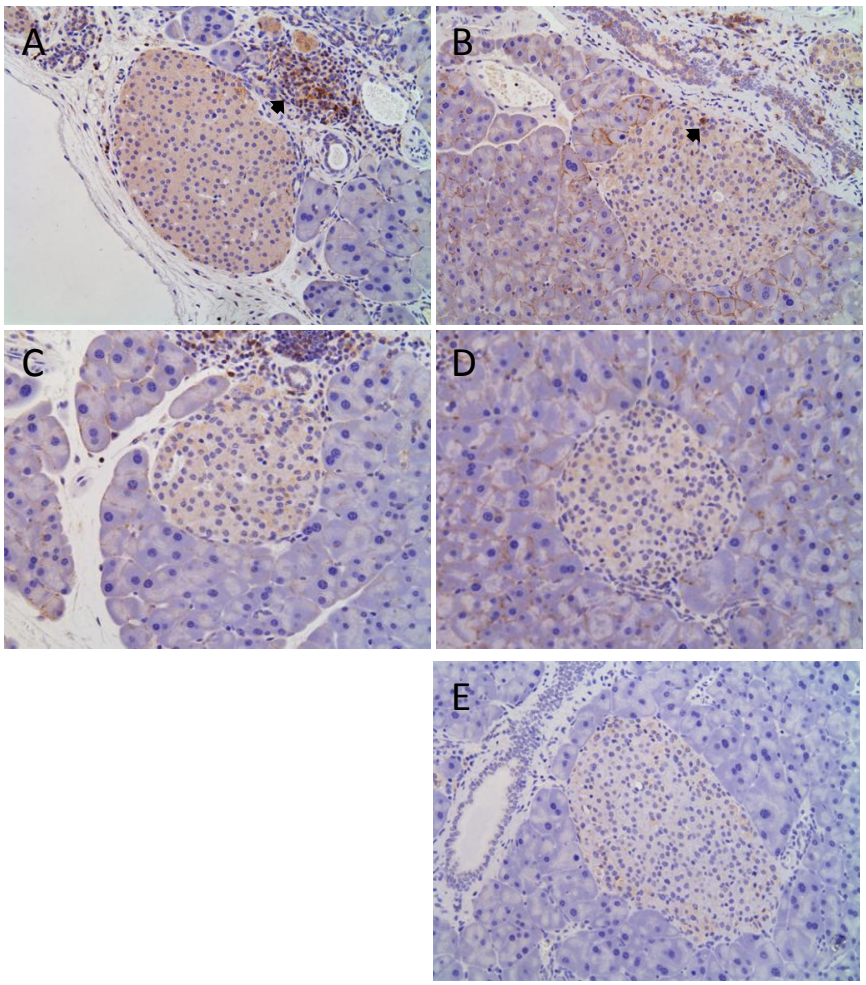

Figure 4.8 Immunohistochemistry for CD3 in islets from WT and KO mice. No CD3-positive cells were observed within islets from WT (A) and KO (C) vehicle-injected mice. A small peri-vascular inflammatory infiltrate adjacent to the islet in panel A, contains numerous CD3-positive cells (arrow). Rare solitary CD3-positive cells were observed in islets from WT STZ-injected mice (B; arrow), while no positive cells were apparent in KO STZ mice (D). E: Islet from WT STZ-injected mouse incubated with an equivalent concentration of rabbit polyclonal immunoglobulin. (Magnification: x200)

and KO vehicle injected animals; rare solitary CD3-positive cells were observed in islets from WT STZ injected mice, and none were seen in islets of KO STZ animals. T cells hence do not appear to constitute an important component of the inflammatory cell infiltrate in pancreatic islets following low dose STZ.

To investigate possible differences in background T cell and macrophage numbers between WT and KO mice, CD3 and Mac-2 immunohistochemistry was also performed on spleen tissue of vehicle-injected mice (Figure 4.9). CD3 staining was observed predominantly within the peri-arteriolar lymphoid sheath in both WT and KO mice with no difference in density or distribution. (Figure 4.9A and B). Mac-2 positive cells were most numerous within the splenic red pulp, with no differences in appearance between WT and KO animals (Figure 4.9C and D).

4.3 Discussion

Current therapy for both type 1 and type 2 diabetes focuses on either replacing or augmenting endogenous pancreatic insulin secretion or enhancing peripheral insulin sensitivity and glucose utilisation. While progressive islet destruction is a feature of both forms of diabetes, no treatments, with the possible exception of GLP-1, exist which interrupt this process (Urusova et al., 2004). In this chapter I have examined the role that P2X7 plays in the pathogenesis of islet injury in a commonly used mouse model of diabetes: low dose STZ. Examining two different strains of P2X7 KO mouse, both showed evidence of pancreatic resistance to the effects of STZ with a reduced proportion of mice becoming diabetic compared to WT, albeit more marked in the Pfizer KO strain. This was corroborated in Pfizer mice by

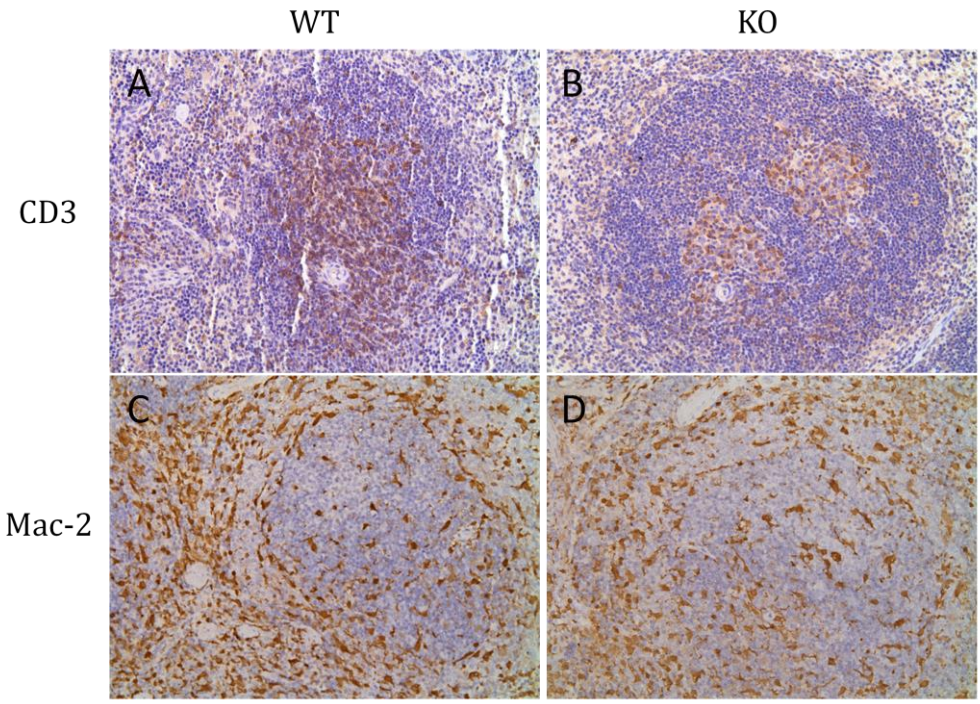

Figure 4.9 Immunohistochemistry for Mac-2 and CD3 in mouse spleen. A,B: CD3 (T cell marker) in WT (A) and KO (B) vehicle-injected mice. CD3 was predominantly localised to the peri-arteriolar lymphoid sheath within the splenic white pulp. Appearances were identical in WT and KO animals. C,D: Mac-2 (macrophage marker) in WT (C) and KO (D) vehicle-injected mice. Mac-2-positive cells were most numerous within the splenic red pulp, with scattered positive cells also visible within white pulp tissue; again, no difference was apparent between WT and KO mice. The number and distribution of T cells and macrophages within the spleen is hence not affected by genetic deficiency of P2X7. (Magnification: x100)

relative preservation of islet architecture and β-cell density compared to WT comparators.

GSK P2X7 KO mice were generated by disruption of exon 1 through insertion of a *LacZ* gene at the beginning of this region (Sim et al., 2004). It has recently been demonstrated that a novel splice variant of P2X7 utilising an alternative exon 1 (P2X7K) escapes inactivation in the GSK mouse, particularly in splenic lymphocytes (Nicke et al., 2009). This receptor is functional, has a greater sensitivity to agonist than the native P2X7A receptor and rapidly triggers membrane permeabilisation as measured by ethidium bromide uptake (Nicke et al., 2009). The Pfizer mouse was generated through targeted disruption of exon 13 (Solle et al., 2001). A C-terminal splice variant (ΔC) escapes deletion in this model also, although this receptor variant is inefficiently trafficked to the cell membrane, transmits only small agonist-evoked currents and exerts a dominant negative effect when co-expressed with P2X7A making this mouse a more 'complete' functional knockout (Masin et al., 2012). These differences in residual receptor expression are likely to explain the difference in protective effect observed between the two KO strains.

An interaction between ATP and the pancreas has been recognised for more than 50 years, with the demonstration that extracellular ATP could stimulate insulin release from rabbit pancreas slices (Rodrigue-Candela et al., 1963). Subsequent work has demonstrated expression of both P2X and P2Y receptor subclasses on exocrine and endocrine cells within the mammalian pancreas, as well as local blood vessels and autonomic nerve terminals (Burnstock and Novak, 2012). P2X7 is expressed in α but not β-cells in both normal rat and mouse pancreas, predominantly at the periphery of the gland (Coutinho-Silva et al., 2003, Coutinho-Silva et al., 2007). Induction of diabetes with STZ in the rat results in progressive accumulation of P2X7-positive α-cells in the centre of the islet, a phenomenon also observed in the NOD mouse and corroborated

by the data in this study (Coutinho-Silva et al., 2003, Coutinho-Silva et al., 2007). In both instances, infiltrating macrophages lacked significant P2X7 positivity, in contrast to splenic and peritoneal macrophages which were typically P2X7-positive. In contrast, P2X7 appears to be widely expressed in human β-cells in addition to α-cells, with marked upregulation in β-cells in obese non-diabetic individuals, but down-regulation in patients with overt diabetes (Glas et al., 2009).

Several studies have previously attempted to address the functional role of P2X7 in diabetic pancreatic injury. Lymphocytes isolated from NOD diabetic mice have been shown to be highly sensitive to P2X7-mediated shedding of CD62L and MHC Class I and also to programmed cell death (Elliott and Higgins, 2004). However, a P2X7 KO NOD stock did not exhibit a reduced incidence of diabetes compared to WT NOD mouse comparators, raising a question as to its importance to the initiation of diabetes in this model (Chen et al., 2011). P2X7-deficiency did, however, completely abrogate the accelerated development of diabetes seen in CD38-deficient NOD mice, where increased NAD-dependent cell death of CD4+ invariant T cells (iNKT) and Foxp3+ regulatory T cells (Tregs) promotes enhanced pancreatic injury (Chen et al., 2006).

Mouse P2X7 can be alternatively activated by ADP-ribosylation, an NAD-dependent process, with P2X7-deficiency presumably protecting iNKTs and Tregs from cell death in this model (Seman et al., 2003). The authors reconcile this finding with the absence of a protective effect on diabetes in CD38 +/+ NOD mice by suggesting that P2X7 may also contribute to suppression of autoreactive pathogenic T cells during development, promoting self-tolerance and balancing the detrimental effect on regulatory cell survival. The effect of P2X7 deficiency on the repertoire of immune cells infiltrating islets was not described in this study. CD38 has also been shown to participate in regulation of spontaneous release of ATP from smooth

muscle, further complicating the findings of this study (Durnin and Mutafova-Yambolieva, 2011).

In another study, the effect of the P2X7 antagonist, oxidized ATP (oATP), was tested on development of autoimmune CD8+ T cell-driven diabetes initiated by islet-specific expression of the LCMV-glycoprotein transgene in RIP-GP mice (Lang et al., 2010). oATP suppressed diabetes in 75% of mice and reduced numbers of activated CD8+ cells, CD4+ and CD11b+ cells within the spleen. The number of CD8+ cells observed infiltrating pancreatic islets was also reduced. oATP has also been shown to prolong graft survival in a murine model of pancreatic islet transplantation (Vergani et al., 2013). This was accompanied by a reduction in the anti-islet Th1 response and an increase in Tregs within the allograft. Graft survival was also prolonged when islets were transplanted to P2X7 KO mice, but to a lesser extent.

Conversely, in a study of β-cell dysfunction due to a high sucrose / high fat diet, P2X7 KO mice displayed severe glucose intolerance and failure to appropriately upregulate β-cell mass compared to WT animals (Glas et al., 2009). This was closely associated with reduced serum levels of IL1-RA, potentially exposing β-cells to increased toxic effects of local IL1β secretion. Islets cultured from P2X7 KO mice showed a defect in glucose-induced insulin release, although expression of P2X7 in β-cells of WT mice was not demonstrated directly.

The reduction in infiltrating macrophages observed in islets of Pfizer mice in the present study suggests that mitigation of the inflammatory response and 'insulinitis' provoked by STZ may underlie pancreatic protection, as opposed to direct protection of β-cells from the initial toxic insult, particularly as no expression of P2X7 could be demonstrated in the body of normal WT islets. The absence of a significant T cell infiltrate in islets from either WT or KO STZ-injected mice, suggest this cell type does not directly contribute to islet

inflammation in this model. Monocytes constitute a similar overall percentage of the circulating leukocyte population in P2X7 KO and WT mice and, together with the finding that macrophage and T cell density and distribution within spleen do not differ between WT and KO mice, it seems unlikely that effects of genetic P2X7 deficiency on monocyte development underlie the present experimental findings (Labasi et al, 2002).

The lack of protection afforded by P2X7 deficiency in NOD mice may be reconciled with our data by considering that STZ represents 'acquired' islet injury (as opposed to an inherent genetic susceptibility to autoimmunity), meaning any effect which P2X7 may have on negative selection of self-reactive thymoctes during development is not of relevance in this model. It is possible that the observed reduction in macrophage infiltration may result from decreased P2X7-dependent secretion of recruitment signals from resident islet cells, in a manner analagous to that seen within the glomerulus (see Chapter 7).

No difference in baseline random glucose was observed between WT and KO mice in this study, in contrast to the elevated fasting glucose seen in younger P2X7 KO mice in the study of Glas et al, although formal tests of glucose tolerance were not conducted. While P2X7 deficiency appears to exert a protective role in murine STZ-induced islet toxicity, the relative contribution of P2X7 and innate immune mechanisms to insulin secretion, β-cell proliferation or apoptosis in human pancreas is not known, meaning the net effect of P2X7 inhibition in human disease is currently difficult to predict. The apparent much greater expression of P2X7 in human β-cells compared to mouse may also impact on this (Coutinho-Silva et al., 2007, Glas et al., 2009).

In summary, the present data suggests that P2X7 deficiency ameliorates inflammatory attack on the islets after low dose STZ making it an interesting possible target in human diabetes. Further studies in isolated human islets,

specifically examining the effect of selective P2X7 antagonists on pancreatotoxic stimuli, will be crucial in advancing the translation of these findings.

CHAPTER 5

Investigating the role of P2X7 in the development of murine diabetic nephropathy using streptozotocin

5.1 Introduction

There is a pressing need to develop new therapies to retard the progression of DN, as the world-wide prevalence of diabetes continues to increase. Current treatments include inhibition of the RAS together with tight glycaemic and blood pressure control; an increasing appreciation that innate immune mechanisms play an important role in disease pathogenesis provides a potential new avenue for intervention (Navarro-Gonzalez and Mora-Fernandez, 2008). Macrophages feature prominently in the glomerular and tubulointerstitial infiltrate observed in DN, and their functional importance has been proven in animal models, making them a prime target for manipulation (Chow et al., 2006, Chow et al., 2007).

P2X7 has an integral role in IL1β and IL18 secretion from macrophages, and genetic deficiency or inhibition of the receptor in animal models of inflammatory disease often reduce accumulation of macrophages at the site of injury (Goncalves et al., 2006, Taylor et al., 2009). Minimal glomerular expression of P2X7 is observed under normal conditions, but marked upregulation has been described in models of both diabetic and hypertensive renal disease (Vonend et al., 2004). In addition, *in vitro* studies suggest that stimulation of P2X7 on mesangial cells by ATP may directly increase ECM synthesis, a central feature of DN, independent of any pro-inflammatory effect (Solini et al., 2005).

The current experiment has sought to investigate the functional role of P2X7 in DN by studying renal injury in WT and GSK P2X7 KO mice after induction of diabetes with low dose STZ. In particular, we have examined the effect of P2X7 deficiency on activation of the innate immune system in DN, by measuring renal inflammatory cytokine production and mononuclear cell infiltration. We selected the low dose STZ model, both because it is well characterised, and because it allows study of the effects of hyperglycaemia on the kidney in relative isolation from confounding insults, such as the obesity and dyslipidaemia observed in type 2 diabetes models and vascular phenotype evident in genetic models such as eNOS KO (see Section 1.9 for further discussion of mouse models of DN). A low dose schedule avoids the majority of direct drug-induced nephrotoxicity observed with high dose induction protocols and, although it induces only mild diabetic kidney injury, has been used successfully elsewhere to examine mechanisms of disease in early DN (eg. (Chow et al., 2006). Older mice (8-12 months) were used in the present study to accelerate progression of DN (Wu et al., 2010a). The GSK KO mouse was chosen for use, both because of local availability, and because amelioration of renal inflammation and injury were observed in the nephrotoxic nephritis model when induced in this P2X7 KO strain (Taylor et al., 2009).

5.2 Results

5.2.1 GSK P2X7 KO mice are not protected from albuminuria or rise in creatinine at 12 weeks after STZ

To ensure that groups were well-matched for degree of hyperglycaemia, only mice achieving and maintaining a BG of 16-33.3mmol/l after STZ injection were studied at the 12 week end-point; details of the proportion of mice falling outside of these limits are described in Chapter 4. Physical and

biochemical data at baseline and week 12 for the mice included in the study are summarised in Table 5.1.

Mean BG (averaged from readings taken between weeks 3 and 12) did not differ between STZ-injected WT and KO groups (Figure 5.1A); BG at week 9 was higher in the KO group (WT STZ vs KO STZ, 22.7 ± 3.4 vs 28.1 ± 4.9 mmol/l; p=0.02), but similar at all other time-points (Figure 5.1B). A trend towards greater % weight loss was observed in KO STZ compared to WT STZ mice (mean difference 5.9%, 95% CI -1.3 to 13.2%).

At 12 weeks, the urine albumin:creatinine ratio (uACR) was elevated in WT STZ mice compared to vehicle-injected controls although this did not reach statistical significance; a trend was seen towards higher uACR values in KO STZ mice compared to WT, albeit with a wide standard deviation of results in the latter group (WT STZ vs KO STZ; 57.0 ± 21.9 vs 158.4 ± 220.6 mg/mmol; 95% CI of difference -44.7 - 247.4 mg/mmol; Figure 5.1C). Serum creatinine was significantly elevated in WT STZ mice compared to controls at this time-point, with no observed difference between WT and KO STZ groups (Figure 5.1D).

5.2.2 P2X7 expression is upregulated in glomeruli of STZ diabetic mice

P2X7 expression in mouse kidney tissue was examined by specific immunohistochemistry using a specific rabbit polyclonal anti-P2X7 antibody (Alomone Labs). Prominent basolateral staining was observed in a subset of tubules in all mice examined (Figure 5.2A), identical to that seen in both human (Chapter 3) and rat (Chapter 6) kidney. This constitutive staining was observed in both WT and KO mice, and, in the latter, is assumed to represent P2X7K splice variant expression (Nicke et al., 2009).

	WT Vehicle (n=8)	**WT STZ** (n=8)	**KO Vehicle** (n=8)	**KO STZ** (n=8)
Age (months)	9.1 ± 0.6	9.5 ± 0.8	9.4 ± 1.2	9.9 ± 0.4
Wk 0 weight (g)	35.0 ± 2.4	36.9 ± 4.0	37.6 ± 4.8	35.6 ± 1.7
% Weight loss (Wk 0 to Wk12)	-1.6 ± 5.6	11.8 ± 8.4[a]	-3.3 ± 4.9	18.7 ± 5.1[b]
Wk 0 BG* (mmol/l)	8.8 ± 1.9	8.0 ± 0.7	8.5 ± 2.5	8.7 ± 1.7
Mean BG (mmol/l) (Wk 3 to Wk 12)	8.3 ± 1.1	25.9 ± 2.6[a]	8.7 ± 1.2	26.6 ± 2.4[b]
Wk 12 uACR† (mg/mmol)	30.9 ± 14.3	57.0 ± 21.9	49.2 ± 36.6	158.4 ± 220.6
Wk 12 Serum Creatinine (µmol/l)	34.8 ± 3.2	53.3 ± 10.1[a]	31.3 ± 3.5	57.1 ± 11.9[b]

Table 5.1 Summary of physical and biochemical data for GSK P2X7 KO mouse DN experiment. [a] $p<0.001$ vs WT vehicle; [b] $p<0.001$ vs KO vehicle. *Data available for a subset of mice: WT vehicle n=8, WT STZ n=6, KO vehicle n=8, KO STZ n=4. † KO vehicle n=7, other groups n=8.

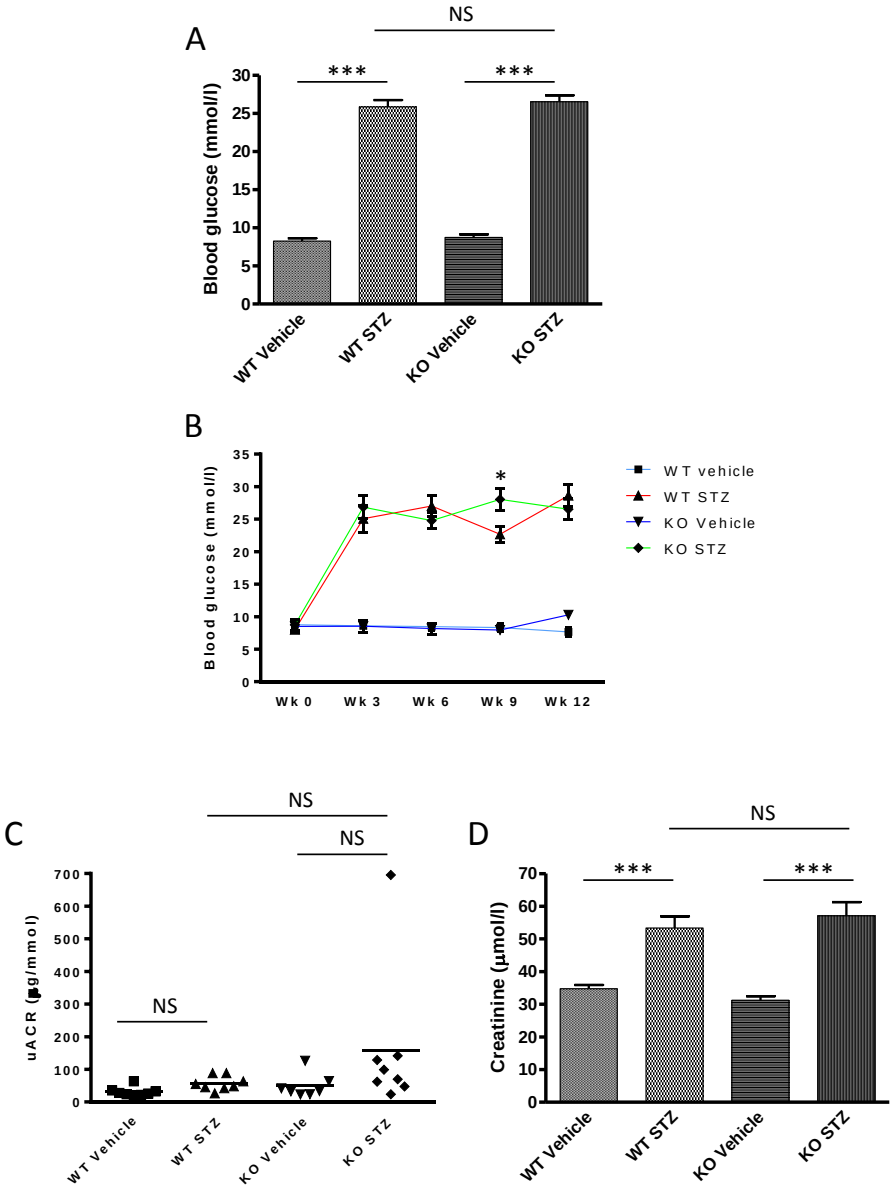

Figure 5.1. Glycaemia and biochemical renal outcomes. A: Mean BG averaged across weeks 3 to 12. Mean BG was equivalent in WT and KO diabetic groups. B: Mean BG at each measurement time-point. KO STZ mice had higher BG at week 9, and similar levels to WT STZ at all other time points. C: uACR at week 12. uACR was elevated in both diabetic groups compared to controls, but failed to reach statistical signficance. A trend towards higher uACR values was seen in KO STZ mice compared to WT, but with a wide standard deviation of values in the former group. D: Serum creatinine at week 12. Creatinine was elevated in both diabetic groups compared to controls, but was equivalent in WT and KO diabetic mice. . *: $p<0.05$; ***: $p<0.001$; NS: Not significant.

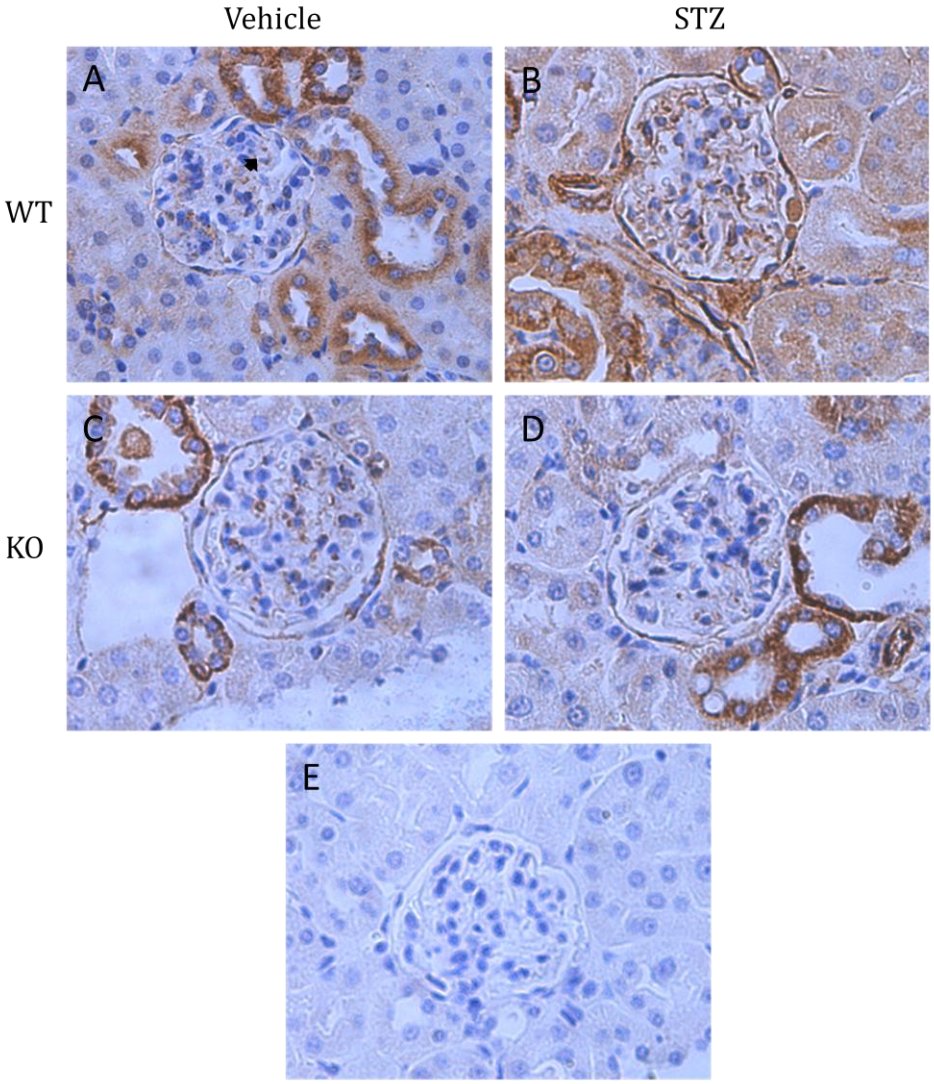

Figure 5.2 Expression of P2X7 in murine DN. A: WT vehicle-injected kidney. Distal tubular staining was present in all kidneys examined, regardless of P2X7 genotype, and showed a similar pattern to that seen in rat and human tissue. Occasional granular 'flecks' of P2X7 staining were observed in some glomeruli (arrow). B: Kidney from WT STZ-injected mouse. Confluent capillary loop staining was observed in the majority of glomeruli, similar to that seen in STZ and GK diabetic rats. C: KO vehicle-injected kidney. Basolateral staining of distal tubules was present in a pattern indistinguishable from WT tissue and is presumed to represent splice-variant receptor expression. D: Tissue from KO STZ-injected kidney. Minimal staining was apparent in glomeruli, contrary to that seen in WT animals. E: Tissue from WT STZ-injected mouse incubated with rabbit polyclonal IgG at a concentration equivalent to the primary antibody. Images shown at x200 magnification.

Minimal glomerular staining was seen in either WT or KO control mice (Figure 5.2A and C). In contrast, WT STZ-injected mice showed marked glomerular P2X7 expression in a capillary loop pattern, in the majority of glomeruli (Figure 5.2B). This capillary loop staining was not seen in KO STZ-injected animals (Figure 5.2D). Glomerular P2X7 staining was not present at 3 weeks after STZ injection in WT mice (data not shown).

5.2.3 Interstitial fibrosis and glomerular hypertrophy are not influenced by P2X7 deficiency

Cortical fibrosis was quantified by image analysis of picrosirius red-stained sections, viewed under double polarised light. Fibrosis was significantly greater in STZ-injected WT mice compared to controls (WT STZ vs WT vehicle; 1.2 ± 0.4 vs 0.7 ± 0.3 % surface area; $p<0.01$), but no difference existed between WT and KO diabetic groups (WT STZ vs KO STZ; 1.2 ± 0.4% vs 1.2 ± 0.3%; $p>0.05$) (Figure 5.3A-E). No correlation was found between interstitial fibrosis and serum creatinine for diabetic mice ($r^2=0.07$, $p=0.32$), suggesting that fibrosis and nephron drop-out was not the prime determinant of the apparent reduction in GFR in this model (Figure 5.4A). Similarly, there was no correlation between uACR and creatinine ($r^2=0.004$, $p=0.82$, as analysed with removal of single outlying datapoint; Figure 5.4B and C). It is hence likely that the apparent reduction in GFR may be due to other factors, such as polyuria-driven volume depletion.

Glomerular hypertrophy was assessed by measurement of mean glomerular area across 30 randomly-selected glomeruli for each animal. A trend was observed towards increased glomerular size in diabetic WT animals compared to controls (WT STZ vs WT vehicle; 4130 ± 851 vs 3655 ± 492 μm^2; 95% CI of difference -457.9 to 1407μm^2), similar to that observed in diabetic

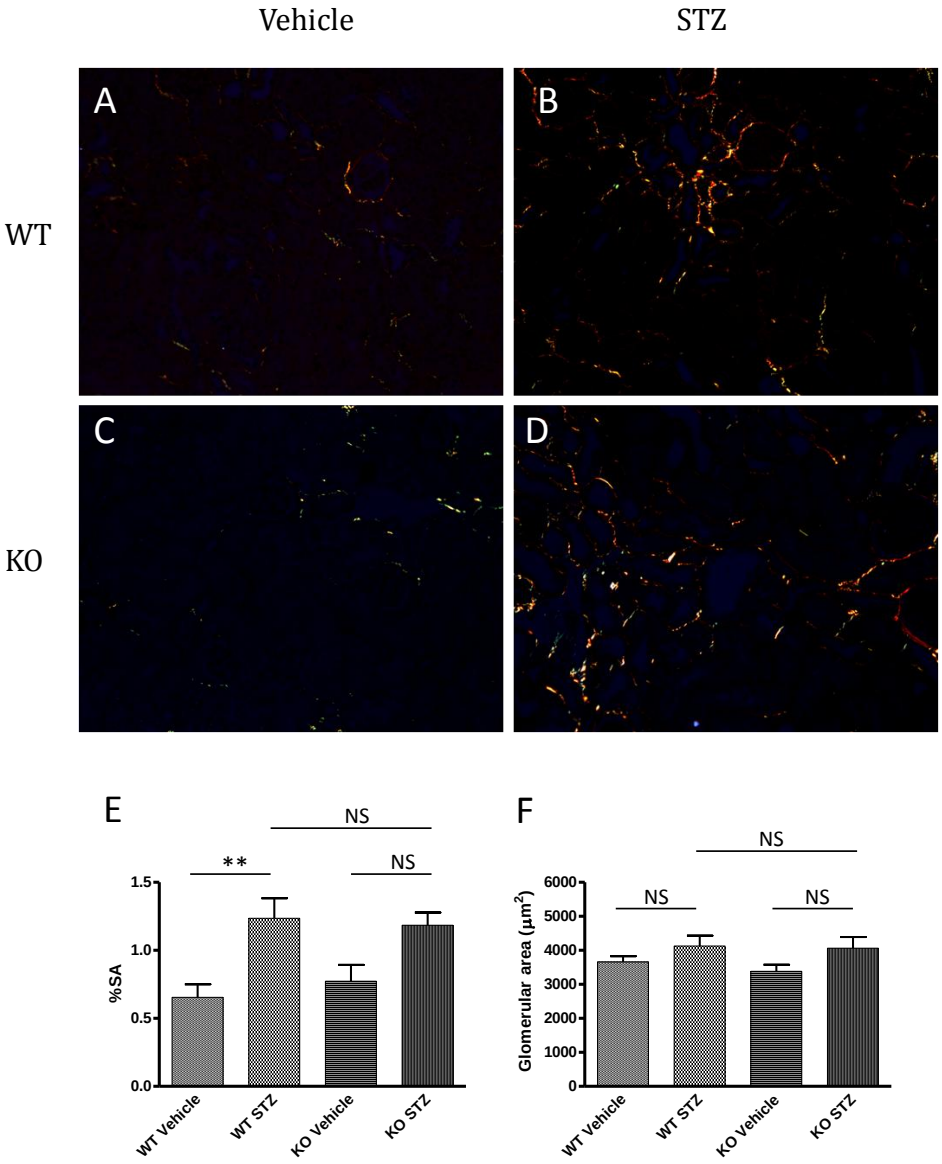

Figure 5.3 Cortical fibrosis and glomerular area in murine DN. A-D: Representative picrosirius red-stained sections viewed under double-polarised light (x200 magnification). E: Picrosirius red-stained cortical area, as determined by image analysis. F: Glomerular area. %SA: % surface area stained with picrosirius red. **: $p<0.01$; NS: Not significant.

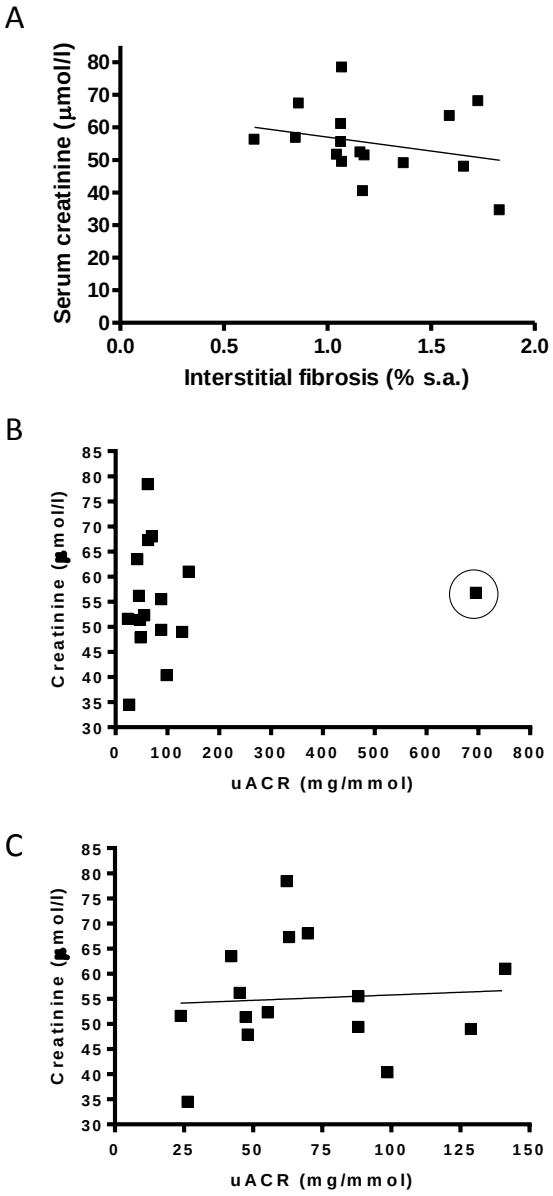

Figure 5.4 Simple Pearson correlation analysis between serum creatinine (dependent variable) and primary determinants of renal function in diabetic mice. A: Scatter plot depicting relationship between serum creatinine and interstitial fibrosis in all diabetic mice (WT and KO), as quantified by picrosirius red-stained surface area. No significant correlation was found between the two variables (r^2=0.07, p=0.32). B: Scatter plot depicting relationship between serum creatinine and uACR in all diabetic mice. Outlying value is circled. C: Data as for figure B but with outlying value removed. No correlation was observed between creatinine and uACR (r^2=0.004, p=0.82). %SA: % surface area stained with picrosirius red.

KO mice compared to KO controls (KO STZ vs KO vehicle; 4060 ± 936 μm^2 vs 3383 ± 549 μm^2; 95% CI of difference -254.6 to 1610 μm^2) (Figure 5.3F). Glomerular size did not differ between WT and KO diabetic mice ($p>0.05$).

Glomerular type IV collagen deposition was examined by immunohistochemisty using a specific rabbit polyclonal anti-type IV collagen antibody (Abcam) and quantified using ImagePro. Glomerular collagen was increased in diabetic WT animals compared to controls (WT STZ vs WT vehicle; 17.8 ± 2.2 vs 13.9 ± 1.5 % surface area; $p<0.01$), with a trend towards reduced levels in KO diabetic animals (WT STZ vs KO STZ; 17.8 ± 2.2 vs 15.2 ± 2.8 % surface area; 95% CI of difference 0.1 to -5.3%); (Figure 5.5).

5.2.4 Diminished glomerular, but not interstitial, macrophage accumulation is observed in GSK P2X7 KO mice

Macrophage infiltration was assessed by immunohistochemistry using a specific rat monoclonal anti-CD68 antibody (Serotec) and quantified for glomerular and tubulointerstitial compartments. At 12 weeks, glomerular macrophage number was significantly elevated in WT diabetic mice compared to controls (WT STZ vs WT vehicle; 0.87 ± 0.53 vs 0.14 ± 0.15 cells per glomerulus; $p<0.001$; Figure 5.6A-E); this was significantly reduced in KO STZ mice (WT STZ vs KO STZ; 0.87 ± 0.53 vs 0.36 ± 0.23 cells per glomerulus; $p<0.01$). A trend towards increased interstitial macrophage accrual was observed in WT diabetic mice compared to WT vehicle, but this did not reach statistical significance (WT STZ vs WT vehicle; 40.6 ± 38.7 vs 13.3 ± 7.5 cells per field; $p>0.05$; Figure 5.6F) nor was a difference observed between WT and KO diabetic animals (WT STZ vs KO STZ; 40.6 ± 38.7 vs 31.3 ± 31.9 cells per field; $p>0.05$).

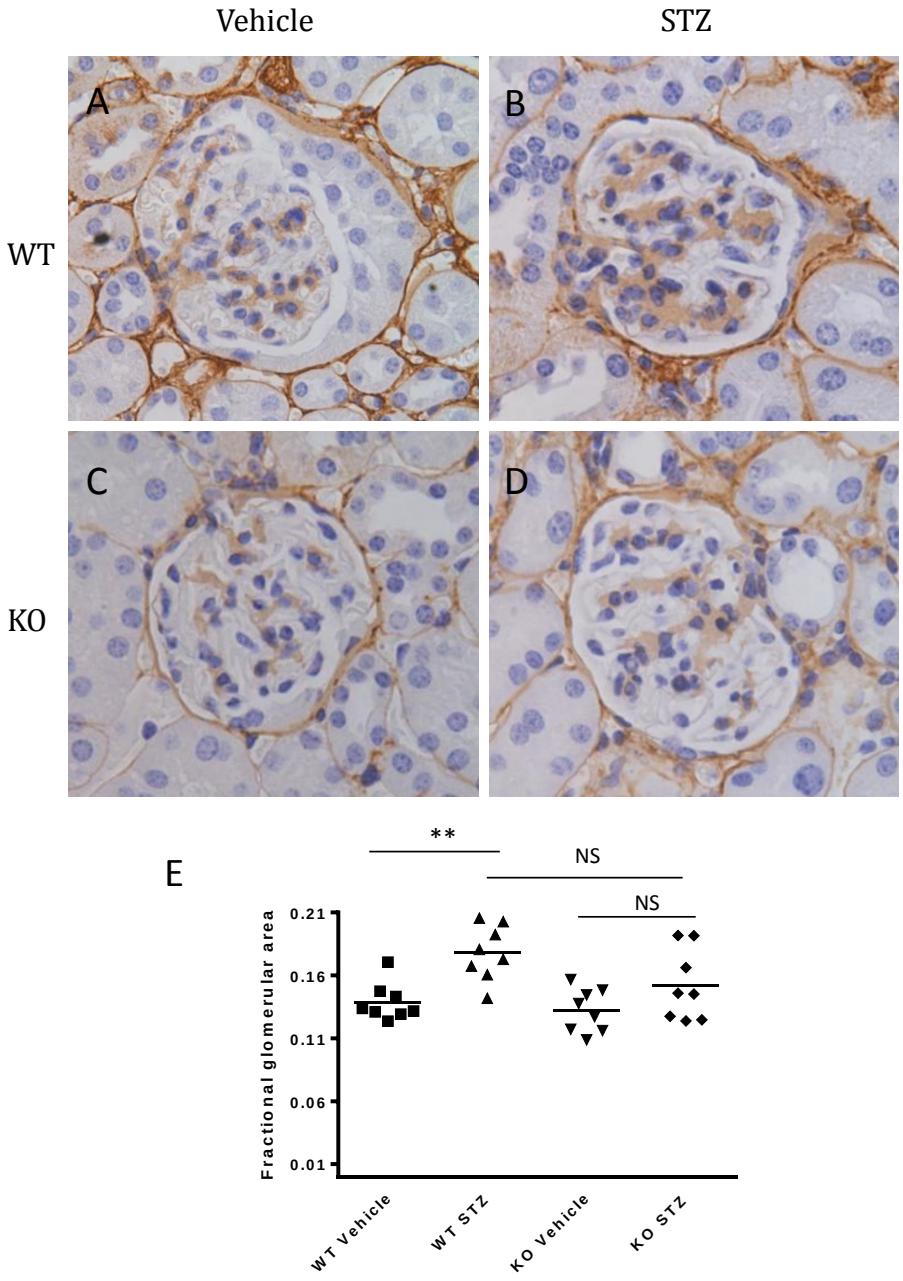

Figure 5.5 Expression of glomerular type IV collagen in murine DN. A-D: Representative glomeruli from each group (x200 magnification). E: Fractional glomerular area stained positive for type IV collagen, as assessed using ImagePro. . **: $p<0.01$; NS: Not significant.

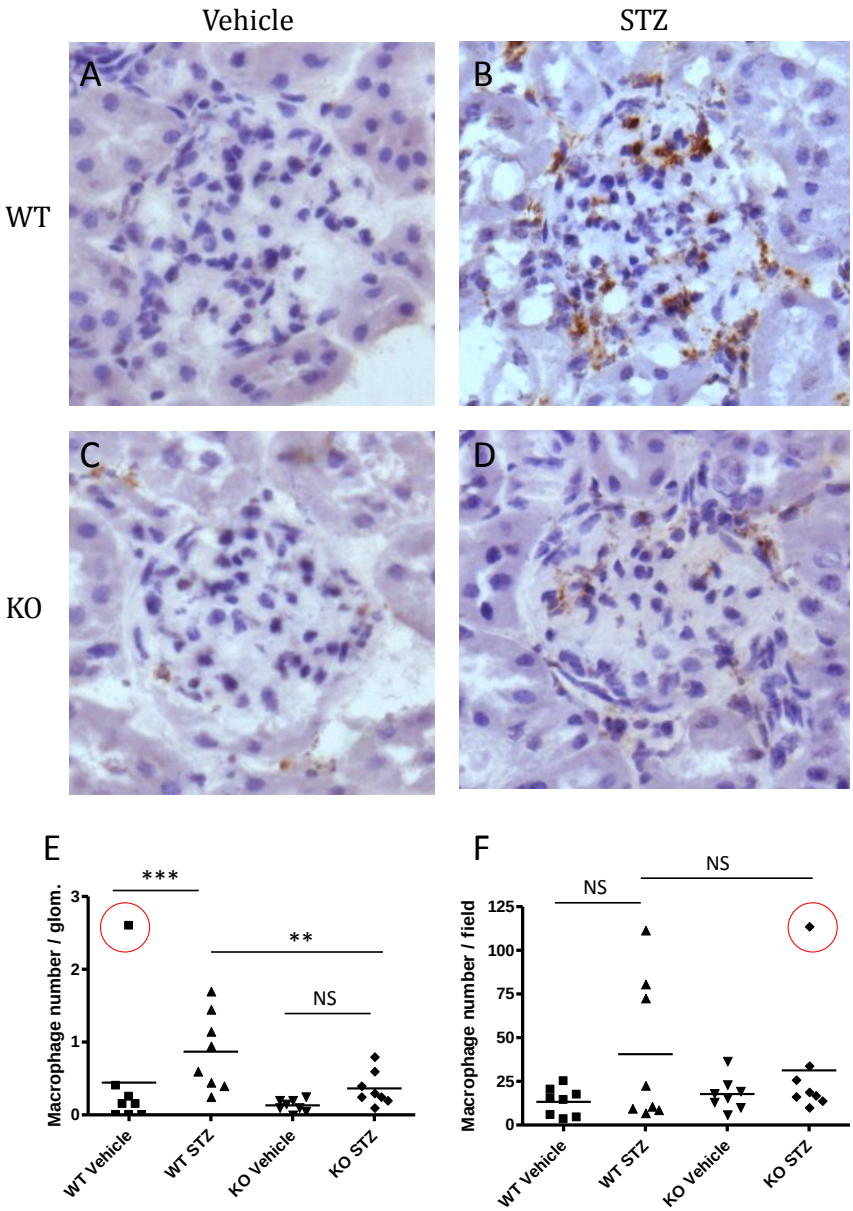

Figure 5.6 Expression of the macrophage marker CD68 in murine DN. A-D: Representative glomeruli (x400 magnification). E: Mean macrophage number per glomerulus. An outlying value in the WT vehicle group, otherwise inconsistent with population data, is circled and was removed from the analysis to facilitate multi-group comparison. F: Mean macrophage number per cortical interstitial field of view. An outlying value in the KO STZ group is circled and was removed from the analysis. **: $p<0.01$; ***: $p<0.001$; NS: Not significant.

Renal cell proliferation was assessed by specific immunohistochemistry for Ki-67, a marker of cell proliferation. Very infrequent Ki-67-positive interstitial cells were observed in all mice, with no difference between groups (data not shown). No signficant glomerular Ki-67 staining was seen in any group, suggesting the observed differences in glomerular macrophage number were not explained by differences in intra-renal macrophage proliferation.

5.2.5 Analysis of mRNA expression of P2X7, inflammasome components, and inflammatory and ECM molecules

Gene expression in whole kidney tissue was studied by qPCR. P2X7 expression was significantly upregulated in WT STZ mice compared to vehicle ($p<0.01$; Figure 5.7A); low level detectable expression in KO animals is presumed to represent P2X7K splice variant expression, as the primers used did not differentiate between P2X7A and K isoforms (it did not prove possible to design specific primers discriminating between the two splice variants, that yielded products short enough for efficient amplification by qPCR).

No significant upregulation of expression was observed for either pro-IL1β or NLRP3, in either WT or KO STZ mice compared to controls (Figure 5.7C and D). Expression of the adaptor molecule apoptosis-associated speck-like protein containing a caspase recruitment domain (ASC; another component of the NLRP3 inflammasome), was elevated in both WT and KO STZ mice compared to controls, reaching statistical significance for the latter ($p<0.01$; Figure 5.7B); no difference was observed between WT and KO diabetic groups. A similar pattern of results was observed for caspase-1. the chemokines MCP-1 and osteopontin, the adhesion molecule ICAM-1, TGFβ, and the ECM molecules COL4A1,

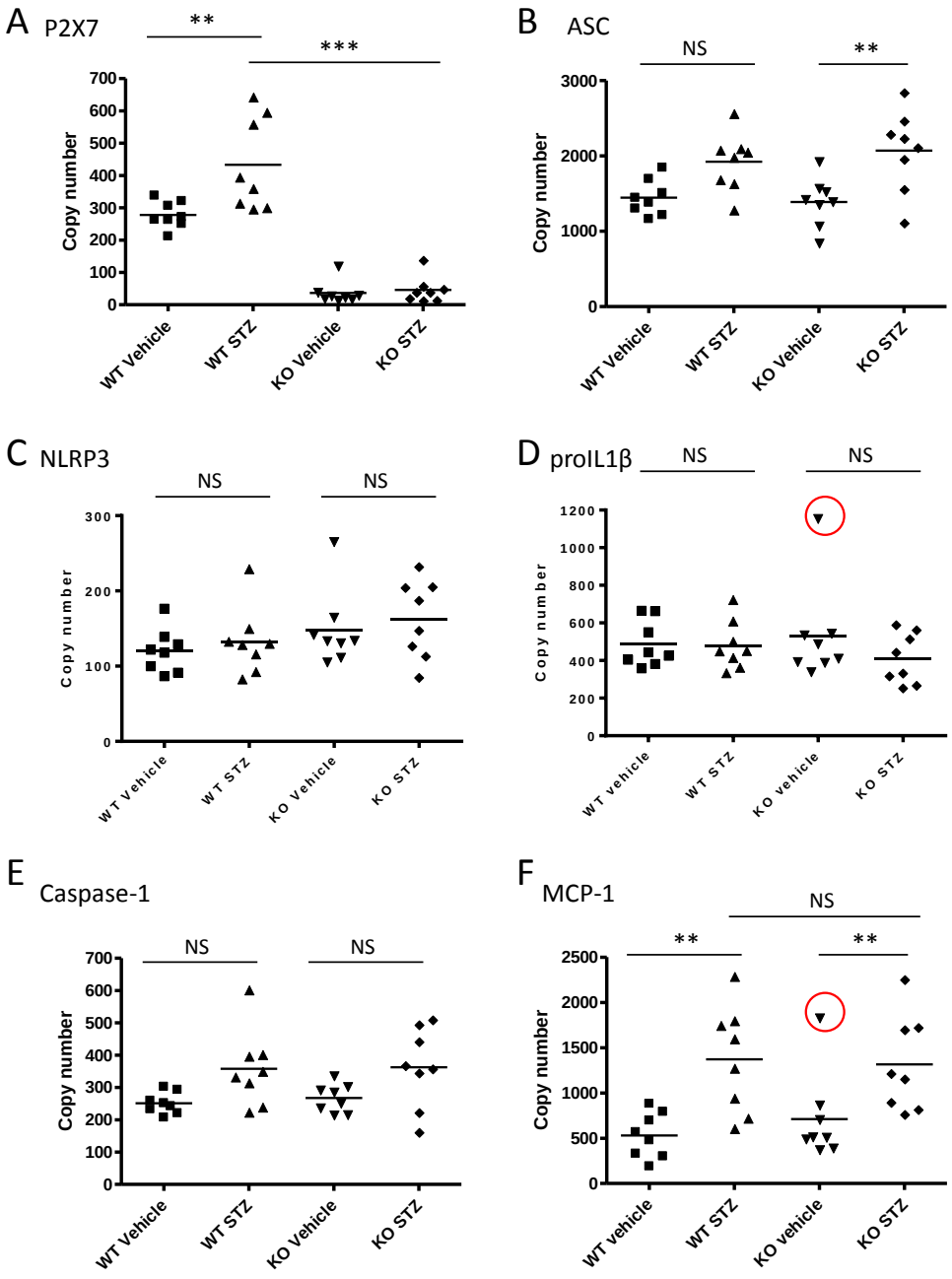

Continued overleaf.

Figure 5.7 Gene expression in murine DN. A: P2X7; B: ASC; C: NLRP3; D: proIL1β; E: Caspase-1; F: MCP-1. Outlying values removed from analysis are marked with red circles. . **: p<0.01; ***: p<0.001; NS: Not significant.

Continued from previous page.

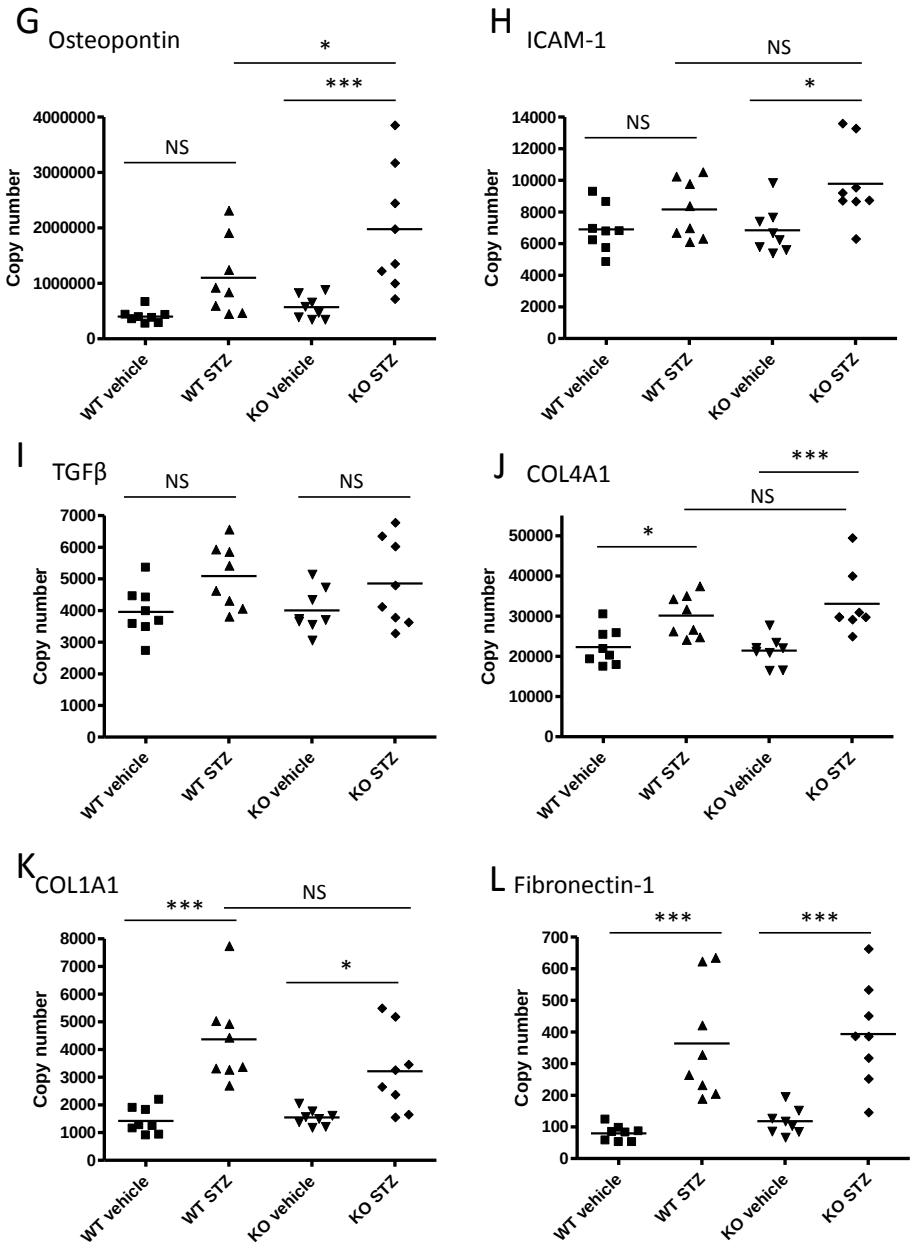

Figure 5.7 Gene expression in mouse DN. G: Osteopontin, H: ICAM-1; I: TGFβ; J: COL4A1; K: COL1A1; L: Fibronectin-1. *: p<0.05; ***: p<0.001; NS: Not significant.

COL1A1 and Fibronectin 1 (Figure 5.7E-L). in the case of osteopontin, expression was increased in KO STZ mice compared to WT STZ ($p<0.05$). A trend towards increased expression of ICAM-1 in KO STZ mice was also apparent (95% CI of difference: -736 to 3992 copies). Reduced COL1A1 expression was seen in KO STZ compared to WT STZ (95% CI of difference: 292 to -2586 copies).

5.3 Discussion

In this study, the role of P2X7 in the development of murine DN has been examined, by inducing diabetes with low dose STZ in WT and GSK P2X7 KO mice. By 12 weeks, early renal injury was apparent in WT mice, with modest albuminuria and tubulointerstitial fibrosis; P2X7 deficiency did not impact on these core features of DN. At this time-point, P2X7 expression, as assessed by immunohistochemistry, was increased in glomeruli of WT diabetic mice compared to vehicle-injected controls. A significant reduction in glomerular, but not interstitial, macrophage number was observed in P2X7 KO diabetic mice compared to WT, suggesting that P2X7 receptor signalling contributes to development of early hyperglycaemia-induced glomerular inflammation.

Renal macrophage infiltration is evident as early as 2 weeks after STZ injection in mice, and studies interfering with macrophage function (by, for instance, disrupting macrophage recruitment signals) have demonstrated important downstream effects on albuminuria, glomerular and interstitial fibrosis and GFR (Chow et al., 2004b, Chow et al., 2006). Although detailed descriptions of macrophage activation state and phenotype in human and animal DN are lacking, the net effect of this infiltrate appears to be deleterious (Lim and Tesch, 2012). The reduction in glomerular macrophage infiltration observed in P2X7-deficient diabetic mice would hence be

predicted to portend an improved outcome, although a longer duration of study would be required to determine this.

Monocytes constitute a similar overall percentage of the circulating leukocyte population in GSK P2X7 KO and WT mice, suggesting reduced glomerular macrophage numbers observed in diabetic KO mice do not merely reflect global deficiency (Labasi et al., 2002). While P2X7 has well-defined roles in the secretion pathway for macrophage-derived inflammatory cytokines, including IL1β and IL18, this, also, does not immediately explain the reduction in glomerular macrophages in diabetic P2X7 KO mice (Surprenant et al., 1996). No difference was detected between WT and KO mice in whole kidney mRNA expression of the macrophage chemokine, MCP-1, while mRNA levels of osteopontin, also involved in macrophage recruitment, and the cell adhesion molecule, ICAM-1, were actually elevated in the KO group. Few proliferating cells were identified within the kidneys of both WT and KO diabetic animals with no difference between groups.

IL1β/IL18 secretion, triggered by P2X7 signalling, is mediated by the NLRP3 inflammsome, which acts as a capase-1 activation platform. A trend towards increased gene expression levels of the NLRP3 inflammasome-associated proteins ASC and caspase-1 was seen both in WT and KO diabetic mice. Increased expression of NLRP3 mRNA is found in a variety of non-diabetic human renal diseases and correlates with renal function (Vilaysane et al., 2010). Moreover, tubular injury, inflammation and fibrosis is reduced after UUO in NLRP3 KO mice, together with maturation of IL1β and IL18 (Vilaysane et al., 2010). NLRP3 inflammasome components, including NLRP3, ASC and caspase-1, are also upregulated in the high-fat diet mouse model of metabolic syndrome, although no mature IL1β or IL18 could be detected in renal cortex in this study (Solini et al., 2013). Levels of mature IL1β and IL18 in the renal cortex were not measured in the current study; while it remains possible that differences in maturation and secretion of these cytokines

underlie the observed amelioration of glomerular inflammation in P2X7 KO mice, the finding that pro-IL1β mRNA was not upregulated by diabetes makes this less likely.

Albuminuria represents the earliest clinical manifestation of DN; although the mechanisms which lead to initiation of albuminuria have not been fully elucidated, VEGF-mediated increases in capillary growth and permeability, deleterious endothelial cell-podocyte crosstalk, RAS activation and podocyte injury and loss all contribute to this process (Wolf et al., 2005, Yuen et al., 2012). P2X7 deficiency had no impact on development of early albuminuria in this study despite the previous observations that podocyte expression of P2X7 increases early in the pathogenesis of STZ-induced diabetes in the rat, and P2X7 agonists increase glucose uptake into podocytes *in vitro* (Vonend et al., 2004, Karczewska et al., 2011). While P2X7 does not appear to contribute to initiation of albuminuria, a longer period of study would be needed to examine its role in progression of glomerular injury to which additional factors, including glomerular inflammation, are of importance. A trend towards reduced glomerular deposition of type IV collagen, another feature of progressive diabetic glomerulopathy, was also apparent in KO mice at 12 weeks.

The absence of an observed effect of P2X7-deficiency on interstitial fibrosis is perhaps surprising in view of previous animal studies, where renal fibrosis after UUO was ameliorated in P2X7 KO mice, as was pulmonary fibrosis provoked by bleomycin (Goncalves et al., 2006, Riteau et al., 2010). In the former study, reduced fibrosis was accompanied by decreased interstitial macrophage infiltration and TGFβ expression; interstitial macrophage number was not significantly increased in WT diabetic mice compared to controls in the present study which may partly explain the lack of efficacy of P2X7-deficiency on interstitial fibrosis (Goncalves et al., 2006).

Of importance, both previous mouse studies examining the role of P2X7 in parenchymal fibrosis were conducted using the Pfizer P2X7 KO mouse, as opposed to the GSK mouse which was used in the present study. As described in Section 2.3.1, GSK P2X7 knockout mice were generated by disruption of exon 1 through insertion of a *LacZ* gene at the beginning of this region(Sim et al., 2004). It has recently been demonstrated that a novel splice variant of P2X7 utilising an alternative exon 1 (P2X7K) escapes inactivation in the GSK mouse, particularly in spleen lymphocytes (Nicke et al., 2009). This receptor is functional, has a greater sensitivity to agonist than the native P2X7A receptor and rapidly triggers membrane permeabilisation as measured by ethidium bromide uptake assays (Nicke et al., 2009). While a C-terminal splice-variant also escapes deletion in the Pfizer KO mouse, this truncated receptor has reduced function and acts in a dominant-negative fashion when co-expressed with P2X7A, making this mouse a functionally 'more complete' P2X7 KO (Masin et al., 2011).

Although attenuated IL1β release has been described in macrophages isolated from both GSK and Pfizer mice, conflicting outcomes have been reported for the two KO strains in the mouse model of experimental auotimmune encephalitis, where disease was exacerbated in GSK mice and suppressed in Pfizer mice (Chen and Brosnan, 2006, Sharp et al., 2008). Differences in residual receptor expression between the two KO strains may explain the absence of an abrogating effect on tubulointerstitial fibrosis and increased mRNA expression of osteopontin seen in diabetic KO mice in this study, and is supported by the observation that tubular immunostaining for P2X7, presumably the P2X7K variant, persists in the GSK KO.

Several other factors may have served to partially mask the full effect of P2X7-deficiency in this experiment. In order to test with specificity the impact of P2X7-deficiency on the renal consequences of sustained hyperglycaemia, it was necessary to exclude a number of mice in which

diabetes either failed to develop after STZ injection, became too severe, or resolved spontaneously. As described in Chapter 4, the proportion of mice developing diabetes by 3 weeks after STZ was reduced in the GSK P2X7 KO group (83% WT vs 72% KO). Similarly, the proportion of mice developing diabetes of excessive severity over the course of the study was also higher among WT animals (33% WT vs 15% KO). Given the finding that P2X7-deficiency attenuates pancreatic islet injury and macrophage infiltration after STZ, it is reasonable to surmise that mice exhibiting more severe pancreatic injury, which were selected out, may also have displayed more exaggerated renal injury. In addition, although levels of hyperglycaemia were similar overall between WT and P2X7 KO mice selected for study, levels were significantly higher in KO animals at one measurement time-point (week 9).

In summary, genetic deficiency of P2X7 imparts a marked amelioration of glomerular inflammation at 12 weeks after induction of diabetes with low dose STZ in the mouse. In combination with established treatments to diminish hyperglycaemia and inhibit RAS activation, targeting of P2X7 signalling may represent an avenue by which to interrupt innate immune system activation in human DN and attenuate disease.

CHAPTER 6

Investigating the role of P2X7 in diabetic nephropathy using a uninephrectomised diabetic rat model

6.1 Introduction

In parallel to conducting experiments in STZ-diabetic mice, we chose to study P2X7 in a rat model of DN, again using STZ to induce diabetes. This was motivated both by the previous observation that P2X7 is upregulated in the glomerulus at an early time-point in this model, and the opportunity to test the effect of a selective antagonist to the P2X7 receptor, for which there are none currently suitable for use in the mouse (Vonend et al., 2004). We selected the STZ model in light of its well-characterised phenotype, primacy of hyperglycaemia as a driver of nephropathy, and to facilitate comparison with the corresponding mouse experiments.

Pilot experiments revealed that STZ-induced diabetes alone produced inadequate evidence of renal injury necessitating the addition of a uninephrectomy (UNx) to accelerate disease. Using this model, a selective P2X7 antagonist was administered twice daily by the IP route between weeks 8 and 12 after injection of STZ, to examine the effect on development of DN and, in particular, activation of the innate immune system.

6.2 Results

6.2.1 Model optimisation

Initial experiments focussed on establishing an in-house diabetic rat model which was both reproducible and manifested sufficient evidence of nephropathy to permit testing of a selective P2X7 antagonist.

6.2.1.i STZ-induced diabetes in male Sprague-Dawley rats

Male Sprague-Dawley rats weighing 200-250g (n=5/group) were administered a single IV dose of STZ (50mg/kg) or vehicle and followed for 21 weeks with periodic urine collection for measurement of albuminuria as a marker of nephropathy. Despite persistent hyperglycaemia in the STZ-treated group, no significant excess of albuminuria was apparent in the diabetic group by 21 weeks (Figure 6.1A and B).

6.2.1.ii STZ-induced diabetes combined with right uninephrectomy in Wistar Han rats

In order to promote more rapid development of nephropathy, rats underwent uninephrectomy (UNx) one week before administration of STZ. A different, nephropathy susceptible rat strain, the Wistar Han, was used to correspond with an established protocol (Dr Tim Johnson, Sheffield Kidney Institute, personal communication). Wistar Han rats proved more sensitive to the effect of STZ than Sprague Dawley, and an initial dose finding study

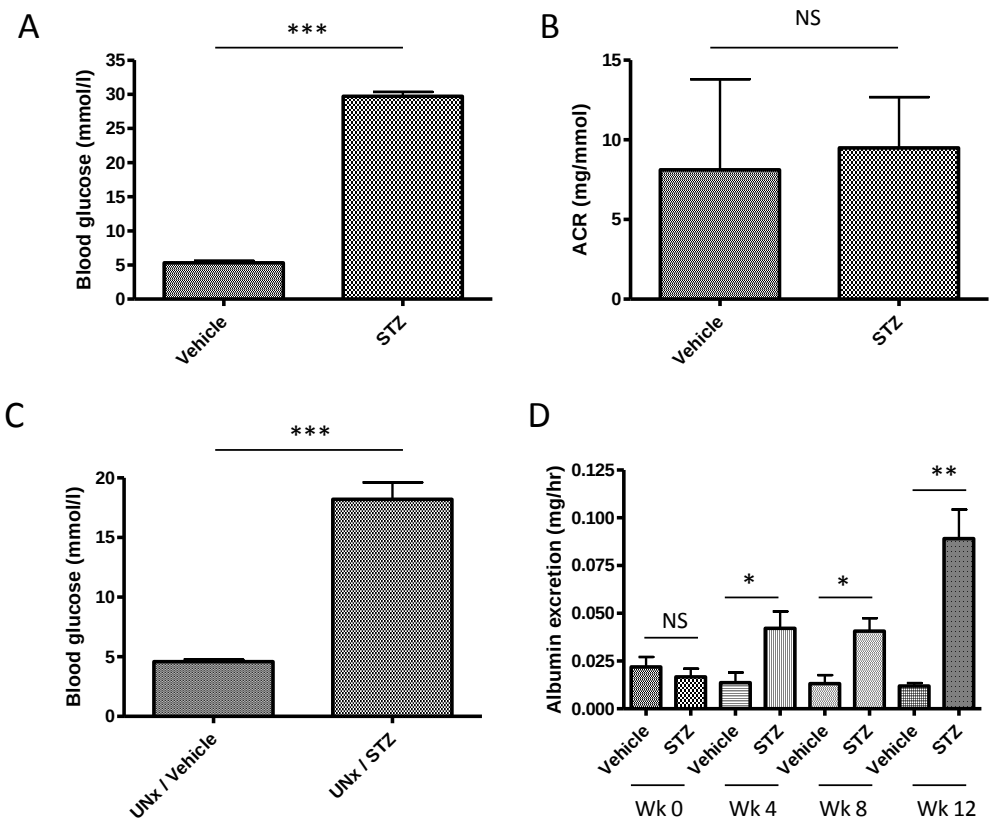

E

	Albumin excretion (mg/hr)			
	Week 0	**Week 4**	**Week 8**	**Week 12**
Unx/Vehicle	0.02 ± 0.01	0.01 ± 0.01	0.01 ± 0.01	0.01 ± 0.00
Unx/STZ	0.02 ± 0.01	0.04 ± 0.02	0.04 ± 0.01	0.09 ± 0.03
P value	0.5	0.03	0.02	0.002

Figure 6.1 Optimisation of a rat model of diabetic nephropathy. A,B: STZ-induced diabetes in male Sprague Dawley rats (n=5/group) C,D,E: STZ-induced diabetes in uninephrectomised Wistar Han rats (vehicle group n=4, diabetic group n=3). A: Mean blood glucose over 21 weeks. STZ-injected animals developed marked and sustained hyperglycaemia. B: Albumin:creatinine ratio. No increase in albuminuria was observed by 21 weeks. C: Mean blood glucose over 12 weeks. D: Albumin excretion over the course of 12 week experiment. A significant excess of albuminuria was present as early as 4 weeks with a further increase by 12 weeks. E: Albumin excretion rate (mg/hr) at each collection time-point, corresponding to graph D. *: $p<0.05$; **: $p<0.01$; ***: $p<0.001$; NS: Not significant.

established 40mg/kg IV as an effective but sub-lethal dose for induction of diabetes. Uninephrectomised male rats weighing 200-250g (n=4/group) were followed for 12 weeks after STZ or vehicle injection with 4 weekly urine collection for measurement of albuminuria and terminal collection of kidney tissue.

One STZ-injected rat spontaneously reverted to normoglycaemia 2 weeks post-injection and was excluded from further analysis; hyperglycaemia was maintained throughout in the remaining 3 diabetic animals (Figure 6.1C). A significant excess of albuminuria was apparent by 4 weeks in the diabetic group, with a further marked increase by week 12 (figure 6.1D and E). No increase in albuminuria was apparent in vehicle-injected uninephrectomised rats compared to baseline pre-nephrectomy values by 12 weeks. The increase in albuminuria by week 4 in diabetic animals was replicated in a second pilot experiment (data not shown).

6.2.2 P2X7 is constitutively expressed in rat distal convoluted tubule and upregulated in the glomerulus with diabetes

P2X7 expression was assessed on rat kidney tissue by immunohistochemistry using a rabbit polyclonal antibody to P2X7. Prominent tubular staining was observed in kidney from all animals tested: UNx diabetic rats, UNx control rats, and normal kidney obtained at the time of nephrectomy (Figure 6.2A and B). The stained tubules appeared most compatible with distal convoluted tubule (DCT), in view of their relatively 'open' appearance (low cuboidal epithelium); staining appeared to be localised predominantly to the basolateral epithelial area. Adjacent sections were subsequently stained for P2X7 and Calbindin D-28K, a protein involved

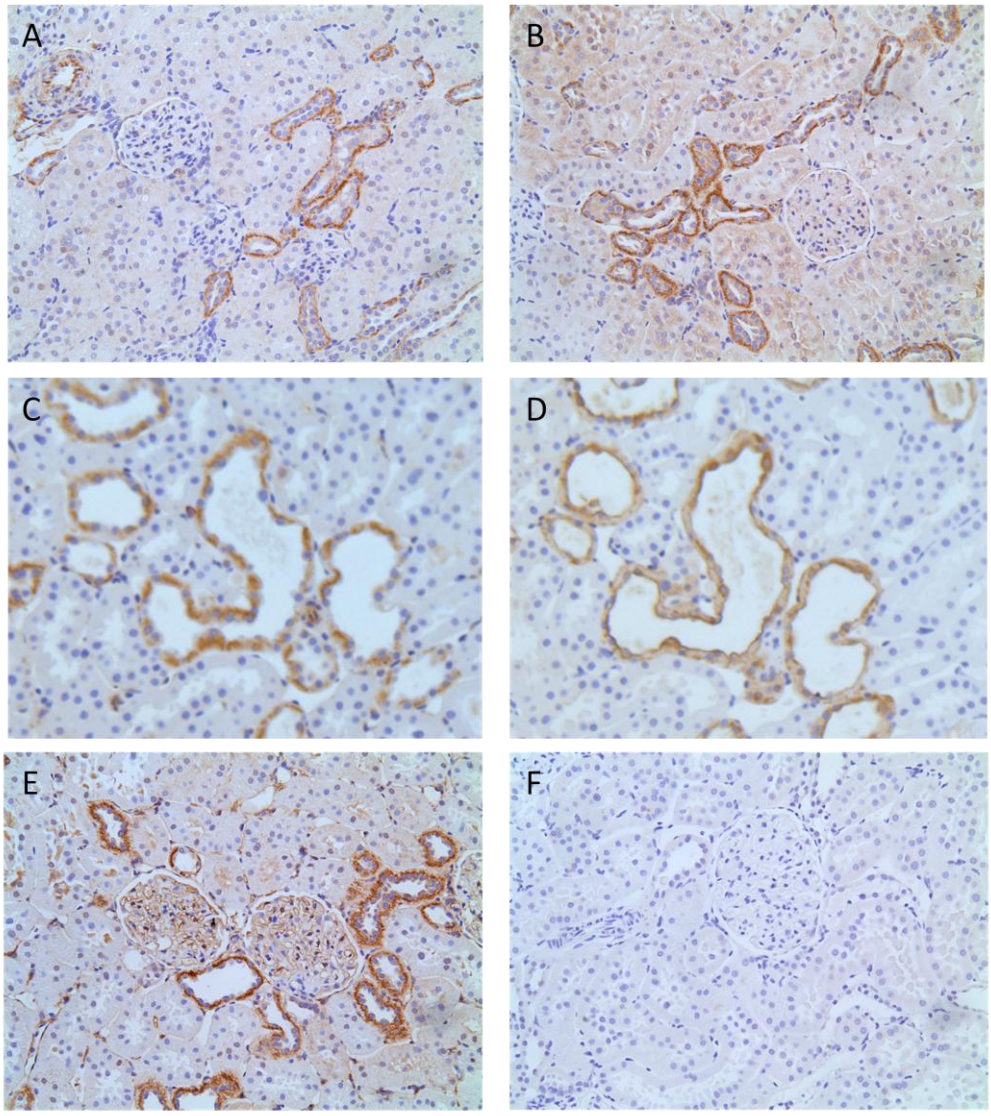

Figure 6.2 Immunohistochemistry for P2X7 in rat kidney. A: Normal Wistar Han kidney collected at nephrectomy. Marked basolateral staining was observed in a subpopulation of tubules while no signficant glomerular positivity was present. B: Kidney tissue from a week 12 vehicle-injected UNx Wistar Han rat. The staining pattern was unchanged from normal kidney with marked tubular positivity. C and D: Immunohistochemistry for P2X7 (C) and Calbindin D-28K (D) on adjacent sections from a vehicle-injected UNx rat. A perfect correspondence between staining patterns was observed indicating that P2X7 is constitutively expressed in rat DCT. E: Week 12 kidney from a STZ-injected UNx rat. In addition to the constitutive DCT staining, marked glomerular capillary loop staining was also apparent. F: Staining in an STZ-injected UNx rat where anti-P2X7 antibody was pre-absorbed with its cognate peptide in a 1:1 ratio, demonstrating the target specificity of the antibody. (x200 magnification)

in calcium transport along the rat DCT, with perfect correspondence of labelling (Figure 6.2C and D) (Rizzo et al., 2004). No significant glomerular P2X7 staining was observed in normal kidney or kidney from UNx control animals. Diffuse capillary loop staining was present in the majority of glomeruli in all diabetic animals examined (Figure 6.2E and Figure 6.3).

6.2.3 Testing the effect of a selective P2X7 antagonist on evolution of diabetic nephropathy

Once a reproducible model of DN had been established, the effect of a selective P2X7 antagonist, AZ11657312, was tested on evolution of disease. Diabetes was induced with STZ and maintained for 8 weeks before administering either drug (at 50mg/kg or 10mg/kg doses) or vehicle IP twice daily between weeks 8 and 12. Previously collected pharmacokinetic data has demonstrated AZ11657312 to be a high-clearance compound, with doses greater than 30mg/kg bd required in rats to maintain plasma levels above the 10x pA_2 value indicative of adequate exposure (AstraZeneca, unpublished data). Urine, serum and kidney tissue were collected for analysis at the end of the experiment.

6.2.4 Selective antagonism of P2X7 does not impact on progression of albuminuria or renal impairment in early experimental DN

Physical and biochemical data at baseline and week 12 is summarised in Table 6.1. BG was carefully controlled in diabetic animals by insertion of SC insulin pellets to gate BG between 16-33.3 mmol/l; the profile of glycaemic control was similar between all 3 diabetic groups (Figure 6.4A). Similarly, mean BG and total insulin dose did not differ between diabetic groups

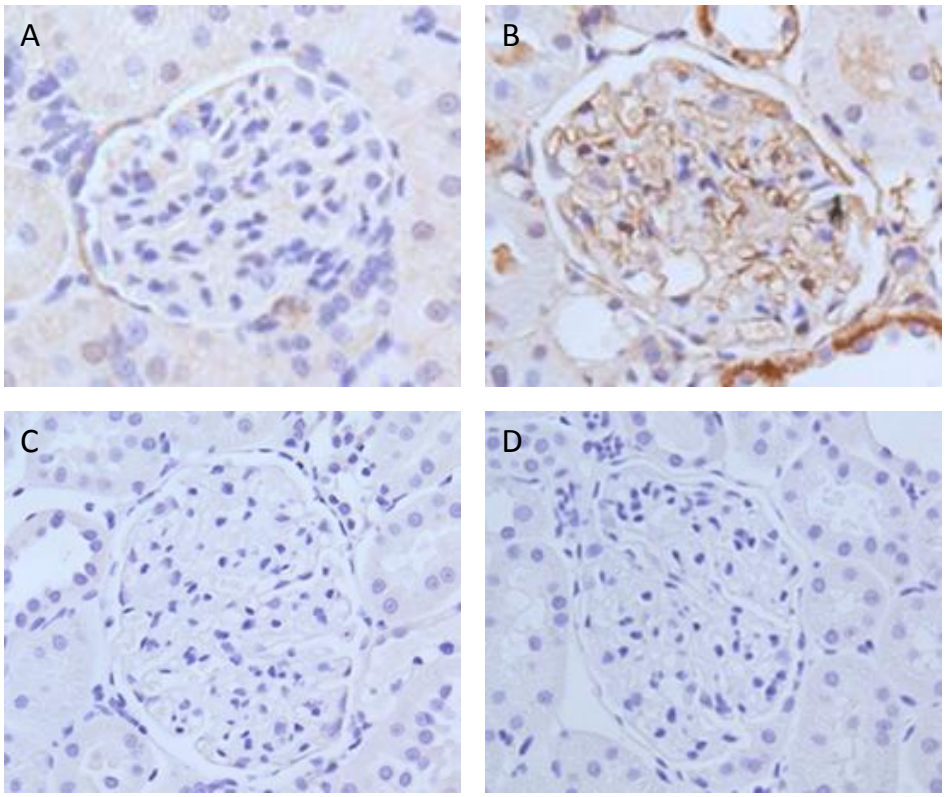

Figure 6.3 Immunohistochemistry for P2X7 in rat glomerulus. A: Glomerulus from normal Wistar Han rat (nephrectomy specimen), negative for P2X7. B: Glomerulus from STZ-injected UNx rat showing diffuse capillary loop staining not evident in controls rats C: Kidney from an STZ-injected rat incubated with anti-P2X7 antibody after pre-absorbing with its cognate peptide; no staining was seen, demonstrating the target specificity of the antibody. D: STZ-injected rat kidney incubated with non-immune polyclonal rabbit IgG applied at the same concentration as the primary antibody. The absence of staining excludes non-specific antigen-independent interactions of immunoglobulin with the tissue. (x200 magnification)

	Sham/ Vehicle (n=8)	**UNx/ Vehicle** (n=8)	**UNX/STZ/ Drug vehicle** (n=8)	**UN X/STZ/ 10mg/kg** (n=8)	**UNx/STZ/ 50 mg/kg** (n=9)
Wk 0 weight (g)	223.8 ± 12.5	218.8 ± 17.2	217.2 ± 13.3	215.3 ± 7.4	224.4 ± 10.3
% Weight gain (Wk 0 to Wk12)	84.0 ± 15.8	84.9 ± 18.7	18.5 ± 8.6[a,b]	23.3 ± 6.1	25.0 ± 10.8
Wk 0 BG (mmol/l)	4.8 ± 0.8	5.8 ± 0.8	5.1 ± 0.6	5.7 ± 1.5	6.0 ± 1.1
Mean BG (mmol/l)	4.6 ± 0.7	4.9 ± 0.6	30.6 ± 0.9[a,b]	30.7 ± 0.9	29.7 ± 1.4
Mean no. insulin pellets	N/A	N/A	3.0 ± 1.5	3.6 ± 1.3	3.9 ± 1.5
Kidney weight : body weight (mg/kg)	2.70 ± 0.29	3.95 ± 0.23[c]	8.17 ± 0.85[a,b]	7.88 ± 0.89	7.24 ± 0.98
Wk 12 AER (mg/hr) *	8.9 ± 2.3	16.0 ± 9.3	50.2 ± 20.3[d]	42.5 ± 17.9	82.3 ± 50.3
Wk 12 Serum Creatinine (µmol/l)	43.7 ± 4.4	48.9 ± 3.3	66.5 ± 5.6[a,b]	71.0 ± 9.1	64.7 ± 7.4

Table 6.1 Summary of physical and biochemical data for rat P2X7 antagonist DN study. [a]: p<0.001 vs sham/ vehicle; [b]: p<0.001 vs UNx/vehicle; [c]: p<0.01 vs sham/vehicle [d]: p<0.05 vs sham/vehicle. *Data presented with outlying values removed, leaving final group numbers: sham/vehicle n=8, Unx/vehicle n=8, Unx/STZ/drug vehicle n=7, Unx/STZ/AZ11657312 10mg/kg n=6, Unx/STZ/AZ11657312 50mg/kg n=9.

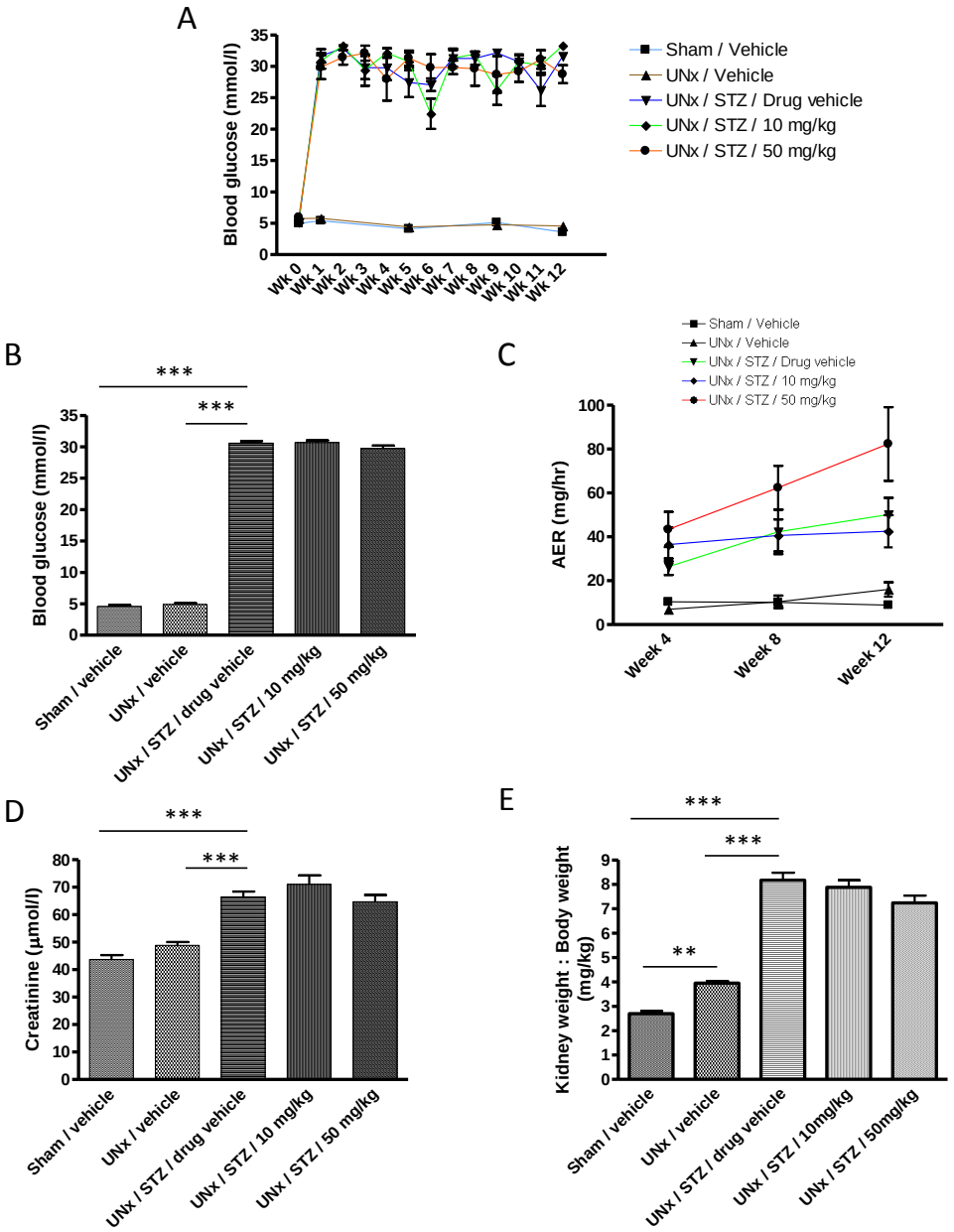

Figure 6.4 Glycaemia and renal outcomes. A: Mean BG at each measurement time-point. BG profile was similar between all 3 diabetic groups. B: Mean BG across weeks 1 to 12. C: Albumin excretion rate from weeks 4 to 12, edited for outlying values (see **Table 6.1** for details) . Although a progressive increase in albuminuria was observed in all 3 diabetic groups, no difference was seen between vehicle and drug treated groups at any time-point. D: Serum creatinine at week 12. E: Kidney weight : body weight. AER: Albumin excretion rate. **: p<0.01; ***: p<0.001.

(FIgure 6.4B). While urine albumin excretion increased progressively from week 4 in diabetic animals, no significant difference was apparent between either drug-treated group and drug vehicle group at week 12 (Figure 6.4C). Serum creatinine was also elevated in diabetic animals compared to both sham-operated and UNx control groups, but did not differ between the three diabetic groups (Figure 6.4D).

Kidney weight : body weight (KW:BW) was increased in UNx/STZ rats 2.1x compared to UNx/controls ($p<0.001$) and 3x compared to sham/controls ($p<0.001$) (Figure 6.4E). A stepwise trend towards decreased KW:BW was seen in antagonist-treated rats (mean reduction 50mg/kg vs drug vehicle groups, 0.933, 95% CI, -0.01 to 1.88). No significant difference in glomerular area was observed among any of the groups studied. No significant interstitial fibrosis was present at 12 weeks in any diabetic or control group as assessed by picrosirius red staining (Data not shown).

6.2.5 Analysis of renal macrophage accumulation

Macrophage infiltration was assessed by immunohistochemistry for CD68 and quantified for glomerular and tubulointerstitial compartments (Figure 6.5). Interstitial macrophage number was significantly increased in diabetic UNx rats compared to both sham-operated and UNx controls ($p<0.05$ for both comparisons) (Figure 6.5A-E). A trend towards reduced interstitial macrophage number was seen in 50 mg/kg (95% CI for difference: 1.5 to -15.9 cells per field) but not 10 mg/kg (95% CI for difference: 11.3 to -6.1 cells per field) P2X7 antagonist-treated rats compared to the drug vehicle group. Macrophage number was significantly reduced in 50mg/kg compared to 10mg/kg antagonist-treated rats ($p<0.05$). Glomerular macrophage number was not increased in diabetic rats compared to controls, and was similar across all 5 groups (Figure 6.5F).

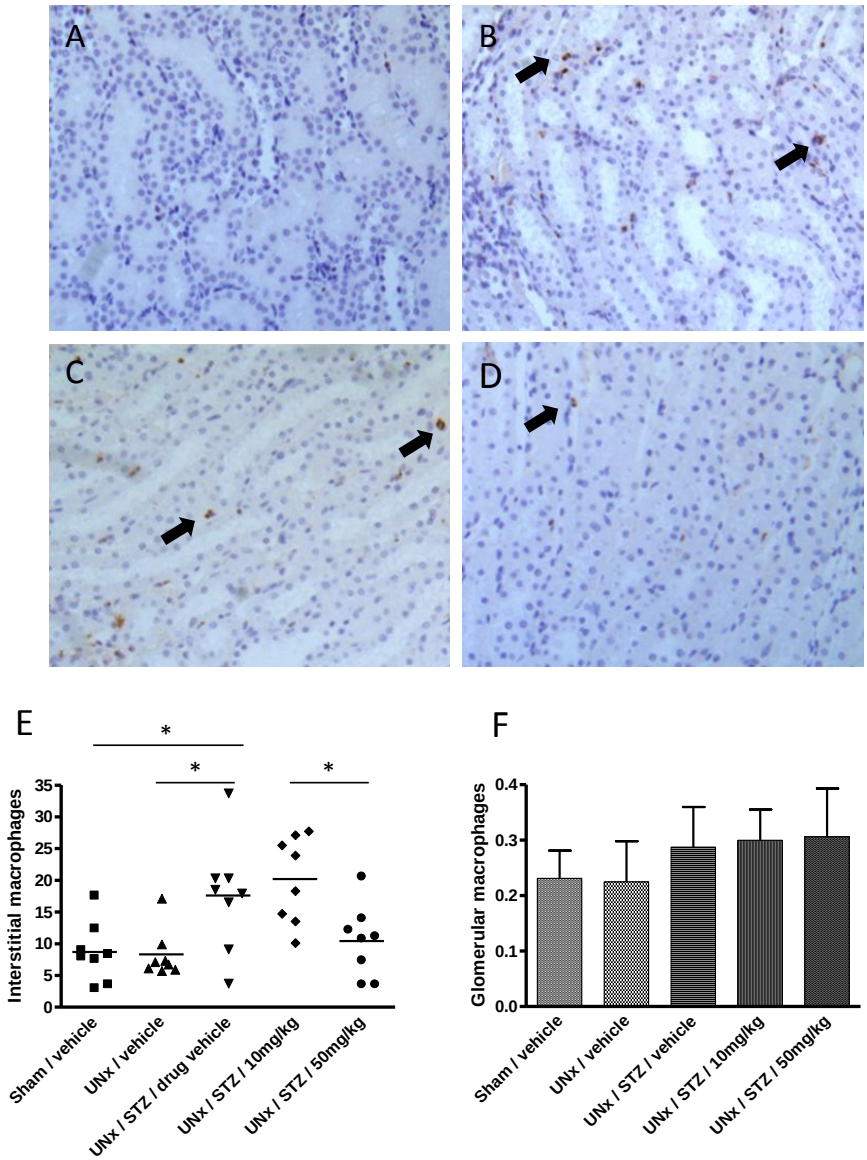

Figure 6.5 Assessment of macrophage infiltration by immunohistochemistry for CD68 (ED-1). A-D: Representative images of the tubulointerstitium (x200 magnification). A: Sham/vehicle-treated rat kidney with minimal macrophage infiltration apparent. B: UNx/STZ/drug vehicle-treated diabetic rat kidney with interstitial macrophage accumulation (arrows). C: Unx/STZ rat treated with 10mg/kg P2X7 antagonist; appearance was similar to rats treated with drug vehicle. D: 50mg/kg P2X7 antagonist-treated rat kidney; interstitial macrophage accumulation was attenuated in the majority of animals. E: Quantification of interstitial macrophage infiltration. F: Quantification of glomerular macrophage infiltration. *: $p<0.05$.

6.2.6 Analysis of mRNA expression of P2X7, inflammatory and ECM molecules

mRNA expression of P2X7, pro-fibrotic and inflammatory cytokines and ECM molecules was examined in homogenised whole kidney tissue by qPCR. (Table 6.2) P2X7 was upregulated significantly in UNx/STZ rats compared to sham/vehicle controls ($p<0.05$), with an trend towards increased expression compared to UNx/vehicle animals. (Figure 6.6A) A step-wise trend towards reduced P2X7 expression was seen in 10mg/kg (mean reduction vs UNx/STZ 4228 copies, 95% CI -7110 to 15570) and 50mg/kg (mean reduction 6649 copies, 95% CI -4369 to 17670) P2X7 antagonist-treated rats.

No significant upregulation of expression was observed in UNx/STZ rats compared to controls for TGFβ, COL4A1, COL1A1 or fibronectin-1, with expression similar across all groups for these mRNAs. pro-IL1β and MCP-1 expression was also similar across all 5 groups.

Expression of the macrophage chemokine, osteopontin, was increased significantly in UNx/STZ rats compared to both non-diabetic groups (Figure 6.6B). A trend towards reduced expression was observed in 10mg/kg antagonist-treated rats (mean reduction vs UNx/STZ 110,100 copies, 95% CI -24170 to 244300), while expression in the 50mg/kg treated group did not differ from drug vehicle. Expression of the cell adhesion molecule, ICAM-1, was also significantly elevated in UNx/STZ rats compared to sham/vehicle ($p<0.01$), with an upward trend compared to UNx/vehicle (mean increase 1385 copies, 95% CI -162.5 to 2933) (Figure 6.6C). The pattern of ICAM-1 expression observed in P2X7 antagonist-treated rats appeared the inverse of that for osteopontin, with a trend towards increased expression in the 10mg/kg group (mean increase vs UNx/STZ 958 copies, 95% CI -590 to 2505) and no difference in 50mg/kg group compared to UNx/STZ.

	Sham / Vehicle (n=8)	**UNx / Vehicle** (n=8)	**UNX /STZ/Drug vehicle** (n=8)	**UNx/STZ/ 10mg/kg** (n=8)	**UNx/STZ/ 50 mg/kg** (n=9)
P2X7 *	11439 ± 1574	20982 ± 9691	25278 ± 7202[a]	21051 ± 7781	18629 ± 10257
COL4A1*	34702 ± 6372	38220 ± 4718	37948 ± 12085	41012 ± 11256	40005 ± 8568
Fibronectin 1	2297 ± 352.8	2472 ± 613.5	2772 ± 754.4	2726 ± 867.7	3081 ± 930.9
COL1A1	6029 ± 1119	7465 ± 2053	5926 ± 2081	5563 ± 1905	7032 ± 1883
TGFβ	3523 ± 461.7	4386 ± 917.1	3654 ± 508.0	4023 ± 910.4	4087 ± 1025
IL1β	400.8 ± 48.4	466.6 ± 146	374.0 ± 62.6	440.1 ± 116	468.5 ± 185.2
MCP-1*	1300 ± 578.3	1760 ± 571.9	1069 ± 258.8	1274 ± 491.5	1564 ± 541.0
Osteopontin*	79236 ± 51446	92476 ± 30445	284762 ± 92792[b,c]	174675 ± 51959[d]	313053 ± 157979
ICAM-1	5288 ± 958.9	5810 ± 734.7	7195 ± 1460[e]	8153 ± 1141	7021 ± 1117

Table 6.2 Summary of qPCR data for rat P2X7 antagonist DN study. Values presented are absolute copy number. [a]: $p<0.05$ vs sham/vehicle; [b]: $p<0.001$ vs sham/vehicle; [c]: $p<0.01$ vs UNx/vehicle. [d]: $p<0.05$ vs 50mg/kg P2X7 antagonist group. [e]: $p<0.01$ vs sham/vehicle. *Data presented with outlying values removed, P2X7 n/group = 7,8,8,8,9; COL1A1 n/group = 8,8,8,7,8; MCP-1 n/group = 8,8,7,8,8; Osteopontin n/group = 8,8,8,7,9.

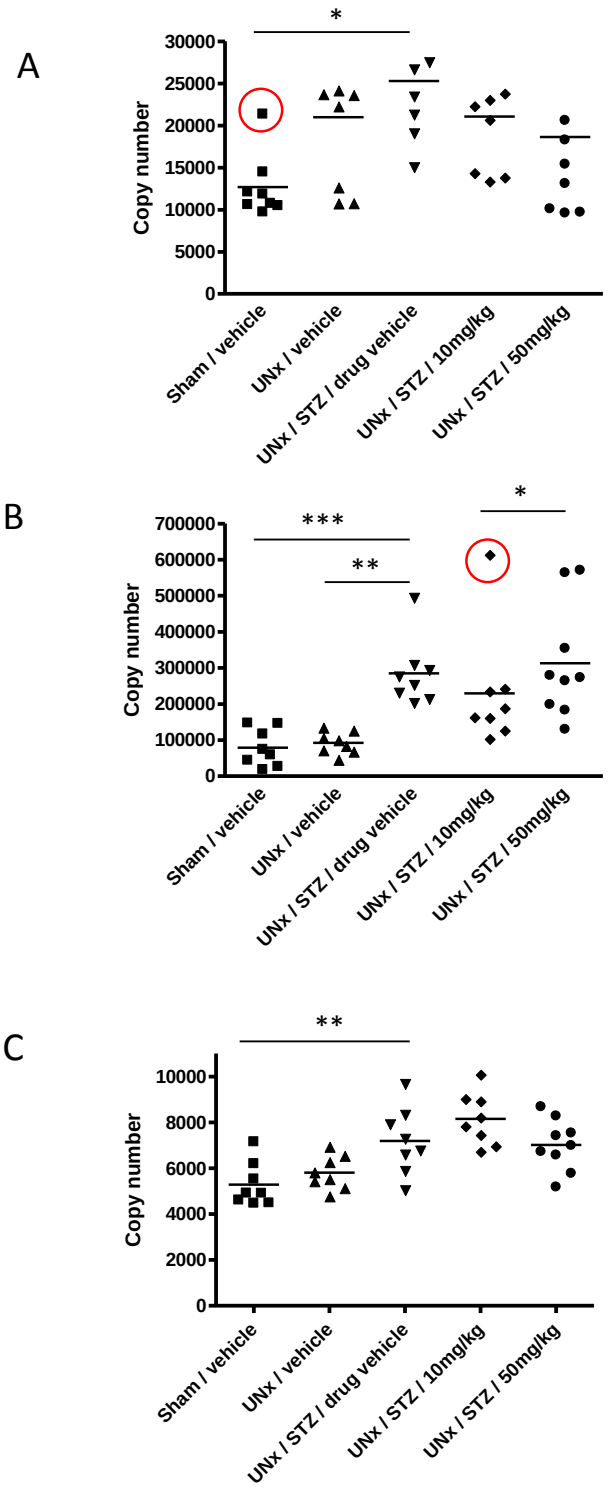

Figure 6.6. qPCR data from rat P2X7 antagonist experiment. A: P2X7, B: Osteopontin. C: ICAM-1. Circled datapoints represent outlying values excluded from analysis. *: $p<0.05$; **: $p<0.01$; ***: $p<0.001$.

6.2.7 P2X7 is upregulated in both glomeruli and peri-tubular capillaries at 12 weeks in a rat model of lean type 2 diabetes

The Goto-Kakasaki rat represents a model of lean type 2 diabetes, accompanied by mild and slowly evolving DN, and is discussed in Section 1.10.3.a. P2X7 expression was examined by specific immunohistochemistry in 12 week old GK rats and age-matched Wistar controls (Figure 6.7). Distal tubular P2X7 expression was observed as previously in control animals, with minimal glomerular staining (Figure 6.7A and C). In addition to tubular staining, GK rats exhibited diffuse capillary loop P2X7 positivity, similar to that observed at 12 weeks after STZ, as well as marked staining of peri-tubular capillaries (Figure 6.7B, D and E). A trend towards increased P2X7 mRNA expression was seen in GK rat kidney compared to Wistar control kidney (Figure 6.7G).

6.3 Discussion

In this experiment, it was sought to test the effect of a selective P2X7 antagonist on the evolution of nephropathy in the uninephrectomised STZ rat model of diabetes. At 12 weeks, this model manifests early DN, with evidence of renal enlargement and increased albumin excretion compared to sham-operated and single kidney controls, but no glomerular hypertrophy, mesangial expansion, interstitial fibrosis or transcriptional upregulation of ECM proteins. While P2X7 expression is upregulated in the diabetic glomerulus at 12 weeks, inhibition with a selective receptor antagonist between weeks 8 and 12 did not modify urinary albumin excretion or final serum creatinine. With the higher, 50mg/kg twice-daily antagonist dose, a trend towards reduced interstitial macrophage accumulation and KW:BW was observed.

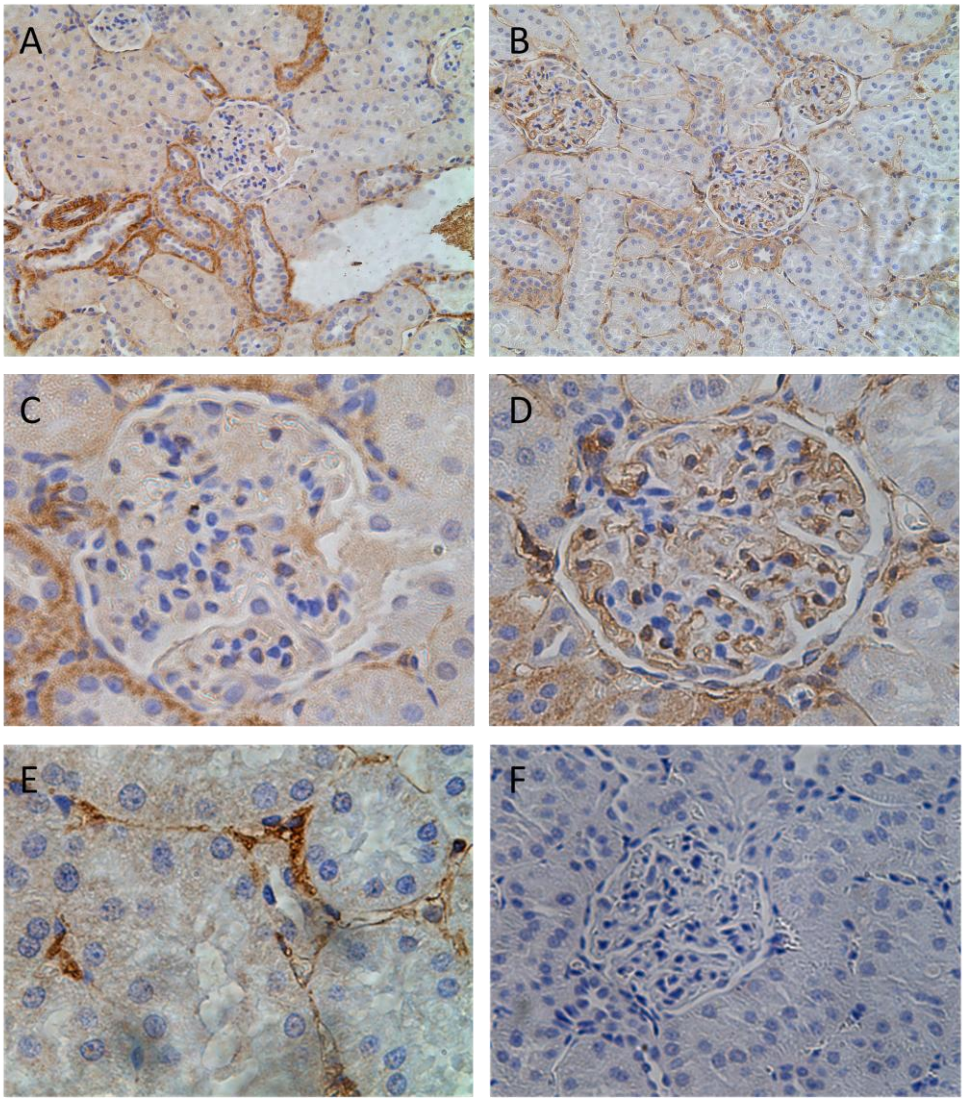

Figure 6.7 Specific IHC for P2X7 in 12 week GK rat. A: Cortex from 12 week Wistar non-diabetic control animal. Basolateral distal tubular staining is apparent, in keeping with findings from normal rats, mice and humans. B: Cortex from 12 week diabetic GK rat. Diffuse capillary loop staining and interstitial staining of per-tubular capillaries is apparent in addition to distal tubular positivity. (x200 magnification) C: High power view of a glomerulus from Wistar control rat. D: Glomerulus from GK rat showing capillary loop staining. E: High power view of tubulo-interstitium in GK rat demonstrating staining of small peri-tubular capillaries. F: Non-immune polyclonal IgG control with no staining.(x400 magnification) G: P2X7 mRNA expression in GK rat kidney measured by qPCR. A trend was seen towards increased expression in GK kidney compared to controls.

AZ11657312 is a highly potent, competitive antagonist at the P2X7 receptor. It was selected from a small molecule drug discovery program, where compounds were screened for inhibitory activity against BzATP-induced pore formation in HEK cells stably transfected with human or rodent P2X7 receptors. *In vivo* efficacy has previously been demonstrated, at a dose of 30-60mg/kg bd, on ankle swelling and mechanical hyperalgesia in the streptococcal cell wall (SCW) rat model of rheumatoid arthritis, and on development of interstitial fibrosis in the rat UUO model (AstraZeneca, unpublished data). Although AZ11657312 is absorbed orally, IP dosing was chosen to maximise bioavailability, with doses separated by ~10-14 hours. The chosen dosing schedule, between week 8, when a separation in albumin excretion between diabetic animals and controls has become clearly evident, and week 12, has relevance to management of human diabetes, where therapy is typically only commenced after signs of DN have become apparent.

The observed lack of impact of P2X7 blockade on albumin excretion is consistent with the experimental findings in GSK P2X7 KO mice and suggests that P2X7 does not contribute mechanistically to the early development of albuminuria. This is despite upregulation of P2X7 expression in the glomerulus at 12 weeks in both mice and rats with STZ-induced diabetes, and also GK lean type 2 diabetic rats. Although not formally co-localised, the pattern of glomerular P2X7 immunostaining is strongly suggestive of an endothelial cell locus of expression as the pattern is reminiscent of that observed with the endothelial cell marker CD31, and not the podocyte antigen, WT-1 (Pusztaszeri et al., 2006, Siu et al., 2006). While this expression does not appear to directly impact on the integrity of the glomerular filtration barrier by week 12, it is conceivable that inducible P2X7 expression may contribute to subsequent glomerular inflammation and disease progression, as occurs in diabetic mice. A longer duration of treatment with the receptor antagonist would be required to test this hypothesis.

Interstitial, but not glomerular, macrophage infiltration was observed in diabetic rats by 12 week, and a trend towards reduced macrophage numbers was observed in 50mg/kg antagonist-treated animals. mRNA for MCP-1, an important chemokine regulating glomerular macrophage recruitment, was not elevated, consistent with the lack of macrophages in this compartment. mRNA for osteopontin, important in co-ordination of interstitial macrophage migration, was upregulated in diabetic rats, with a trend towards reduced mRNA levels evident in 10mg/kg antagonist-treated animals. A trend towards *increased* expression of ICAM-1 mRNA, important in leucocyte adhesion, was also observed in 10mg/kg antagonist-treated rats, and may represent a reciprocal compensatory phenomenon. These findings are comparable to those seen in P2X7 KO mice, where glomerular macrophage infiltration was suppressed compared to WT. Although no significant interstitial fibrosis was apparent by 12 weeks in diabetic rats, one may predict that a reduction in interstitial macrophage infiltration may portend milder disease, were later time-points to be assessed (Chow et al., 2004b).

In summary, this study suggests, but does not conclusively prove, that inhibition of P2X7 by administration of a selective receptor antagonist ameliorates the interstitial inflammatory response observed in early DN in the rat. While longer-term studies are required to confirm efficacy against progressive disease, these data provide encouragement for the development of P2X7 antagonists as an adjunct to current standard therapy in human diabetic disease.

CHAPTER 7

Investigating the effects of diabetic and purinergic stimuli on P2X7 expression and MCP-1 secretion by resident glomerular cells *in vitro*

7.1 Introduction

Diabetic nephropathy (DN) is primarily characterised by its glomerular phenotype, histologically comprising GBM thickening and progressive mesangial sclerosis and manifesting clinically as proteinuria (Tervaert et al., 2010). All resident glomerular cell types are affected by the prevailing metabolic and haemodynamic disturbances: podocyte injury and loss occurs early, denuding areas of the GBM and provoking architectural disturbance in neighbouring epithelial cells; endothelial cells show swelling and thinning of the glycocalyx; and mesangial cells proliferate and elaborate excessive extracellular matrix (ECM) components (Gnudi, 2012). An early and prominent influx of macrophages into glomeruli is observed in experimental DN as early as day 3, preceding classical histological changes and preventable with insulin (Young et al., 1995). Interrupting this macrophage accumulation, either by depletion or interfering with critical adhesion molecules or chemokine signals, has been shown to attenuate glomerular injury, proving a critical role for this cell type in the evolution of DN (Lim and Tesch, 2012).

Although numerous inflammatory molecules have been linked to renal leukocyte recruitment in DN (reviewed in Chapter 1), the chemokine MCP-1 currently has the strongest evidence for an important functional role (Chow

et al., 2006, Lim and Tesch, 2012). MCP-1 is synthesised by all resident glomerular cell types as well as mononuclear cells (Kim and Tam, 2011). Hyperglycaemia induces an upregulation of MCP-1 protein production and release in both mesangial cells and podocytes *in vitro* (Ihm et al., 1998, Han et al., 2004). In addition to its role as a chemoattractant, MCP-1 has been demonstrated to mediate effects on podocyte mobility and albumin permeability, podocyte apoptosis and mesangial cell synthesis of ECM proteins, potentially positioning it as a central player in the pathogenesis of diabetic glomerulopathy (Park et al., 2008, Lee et al., 2009, Nam et al., 2012).

Previous studies of P2X7 in DN have demonstrated upregulation of mRNA and protein in all glomerular cell types, although predominantly the podocyte, at an early stage of disease development (Vonend et al., 2004). P2X7 has also been directly linked to the synthesis of ECM proteins in rat podocytes cultured under hyperglycaemic conditions *in vitro* (Solini et al., 2005). When studied in experimental nephrotoxic nephritis, a model of inflammatory glomerular disease, genetic P2X7 deficiency or inhibition markedly reduced the influx of macrophages into glomeruli and almost entirely abolished urinary excretion of MCP-1 (Taylor et al., 2009). When studied in astrocytes and microglia, application of the P2X7 agonist BzATP resulted in increased expression of MCP-1 (Panenka et al., 2001, Fang et al., 2011).

In view of these observations together with data from my experiments using the GSK P2X7 KO mouse (Chapter 5), showing a reduction in glomerular macrophage infiltration after induction of diabetes with STZ compared to WT animals, it was hypothesised that the diabetic milieu may upregulate P2X7 expression in glomerular cells and provoke a consequent increase in MCP-1 release. Hence to test this hypothesis, it was chosen to study the effect of hyperglycaemia on P2X7 expression and MCP-1 secretion from both human podocytes and mesangial cells *in vitro*.

7.2 Results

7.2.1 Characterisation of podocytes

Conditionally-immortalised human podocytes (a gift of Prof. Moin Saleem) were allowed to proliferate at 33^{o}C in a medium approximating human euglycaemia (4mM D-glucose). Cells were then transferred to 37^{o}C for 2 weeks to inactivate the temperature-sensitive SV40 T transgene and trigger subsequent differentiation to a mature form. Efforts were made to characterise the differentiated cells prior to further study to ensure they were adequately recapitulating the anticipated mature phenotype.

Cells grown at 33^{o}C showed a cobblestone morphology (typical for epithelial cells) but after transfer to 37^{o}C and arrest of proliferation underwent a gradual change in appearance with irregular enlargement of the cell body and appearance of long spindle-like cytoplasmic processes (Figure 7.1). The majority of cells underwent these changes, consistent with the original published report of their behaviour, although occasional small rafts of undifferentiated cells were observed. (Saleem et al., 2002) Expression of the slit-diaphragm protein nephrin was confirmed in mature cells by specific immunofluorescence: a diffuse cytoplasmic staining pattern was observed in differentiated cells as opposed to a peri-nuclear distribution in proliferating cells, suggesting cellular redistribution of the protein during the maturation process. Podocin was also examined by specific immunofluorescence and showed an increase in cytoplasmic staining intensity during the maturation process although unexpected nuclear staining was also prominent at all time-points. Expression of SV40 large T antigen was examined by Western blot; expression level appeared unchanged across all-time points examined suggesting incomplete inactivation of the transgene by temperature modulation.

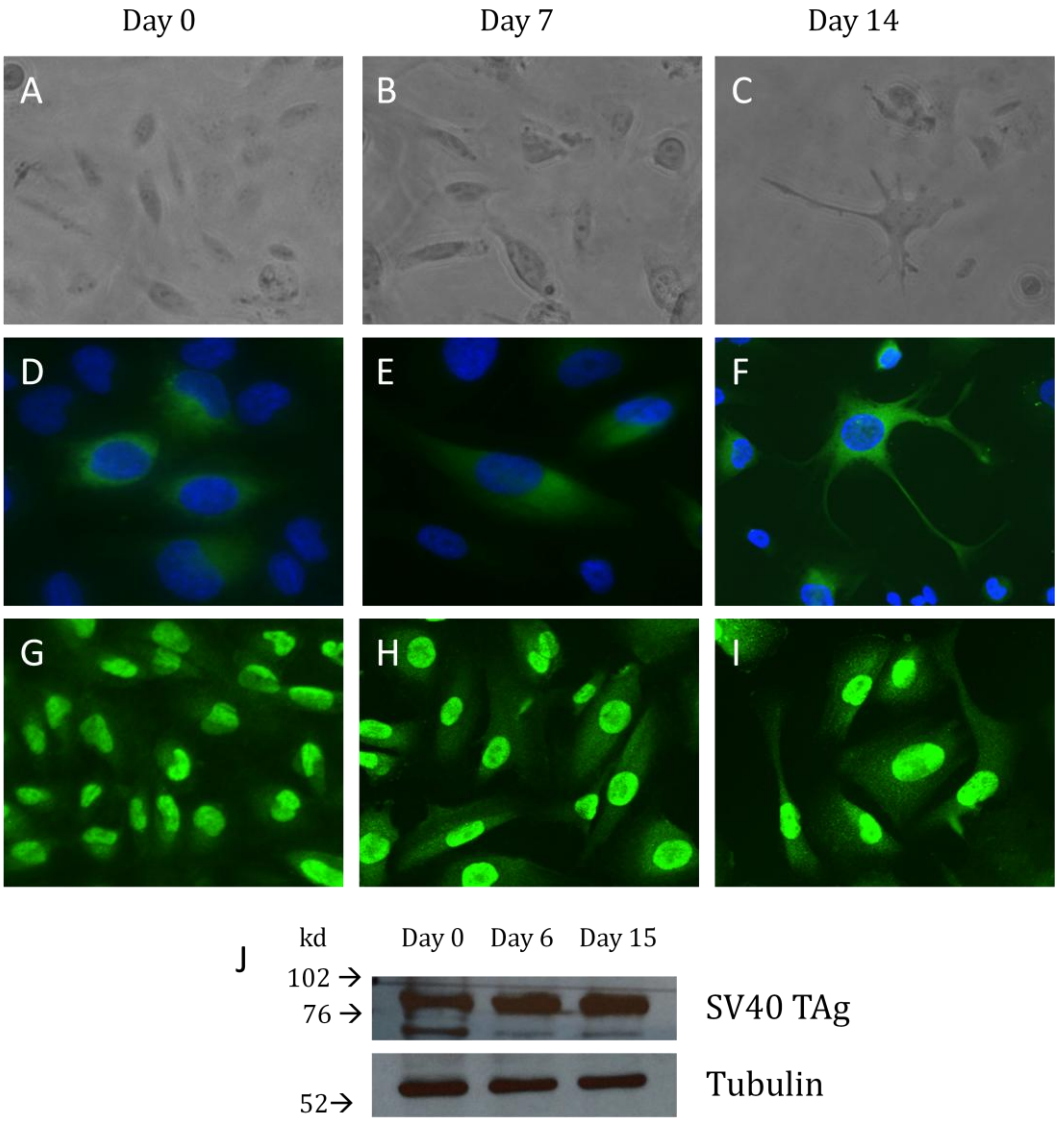

Figure 7.1 Characterisation of AB8/13 conditionally immortalised human podocyte cell line. A-C: Phase- contrast micrographs illustrating the change in cellular morphology during differentiation at 37°C. Cells bodies elongate and develop long slender cytoplasmic processes. D-F: Specific immunofluorescence for nephrin (green) with DAPI nuclear counterstain (blue). Initial staining (D) is faint and peri-nuclear but by day 14 (F) this extends throughout the cytoplasm. G-I: Immunofluorescence for podocin (green). Cytoplasmic fluorescence intensity increases with time although nuclear staining is prominent throughout. J: Immunoblot for SV40 T antigen. Expression levels do not appear to decrease despite two weeks growth at the inactivating higher temperature. This suggests proliferative behaviour may not be fully inhibited by the ambient temperature switch as reported.

7.2.2 Secretion of MCP-1 from human podocytes exposed to hyperglycaemia is inconsistent between experiments

The capacity of mature podocytes to secrete MCP-1 was first tested by stimulating them with the inflammatory cytokine TNFα (10 ng/ml) for 48 hours. TNFα provoked a 5-fold rise in MCP-1 secretion, as measured in conditioned media by specific ELISA, compared to unstimulated cells. (Figure 7.2A) Fully differentiated podocytes were subsequently cultured for 48 hours in hyperglycaemic (30mM D-glucose) or euglycaemic (4mM) media, or with an osmotically equivalent concentration of the metabolically inactive stereoisomer L-glucose (26mM L-glucose + 4mM D-glucose). Although an increase in MCP-1 secretion was observed with hyperglycaemia, the magnitude of the response was variable between experiments (Figure 7.2B,C), as was the proportion of non-adherent cells observed at the point of supernatant collection. No significant increase in MCP-1 was observed after culture in 30mM D-glucose for 96 hours, while MCP-1 secretion from cells incubated with L-glucose was significantly reduced compared to 4mM D-glucose controls by this time (Figure 7.2D).

A single experiment was performed with the selective P2X7 antagonist A438079 (10μM) added to cultures with or without hyperglycaemic medium for 48 hours (Figure 7.2E). A significant *increase* in MCP-1 release was observed in the presence of A438079 from cells grown in both 4mM D-glucose and 30mM D-glucose, although hyperglycaemia alone did not increase MCP-1 levels compared to euglycaemia in this experiment. A438079 did not influence the secretion of MCP-1 induced by culture with TNFα for 48 hours (Figure 7.2F).

In view of the difficulties in establishing a reproducible response of the podocytes to hyperglycaemic challenge in terms of MCP-1 secretion, no

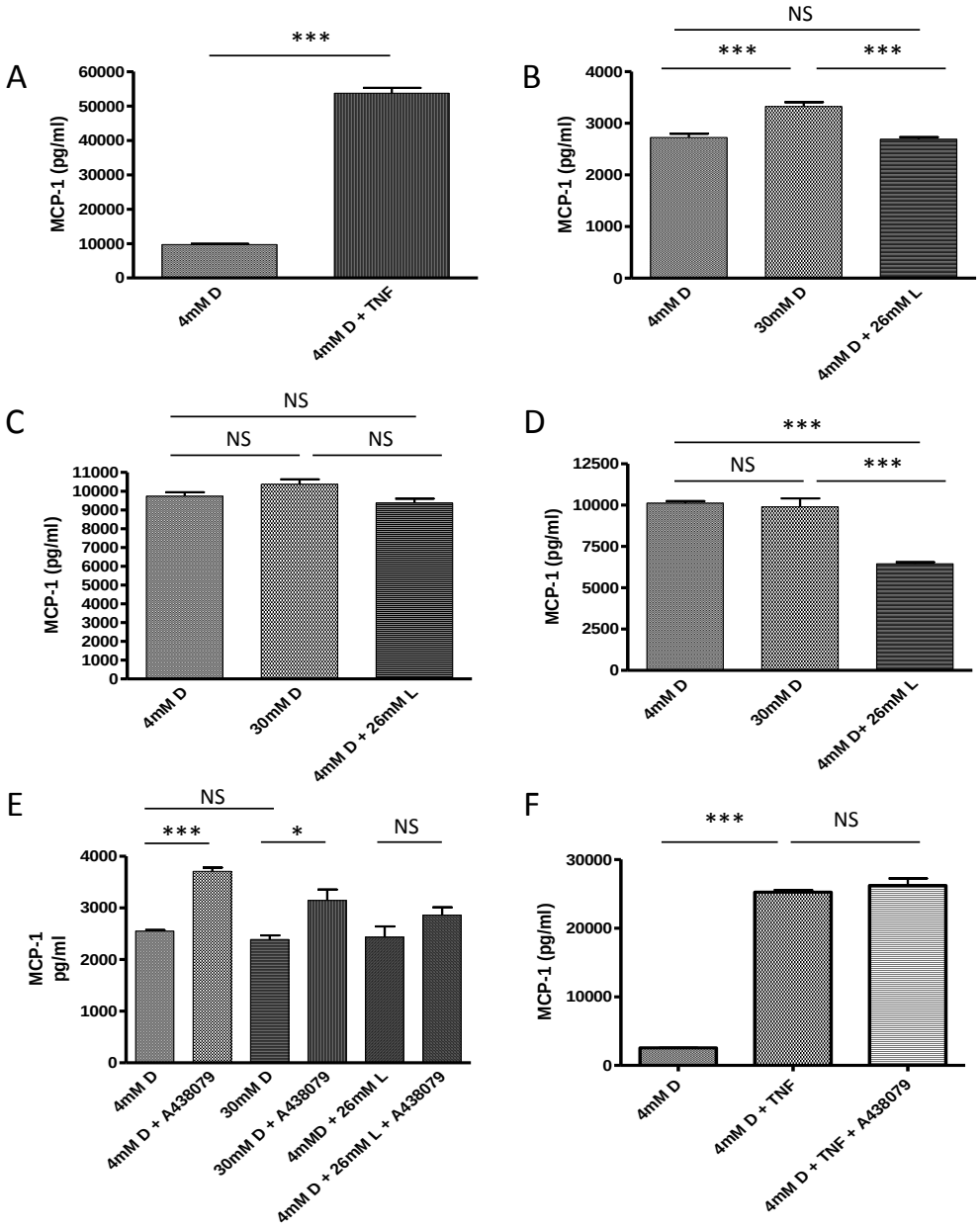

Figure 7.2 Podocyte MCP-1 secretion under hyperglycaemic and inflammatory stress. A: Stimulation with TNFα (10ng/ml) for 48 hours provoked a 5-fold rise in MCP-1 secretion compared to basal 4mM D-glucose conditions. B,C: Two illustrative experiments of stimulation with 30mM D-glucose or osmotic control for 48 hours showing the observed increase in MCP-1 secretion was inconsistent in magnitude. D: No excess of MCP-1 was observed when cells were cultured in 30mM D-glucose for 96 hours although MCP-1 secretion was reduced from cells cultured in L-glucose compared to 4mM D-glucose controls. E: A438079 (10μM) provoked a *rise* in MCP-1 secretion under both normal and high glucose conditions, although hyperglycaemia itself did not increase secretion in this experiment. F: A438079 (10μM) had no effect on the increased MCP-1 secretion provoked by TNFα (10ng/ml). N=3-4/group in all experiments. D: D-glucose; L: L-glucose. *: $p<0.05$; ***: $p<0.001$; NS: Not significant.

further investigations were undertaken of the role of the P2X7 receptor in this cell line.

7.2.3 Secretion of MCP-1 from transformed human mesangial cells exposed to hyperglycaemia is inconsistent between experiments

A transformed human mesangial cell line (tHMC) was available (see Section 2.16.2.i) which had been used with success locally for other applications, hence initial studies of the mesangial MCP-1 response to hyperglycaemia were performed using these. In the same manner as for podocytes, an initial stimulation was performed with TNFα to confirm whether tHMC secrete MCP-1 in respone to a robust inflammatory stimulus. TNFα provoked an 8-fold rise in MCP-1 secretion compared to unstimulated cells (Figure 7.3A). As with the podocyte line, mesangial cells were then incubated for 48 hours in high or low glucose or L-glucose as an osmotic control. Over four experiments the magnitude of MCP-1 response to hyperglycaemia proved highly variable (Figure 7.3B). In those experiments where a significant increase in secretion in response to hyperglycaemia was observed, no difference was seen as compared to the L-glucose control, suggesting any such effect was a direct consequence of changes in tonicity of the culture milieu. For these reasons, no further investigations were undertaken with this cell line.

7.2.4 Hyperglycaemia induces a reproducible rise in MCP-1 secretion, but not IL1β, from primary human mesangial cells, independent of its osmotic effect

In view of the inconsistent response to hyperglycaemia observed with transformed mesangial cells, further experiments were undertaken with

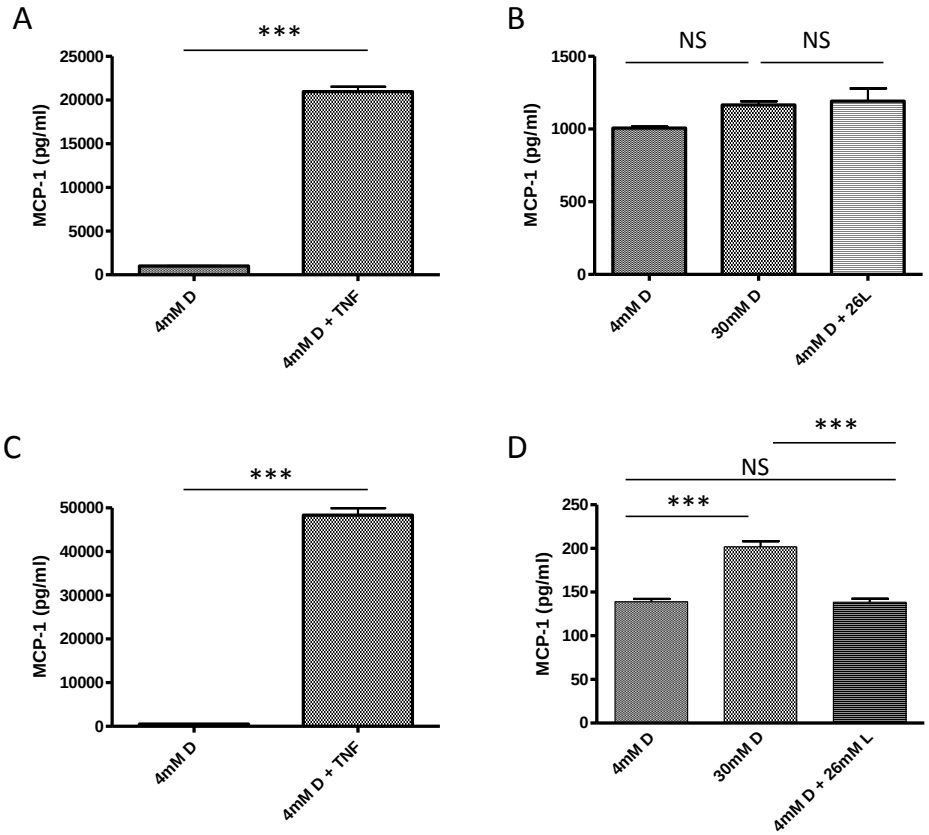

Figure 7.3 MCP-1 secretion from transformed and primary HMCs under hyperglycaemic and inflammatory stress. A: Stimulation of transformed HMCs with TNFα (10ng/ml) for 48 hours provoked an 8-fold rise in MCP-1 secretion compared to basal glycaemic conditions alone. B: A representative trial of MCP-1 secretion from transformed HMCs under hyperglycaemic conditions. The rise in MCP-1 secretion in response to hyperglycaemia was variable and when present, did not differ from the effect of the osmotic control. C: Stimulation of primary HMCs with TNFα (10ng/ml) for 48 hours provoked a 90-fold rise in MCP-1 secretion compared to basal glycaemic conditions alone. D: Culture of primary HMCs in 30 mM D-glucose provoked a robust increase in MCP-1 secretion that was not reproduced by an equivalent concentration of L-glucose, suggesting the response was independent of the hypertonic effect of hyperglycaemia. N= 3-4/group in all experiments. ***: $p<0.001$; NS: Not significant.

commercially-available human primary mesangial cells (pHMC). The ability of these cells to secrete MCP-1 when exposed to a robust inflammatory cytokine stimulus (TNFα 10ng/ml) was again assessed. TNFα provoked a 90-fold rise in MCP-1 secretion compared to unstimulated cells. (Figure 7.3C). On incubation of cells with 30mM D-glucose for 48 hours, in all experiments a rise in MCP-1 of 25-50% was observed compared to cells grown in 4mM D-glucose (Figure 7.3D). No rise in MCP-1 was elicited with an osmotically equivalent concentration of L-glucose.

To ascertain whether pHMCs are capable of significant IL1β release, cells were exposed to TNFα 10ng/ml for 48 hours and IL1β was measured in supernatant by specific ELISA. No IL1β was detectable in supernatants from either TNFα stimulated or unstimulated cells. In a single experiment, IL1β was also undetectable after cells were cultured in either 30mM D-glucose or an osmotically equivalent concentration of L-glucose for 48 hours.

Given the importance of ATP as a stimulus for IL1β maturation and release from macrophages, IL1β was also measured in pHMC supernatants in a single experiment following 30 minutes exposure to 5mM ATP, after pre-culture in either 4mM or 30mM D-glucose media or 4mM D-glucose media supplemented with TNFα (10ng/ml) for 48 hours. Again, no IL1β was detectable in cell culture supernatants of any group. pHMC hence do not appear capable of significant mature IL1β secretion under the culture conditions used in this study.

7.2.5 P2X7 is constitutively expressed in pHMC with cellular redistribution on exposure to hyperglycaemia

P2X7 expression in pHMC was examined using Western blotting of cell lysates and specific immunofluorescence staining of fixed cells. Using a monoclonal anti-P2X7 primary antibody, a band of the anticipated molecular weight (72kD) was observed in lysates from cells grown for 48 hours in both 4mM and 30mM D-glucose media (Figure 7.4A). A trend towards increased P2X7 expression, as quantified by band densitometry, was apparent in cells grown under hyperglycaemic conditions (Figure 7.4B) P2X7 was also present but not upregulated in cells stimulated with TNFα 10ng/ml (data not shown).

Intensity of cytoplasmic staining for P2X7 by immunofluorescence (using the same monoclonal anti-P2X7 antibody) appeared greater in cells cultured in a hyperglycaemic milieu than low glucose conditions (Figure 7.4C,D). Occasional peripheral ring-like figures, presumed to represent coalescence of P2X7 molecules into pore-like structures were also observed (Figure 7.4E), as have been described elsewhere, suggesting that hyperglycaemia can provoke cellular redistribution of the pre-formed protein (Solini et al., 2005).

7.2.6 P2X7 contributes to regulation of MCP-1 secretion from pHMC exposed to hyperglycaemia

The effect of a small molecule selective P2X7 antagonist, A438079, on MCP-1 secretion from pHMC exposed to hyperglycaemia was tested. At 10μM concentration, A438079 reduced hyperglycaemia-induced MCP-1 secretion by 43.9 ± 61.0% aggregated over 9 separate experiments ($p=0.057$; paired *t*-test), although some variability in response was observed between experiments. (Figure 7.5A,B). This effect was sustained across the range of

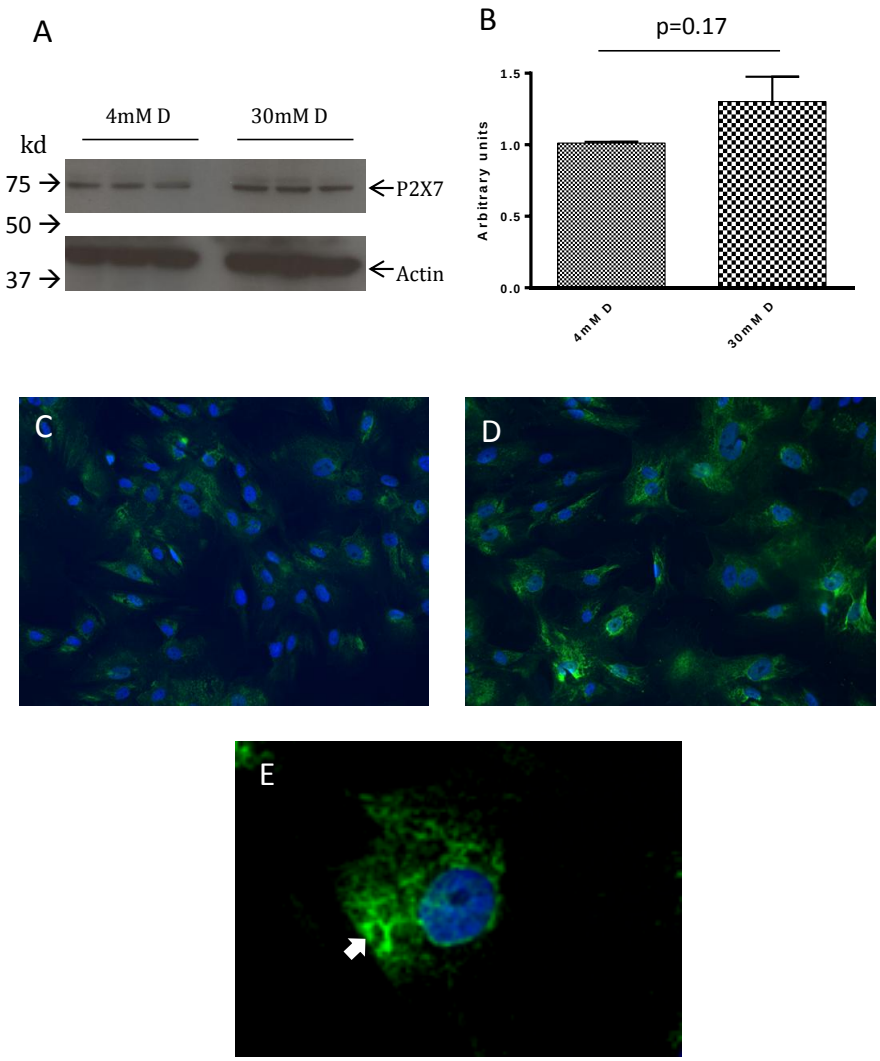

Figure 7.4 P2X7 expression in primary HMCs. A,B: Specific immunoblot for P2X7 with an actin loading control (A) and P2X7 expression quantified by densitometry (B). P2X7 was expressed under basal culture conditions, with a trend towards upregulated expression after culture in hyperglycaemic medium. C,D,E: Specific immunofluorescence for P2X7. C: P2X7 expression under basal glucose conditions. D: P2X7 expression under hyperglycaemic conditions. Intensity of cytoplasmic staining for P2X7 appeared increased under high glucose conditions with an increased incidence of organised peripheral ring-like structures (E, arrow).

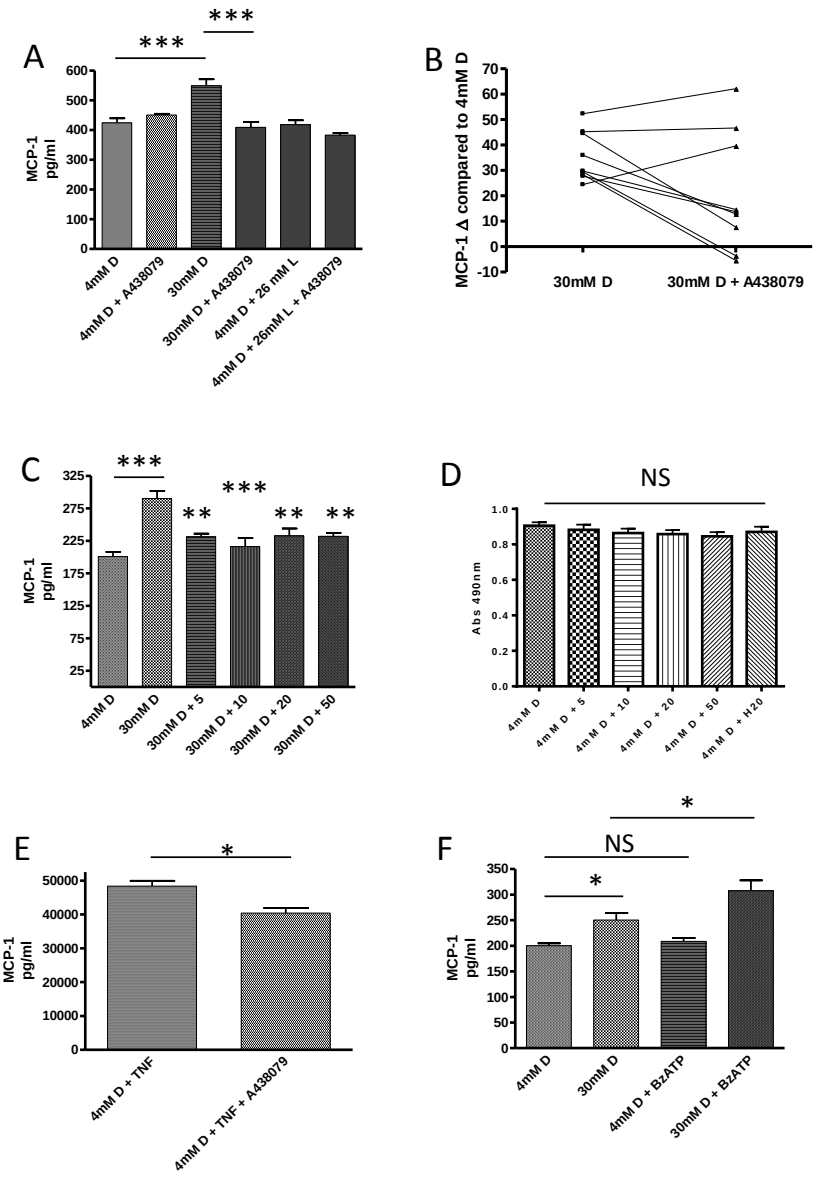

Figure 7.5 P2X7 contributes to regulation of hyperglycaemia-induced MCP-1 secretion from primary HMCs. A,B,C: Effect of the small molecule selective P2X7 antagonist A438079 on hyperglycaemia-induced MCP-1 release. A: An example of an experiment where A438079 (10μM) was added to cells grown either in 4mM or 30mmM D-glucose or L-glucose as an osmotic control. In this instance, A438079 suppressed hyperglycaemia-induced MCP-1 release to basal levels. B: Over 9 independent experiments, an average reduction in MCP-1 secretion of 43.9 ± 61.0% was observed, with inhibition observed in 6/9 trials and no effect or increased secretion in 3/9. C: No apparent dose-dependence was seen over a range of concentrations of A438079 from 5 to 50 μM, with all proving equally effective (all comparisons to 30mM D-glucose group). D: Assessment of A438079 cytotoxicity using MTS assay. A438079 had no effect on cell viability as assessed over the 5 to 50μM concentration range. E: Effect of A438079 on TNFα-induced MCP-1 release. A438079 (10 μM) partially inhibited TNFα stimulated MCP-1 release (18.6 ± 3.0% reduction). F: The P2X7 agonist BzATP (100μM) provoked an additive increase in MCP-1 secretion under high glucose, but not low glucose, conditions. N=3-4/group D: D-glucose; L: L-glucose. *: $p<0.05$; **: $p<0.01$; ***: $p<0.001$; NS: Not significant.

concentrations of A438079 tested (5-50μM) (Figure 7.5C). A438079 also produced a proportionally smaller but significant reduction in MCP-1 secretion after stimulation with TNFα 10 ng/ml (18.6 ± 3.0% reduction compared to TNFα alone) (Figure 7.5E). No evidence of cytotoxicity was observed with A438079, as measured by MTS assay, over a range of concentrations from 5 to 50 μM (Figure 7.5D). The P2X7 agonist BzATP had no effect on MCP-1 secretion when added to cells incubated in 4mM D-glucose, but provoked a significant additive increase in MCP-1 secretion when applied to cells incubated in 30mM D-glucose (114.1% increase compared to baseline vs 30mM D-glucose alone, $p<0.05$, pooled data from two trials) (Figure 7.5F).

7.2.7 The ATP-hydrolysing enzyme apyrase enhances MCP-1 secretion from pHMC.

Apyrase efficiently hydrolyses ATP to yield AMP and inorganic phosphate. ATP is the dominant agonist of P2X7 and indeed all P2X family receptors. Given the observed partial P2X7-dependence of pHMC MCP-1 secretion, apyrase was added to cultures in the expectation that MCP-1 secretion would be attenuated as agonist at the P2X7 receptor (ATP) would be degraded.

Addition of apyrase (5 U/ml) to cultures led to an *increase* in MCP-1 secretion, most marked under hyperglycaemic conditions (78.8 ± 65.4% increase compared to 30mM D-glucose alone) (Figure 7.6A) The rise in MCP-1 under hyperglycaemic conditions was dependent on the concentration of apyrase added (Figure 7.6B).

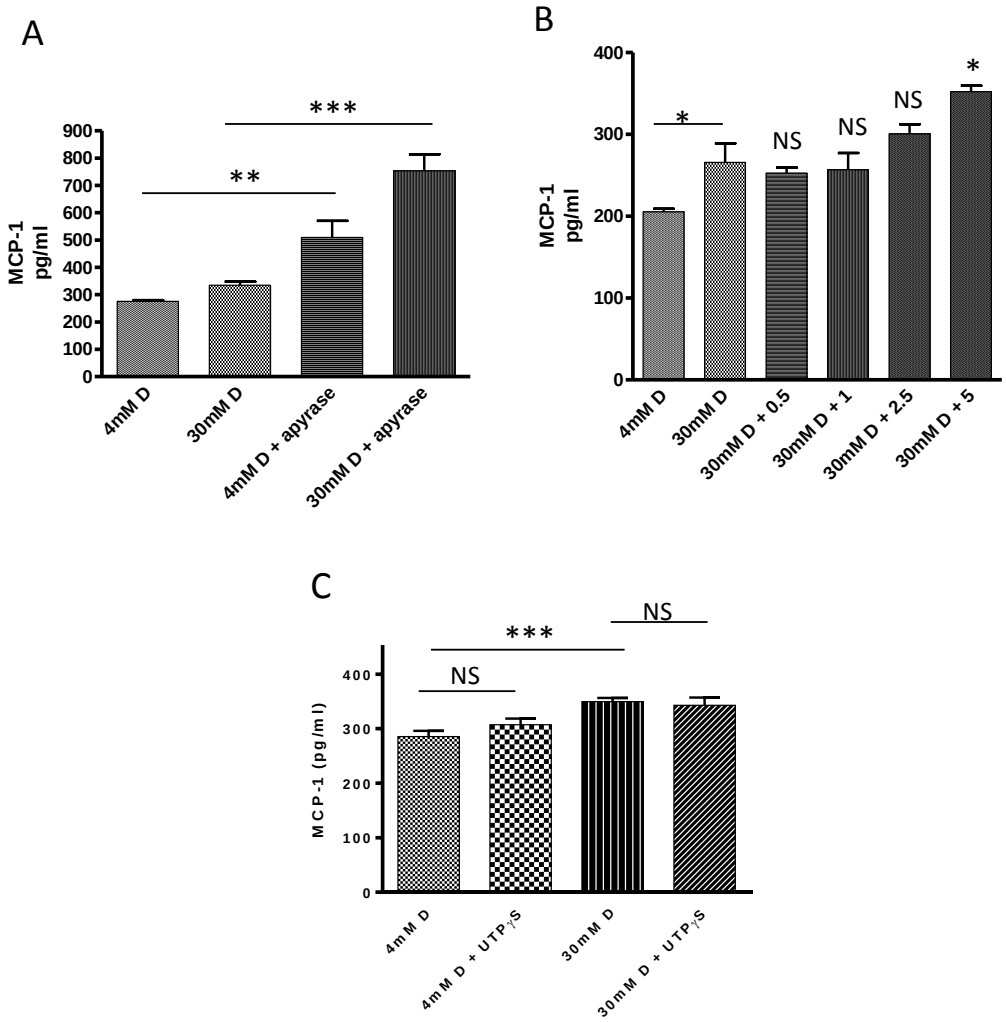

Figure 7.6 ATP may regulate hyperglycaemia-induced MCP-1 secretion via multiple P2 receptors. A,B: Incubation of HMCs with the ATP hydrolysing agent apyrase, in the presence or absence of hyperglycaemia. A; Apyrase (5U/ml) induced a *rise* in MCP-1 secretion under both normal and high glucose conditions. B: The effect of a range of concentrations (0.5 – 5U/ml) were examined; a trend towards increased MCP-1 secretion with increasing apyrase concentration became statistically significant at 5U/ml. C: The P2Y2/4 agonist, UTPγS, at 10μM produced a small but non-significant rise in MCP-1 release under low glucose conditions but the opposite effect under high glucose conditions. D: D-glucose. *: $p<0.05$; **: $p<0.01$; ***: $p<0.001$; NS: Not significant.

7.2.8 Hyperglycaemia-induced MCP-1 secretion may be regulated by multiple competing purinoceptor signals

The observed enhancement of MCP-1 release with the addition of the ATP-hydrolysing enzyme apyrase raises the possibility that ATP or adenosine may provoke differential effects on MCP-1 secretion from HMCs, presumably as a result of activity at multiple receptors. ATP is the dominant agonist at all P2X receptors and several P2Y receptors including P2Y2 and P2Y11. To investigate this further, cells were cultured in the presence of 5-BDBD, a potent P2X4 receptor antagonist, and UTPγS, an agonist at the P2Y2 and P2Y4 receptors, both of which have been implicated in inhibitory effects on ECM production in rat MCs (Solini et al., 2005). Expression of both P2X4 and P2Y2 has previously been demonstrated in pHMC cultures (Solini et al., 2007).

UTPγS (10μM) produced a trend towards increased MCP-1 release under normoglycaemic conditions (7.6% increase vs 4mM D-glucose, $p>0.05$) but a trend towards reduced MCP-1 secretion under hyperglycaemic conditions (10.3% reduction compared to basal secretion vs 30mM D-glucose, $p>0.05$, pooled data from 2 trials.) (Figure 7.6C).

P2X4 expression in pHMC was examined using Western blotting of cell lysates. Using a polyclonal anti-P2X4 primary antibody, a band of the anticipated molecular weight (62kD) was observed in lysates from cells grown for 48 hours in both 4mM and 30mM D-glucose media (Figure 7.7A). A trend towards increased P2X4 expression, as quantified by band densitometry, was apparent in cells grown under hyperglycaemic conditions (Figure 7.7B). Addition of 5-BDBD (10μM) to cultures provoked an additional *increase* in MCP-1 release under high glucose, but not low glucose, conditions (85.9% increase compared to 30mmM D-glucose alone, $p<0.05$, pooled data

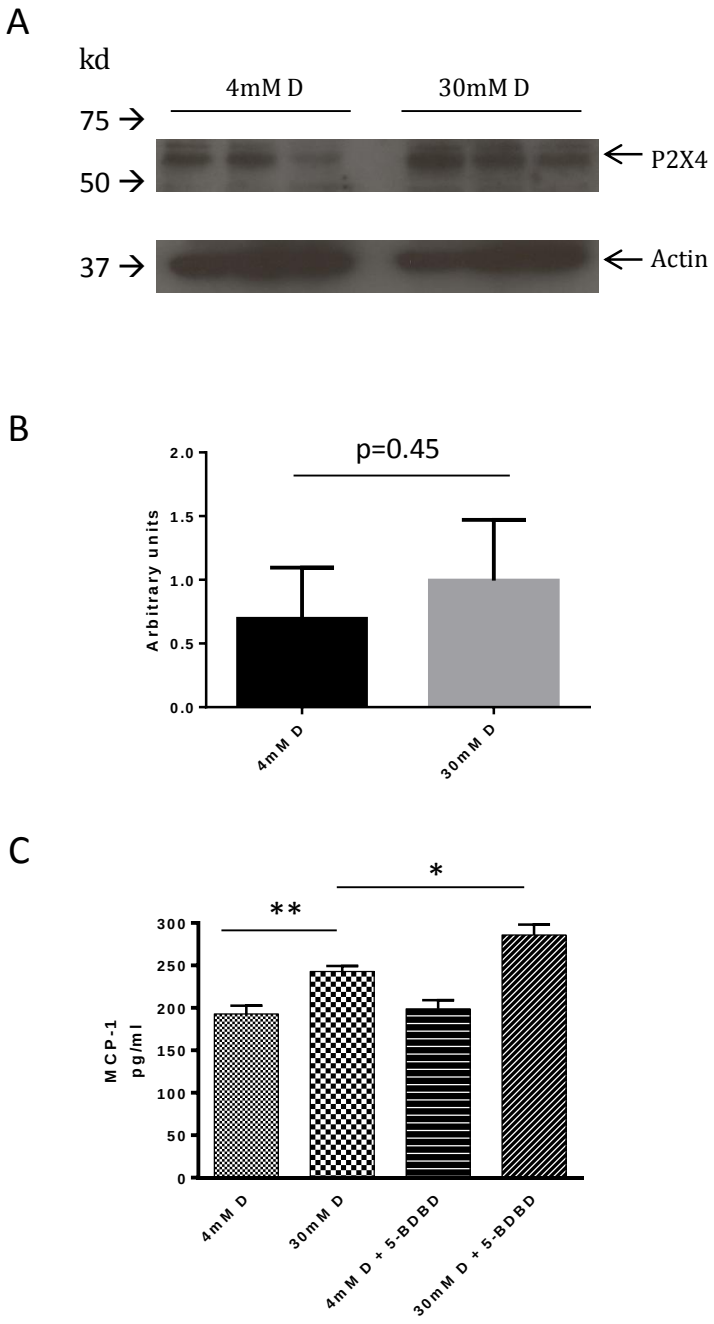

Figure 7.7 P2X4 is antagonistic to P2X7 with respect to hyperglycaemia-induced MCP-1 secretion. A,B: Specific immunoblot for P2X4 with an actin loading control (A) and P2X4 expression quantified by densitometry (B). P2X4 was expressed under basal culture conditions, with a trend towards upregulated expression after culture in hyperglycaemic medium. C: Incubation with the selective P2X4 antagonist. 5-BDBD, at 10μM produced an additive rise in MCP-1 secretion under hyperglycaemic conditions, but did not augment MCP-1 release in normoglycemia. D: D-glucose. *: $p<0.05$; **: $p<0.01$.

from two trials), suggesting that signalling via P2X4 and P2X7 is antagonistic with respect to MCP-1 release (Figure 7.7C).

7.3 Discussion

Renal infiltration by macrophages plays an important role in the pathogenesis of DN and represents a novel facet of disease to target therapeutically. Based on data presented elsewhere in this thesis (Chapters 4 and 5), expression of P2X7 appears to be required for development of the expected inflammatory response observed in both the pancreas after induction of diabetes with STZ, and in the kidney during hyperglycaemia. In this chapter, I have examined the production of the key macrophage chemokine MCP-1 by different resident glomerular cells in response to hyperglycaemia and the P2X7-dependence of this response in primary HMCs. While conditionally-immortalised human podocytes and transformed HMCs both exhibited a marked increase in MCP-1 secretion in response to stimulation with TNFα, confirming their potential to upregulate and secrete this cytokine under inflammatory stress, neither cell line displayed a robust or reproducible response to hyperglycaemia. Consequently, neither line was suitable for further investigation of P2X7 in this context.

Conversely, primary HMCs exhibited a reproducible increase in MCP-1 secretion when cultured in high glucose, which was independent of osmotic stress, making these cells an excellent model for further study. Using this model, I have demonstrated that glucose-induced MCP-1 release is, at least in part, dependent on the P2X7 receptor. Surprisingly, hydrolysis of ATP with apyrase produced the opposite direction of response to P2X7 blockade, suggesting involvement of other P1 or P2 receptors in the modulation of MCP-1 release. Selective blockade of P2X4 also enhanced MCP-1 release,

suggesting this may be one such receptor antagonising the effect of P2X7. The implication is that competing signals through P1 or P2 receptors may 'fine tune' local MCP-1 release depending on current levels of receptor expression, local concentration of ATP or ectonucleotidase activity. The role of adenosine in regulating MCP-1 release from pHMCs was not tested in this study, but represents an important focus for future research, particularly as CD73, an important source of local adenosine production, is upregulated in the kidneys of mice with DN (Tak et al., 2013).

Expression of P2X7, albeit at low levels, has previously been demonstrated at both mRNA and protein levels in human and rat MCs (Solini et al., 2005, Solini et al., 2007). P2X7 mRNA can be upregulated in rat MCs through stimulation by TNFα, although not reportedly by hyperglycaemia (Harada et al., 2000, Solini et al., 2005). When present, P2X7 is typically reported to form ring-like structures at the periphery of the cell visualised by specific immunofluoresence; the incidence of such structures is enhanced in fibroblasts by hyperglycaemia, mirroring the findings in this study (Solini et al., 2000). P2X7 has previously been shown to mediate ATP-induced apoptosis in rat MCs, although this does not appear to be true in human MCs where P2X4 has a more prominent role at least under basal conditions (Schulze-Lohoff et al., 1998, Harada et al., 2000, Solini et al., 2007).

Unlike in macrophages where P2X7 has a clear role in the inflammatory cascade and cytokine release, the role of P2X7 in secretion of inflammatory molecules from MCs has not been studied. MCs do not represent a major source of IL-1, the cytokine most tightly linked to P2X7, although upregulation of IL1β mRNA in MCs has been shown in the rat model of anti-GBM nephritis and small detectable increases in IL1β secretion have been observed in response to hyperglycaemia in HMCs *in vitro* (Tesch et al., 1997, Wu et al., 2010b). MCs do, however, represent an important source of other inflammatory mediators including TNFα, MCP-1 and MIP-1α (Wu et al.,

2010b). IL1β itself represents an important inducer of MCP-1 secretion from MCs, while IL1-RA, the endogenous IL-1 antagonist, almost entirely suppresses leukocyte infiltration in experimental models of glomerulonephritis (Lan et al., 1993, Chikaraishi et al., 2001).

In this study, negligible IL1β release could be detected from MCs, whether cultured for 48 hours in normal or high glucose or in the presence of TNFα, or after 30 minute application of 5mM ATP following preculture in TNFα-supplemented medium, a potent combination inducing IL1β maturation and release from macrophages (Franchi et al., 2009). Although this does not entirely exclude the possibility of low level hyperglycaemia-induced, P2X7-dependent IL1β release acting in a paracrine fashion to upregulate MCP-1, it seems probable that P2X7 regulates MCP-1 synthesis or release via an independent mechanism. Experiments performed in astrocytes have suggested that P2X7 acts to increase MCP-1 expression via activation of the mitogen-activated protein kinases (MAPK) ERK1/2 and p38, discrete from the caspase-1 pathway associated with IL1β release (Panenka et al., 2001).

Work examining ECM protein production from rat MCs exposed to hyperglycaemia has demonstrated how competing signals through P2 receptors may provoke opposing effects (Solini et al., 2005). The authors demonstrated that a range of P2X and P2Y receptor subtypes are expressed in MCs and extracellular ATP levels rose after exposure to hyperglycaemia. In this system, stimulation with ATP and BzATP (presumed to be acting via the P2X7 receptor) led to a dose-dependent increase in ECM production under both normal and high glucose conditions while the P2Y agonist, UTP, led to a reduction in ECM synthesis. The data presented in this thesis suggests a similar balance of competing purinoceptor signals may exist in the control of MCP-1 secretion by MCs, with a suggestion of functional antagonism between P2X7 and P2X4. Physiological antagonism between P2X7 and P2X4 has been described in the normal control of renal arterial resistance in the rat,

although *in vitro* studies of P2X4 in renal tubular epithelial cells have suggested they transduce a pro-inflammatory response after high glucose stimulation, contrary to the present findings in mesangial cells (Chen et al., 2013, Menzies et al., 2013).

P2X4 shares structural and functional similarities with P2X7, including the ability to undergo pore-like transformation, and is frequently co-expressed with P2X7, although its affinity for ATP is considerably higher (Guo et al., 2007). Previous descriptions of interaction between P2X4 and P2X7 have been co-operative, for instance in the facilitation of cytokine release and apoptosis from murine macrophages, while receptor subunits of the two receptors may be capable of forming heteromeric channels (Guo et al., 2007, Kawano et al., 2012, Sakaki et al., 2013). Although no statistically significant effect was noted with UTPγS, a P2Y2/4 agonist, it should be noted that BzATP possesses antagonistic properties at P2Y1 and P2Y4 receptors in addition to agonism at P2X7 and hence the possibility of a role for P2Y receptors in the modulation of MCP-1 release is not excluded (Vigne et al., 1999, Wildman et al., 2003).

In summary, P2 receptors appear to play a clear role in the regulation of MCP-1 release from MCs *in vitro*, and, by corollary, organisation of the glomerular inflammatory response to hyperglycaemia. Future efforts to delineate the P2 receptor dependency of inflammatory cytokine release from other resident renal cell types will be needed to ascertain whether pharmacological manipulation of individual or multiple P2 receptors *in vivo* would be anticipated to have a net beneficial effect. The data presented is consistent with the observation that renal macrophage recruitment is attenuated when P2X7 is deficient, and provides a putative mechanism for this phenomenon.

CHAPTER 8

Discussion

8.1 Summary of key findings and evaluation of the experimental hypotheses

The work described in this thesis has been conducted to test a central research question: "Does P2X7 contribute to the pathogenesis of diabetic nephropathy?". The following novel findings have emerged from this research:

- P2X7 is constitutively expressed in distal convoluted tubule in human, rat and mouse kidney, with glomerular upregulation apparent in all three species when diabetes is present.

- P2X7 is required for development of insulinitis after low dose STZ in the mouse, with partial protection against induction of diabetes observed in Pfizer P2X7 KO animals.

- P2X7 contributes mechanistically to the glomerular inflammatory response observed after low dose STZ in the mouse.

- P2X7 is expressed in human mesangial cells *in vitro* and contributes to chemokine production after exposure to hyperglycaemia. Competing purinoceptor signals appear able to modulate this response.

With reference to the main research question, it also serves to highlight those findings which have proved either negative or equivocal:

- Genetic P2X7 deficiency in the mouse did not ameliorate albuminuria, interstitial fibrosis or loss of GFR at the early (12 week) time-point studied, and mRNA levels of the chemokine osteopontin were actually *increased*.

- No statistically significant effect was observed on any measured parameter when uninephrectomised diabetic rats were treated with a selective P2X7 antagonist between weeks 8 and 12, although a trend towards reduced interstitial macrophage infiltration was apparent in high-dose (50mg/kg) antagonist-treated animals.

Taken together, these findings suggest that P2X7 has an important role in facilitating activation of the innate immune system in experimental diabetes induced with STZ. While this function may, in part, derive from the well-characterised role of P2X7 in IL1β/IL18 maturation and release from inflammatory cells (Surprenant et al,. 1996), the *in vitro* data obtained in mesangial cells suggests that P2X7 activation may directly or indirectly influence production of other cytokines crucial to the inflammatory response, such as MCP-1, by resident renal cell types. The similar histological patterns of receptor expression observed in all three species studied suggest that these findings may potentially translate to human disease.

8.2 P2X7 and albuminuria

While both rat and mouse models of DN histologically displayed early disease, increased albumin excretion was present in diseased animals, and

was unaffected by P2X7 deficiency or inhibition. Hence, it appears that P2X7 activation does not contribute to the mechanism by which albuminuria is initiated despite its early glomerular upregulation in diabetes. The effect of P2X7 deficiency on podocyte detachment and apoptosis, an important early event in diabetic glomerulopathy, was not directly examined in this study, and would merit further investigation; reduced glomerular cell apoptosis has previously been demonstrated in the GSK P2X7 KO mouse in the high fat diet model of metabolic syndrome (Solini et al., 2013). Previous studies have demonstrated that renal macrophage infiltration drives progressive disease in both glomerular and interstitial compartments in DN; given the reduced accumulation of glomerular macrophages observed in diabetic P2X7 KO mice, it is tempting to speculate that P2X7 may contribute to this disease amplification loop, but longer term study of models displaying a more severe disease phenotype would be required to confirm this (Chow et al., 2006, Chow et al., 2007).

8.3 P2X7, interstitial fibrosis and splice variant receptor expression in KO mice

A moderate amount of interstitial fibrosis, typically associated with advanced DN, was observed in the mouse model of STZ-induced DN, and was not ameliorated in GSK P2X7 KO mice. The quantity of interstitial fibrosis appeared somewhat disproportionate to the degree of glomerulopathy; the absence of an increase in interstitial macrophage number in WT diabetic mice is also surprising, as local inflammation is an important driver of tubulointerstitial injury in this model (Chow et al., 2004b). These findings may reflect the use of older, 8-12 month old mice in the study, but may also imply the contribution of other mechanisms of interstitial injury. While STZ has been shown to cause minimal direct nephrotoxicity when administered in a low dose protocol (with hyperglycaemia fully corrected by insulin

treatment), this has not been replicated in aged mice where the threshold of injury may be lower (Chow et al., 2006). Similarly, tolerance of severe polyuria and relative hypovolaemia may be altered in older mice, also predisposing to tubular injury.

However, the lack of impact of P2X7 deficiency on tubulointerstitial fibrosis remains surprising. A previous study investigating the effect of P2X7 deficiency on tubulointerstitial fibrosis, using the UUO model in Pfizer P2X7 KO mice, showed reduced fibrosis, TGFβ expression and interstitial macrophage accumulation (Goncalves et al., 2006). Similarly, pulmonary fibrosis after bleomycin was ameliorated in the Pfizer mouse (Riteau et al., 2010). Interstitial fibrosis measurements were not reported in the study of high fat diet-induced metabolic syndrome in GSK P2X7 KO mice (Solini et al., 2013).

As discussed previously (Chapter 5), neither available P2X7 KO mouse represents a true 'global' receptor knockout. The GSK mouse retains a functional exon 1 splice variant (P2X7K) which displays increased sensitivity of pore-formation to BzATP, is insensitive to the P451L single nucleotide polymorphism (SNP), and is the receptor subtype that mediates NAD-dependent ADP-ribosylation; P2X7K is absent in the Pfizer mouse (Xu et al., 2012). While P2X7K has a relatively restricted tissue distribution compared to P2X7A, it is known to be present in T lymphocytes and spleen; expression in kidney has not been studied (Nicke et al., 2009). Although no significant glomerular P2X7 expression was observed in GSK P2X7 KO mice, residual receptor expression was demonstrated by immunohistochemistry in a subset of renal tubules in this study, however the precise receptor variant was not characterised. It is likely that persistent tubular expression of the functional P2X7K splice variant underlies the lack of protection against tubulointerstitial fibrosis seen in the GSK KO mouse in this model of DN.

Pfizer P2X7 KO mice also express a splice variant receptor which escapes deletion (Masin et al., 2011). This ΔC-terminal splice variant receptor has reduced function and, when co-expressed with P2X7A, exerts a dominant-negative effect. Immunohistochemistry for P2X7 performed on pancreas from Pfizer KO mice, using an antibody raised against the distal C-terminus of P2X7 (APR-004, Alomone Labs), revealed positive staining in a distribution similar to that seen in WT mice, albeit with reduced frequency of positive cells. The staining pattern in WT mice recapitulated published data obtained using a different antibody (Roche Bioscience) also recognising the C-terminal domain (Coutinho-Silva et al., 2007). APR-004 does not recognise the ΔC-terminal splice variant, but has previously been used to demonstrate residual receptor expression within brain tissue of the Pfizer KO mouse, while confirming absence of expression in macrophages (Sanchez-Nogueiro et al., 2005, Masin et al., 2011). Taken together, these findings strongly suggest the existence of at least one additonal, uncharacterised, splice variant which escapes deletion in the Pfizer KO mouse, further complicating interpretation of data obtained in experiments using this strain.

8.4 P2X7 and glomerular macrophage infiltration

The reduction in glomerular macrophage numbers observed in GSK P2X7 KO mice prompted subsequent *in vitro* studies using resident glomerular cells; these experiments suggest that P2X7 may regulate secretion of MCP-1 from mesangial cells under hyperglycaemic conditions. MCP-1 has a key role in mediating monocyte/macrophage infiltration in acute and chronic glomerular inflammatory conditions, and also in experimental DN (Wenzel et al., 1997, Fujinaka et al., 1997, Chow et al., 2006). Amelioration of murine nephrotoxic nephritis by genetic P2X7 deficiency in the GSK KO mouse, was associated with almost complete suppression of urinary MCP-1 secretion, disproportionate to the reduction in glomerular macrophage number,

suggesting a possible causal relationship as opposed to a bystander effect (Taylor et al., 2009). IL1β is a potent inducer of MCP-1 secretion from human mesangial cells (Lee et al., 2003). IL1β could not be detected by ELISA in cell culture supernatants, when cells were exposed to either TNFα or hyperglycaemia for 48 hours, with or without a subsequent 30 minute exposure to 5mM ATP. The combination of priming with TNFα followed by a short exposure to ATP represents a robust stimulus to pro-IL1β maturation and release in macrophages, and would be anticipated to demonstrate IL1β release from mesangial cells if capable of doing so (Franchi et al., 2009). The possibility still remains, however, that low level IL1β release (below the threshold of detection by ELISA) acts in an autrocrine or paracrine fashion to stimulate MCP-1 release and underlies the association between P2X7 and MCP-1 production.

While mRNA expression of MCP-1 in whole kidney tissue lysates was increased in WT diabetic mice, no reduction was observed in GSK KO animals, and transcriptional levels of osteopontin, another chemokine, were actually elevated in the KO group. This may, in part, be explained by the observed differences in outcome between glomerular and interstitial compartments, as discussed above, and also residual P2X7 receptor expression at these two sites. A clearer appreciation of the effect of P2X7 deficiency on chemokine expression in this model may have been gained either by analysing transcriptional changes in isolated glomerular mRNA, or by performing specific immunohistochemistry and separately assessing staining in glomerular and interstitial compartments.

8.5 P2X7 and pancreatic injury

The serendipitous observation that GSK P2X7 KO mice appeared protected from the induction of diabetes with STZ was explored more closely in the Pfizer P2X7 KO; in this mouse, protection from diabetes was clear-cut, with reduced islet inflammation and macrophage infiltration. In contrast to human disease, few T lymphocytes were seen accumulating in islets in this mouse model, although macrophages also form part of the islet inflammatory infiltrate in human type 1 diabetes, and interest has grown in targeting innate immune pathways to slow pancreatic destruction (Foulis, 2008, Mandrup-Poulsen et al., 2010).

IL1β, the release of which from macrophages is partly dependent on P2X7 activation, has attracted particular attention; β-cells are highly sensitive to IL1β-induced apoptosis, and IL1β is also able to polarise T cells towards a pro-inflammatory phenotype (such as TH_1 or TH_{17}) (Mandrup-Poulsen et al., 2010). A recent clinical trial compared the effect of either the IL1 receptor antagonist anakinra, or the monoclonal anti-IL1 antibody canakinumab, against placebo in patients with newly diagnosed type 1 diabetes. Monotherapy with these drugs did not prove effective in retarding disease progression, although hope remains that such a strategy may be clinically useful if combined with simultaneous manipulation of the adaptive immune response (Moran et al., 2013).

As discussed in the context of DN, it is likely that P2X7 may also induce local inflammation and tissue injury via IL1β-independent mechanisms. Like mesangial cells, β-cells also secrete MCP-1, raising the possibility that P2X7 activation may drive macrophage recruitment via increased secretion of this chemokine (Chen et al., 2001). P2X7 may also mediate direct ATP-induced cell death in β-cells, similar to the effect of ADP acting via the P2Y13 receptor (Tan et al., 2010). Notably, ATP stimulation also inhibits the suppressive

potential and stability of regulatory T cells via the P2X7 receptor, while P2X7 has been shown to have a role in driving T cell lineage decisions in the thymus (Schenk et al., 2011, Frascoli et al., 2012). This pleiotropic effect on the immune system renders P2X7 an important candidate for further study, suggesting manipulation of P2X7 may yield benefits beyond simple downsteam inhibition of IL1β.

As discussed in Chapter 4, Pfizer P2X7 KO mice fed a high sucrose/high fat diet exhibited severe glucose intolerance and failure to appropriately increase β-cell mass, accompanied by reduced circulating IL1-RA levels (Glas et al., 2009). This suggests pancreatic P2X7 signalling may be either beneficial or deleterious depending on the mechanism of islet injury or time-point of disease (Glas et al., 2009). This, combined with differences in P2X7 expression between human and rodent islets, make the clinical effects of P2X7 antagonism in human disease difficult to predict and mandate further study in human tissue before considering a clinical trial of a selective P2X7 inhibitor.

8.6 Potential translational relevance of findings

How may the findings in this study translate to opportunities in the treatment of human disease? Current therapy in DN centres on good glycaemic and blood pressure control and use of ACE inhibitors primarily to reduce glomerular hypertension and albuminuria. Targeting of innate immune mechanisms and, more specifically, macrophage activation, represents a potential avenue for adjunctive therapy to delay progression of disease. Selective antagonism of P2X7 may provide one option by which to achieve this, particularly since orally-active selective human P2X7

antagonists are already available and have proved well tolerated in clinical studies to date (Arulkumaran et al., 2011).

Evidence of benefit in pre-clinical studies would need to be strengthened prior to considering clinical translation, for instance through examining the effect of long-term P2X7 receptor antagonism in a mouse model which exhibits convincing evidence of established DN (eg. STZ diabetic eNOS KO mice). The present study has also brought into focus the functional importance of P2X7 receptor splice variant expression, and the expression profile for receptor variants and relative potency of antagonists at these isoforms in both rodents and humans should be considered when planning any future human study.

8.7 Limitations of the work, potential experimental refinements and future research

Limitations of the animal models employed to examine the functional role of P2X7 in DN have been discussed throughout this thesis. A number of modifications and refinements to the experimental protocols may, however, have yielded more clear-cut answers to the experimental hypotheses.

8.7.1 Choice of mouse and genetic background

The C57BL/6 background is relatively resistant to the renal consequences of diabetes and work to understand the genetic basis for this is on-going (Brosius et al., 2009). Use of aged male mice in this study enhanced the severity of disease, although the DN phenotype after 12 weeks would still be

regarded as 'mild'. Although the model proved sufficient to delineate an effect of P2X7 deficiency on glomerular macrophage accumulation, it was not possible to conclude whether 'harder' signs of established DN, such as development of typical glomerular lesions, are similarly ameliorated. Back-crossing the KO mouse onto a more susceptible genetic background (eg. DBA/2) may have helped provide a more robust disease phenotype, and this is currently being performed in the laboratory with the Pfizer mouse to permit study of P2X7 in a mouse model of uraemic vascular calcification (Gurley et al., 2006).

C57BL/6 is also notable for carrying the P451L single nucleotide polymorphism in P2X7 which confers drastically reduced sensitivity to ATP-induced pore formation and knock-on effects on P2X7-mediated apoptosis and cytokine release (Adriouch et al., 2002). Testing the effect of the P2X7 KO against a mouse already carrying a hypofunctional receptor may thus have led to underestimation of treatment effect.

Finally, as discussed at length, the GSK P2X7 KO mouse does not represent a true global receptor KO. While the Pfizer KO also expresses splice variants which escape deletion, the functional difference between the animals is emphasised by the differing degrees of resistance to diabetes induction apparent in this study. Any future experiments should employ the Pfizer KO in preference to the GSK.

8.7.2 Choice of mouse model

While STZ-induced diabetes remains a useful tool due to the production of a relatively 'pure' hyperglycaemic phenotype, renal disease is strain-dependent, generally mild, and potentially confounded by direct renal

tubular toxicity. Newer genetic models of disease, in particular eNOS KO mice combined with low dose STZ, present a more robust and severe phenotype, even on a C57BL/6 background (Kanetsuna et al., 2007).

Using this model it would be feasible to test the effect of P2X7 deficiency with or without co-administration of an ACE inhibitor to simulate a proposed treatment regimen in humans. Demonstration of an additive effect would provide strong pre-clinical evidence for P2X7 inhibition in human disease. A similar protocol could be undertaken in *db/db* mice with co-existent eNOS deficiency, to test the hypothesis in a model of accelerated nephropathy in type 2 diabetes.

8.7.3 Downstream mechanisms of P2X7 signalling in DN

Although this study has produced several findings regarding the mechanism by which P2X7 signalling contributes to pathogenesis of DN, refinements to the experimental protocol could have yielded further insights. In the mouse study of DN, Isolation of glomeruli, either by sieving of renal tissue or laser-capture micro-dissection, would have allowed analysis of transcriptional changes in the glomeruli alone, and overcome problems interpreting data in the light of diverging responses of glomerular and interstitial compartments to the effect of P2X7 gene deletion. This is particularly pertinent in view of the apparent differences in residual receptor splice variant expression between glomeruli and tubules in the GSK KO mouse.

The association between P2X7 and inflammatory cytokine release from resident glomerular cells could also be further dissected. The extended pattern of inflammatory and pro-fibrotic cytokines released under conditions of hyperglycaemia, with or without P2X7 blockade, could be assayed using a

high-sensitivity bead-based multiplex assay, to determine the specificity of the observed relationship with MCP-1. This approach could also be complemented by transcriptional analysis of a similar range of mediators. The caspase-1/IL1β dependence of P2X7-mediated MCP-1 release could be further explored by repeating experiments in the presence of a caspase-1 inhibitor. Similar approaches could be used to investigate the role of the large pore pathway and ERK signalling in P2X7-induced MCP-1 release, by using selective inhibitors of panx-1 and ERK-1or -2 respectively. Similar studies undertaken in an alternative podocyte cell-line would resolve whether these responses are common to other resident renal cells. Finally, additional work using modulators of adenosine signalling (eg adenosine deaminase) would determine whether the observed increase in hyperglycaemia-induced MCP-1 release from pHMCs with apyrase is, in fact, adenosine dependent.

8.7.4 P2X7, islet inflammation and diabetes

The finding that P2X7 deficiency protects mice against induction of diabetes with STZ may be relevant to the pathogenesis of human type 1 diabetes but requires further investigation. Administration of low dose STZ to P2X7 KO mice chimaeric for WT bone marrow would help elucidate the relative contribution of P2X7 signalling in peripheral immune cells to this protective effect. Similar studies using a genetically engineered cell-type specific P2X7 KO, harnessing for instance, the insulin gene promoter to isolate P2X7 gene silencing in β cells, would provide complementary information on the role of P2X7 in resident islet cells.

A further experiment could assess the effect of selective pharmacological inhibition of P2X7 on *induction* of STZ diabetes in the rat, with the caveat that this is less dependent on an autoimmune insulinitis than low dose STZ in the

mouse. *In vitro* studies, ideally using islets extracted from normal healthy human pancreas, would help delineate the consequences of P2X7 activation on cytokine and chemokine release and cell survival, and the effect of P2X7 receptor blockade on the response to injurious stimuli, including STZ and hyperglycaemia, could be studied.

8.8 Conclusion

P2X7 is not significantly expressed in the normal glomerulus, but is upregulated in this location at an early timepoint in rodent models of both type 1 and type 2 diabetes as well as human disease. P2X7 contributes to both glomerular and pancreatic islet inflammation after STZ, with partial protection against STZ diabetes observed in Pfizer P2X7 KO mice. P2X7 appears to regulate secretion of the pro-inflammatory chemokine, MCP-1, from primary human mesangial cells under diabetic conditions, as part of a wider spectrum of purinoceptor responses.

These findings place P2X7 firmly at the heart of the innate immune response observed in experimental diabetes and DN. The human biopsy tissue study and human cell culture data presented in this thesis, correspond well with the results from animal models, boding well for future translational efforts.

Further pre-clinical studies, primarily designed to test the effect of P2X7 signalling on major long-term renal outcomes in DN (eg. glomerulosclerosis, interstitial fibrosis and loss of GFR), are required before receptor antagonists can be trialled in human disease, together with exhaustive characterisation of receptor splice variant expression in human immune cells and kidney.

ABSTRACTS, PUBLICATIONS AND PRESENTATIONS

Peer-reviewed paper

BOOTH, J.W., TAM F.W., UNWIN, R.J. 2012. P2 purinoceptors: Renal pathophysiology and therapeutic potential. *Clin Nephrol,* 78, 154-63

Publication in Abstract

BOOTH, J.W., NORMAN, J. T., TAM F.W., UNWIN, R.J. 2013. P2X7 deficiency attenutates renal inflammation and pancreatic beta cell injury in experimental diabetes. Poster presentation at American Society of Nephrology conference, San Diego, USA.

BOOTH, J.W., NORMAN, J. T., TAM F.W., UNWIN, R.J. 2013. P2X7 deficiency attenutates renal inflammation and pancreatic beta cell injury in experimental diabetes. Oral presentation at British Renal Association conference, Bournemouth, UK.

REFERENCES

ABBRACCHIO, M. P., BURNSTOCK, G., BOEYNAEMS, J. M., BARNARD, E. A., BOYER, J. L., KENNEDY, C., KNIGHT, G. E., FUMAGALLI, M., GACHET, C., JACOBSON, K. A. & WEISMAN, G. A. 2006. International Union of Pharmacology LVIII: update on the P2Y G protein-coupled nucleotide receptors: from molecular mechanisms and pathophysiology to therapy. *Pharmacol Rev,* 58**,** 281-341.

ADHIKARY, L., CHOW, F., NIKOLIC-PATERSON, D. J., STAMBE, C., DOWLING, J., ATKINS, R. C. & TESCH, G. H. 2004. Abnormal p38 mitogen-activated protein kinase signalling in human and experimental diabetic nephropathy. *Diabetologia,* 47**,** 1210-22.

ADINOLFI, E., CALLEGARI, M. G., FERRARI, D., BOLOGNESI, C., MINELLI, M., WIECKOWSKI, M. R., PINTON, P., RIZZUTO, R. & DI VIRGILIO, F. 2005. Basal activation of the P2X7 ATP receptor elevates mitochondrial calcium and potential, increases cellular ATP levels, and promotes serum-independent growth. *Mol Biol Cell,* 16**,** 3260-72.

ADINOLFI, E., CIRILLO, M., WOLTERSDORF, R., FALZONI, S., CHIOZZI, P., PELLEGATTI, P., CALLEGARI, M. G., SANDONA, D., MARKWARDT, F., SCHMALZING, G. & DI VIRGILIO, F. 2010. Trophic activity of a naturally occurring truncated isoform of the P2X7 receptor. *Faseb j,* 24**,** 3393-404.

ADINOLFI, E., RAFFAGHELLO, L., GIULIANI, A. L., CAVAZZINI, L., CAPECE, M., CHIOZZI, P., BIANCHI, G., KROEMER, G., PISTOIA, V. & DI VIRGILIO, F. 2012. Expression of P2X7 receptor increases in vivo tumor growth. *Cancer Res,* 72**,** 2957-69.

ADRIOUCH, S., DOX, C., WELGE, V., SEMAN, M., KOCH-NOLTE, F. & HAAG, F. 2002. Cutting edge: a natural P451L mutation in the cytoplasmic domain impairs the function of the mouse P2X7 receptor. *J Immunol,* 169**,** 4108-12.

ALPERS, C. E. & HUDKINS, K. L. 2011. Mouse models of diabetic nephropathy. *Curr Opin Nephrol Hypertens,* 20**,** 278-84.

ALZOLA, E., PEREZ-ETXEBARRIA, A., KABRE, E., FOGARTY, D. J., METIOUI, M., CHAIB, N., MACARULLA, J. M., MATUTE, C., DEHAYE, J. P. & MARINO, A. 1998. Activation by P2X7 agonists of two phospholipases A2 (PLA2) in ductal cells of rat submandibular gland. Coupling of the calcium-independent PLA2 with kallikrein secretion. *J Biol Chem,* 273**,** 30208-17.

AMOROSO, F., FALZONI, S., ADINOLFI, E., FERRARI, D. & DI VIRGILIO, F. 2012. The P2X7 receptor is a key modulator of aerobic glycolysis. *Cell Death Dis,* 3**,** e370.

ANDREI, C., MARGIOCCO, P., POGGI, A., LOTTI, L. V., TORRISI, M. R. & RUBARTELLI, A. 2004. Phospholipases C and A2 control lysosome-mediated IL-1 beta secretion: Implications for inflammatory processes. *Proc Natl Acad Sci U S A,* 101**,** 9745-50.

ANTONIO, L. S., STEWART, A. P., XU, X. J., VARANDA, W. A., MURRELL-LAGNADO, R. D. & EDWARDSON, J. M. 2011. P2X4 receptors interact with both P2X2 and P2X7 receptors in the form of homotrimers. *Br J Pharmacol,* 163**,** 1069-77.

ARULKUMARAN, N., UNWIN, R. J. & TAM, F. W. 2011. A potential therapeutic role for P2X7 receptor (P2X7R) antagonists in the treatment of inflammatory diseases. *Expert Opin Investig Drugs,* 20**,** 897-915.

ATKINSON, M. A. & LEITER, E. H. 1999. The NOD mouse model of type 1 diabetes: as good as it gets? *Nat Med,* 5**,** 601-4.

AWAD, A. S., KINSEY, G. R., KHUTSISHVILI, K., GAO, T., BOLTON, W. K. & OKUSA, M. D. 2011. Monocyte/macrophage chemokine receptor CCR2 mediates diabetic renal injury. *Am J Physiol Renal Physiol,* 6, 1358-66

BADAL, S. S. & DANESH, F. R. 2012. Strategies to reverse endothelial dysfunction in diabetic nephropathy. *Kidney Int*, 82, 1151-4

BAGCHUS, W. M., HOEDEMAEKER, P. J., ROZING, J. & BAKKER, W. W. 1986. Glomerulonephritis induced by monoclonal anti-Thy 1.1 antibodies. A sequential histological and ultrastructural study in the rat. *Lab Invest,* 55**,** 680-7.

BARDINI, M., LEE, H. Y. & BURNSTOCK, G. 2000. Distribution of P2X receptor subtypes in the rat female reproductive tract at late pro-oestrus/early oestrus. *Cell Tissue Res,* 299**,** 105-13.

BARICORDI, O. R., MELCHIORRI, L., ADINOLFI, E., FALZONI, S., CHIOZZI, P., BUELL, G. & DI VIRGILIO, F. 1999. Increased proliferation rate of lymphoid cells transfected with the P2X(7) ATP receptor. *J Biol Chem,* 274**,** 33206-8.

BENDING, J. J., LOBO-YEO, A., VERGANI, D. & VIBERTI, G. C. 1988. Proteinuria and activated T-lymphocytes in diabetic nephropathy. *Diabetes,* 37**,** 507-11.

BIANCO, F., PRAVETTONI, E., COLOMBO, A., SCHENK, U., MOLLER, T., MATTEOLI, M. & VERDERIO, C. 2005. Astrocyte-derived ATP induces vesicle shedding and IL-1 beta release from microglia. *J Immunol,* 174**,** 7268-77.

BIANCO, F., CERUTI, S., COLOMBO, A., FUMAGALLI, M., FERRARI, D., PIZZIRANI, C., MATTEOLI, M., DI VIRGILIO, F., ABBRACCHIO, M. P. & VERDERIO, C. 2006. A role for P2X7 in microglial proliferation. *J Neurochem,* 99**,** 745-58.

BOHLE, A., WEHRMANN, M., BOGENSCHUTZ, O., BATZ, C., MULLER, C. A. & MULLER, G. A. 1991. The pathogenesis of chronic renal failure in diabetic nephropathy. Investigation of 488 cases of diabetic glomerulosclerosis. *Pathol Res Pract,* 187**,** 251-9.

BOWER, G., BROWN, D. M., STEFFES, M. W., VERNIER, R. L. & MAUER, S. M. 1980. Studies of the glomerular mesangium and the juxtaglomerular apparatus in the genetically diabetic mouse. *Lab Invest,* 43**,** 333-41.

BREYER, M. D., BOTTINGER, E., BROSIUS, F. C., 3RD, COFFMAN, T. M., HARRIS, R. C., HEILIG, C. W. & SHARMA, K. 2005. Mouse models of diabetic nephropathy. *J Am Soc Nephrol,* 16**,** 27-45.

BROSIUS, F. C., 3RD, ALPERS, C. E., BOTTINGER, E. P., BREYER, M. D., COFFMAN, T. M., GURLEY, S. B., HARRIS, R. C., KAKOKI, M., KRETZLER, M., LEITER, E. H., LEVI, M., MCINDOE, R. A., SHARMA, K., SMITHIES, O., SUSZTAK, K., TAKAHASHI, N. & TAKAHASHI, T. 2009. Mouse models of diabetic nephropathy. *J Am Soc Nephrol,* 20**,** 2503-12.

BROWNE, L. E. & NORTH, R. A. 2013. P2X receptor intermediate activation states have altered nucleotide selectivity. *J Neurosci,* 33**,** 14801-8.

BUCHHOLZ, B., TESCHEMACHER, B., SCHLEY, G., SCHILLERS, H. & ECKARDT, K. U. 2011. Formation of cysts by principal-like MDCK cells depends on the synergy of cAMP- and ATP-mediated fluid secretion. *J Mol Med,* 89**,** 251-61.

BUELL, G. N., TALABOT, F., GOS, A., LORENZ, J., LAI, E., MORRIS, M. A. & ANTONARAKIS, S. E. 1998. Gene structure and chromosomal localization of the human P2X7 receptor. *Receptors Channels,* 5**,** 347-54.

BURNSTOCK, G., CAMPBELL, G., SATCHELL, D. & SMYTHE, A. 1970. Evidence that adenosine triphosphate or a related nucleotide is the transmitter substance released by non-adrenergic inhibitory nerves in the gut. *Br J Pharmacol,* 40**,** 668-88.

BURNSTOCK, G. 2006. Pathophysiology and therapeutic potential of purinergic signaling. *Pharmacol Rev,* 58**,** 58-86.

BURNSTOCK, G. & NOVAK, I. 2012. Purinergic signalling in the pancreas in health and disease. *J Endocrinol.* 213, 123-41

BURNSTOCK, G. 2013. Purinergic mechanisms and pain-An update. *Eur J Pharmacol*. http://dx.doi.org/10.1016/j.ejphar.2013.01.078 (Epub ahead of print)

BYRNE, C., FORD, D., GILG, J., ANSELL, D. & FEEHALLY, J. 2010. UK Renal Registry 12th Annual Report (December 2009): chapter 3: UK ESRD incident rates in 2008: national and centre-specific analyses. *Nephron Clin Pract,* 115 Suppl 1**,** c9-39.

CALVET, J. P. 2002. Cilia in PKD--letting it all hang out. *J Am Soc Nephrol,* 13**,** 2614-6.

CHANG, M. Y., LU, J. K., TIAN, Y. C., CHEN, Y. C., HUNG, C. C., HUANG, Y. H., CHEN, Y. H., WU, M. S., YANG, C. W. & CHENG, Y. C. 2011. Inhibition of the P2X7 receptor reduces cystogenesis in PKD. *J Am Soc Nephrol,* 22**,** 1696-706.

CHEN, M. C., PROOST, P., GYSEMANS, C., MATHIEU, C. & EIZIRIK, D. L. 2001. Monocyte chemoattractant protein-1 is expressed in pancreatic islets from prediabetic NOD mice and in interleukin-1 beta-exposed human and rat islet cells. *Diabetologia,* 44**,** 325-32.

CHEN, S., LEE, J. S., IGLESIAS-DE LA CRUZ, M. C., WANG, A., IZQUIERDO-LAHUERTA, A., GANDHI, N. K., DANESH, F. R., WOLF, G. & ZIYADEH, F. N. 2005. Angiotensin II stimulates alpha3(IV) collagen production in mouse podocytes via TGF-beta and VEGF signalling: implications for diabetic glomerulopathy. *Nephrol Dial Transplant,* 20**,** 1320-8.

CHEN, J., CHEN, Y. G., REIFSNYDER, P. C., SCHOTT, W. H., LEE, C. H., OSBORNE, M., SCHEUPLEIN, F., HAAG, F., KOCH-NOLTE, F., SERREZE, D. V. & LEITER, E. H. 2006. Targeted disruption of CD38 accelerates autoimmune diabetes in NOD/Lt mice by enhancing autoimmunity in an ADP-ribosyltransferase 2-dependent fashion. *J Immunol,* 176**,** 4590-9.

CHEN, L. & BROSNAN, C. F. 2006. Exacerbation of experimental autoimmune encephalomyelitis in P2X7R-/- mice: evidence for loss of apoptotic activity in lymphocytes. *J Immunol,* 176**,** 3115-26.

CHEN, Y. G., SCHEUPLEIN, F., DRIVER, J. P., HEWES, A. A., REIFSNYDER, P. C., LEITER, E. H. & SERREZE, D. V. 2011. Testing the role of P2X7 receptors in the development of type 1 diabetes in nonobese diabetic mice. *J Immunol.* 7, 4278-84

CHEN, K., ZHANG, J., ZHANG, W., YANG, J., LI, K. & HE, Y. 2013. ATP-P2X4 signaling mediates NLRP3 inflammasome activation: a novel pathway of diabetic nephropathy. *Int J Biochem Cell Biol,* 45**,** 932-43.

CHESSELL, I. P., HATCHER, J. P., BOUNTRA, C., MICHEL, A. D., HUGHES, J. P., GREEN, P., EGERTON, J., MURFIN, M., RICHARDSON, J., PECK, W. L., GRAHAMES, C. B., CASULA, M. A., YIANGOU, Y., BIRCH, R., ANAND, P. & BUELL, G. N. 2005. Disruption of the P2X7 purinoceptor gene abolishes chronic inflammatory and neuropathic pain. *Pain,* 114**,** 386-96.

CHIKARAISHI, A., HIRAHASHI, J., TAKASE, O., MARUMO, T., HISHIKAWA, K., HAYASHI, M. & SARUTA, T. 2001. Tranilast inhibits interleukin-1beta-induced monocyte chemoattractant protein-1 expression in rat mesangial cells. *Eur J Pharmacol.* 427, 151-8

CHOW, F., OZOLS, E., NIKOLIC-PATERSON, D. J., ATKINS, R. C. & TESCH, G. H. 2004a. Macrophages in mouse type 2 diabetic nephropathy: correlation with diabetic state and progressive renal injury. *Kidney Int,* 65**,** 116-28.

CHOW, F. Y., NIKOLIC-PATERSON, D. J., ATKINS, R. C. & TESCH, G. H. 2004b. Macrophages in streptozotocin-induced diabetic nephropathy: potential role in renal fibrosis. *Nephrol Dial Transplant.* 19, 2987-96.

CHOW, F. Y., NIKOLIC-PATERSON, D. J., OZOLS, E., ATKINS, R. C. & TESCH, G. H. 2005. Intercellular adhesion molecule-1 deficiency is protective against nephropathy in type 2 diabetic db/db mice. *J Am Soc Nephrol.* 6, 1711-22

CHOW, F. Y., NIKOLIC-PATERSON, D. J., OZOLS, E., ATKINS, R. C., ROLLIN, B. J. & TESCH, G. H. 2006. Monocyte chemoattractant protein-1 promotes the development of diabetic renal injury in streptozotocin-treated mice. *Kidney Int.* 69, 73-80.

CHOW, F. Y., NIKOLIC-PATERSON, D. J., MA, F. Y., OZOLS, E., ROLLINS, B. J. & TESCH, G. H. 2007. Monocyte chemoattractant protein-1-induced tissue inflammation is critical for the development of renal injury but not type 2 diabetes in obese db/db mice. *Diabetologia,* 50**,** 471-80.

CHOW, S. C., KASS, G. E. & ORRENIUS, S. 1997. Purines and their roles in apoptosis. *Neuropharmacology,* 36**,** 1149-56.

CLARK, J. B., PALMER, C. J. & SHAW, W. N. 1983. The diabetic Zucker fatty rat. *Proc Soc Exp Biol Med,* 173**,** 68-75.

COMMUNI, D., JANSSENS, R., SUAREZ-HUERTA, N., ROBAYE, B. & BOEYNAEMS, J. M. 2000. Advances in signalling by extracellular nucleotides. the role and transduction mechanisms of P2Y receptors. *Cell Signal,* 12**,** 351-60.

CONWAY, B. R., RENNIE, J., BAILEY, M. A., DUNBAR, D. R., MANNING, J. R., BELLAMY, C. O., HUGHES, J. & MULLINS, J. J. 2012. Hyperglycemia and renin-dependent hypertension synergize to model diabetic nephropathy. *J Am Soc Nephrol,* 23**,** 405-11.

COUTINHO-SILVA, R., PARSONS, M., ROBSON, T., LINCOLN, J. & BURNSTOCK, G. 2003. P2X and P2Y purinoceptor expression in pancreas from streptozotocin-diabetic rats. *Mol Cell Endocrinol.* 204, 141-54

COUTINHO-SILVA, R., ROBSON, T., BEALES, P. E. & BURNSTOCK, G. 2007. Changes in expression of P2X7 receptors in NOD mouse pancreas during the development of diabetes. *Autoimmunity.* 40, 108-16

CRUWYS, S., MIDHA, A., RENDALL, E., MCCORMICK, M., NICOL, A., FOSTER, M., AND BRADDOCK, M. 2007 Antagonism of the P2X7 receptor attenuates joint destruction in a model of arthritis. *Proceedings of the Annual Meeting of American College of Rheumatology*; Nov 6–11; Boston, MA; presentation no. 1772.

DEJI, N., KUME, S., ARAKI, S., SOUMURA, M., SUGIMOTO, T., ISSHIKI, K., CHIN-KANASAKI, M., SAKAGUCHI, M., KOYA, D., HANEDA, M., KASHIWAGI, A. & UZU, T. 2009. Structural and functional changes in the kidneys of high-fat diet-induced obese mice. *Am J Physiol Renal Physiol.* 296, 118-26

DI VIRGILIO, F., CHIOZZI, P., FALZONI, S., FERRARI, D., SANZ, J. M., VENKETARAMAN, V. & BARICORDI, O. R. 1998. Cytolytic P2X purinoceptors. *Cell Death Differ,* 5**,** 191-9.

DI VIRGILIO, F. 2007. Liaisons dangereuses: P2X(7) and the inflammasome. *Trends Pharmacol Sci,* 28**,** 465-72.

DOI, K., MATSUZAKI, H., TSUDA, T. & ONODERA, T. 1989. Rapid development of renal lesions in diabetic DBA mice infected with the D-variant of encephalomyocarditis virus (EMC-D). *Br J Exp Pathol,* 70**,** 275-81.

DOI, T., HATTORI, M., AGODOA, L. Y., SATO, T., YOSHIDA, H., STRIKER, L. J. & STRIKER, G. E. 1990. Glomerular lesions in nonobese diabetic mouse: before and after the onset of hyperglycemia. *Lab Invest,* 63**,** 204-12.

DONADELLI, R., ZANCHI, C., MORIGI, M., BUELLI, S., BATANI, C., TOMASONI, S., CORNA, D., ROTTOLI, D., BENIGNI, A., ABBATE, M., REMUZZI, G. & ZOJA, C. 2003. Protein overload induces fractalkine upregulation in proximal tubular cells through nuclear factor kappaB- and p38 mitogen-activated protein kinase-dependent pathways. *J Am Soc Nephrol,* 14**,** 2436-46.

DONNELLY-ROBERTS, D. L., NAMOVIC, M. T., FALTYNEK, C. R. & JARVIS, M. F. 2004. Mitogen-activated protein kinase and caspase signaling pathways are required for P2X7 receptor (P2X7R)-induced pore formation in human THP-1 cells. *J Pharmacol Exp Ther,* 308**,** 1053-61.

DONNELLY-ROBERTS, D. L. & JARVIS, M. F. 2007. Discovery of P2X7 receptor-selective antagonists offers new insights into P2X7 receptor function and indicates a role in chronic pain states. *Br J Pharmacol,* 151**,** 571-9.

DU, X. L., EDELSTEIN, D., DIMMELER, S., JU, Q., SUI, C. & BROWNLEE, M. 2001. Hyperglycemia inhibits endothelial nitric oxide synthase activity by posttranslational modification at the Akt site. *J Clin Invest,* 108**,** 1341-8.

DURNIN, L. & MUTAFOVA-YAMBOLIEVA, V. N. 2011. Cyclic ADP-ribose requires CD38 to regulate the release of ATP in visceral smooth muscle. *Febs j,* 278**,** 3095-108.

EL-MOATASSIM, C. & DUBYAK, G. R. 1992. A novel pathway for the activation of phospholipase D by P2z purinergic receptors in BAC1.2F5 macrophages. *J Biol Chem,* 267**,** 23664-73.

ELLER, K., KIRSCH, A., WOLF, A. M., SOPPER, S., TAGWERKER, A., STANZL, U., WOLF, D., PATSCH, W., ROSENKRANZ, A. R. & ELLER, P. 2011. Potential role of regulatory T cells in reversing obesity-linked insulin resistance and diabetic nephropathy. *Diabetes.* 60, 2954-62

ELLIOTT, J. I. & HIGGINS, C. F. 2004. Major histocompatibility complex class I shedding and programmed cell death stimulated through the proinflammatory P2X7 receptor: a candidate susceptibility gene for NOD diabetes. *Diabetes.* 53, 2012-7

ELSSNER, A., DUNCAN, M., GAVRILIN, M. & WEWERS, M. D. 2004. A novel P2X7 receptor activator, the human cathelicidin-derived peptide LL37, induces IL-1 beta processing and release. *J Immunol,* 172**,** 4987-94.

ENGVALL, E. & PERLMANN, P. 1971. Enzyme-linked immunosorbent assay (ELISA). Quantitative assay of immunoglobulin G. *Immunochemistry,* 8**,** 871-4.

EPSTEIN, P. N., OVERBEEK, P. A. & MEANS, A. R. 1989. Calmodulin-induced early-onset diabetes in transgenic mice. *Cell,* 58**,** 1067-73.

EZZIDI, I., MTIRAOUI, N., MOHAMED, M. B., MAHJOUB, T., KACEM, M. & ALMAWI, W. Y. 2008. Association of endothelial nitric oxide synthase Glu298Asp, 4b/a, and -786T>C gene variants with diabetic nephropathy. *J Diabetes Complications.* 22, 331-8

FANG, K. M., WANG, Y. L., HUANG, M. C., SUN, S. H., CHENG, H. & TZENG, S. F. 2011. Expression of macrophage inflammatory protein-1alpha and monocyte chemoattractant protein-1 in glioma-infiltrating microglia: involvement of ATP and P2X(7) receptor. *J Neurosci Res,* 89**,** 199-211.

FEEHALLY, J., FLOEGE, J. & JOHNSON, R. 2007. *Comprehensive Clinical Nephrology*, Mosby, Inc. Chapter 29, pages 359-376

FERRARI, D., CHIOZZI, P., FALZONI, S., DAL SUSINO, M., MELCHIORRI, L., BARICORDI, O. R. & DI VIRGILIO, F. 1997. Extracellular ATP triggers IL-1 beta release by activating the purinergic P2Z receptor of human macrophages. *J Immunol,* 159**,** 1451-8.

FERRARI, D., PIZZIRANI, C., ADINOLFI, E., LEMOLI, R. M., CURTI, A., IDZKO, M., PANTHER, E. & DI VIRGILIO, F. 2006. The P2X7 receptor: a key player in IL-1 processing and release. *J Immunol,* 176**,** 3877-83.

FIORETTO, P., STEFFES, M. W., SUTHERLAND, D. E. & MAUER, M. 1995. Sequential renal biopsies in insulin-dependent diabetic patients: structural factors associated with clinical progression. *Kidney Int,* 48**,** 1929-35.

FORBES, J. M. & COOPER, M. E. 2013. Mechanisms of diabetic complications. *Physiol Rev,* 93**,** 137-88.

FOULIS, A. K. 2008. Pancreatic pathology in type 1 diabetes in human. *Novartis Found Symp,* 292**,** 2-13

FOX, C. H., JOHNSON, F. B., WHITING, J. & ROLLER, P. P. 1985. Formaldehyde fixation. *J Histochem Cytochem,* 33**,** 845-53.

FRANCHI, L., EIGENBROD, T. & NUNEZ, G. 2009. Cutting edge: TNF-alpha mediates sensitization to ATP and silica via the NLRP3 inflammasome in the absence of microbial stimulation. *J Immunol,* 183**,** 792-6.

FRASCOLI, M., MARCANDALLI, J., SCHENK, U. & GRASSI, F. 2012. Purinergic P2X7 receptor drives T cell lineage choice and shapes peripheral gammadelta cells. *J Immunol,* 189**,** 174-80.

FUJINAKA, H., YAMAMOTO, T., TAKEYA, M., FENG, L., KAWASAKI, K., YAOITA, E., KONDO, D., WILSON, C. B., UCHIYAMA, M. & KIHARA, I. 1997. Suppression of anti-glomerular basement membrane nephritis by administration of anti-monocyte chemoattractant protein-1 antibody in WKY rats. *J Am Soc Nephrol,* 8**,** 1174-8.

GARCIA-MARCOS, M., POCHET, S., MARINO, A. & DEHAYE, J. P. 2006. P2X7 and phospholipid signalling: the search of the "missing link" in epithelial cells. *Cell Signal,* 18**,** 2098-104.

GARGETT, C. E., CORNISH, E. J. & WILEY, J. S. 1996. Phospholipase D activation by P2Z-purinoceptor agonists in human lymphocytes is dependent on bivalent cation influx. *Biochem J,* 313**,** 529-35.

GAUER, S., SICHLER, O., OBERMULLER, N., HOLZMANN, Y., KISS, E., SOBKOWIAK, E., PFEILSCHIFTER, J., GEIGER, H., MUHL, H. & HAUSER, I. A. 2007. IL-18 is expressed in the intercalated cell of human kidney. *Kidney Int,* 72**,** 1081-7.

GEISSMANN, F., MANZ, M. G., JUNG, S., SIEWEKE, M. H., MERAD, M. & LEY, K. 2010. Development of monocytes, macrophages, and dendritic cells. *Science.* 327, 656-61

GLAS, R., SAUTER, N. S., SCHULTHESS, F. T., SHU, L., OBERHOLZER, J. & MAEDLER, K. 2009. Purinergic P2X7 receptors regulate secretion of interleukin-1 receptor antagonist and beta cell function and survival. *Diabetologia,* 52**,** 1579-88.

GNUDI, L. 2012. Cellular and molecular mechanisms of diabetic glomerulopathy. *Nephrol Dial Transplant.* 7, 2642-9

GONCALVES, R. G., GABRICH, L., ROSARIO, A., JR., TAKIYA, C. M., FERREIRA, M. L., CHIARINI, L. B., PERSECHINI, P. M., COUTINHO-SILVA, R. & LEITE, M., JR. 2006. The role of purinergic P2X7 receptors in the inflammation and fibrosis of unilateral ureteral obstruction in mice. *Kidney Int.* 70, 1599-606

GORDON, S. 2002. Pattern recognition receptors: doubling up for the innate immune response. *Cell.* 111, 927-30

GORDON, S. & MARTINEZ, F. O. 2010. Alternative activation of macrophages: mechanism and functions. *Immunity.* 32, 593-604

GOTO, Y., KAKIZAKI, M. & MASAKI, N. 1976. Production of spontaneous diabetic rats by repetition of selective breeding. *Tohoku J Exp Med,* 119**,** 85-90.

GRACIANO, M. L., NISHIYAMA, A., JACKSON, K., SETH, D. M., ORTIZ, R. M., PRIETO-CARRASQUERO, M. C., KOBORI, H. & NAVAR, L. G. 2008. Purinergic receptors contribute to early mesangial cell transformation and renal vessel hypertrophy during angiotensin II-induced hypertension. *Am J Physiol Renal Physiol,* 294**,** 161-9.

GROSCHEL-STEWART, U., BARDINI, M., ROBSON, T. & BURNSTOCK, G. 1999. Localisation of P2X5 and P2X7 receptors by immunohistochemistry in rat stratified squamous epithelia. *Cell Tissue Res,* 296**,** 599-605.

GU, B. J., ZHANG, W. Y., BENDALL, L. J., CHESSELL, I. P., BUELL, G. N. & WILEY, J. S. 2000. Expression of P2X(7) purinoceptors on human lymphocytes and monocytes: evidence for nonfunctional P2X(7) receptors. *Am J Physiol Cell Physiol,* 279**,** 1189-97.

GU, B. J., ZHANG, W., WORTHINGTON, R. A., SLUYTER, R., DAO-UNG, P., PETROU, S., BARDEN, J. A. & WILEY, J. S. 2001. A Glu-496 to Ala polymorphism leads to loss of function of the human P2X7 receptor. *J Biol Chem,* 276**,** 11135-42.

GU, B. J., RATHSAM, C., STOKES, L., MCGEACHIE, A. B. & WILEY, J. S. 2009. Extracellular ATP dissociates nonmuscle myosin from P2X(7) complex: this dissociation regulates P2X(7) pore formation. *Am J Physiol Cell Physiol,* 297**,** 430-9.

GU, B. J., SAUNDERS, B. M., JURSIK, C. & WILEY, J. S. 2010. The P2X7-nonmuscle myosin membrane complex regulates phagocytosis of nonopsonized particles and bacteria by a pathway attenuated by extracellular ATP. *Blood,* 115**,** 1621-31.

GU, B. J., SAUNDERS, B. M., PETROU, S. & WILEY, J. S. 2011. P2X(7) is a scavenger receptor for apoptotic cells in the absence of its ligand, extracellular ATP. *J Immunol,* 187**,** 2365-75.

GUO, C., MASIN, M., QURESHI, O. S. & MURRELL-LAGNADO, R. D. 2007. Evidence for functional P2X4/P2X7 heteromeric receptors. *Mol Pharmacol.* 72, 1147-56.

GURLEY, S. B., CLARE, S. E., SNOW, K. P., HU, A., MEYER, T. W. & COFFMAN, T. M. 2006. Impact of genetic background on nephropathy in diabetic mice. *Am J Physiol Renal Physiol.* 290, 214-22.

GURLEY, S. B., MACH, C. L., STEGBAUER, J., YANG, J., SNOW, K. P., HU, A., MEYER, T. W. & COFFMAN, T. M. 2010. Influence of genetic background on albuminuria and kidney injury in Ins2(+/C96Y) (Akita) mice. *Am J Physiol Renal Physiol.* 298, 788-95.

HALIMI, J. M. 2012. The emerging concept of chronic kidney disease without clinical proteinuria in diabetic patients. *Diabetes Metab,* 38**,** 291-7.

HAN, S. Y., SO, G. A., JEE, Y. H., HAN, K. H., KANG, Y. S., KIM, H. K., KANG, S. W., HAN, D. S., HAN, J. Y. & CHA, D. R. 2004. Effect of retinoic acid in experimental diabetic nephropathy. *Immunol Cell Biol.* 82, 568-76.

HARADA, H., CHAN, C. M., LOESCH, A., UNWIN, R. & BURNSTOCK, G. 2000. Induction of proliferation and apoptotic cell death via P2Y and P2X receptors, respectively, in rat glomerular mesangial cells. *Kidney Int.* 57, 949-58.

HASEGAWA, G., NAKANO, K., SAWADA, M., UNO, K., SHIBAYAMA, Y., IENAGA, K. & KONDO, M. 1991. Possible role of tumor necrosis factor and interleukin-1 in the development of diabetic nephropathy. *Kidney Int,* 40**,** 1007-12.

HATTORI, M. & GOUAUX, E. 2012. Molecular mechanism of ATP binding and ion channel activation in P2X receptors. *Nature,* 485, 207-12.

HIBELL, A. D., THOMPSON, K. M., XING, M., HUMPHREY, P. P. & MICHEL, A. D. 2001. Complexities of measuring antagonist potency at P2X(7) receptor orthologs. *J Pharmacol Exp Ther,* 296**,** 947-57.

HILLMAN, K. A., JOHNSON, T. M., WINYARD, P. J., BURNSTOCK, G., UNWIN, R. J. & WOOLF, A. S. 2002. P2X(7) receptors are expressed during mouse nephrogenesis and in collecting duct cysts of the cpk/cpk mouse. *Exp Nephrol,* 10**,** 34-42.

HILLMAN, K. A., WOOLF, A. S., JOHNSON, T. M., WADE, A., UNWIN, R. J. & WINYARD, P. J. 2004. The P2X7 ATP receptor modulates renal cyst development in vitro. *Biochem Biophys Res Commun,* 322**,** 434-9.

HIRATA, K., SHIKATA, K., MATSUDA, M., AKIYAMA, K., SUGIMOTO, H., KUSHIRO, M. & MAKINO, H. 1998. Increased expression of selectins in kidneys of patients with diabetic nephropathy. *Diabetologia,* 41**,** 185-92.

HO, M. K. & SPRINGER, T. A. 1982. Mac-2, a novel 32,000 Mr mouse macrophage subpopulation-specific antigen defined by monoclonal antibodies. *J Immunol,* 128**,** 1221-8.

HOHENSTEIN, B., RENK, S., LANG, K., DANIEL, C., FREUND, M., LEON, C., AMANN, K. U., GACHET, C. & HUGO, C. P. 2007. P2Y1 gene deficiency protects from renal disease progression and capillary rarefaction during passive crescentic glomerulonephritis. *J Am Soc Nephrol,* 18**,** 494-505.

HONORE, P., DONNELLY-ROBERTS, D., NAMOVIC, M. T., HSIEH, G., ZHU, C. Z., MIKUSA, J. P., HERNANDEZ, G., ZHONG, C., GAUVIN, D. M., CHANDRAN, P., HARRIS, R., MEDRANO, A. P., CARROLL, W., MARSH, K., SULLIVAN, J. P., FALTYNEK, C. R. & JARVIS, M. F. 2006. A-740003 [N-(1-{[(cyanoimino)(5-quinolinylamino) methyl]amino}-2,2-dimethylpropyl)-2-(3,4-dimethoxyphenyl)acetamide], a novel and selective P2X7 receptor antagonist, dose-dependently reduces neuropathic pain in the rat. *J Pharmacol Exp Ther,* 319**,** 1376-85.

HUANG, G., ASHTON, C., KUMBHANI, D. S. & YING, Q. L. 2011. Genetic manipulations in the rat: progress and prospects. *Curr Opin Nephrol Hypertens,* 20**,** 391-9.

HUANG, L., HAYLOR, J. L., HAU, Z., JONES, R. A., VICKERS, M. E., WAGNER, B., GRIFFIN, M., SAINT, R. E., COUTTS, I. G., EL NAHAS, A. M. & JOHNSON, T. S. 2009. Transglutaminase inhibition ameliorates experimental diabetic nephropathy. *Kidney Int.* 76, 383-94.

HUGO, C., SHANKLAND, S. J., BOWEN-POPE, D. F., COUSER, W. G. & JOHNSON, R. J. 1997. Extraglomerular origin of the mesangial cell after injury. A new role of the juxtaglomerular apparatus. *J Clin Invest,* 100**,** 786-94.

HUMMEL, K. P., DICKIE, M. M. & COLEMAN, D. L. 1966. Diabetes, a new mutation in the mouse. *Science,* 153**,** 1127-8.

IHM, C. G., PARK, J. K., HONG, S. P., LEE, T. W., CHO, B. S., KIM, M. J., CHA, D. R. & HA, H. 1998. A high glucose concentration stimulates the expression of monocyte chemotactic peptide 1 in human mesangial cells. *Nephron.* 79, 33-7.

IMANI, F., HORII, Y., SUTHANTHIRAN, M., SKOLNIK, E. Y., MAKITA, Z., SHARMA, V., SEHAJPAL, P. & VLASSARA, H. 1993. Advanced glycosylation endproduct-specific receptors on human and rat T-lymphocytes mediate synthesis of interferon gamma: role in tissue remodeling. *J Exp Med,* 178**,** 2165-72.

IN'T VELD, P. 2011. Insulitis in human type 1 diabetes: The quest for an elusive lesion. *Islets.* 3, 131-8

INA, K., KITAMURA, H., OKEDA, T., NAGAI, K., LIU, Z. Y., MATSUDA, M. & FUJIKURA, Y. 1999. Vascular cell adhesion molecule-1 expression in the renal interstitium of diabetic KKAy mice. *Diabetes Res Clin Pract.* 44, 1-8.

INSCHO, E. W., COOK, A. K., CLARKE, A., ZHANG, S. & GUAN, Z. 2011. P2X1 Receptor-Mediated Vasoconstriction of Afferent Arterioles in Angiotensin II-Infused Hypertensive Rats Fed a High-Salt Diet. *Hypertension,* 57**,** 780-7.

JENSEN, M. E., ODGAARD, E., CHRISTENSEN, M. H., PRAETORIUS, H. A. & LEIPZIGER, J. 2007. Flow-induced [Ca2+]i increase depends on nucleotide release and subsequent purinergic signaling in the intact nephron. *J Am Soc Nephrol,* 18**,** 2062-70.

JI, X., NAITO, Y., HIROKAWA, G., WENG, H., HIURA, Y., TAKAHASHI, R. & IWAI, N. 2011. P2X(7) receptor antagonism attenuates the hypertension and renal injury in Dahl salt-sensitive rats. *Hypertens Res*. 35, 173-9

JUNAID, A. & AMARA, F. M. 2004. Osteopontin: correlation with interstitial fibrosis in human diabetic kidney and PI3-kinase-mediated enhancement of expression by glucose in human proximal tubular epithelial cells. *Histopathology.* 44, 136-46

JUNOD, A., LAMBERT, A. E., ORCI, L., PICTET, R., GONET, A. E. & RENOLD, A. E. 1967. Studies of the diabetogenic action of streptozotocin. *Proc Soc Exp Biol Med,* 126**,** 201-5.

JUNQUEIRA, L. C., BIGNOLAS, G. & BRENTANI, R. R. 1979. Picrosirius staining plus polarization microscopy, a specific method for collagen detection in tissue sections. *Histochem J,* 11**,** 447-55.

KALANTARINIA, K., AWAD, A. S. & SIRAGY, H. M. 2003. Urinary and renal interstitial concentrations of TNF-alpha increase prior to the rise in albuminuria in diabetic rats. *Kidney Int.* 64, 1208-13

KANETSUNA, Y., TAKAHASHI, K., NAGATA, M., GANNON, M. A., BREYER, M. D., HARRIS, R. C. & TAKAHASHI, T. 2007. Deficiency of endothelial nitric-oxide synthase confers susceptibility to diabetic nephropathy in nephropathy-resistant inbred mice. *Am J Pathol.* 170, 1473-84

KANWAR, Y. S., SUN, L., XIE, P., LIU, F. Y. & CHEN, S. 2011. A glimpse of various pathogenetic mechanisms of diabetic nephropathy. *Annu Rev Pathol,* 6**,** 395-423.

KARCZEWSKA, J., PIWKOWSKA, A., ROGACKA, D., STEPINSKI, J., ANGIELSKI, S. & JANKOWSKI, M. 2011. Purinergic modulation of glucose uptake into cultured rat podocytes: effect of diabetic milieu. *Biochem Biophys Res Commun,* 404**,** 723-7.

KAWANO, A., TSUKIMOTO, M., MORI, D., NOGUCHI, T., HARADA, H., TAKENOUCHI, T., KITANI, H. & KOJIMA, S. 2012. Regulation of P2X7-dependent inflammatory functions by P2X4 receptor in mouse macrophages. *Biochem Biophys Res Commun.* 420, 102-7.

KAWANO, K., HIRASHIMA, T., MORI, S., SAITOH, Y., KUROSUMI, M. & NATORI, T. 1992. Spontaneous long-term hyperglycemic rat with diabetic complications. Otsuka Long-Evans Tokushima Fatty (OLETF) strain. *Diabetes,* 41**,** 1422-8.

KAWATE, T., MICHEL, J. C., BIRDSONG, W. T. & GOUAUX, E. 2009. Crystal structure of the ATP-gated P2X(4) ion channel in the closed state. *Nature,* 460**,** 592-8.

KELLY, D. J., WILKINSON-BERKA, J. L., ALLEN, T. J., COOPER, M. E. & SKINNER, S. L. 1998. A new model of diabetic nephropathy with progressive renal impairment in the transgenic (mRen-2)27 rat (TGR). *Kidney Int,* 54**,** 343-52.

KELLY, K. J. & DOMINGUEZ, J. H. 2010. Rapid progression of diabetic nephropathy is linked to inflammation and episodes of acute renal failure. *Am J Nephrol.* 32, 469-75

KEYSTONE, E. C., WANG, M. M., LAYTON, M., HOLLIS, S. & MCINNES, I. B. 2011. Clinical evaluation of the efficacy of the P2X7 purinergic receptor antagonist AZD9056 on the signs and symptoms of rheumatoid arthritis in patients with active disease despite treatment with methotrexate or sulphasalazine. *Ann Rheum Dis*. 71, 2064.

KHAKH, B. S. & NORTH, R. A. 2006. P2X receptors as cell-surface ATP sensors in health and disease. *Nature,* 442**,** 527-32.

KIKUCHI, Y., IKEE, R., HEMMI, N., HYODO, N., SAIGUSA, T., NAMIKOSHI, T., YAMADA, M., SUZUKI, S. & MIURA, S. 2004. Fractalkine and its receptor, CX3CR1, upregulation in streptozotocin-induced diabetic kidneys. *Nephron Exp Nephrol.* 97, e17-25.

KIM, M. J. & TAM, F. W. 2011. Urinary monocyte chemoattractant protein-1 in renal disease. *Clin Chim Acta.* 412, 2022-30.

KING, B. F. 2007. Novel P2X7 receptor antagonists ease the pain. *Br J Pharmacol,* 151**,** 565-7.

KISHORE, B. K., CHOU, C. L. & KNEPPER, M. A. 1995. Extracellular nucleotide receptor inhibits AVP-stimulated water permeability in inner medullary collecting duct. *Am J Physiol,* 269**,** 863-9.

KISHORE, B. K., KRANE, C. M., MILLER, R. L., SHI, H., ZHANG, P., HEMMERT, A., SUN, R. & NELSON, R. D. 2005. P2Y2 receptor mRNA and protein expression is altered in inner medullas of hydrated and dehydrated rats: relevance to AVP-independent regulation of IMCD function. *Am J Physiol Renal Physiol,* 288**,** 1164-72.

KLAHR, S. 2001. Urinary tract obstruction. *Semin Nephrol,* 21**,** 133-45.

KRAYNAK, A. R., STORER, R. D., JENSEN, R. D., KLOSS, M. W., SOPER, K. A., CLAIR, J. H., DELUCA, J. G., NICHOLS, W. W. & EYDELLOTH, R. S. 1995. Extent and persistence of streptozotocin-induced DNA damage and cell proliferation in rat kidney as determined by in vivo alkaline elution and BrdUrd labeling assays. *Toxicol Appl Pharmacol.* 135, 279-86

KUME, S., UZU, T., ARAKI, S., SUGIMOTO, T., ISSHIKI, K., CHIN-KANASAKI, M., SAKAGUCHI, M., KUBOTA, N., TERAUCHI, Y., KADOWAKI, T., HANEDA, M., KASHIWAGI, A. & KOYA, D. 2007. Role of altered renal lipid metabolism in the development of renal injury induced by a high-fat diet. *J Am Soc Nephrol.* 18, 2715-23

LABASI, J. M., PETRUSHOVA, N., DONOVAN, C., MCCURDY, S., LIRA, P., PAYETTE, M. M., BRISSETTE, W., WICKS, J. R., AUDOLY, L. & GABEL, C. A. 2002. Absence of the P2X7 receptor alters leukocyte function and attenuates an inflammatory response. *J Immunol,* 168**,** 6436-45.

LAN, H. Y., NIKOLIC-PATERSON, D. J., ZARAMA, M., VANNICE, J. L. & ATKINS, R. C. 1993. Suppression of experimental crescentic glomerulonephritis by the interleukin-1 receptor antagonist. *Kidney Int,* 43**,** 479-85.

LANG, P. A., MERKLER, D., FUNKNER, P., SHAABANI, N., MERYK, A., KRINGS, C., BARTHUBER, C., RECHER, M., BRUCK, W., HAUSSINGER, D., OHASHI, P. S. & LANG, K. S. 2010. Oxidized ATP inhibits T-cell-mediated autoimmunity. *Eur J Immunol,* 40**,** 2401-8.

LEE, E. Y., CHUNG, C. H., KHOURY, C. C., YEO, T. K., PYAGAY, P. E., WANG, A. & CHEN, S. 2009. The monocyte chemoattractant protein-1/CCR2 loop, inducible by TGF-beta, increases podocyte motility and albumin permeability. *Am J Physiol Renal Physiol.* 297, 85-94

LEE, H. Y., BARDINI, M. & BURNSTOCK, G. 2000. Distribution of P2X receptors in the urinary bladder and the ureter of the rat. *J Urol,* 163**,** 2002-7.

LEE, M. J., YANG, C. W., JIN, D. C., CHANG, Y. S., BANG, B. K. & KIM, Y. S. 2003. Bone morphogenetic protein-7 inhibits constitutive and interleukin-1 beta-induced monocyte chemoattractant protein-1 expression in human mesangial cells: role for JNK/AP-1 pathway. *J Immunol,* 170**,** 2557-63.

LEE, T. N., ALBORN, W. E., KNIERMAN, M. D. & KONRAD, R. J. 2006. The diabetogenic antibiotic streptozotocin modifies the tryptic digest pattern for peptides of the enzyme O-GlcNAc-selective N-acetyl-beta-d-glucosaminidase that contain amino acid residues essential for enzymatic activity. *Biochem Pharmacol.* 72, 710-8.

LEES, M. P., FULLER, S. J., MCLEOD, R., BOULTER, N. R., MILLER, C. M., ZAKRZEWSKI, A. M., MUI, E. J., WITOLA, W. H., COYNE, J. J., HARGRAVE, A. C., JAMIESON, S. E., BLACKWELL, J. M., WILEY, J. S. & SMITH, N. C. 2010. P2X7 receptor-mediated killing of an intracellular parasite, Toxoplasma gondii, by human and murine macrophages. *J Immunol,* 184**,** 7040-6.

LENZEN, S. 2008. The mechanisms of alloxan- and streptozotocin-induced diabetes. *Diabetologia,* 51**,** 216-26.

LEON, C., HECHLER, B., FREUND, M., ECKLY, A., VIAL, C., OHLMANN, P., DIERICH, A., LEMEUR, M., CAZENAVE, J. P. & GACHET, C. 1999. Defective platelet aggregation and increased resistance to thrombosis in purinergic P2Y(1) receptor-null mice. *J Clin Invest,* 104**,** 1731-7.

LI, F., YANG, N., ZHANG, L., TAN, H., HUANG, B., LIANG, Y., CHEN, M. & YU, X. 2010. Increased expression of toll-like receptor 2 in rat diabetic nephropathy. *Am J Nephrol,* 32**,** 179-86.

LI, J., LIU, D., KE, H. Z., DUNCAN, R. L. & TURNER, C. H. 2005. The P2X7 nucleotide receptor mediates skeletal mechanotransduction. *J Biol Chem,* 280**,** 42952-9.

LIKE, A. A. & ROSSINI, A. A. 1976. Streptozotocin-induced pancreatic insulitis: new model of diabetes mellitus. *Science,* 193**,** 415-7.

LIKE, A. A., APPEL, M. C., WILLIAMS, R. M. & ROSSINI, A. A. 1978. Streptozotocin-induced pancreatic insulitis in mice. Morphologic and physiologic studies. *Lab Invest,* 38**,** 470-86.

LIM, A. K., MA, F. Y., NIKOLIC-PATERSON, D. J., KITCHING, A. R., THOMAS, M. C. & TESCH, G. H. 2010. Lymphocytes promote albuminuria, but not renal dysfunction or histological damage in a mouse model of diabetic renal injury. *Diabetologia,* 53**,** 1772-82.

LIM, A. K., MA, F. Y., NIKOLIC-PATERSON, D. J., THOMAS, M. C., HURST, L. A. & TESCH, G. H. 2009. Antibody blockade of c-fms suppresses the progression of inflammation and injury in early diabetic nephropathy in obese db/db mice. *Diabetologia,* 52**,** 1669-79.

LIM, A. K. & TESCH, G. H. 2012. Inflammation in diabetic nephropathy. *Mediators Inflamm,* 2012**,** 146154.

LIN, J., GLYNN, R. J., RIFAI, N., MANSON, J. E., RIDKER, P. M., NATHAN, D. M. & SCHAUMBERG, D. A. 2008. Inflammation and progressive nephropathy in type 1 diabetes in the diabetes control and complications trial. *Diabetes Care.* 31, 2338-43

LIN, M., YIU, W. H., WU, H. J., CHAN, L. Y., LEUNG, J. C., AU, W. S., CHAN, K. W., LAI, K. N. & TANG, S. C. 2012. Toll-like receptor 4 promotes tubular inflammation in diabetic nephropathy. *J Am Soc Nephrol,* 23**,** 86-102.

LIN, M., YIU, W. H., LI, R. X., WU, H. J., WONG, D. W., CHAN, L. Y., LEUNG, J. C., LAI, K. N. & TANG, S. C. 2013. The TLR4 antagonist CRX-526 protects against advanced diabetic nephropathy. *Kidney Int,* 83**,** 887-900.

LOUTZENHISER, R., GRIFFIN, K. A. & BIDANI, A. K. 2006. Systolic blood pressure as the trigger for the renal myogenic response: protective or autoregulatory? *Curr Opin Nephrol Hypertens,* 15**,** 41-9.

MA, L. J. & FOGO, A. B. 2003. Model of robust induction of glomerulosclerosis in mice: importance of genetic background. *Kidney Int.* 64, 350-5

MACKENZIE, A. B., YOUNG, M. T., ADINOLFI, E. & SURPRENANT, A. 2005. Pseudoapoptosis induced by brief activation of ATP-gated P2X7 receptors. *J Biol Chem,* 280**,** 33968-76.

MAKINO, S., KUNIMOTO, K., MURAOKA, Y., MIZUSHIMA, Y., KATAGIRI, K. & TOCHINO, Y. 1980. Breeding of a non-obese, diabetic strain of mice. *Jikken Dobutsu,* 29**,** 1-13.

MANDRUP-POULSEN, T., PICKERSGILL, L. & DONATH, M. Y. 2010. Blockade of interleukin 1 in type 1 diabetes mellitus. *Nat Rev Endocrinol,* 6**,** 158-66.

MANGOO-KARIM, R., UCHIC, M., LECHENE, C. & GRANTHAM, J. J. 1989. Renal epithelial cyst formation and enlargement in vitro: dependence on cAMP. *Proc Natl Acad Sci U S A,* 86**,** 6007-11.

MARINO, E. & CARDIER, J. E. 2003. Differential effect of IL-18 on endothelial cell apoptosis mediated by TNF-alpha and Fas (CD95). *Cytokine.* 22, 142-8.

MARQUES-DA-SILVA, C., CHAVES, M. M., CASTRO, N. G., COUTINHO-SILVA, R. & GUIMARAES, M. Z. 2011. Colchicine inhibits cationic dye uptake induced by ATP in P2X2 and P2X7 receptor-expressing cells: implications for its therapeutic action. *Br J Pharmacol,* 163**,** 912-26.

MASIN, M., YOUNG, C., LIM, K., BARNES, S. J., XU, X. J., MARSCHALL, V., BRUTKOWSKI, W., MOONEY, E. R., GORECKI, D. C. & MURRELL-LAGNADO, R. 2012. Expression, assembly and function of novel C-terminal truncated variants of the mouse P2X7 receptor: re-evaluation of P2X7 knockouts. *Br J Pharmacol,* 165**,** 978-93.

MASON, R. M. & WAHAB, N. A. 2003. Extracellular matrix metabolism in diabetic nephropathy. *J Am Soc Nephrol,* 14**,** 1358-73.

MCADOO, S. P., TAM, F. W. & PUSEY, C. D. 2010. Disease models of rapidly progressive glomerulonephritis. *Drug Discovery Today: Disease Models,* 7**,** 43-50.

MCDONALD, B., PITTMAN, K., MENEZES, G. B., HIROTA, S. A., SLABA, I., WATERHOUSE, C. C., BECK, P. L., MURUVE, D. A. & KUBES, P. 2010. Intravascular danger signals guide neutrophils to sites of sterile inflammation. *Science,* 330**,** 362-6.

MELCION, C., LACHMAN, L., KILLEN, P. D., MOREL-MAROGER, L. & STRIKER, G. E. 1982. Mesangial cells, effect of monocyte products on proliferation and matrix synthesis. *Transplant Proc,* 14**,** 559-64.

MELNIKOV, V. Y., ECDER, T., FANTUZZI, G., SIEGMUND, B., LUCIA, M. S., DINARELLO, C. A., SCHRIER, R. W. & EDELSTEIN, C. L. 2001. Impaired IL-18 processing protects caspase-1-deficient mice from ischemic acute renal failure. *J Clin Invest,* 107**,** 1145-52.

MENZIES, R. I., UNWIN, R. J., DASH, R. K., BEARD, D. A., COWLEY, A. W., JR., CARLSON, B. E., MULLINS, J. J. & BAILEY, M. A. 2013. Effect of P2X4 and P2X7 receptor antagonism on the pressure diuresis relationship in rats. *Front Physiol,* 4**,** 305.

MEZZANO, S., AROS, C., DROGUETT, A., BURGOS, M. E., ARDILES, L., FLORES, C., SCHNEIDER, H., RUIZ-ORTEGA, M. & EGIDO, J. 2004. NF-kappaB activation and overexpression of regulated genes in human diabetic nephropathy. *Nephrol Dial Transplant.* 19, 2505-12

MICHEL, A. D., CHESSELL, I. P. & HUMPHREY, P. P. 1999. Ionic effects on human recombinant P2X7 receptor function. *Naunyn Schmiedebergs Arch Pharmacol,* 359**,** 102-9.

MISHRA, A. 2013. New insights of P2X7 receptor signaling pathway in alveolar functions. *J Biomed Sci,* 20**,** 26.

MOON, J. Y., JEONG, K. H., LEE, T. W., IHM, C. G., LIM, S. J. & LEE, S. H. 2012. Aberrant recruitment and activation of T cells in diabetic nephropathy. *Am J Nephrol.* 35, 164-74

MORAN, A., BUNDY, B., BECKER, D. J., DIMEGLIO, L. A., GITELMAN, S. E., GOLAND, R., GREENBAUM, C. J., HEROLD, K. C., MARKS, J. B., RASKIN, P., SANDA, S., SCHATZ, D., WHERRETT, D. K., WILSON, D. M., KRISCHER, J. P., SKYLER, J. S., PICKERSGILL, L., DE KONING, E., ZIEGLER, A. G., BOEHM, B., BADENHOOP, K., SCHLOOT, N., BAK, J. F., POZZILLI, P., MAURICIO, D., DONATH, M. Y., CASTANO, L., WAGNER, A., LERVANG, H. H., PERRILD, H., MANDRUP-POULSEN, T., POCIOT, F. & DINARELLO, C. A. 2013. Interleukin-1 antagonism in type 1 diabetes of recent onset: two multicentre, randomised, double-blind, placebo-controlled trials. *Lancet,* 381**,** 1905-15.

MORIWAKI, Y., YAMAMOTO, T., SHIBUTANI, Y., AOKI, E., TSUTSUMI, Z., TAKAHASHI, S., OKAMURA, H., KOGA, M., FUKUCHI, M. & HADA, T. 2003. Elevated levels of interleukin-18 and tumor necrosis factor-alpha in serum of patients with type 2 diabetes mellitus: relationship with diabetic nephropathy. *Metabolism.* 52, 605-8

MORIWAKI, Y., INOKUCHI, T., YAMAMOTO, A., KA, T., TSUTSUMI, Z., TAKAHASHI, S. & YAMAMOTO, T. 2007. Effect of TNF-alpha inhibition on urinary albumin excretion in experimental diabetic rats. *Acta Diabetol,* 44**,** 215-8.

MORIYA, R., MANIVEL, J. C. & MAUER, M. 2004. Juxtaglomerular apparatus T-cell infiltration affects glomerular structure in Type 1 diabetic patients. *Diabetologia,* 47**,** 82-8.

NAGAO, T., OKURA, T., IRITA, J., JOTOKU, M., ENOMOTO, D., DESILVA, V. R., MIYOSHI, K., KURATA, M., MATSUI, Y., UEDE, T. & HIGAKI, J. 2012. Osteopontin plays a critical role in interstitial fibrosis but not glomerular sclerosis in diabetic nephropathy. *Nephron Extra.* 2, 87-103

NAKAGAWA, T., SATO, W., GLUSHAKOVA, O., HEINIG, M., CLARKE, T., CAMPBELL-THOMPSON, M., YUZAWA, Y., ATKINSON, M. A., JOHNSON, R. J. & CROKER, B. 2007. Diabetic endothelial nitric oxide synthase knockout mice develop advanced diabetic nephropathy. *J Am Soc Nephrol.* 18, 539-50

NAKAMURA, A., SHIKATA, K., HIRAMATSU, M., NAKATOU, T., KITAMURA, T., WADA, J., ITOSHIMA, T. & MAKINO, H. 2005. Serum interleukin-18 levels are associated with nephropathy and atherosclerosis in Japanese patients with type 2 diabetes. *Diabetes Care.* 28, 2890-5

NAKAMURA, S., LI, H., ADIJIANG, A., PISCHETSRIEDER, M. & NIWA, T. 2007. Pyridoxal phosphate prevents progression of diabetic nephropathy. *Nephrol Dial Transplant.* 22, 2165-74

NAM, B. Y., PAENG, J., KIM, S. H., LEE, S. H., KIM DO, H., KANG, H. Y., LI, J. J., KWAK, S. J., PARK, J. T., YOO, T. H., HAN, S. H., KIM, D. K. & KANG, S. W. 2012. The MCP-1/CCR2 axis in podocytes is involved in apoptosis induced by diabetic conditions. *Apoptosis,* 17**,** 1-13.

NAULI, S. M., ALENGHAT, F. J., LUO, Y., WILLIAMS, E., VASSILEV, P., LI, X., ELIA, A. E., LU, W., BROWN, E. M., QUINN, S. J., INGBER, D. E. & ZHOU, J. 2003. Polycystins 1 and 2 mediate mechanosensation in the primary cilium of kidney cells. *Nat Genet,* 33**,** 129-37.

NAVARRO, J. F., MILENA, F. J., MORA, C., LEON, C. & GARCIA, J. 2006. Renal pro-inflammatory cytokine gene expression in diabetic nephropathy: effect of angiotensin-converting enzyme inhibition and pentoxifylline administration. *Am J Nephrol.* 26, 562-70

NAVARRO-GONZALEZ, J. F. & MORA-FERNANDEZ, C. 2008. The role of inflammatory cytokines in diabetic nephropathy. *J Am Soc Nephrol,* 19**,** 433-42.

NAVARRO-GONZALEZ, J. F., MORA-FERNANDEZ, C., MUROS DE FUENTES, M. & GARCIA-PEREZ, J. 2011. Inflammatory molecules and pathways in the pathogenesis of diabetic nephropathy. *Nat Rev Nephrol.* 7, 327-40

NELSON, P. J., REES, A. J., GRIFFIN, M. D., HUGHES, J., KURTS, C. & DUFFIELD, J. 2012. The renal mononuclear phagocytic system. *J Am Soc Nephrol.* 23, 194-203

NGUYEN, D., PING, F., MU, W., HILL, P., ATKINS, R. C. & CHADBAN, S. J. 2006. Macrophage accumulation in human progressive diabetic nephropathy. *Nephrology (Carlton).* 11, 226-31

NICKE, A., KUAN, Y. H., MASIN, M., RETTINGER, J., MARQUEZ-KLAKA, B., BENDER, O., GORECKI, D. C., MURRELL-LAGNADO, R. D. & SOTO, F. 2009. A functional P2X7 splice variant with an alternative transmembrane domain 1 escapes gene inactivation in P2X7 knock-out mice. *J Biol Chem,* 284**,** 25813-22.

NORTH, R. A. 2002. Molecular physiology of P2X receptors. *Physiol Rev,* 82**,** 1013-67.

OKADA, S., SHIKATA, K., MATSUDA, M., OGAWA, D., USUI, H., KIDO, Y., NAGASE, R., WADA, J., SHIKATA, Y. & MAKINO, H. 2003. Intercellular adhesion molecule-1-deficient mice are resistant against renal injury after induction of diabetes. *Diabetes,* 52**,** 2586-93.

OKADA, T., NAGAO, T., MATSUMOTO, H., NAGAOKA, Y., WADA, T. & NAKAO, T. 2012. Histological predictors for renal prognosis in diabetic nephropathy in diabetes mellitus type 2 patients with overt proteinuria. *Nephrology (Carlton),* 17**,** 68-75.

OSICKA, T. M., YU, Y., PANAGIOTOPOULOS, S., CLAVANT, S. P., KIRIAZIS, Z., PIKE, R. N., PRATT, L. M., RUSSO, L. M., KEMP, B. E., COMPER, W. D. & JERUMS, G. 2000. Prevention of albuminuria by aminoguanidine or ramipril in streptozotocin-induced diabetic rats is associated with the normalization of glomerular protein kinase C. *Diabetes,* 49**,** 87-93.

OSMOND, D. A. & INSCHO, E. W. 2010. P2X(1) receptor blockade inhibits whole kidney autoregulation of renal blood flow in vivo. *Am J Physiol Renal Physiol,* 298**,** 1360-8.

PALOMINO-DOZA, J., RAHMAN, T. J., AVERY, P. J., MAYOSI, B. M., FARRALL, M., WATKINS, H., EDWARDS, C. R. & KEAVNEY, B. 2008. Ambulatory blood pressure is associated with polymorphic variation in P2X receptor genes. *Hypertension,* 52**,** 980-5.

PANCHAL, S. K. & BROWN, L. 2011. Rodent models for metabolic syndrome research. *J Biomed Biotechnol,* 2011**,** 351982.

PANENKA, W., JIJON, H., HERX, L. M., ARMSTRONG, J. N., FEIGHAN, D., WEI, T., YONG, V. W., RANSOHOFF, R. M. & MACVICAR, B. A. 2001. P2X7-like receptor activation in astrocytes increases chemokine monocyte chemoattractant protein-1 expression via mitogen-activated protein kinase. *J Neurosci.* United States. 21, 7135-42

PARK, C. W., KIM, J. H., LEE, J. H., KIM, Y. S., AHN, H. J., SHIN, Y. S., KIM, S. Y., CHOI, E. J., CHANG, Y. S. & BANG, B. K. 2000. High glucose-induced intercellular adhesion molecule-1 (ICAM-1) expression through an osmotic effect in rat mesangial cells is PKC-NF-kappa B-dependent. *Diabetologia,* 43**,** 1544-53.

PARK, J., RYU, D. R., LI, J. J., JUNG, D. S., KWAK, S. J., LEE, S. H., YOO, T. H., HAN, S. H., LEE, J. E., KIM, D. K., MOON, S. J., KIM, K., HAN, D. S. & KANG, S. W. 2008. MCP-1/CCR2 system is involved in high glucose-induced fibronectin and type IV collagen expression in cultured mesangial cells. *Am J Physiol Renal Physiol.* 295, 749-57

PELEGRIN, P. & SURPRENANT, A. 2006. Pannexin-1 mediates large pore formation and interleukin-1beta release by the ATP-gated P2X7 receptor. *Embo j,* 25**,** 5071-82.

PELEGRIN, P. & SURPRENANT, A. 2009. The P2X(7) receptor-pannexin connection to dye uptake and IL-1beta release. *Purinergic Signal,* 5**,** 129-37.

PELEGRIN, P. 2011. The many ways for P2X7 receptor pore dilatation. *British journal of pharmacology*. 163, 908-11

PERRIN, N. E., TORBJORNSDOTTER, T. B., JAREMKO, G. A. & BERG, U. B. 2006. The course of diabetic glomerulopathy in patients with type I diabetes: a 6-year follow-up with serial biopsies. *Kidney Int.* 69, 699-705

PETI-PETERDI, J. 2006. Calcium wave of tubuloglomerular feedback. *Am J Physiol Renal Physiol,* 291**,** 473-80.

PFEILSCHIFTER, J., PIGNAT, W., VOSBECK, K. & MARKI, F. 1989. Interleukin 1 and tumor necrosis factor synergistically stimulate prostaglandin synthesis and phospholipase A2 release from rat renal mesangial cells. *Biochem Biophys Res Commun.* 159, 385-94

PHILLIPS, A. O., BABOOLAL, K., RILEY, S., GRONE, H., JANSSEN, U., STEADMAN, R., WILLIAMS, J. & FLOEGE, J. 2001. Association of prolonged hyperglycemia with glomerular hypertrophy and renal basement membrane thickening in the Goto Kakizaki model of non-insulin-dependent diabetes mellitus. *Am J Kidney Dis.* 37, 400-10.

PIZZO, P., MURGIA, M., ZAMBON, A., ZANOVELLO, P., BRONTE, V., PIETROBON, D. & DI VIRGILIO, F. 1992. Role of P2z purinergic receptors in ATP-mediated killing of tumor necrosis factor (TNF)-sensitive and TNF-resistant L929 fibroblasts. *J Immunol,* 149**,** 3372-8.

POCHET, S., GOMEZ-MUNOZ, A., MARINO, A. & DEHAYE, J. P. 2003. Regulation of phospholipase D by P2X7 receptors in submandibular ductal cells. *Cell Signal,* 15**,** 927-35.

POCHYNYUK, O., BUGAJ, V., RIEG, T., INSEL, P. A., MIRONOVA, E., VALLON, V. & STOCKAND, J. D. 2008. Paracrine regulation of the epithelial Na+ channel in the mammalian collecting duct by purinergic P2Y2 receptor tone. *J Biol Chem,* 283**,** 36599-607.

PONNUSAMY, M., MA, L., GONG, R., PANG, M., CHIN, Y. E. & ZHUANG, S. 2011. P2X7 receptors mediate deleterious renal epithelial-fibroblast cross talk. *Am J Physiol Renal Physiol,* 300**,** 62-70.

PRAETORIUS, H. A. & SPRING, K. R. 2001. Bending the MDCK cell primary cilium increases intracellular calcium. *J Membr Biol,* 184**,** 71-9.

PRAETORIUS, H. A. & LEIPZIGER, J. 2009a. ATP release from non-excitable cells. *Purinergic Signal,* 5**,** 433-46.

PRAETORIUS, H. A. & LEIPZIGER, J. 2009b. Released nucleotides amplify the cilium-dependent, flow-induced [Ca2+]i response in MDCK cells. *Acta Physiol (Oxf),* 197**,** 241-51.

PREDESCU, D., PREDESCU, S., SHIMIZU, J., MIYAWAKI-SHIMIZU, K. & MALIK, A. B. 2005. Constitutive eNOS-derived nitric oxide is a determinant of endothelial junctional integrity. *Am J Physiol Lung Cell Mol Physiol.* 289, 371-81

PUSZTASZERI, M. P., SEELENTAG, W. & BOSMAN, F. T. 2006. Immunohistochemical expression of endothelial markers CD31, CD34, von Willebrand factor, and Fli-1 in normal human tissues. *J Histochem Cytochem,* 54**,** 385-95.

QIAN, Y., FELDMAN, E., PENNATHUR, S., KRETZLER, M. & BROSIUS, F. C., 3RD 2008. From fibrosis to sclerosis: mechanisms of glomerulosclerosis in diabetic nephropathy. *Diabetes,* 57**,** 1439-45.

RABB, H., DANIELS, F., O'DONNELL, M., HAQ, M., SABA, S. R., KEANE, W. & TANG, W. W. 2000. Pathophysiological role of T lymphocytes in renal ischemia-reperfusion injury in mice. *Am J Physiol Renal Physiol,* 279**,** 525-31.

RASSENDREN, F., BUELL, G. N., VIRGINIO, C., COLLO, G., NORTH, R. A. & SURPRENANT, A. 1997. The permeabilizing ATP receptor, P2X7. Cloning and expression of a human cDNA. *J Biol Chem,* 272**,** 5482-6.

REDDY, G. R., KOTLYAREVSKA, K., RANSOM, R. F. & MENON, R. K. 2008. The podocyte and diabetes mellitus: is the podocyte the key to the origins of diabetic nephropathy? *Curr Opin Nephrol Hypertens,* 17**,** 32-6.

REN, Y., GARVIN, J. L., LIU, R. & CARRETERO, O. A. 2004. Role of macula densa adenosine triphosphate (ATP) in tubuloglomerular feedback. *Kidney Int,* 66**,** 1479-85.

RIEG, T., BUNDEY, R. A., CHEN, Y., DESCHENES, G., JUNGER, W., INSEL, P. A. & VALLON, V. 2007. Mice lacking P2Y2 receptors have salt-resistant hypertension and facilitated renal Na+ and water reabsorption. *Faseb j.* 21**,** 3717-26.

RITEAU, N., GASSE, P., FAUCONNIER, L., GOMBAULT, A., COUEGNAT, M., FICK, L., KANELLOPOULOS, J., QUESNIAUX, V. F., MARCHAND-ADAM, S., CRESTANI, B., RYFFEL, B. & COUILLIN, I. 2010. Extracellular ATP is a danger signal activating P2X7 receptor in lung inflammation and fibrosis. *Am J Respir Crit Care Med,* 182**,** 774-83.

RIVERO, A., MORA, C., MUROS, M., GARCIA, J., HERRERA, H. & NAVARRO-GONZALEZ, J. F. 2009. Pathogenic perspectives for the role of inflammation in diabetic nephropathy. *Clin Sci (Lond).* 116, 479-92

RIZZO, M., METAFORA, S., MORELLI, F., RUSSO, F., CIANI, F. & CAPASSO, G. 2004. Chronic administration of bumetanide upregulates calbindin D28k mRNA and protein abundance in rat distal convoluted tubules. *Nephron Physiol,* 97**,** 16-22.

RODRIGUE-CANDELA, J. L., MARTIN-HERNANDEZ, D. & CASTILLA-CORTAZAR, T. 1963. Stimulation of insulin secretion in vitro by adenosine triphosphate. *Nature,* 197**,** 1304.

ROGER, S., GILLET, L., BAROJA-MAZO, A., SURPRENANT, A. & PELEGRIN, P. 2010. C-terminal calmodulin-binding motif differentially controls human and rat P2X7 receptor current facilitation. *J Biol Chem,* 285**,** 17514-24.

RON, D. 2002. Proteotoxicity in the endoplasmic reticulum: lessons from the Akita diabetic mouse. *J Clin Invest,* 109**,** 443-5.

ROSIN, D. L. & OKUSA, M. D. 2011. Dangers within: DAMP responses to damage and cell death in kidney disease. *J Am Soc Nephrol,* 22**,** 416-25.

ROST, S., DANIEL, C., SCHULZE-LOHOFF, E., BAUMERT, H. G., LAMBRECHT, G. & HUGO, C. 2002. P2 receptor antagonist PPADS inhibits mesangial cell proliferation in experimental mesangial proliferative glomerulonephritis. *Kidney Int,* 62**,** 1659-71.

ROXBURGH, S. A., KATTLA, J. J., CURRAN, S. P., O'MEARA, Y. M., POLLOCK, C. A., GOLDSCHMEDING, R., GODSON, C., MARTIN, F. & BRAZIL, D. P. 2009. Allelic depletion of grem1 attenuates diabetic kidney disease. *Diabetes.* 58, 1641-50

ROYALL, J. A., BERKOW, R. L., BECKMAN, J. S., CUNNINGHAM, M. K., MATALON, S. & FREEMAN, B. A. 1989. Tumor necrosis factor and interleukin 1 alpha increase vascular endothelial permeability. *Am J Physiol,* 257**,** 399-410.

RUBIO-GUERRA, A. F., VARGAS-ROBLES, H., LOZANO NUEVO, J. J. & ESCALANTE-ACOSTA, B. A. 2009. Correlation between circulating adhesion molecule levels and albuminuria in type-2 diabetic hypertensive patients. *Kidney Blood Press Res.* 32, 106-9

SAKAKI, H., FUJIWAKI, T., TSUKIMOTO, M., KAWANO, A., HARADA, H. & KOJIMA, S. 2013. P2X4 receptor regulates P2X7 receptor-dependent IL-1beta and IL-18 release in mouse bone marrow-derived dendritic cells. *Biochem Biophys Res Commun,* 432**,** 406-11.

SALEEM, M. A., O'HARE, M. J., REISER, J., COWARD, R. J., INWARD, C. D., FARREN, T., XING, C. Y., NI, L., MATHIESON, P. W. & MUNDEL, P. 2002. A conditionally immortalized human podocyte cell line demonstrating nephrin and podocin expression. *J Am Soc Nephrol,* 13**,** 630-8.

SANAI, T., SOBKA, T., JOHNSON, T., EL-ESSAWY, M., MUCHANETA-KUBARA, E. C., BEN GHARBIA, O., EL OLDROYD, S. & NAHAS, A. M. 2000. Expression of cytoskeletal proteins during the course of experimental diabetic nephropathy. *Diabetologia,* 43**,** 91-100.

SANCHEZ-NOGUEIRO, J., MARIN-GARCIA, P. & MIRAS-PORTUGAL, M. T. 2005. Characterization of a functional P2X(7)-like receptor in cerebellar granule neurons from P2X(7) knockout mice. *FEBS Lett,* 579**,** 3783-8.

SATO, N., KOMATSU, K. & KURUMATANI, H. 2003. Late onset of diabetic nephropathy in spontaneously diabetic GK rats. *Am J Nephrol.* 23, 334-42

SAVIGE, J., GREGORY, M., GROSS, O., KASHTAN, C., DING, J. & FLINTER, F. 2013. Expert guidelines for the management of Alport syndrome and thin basement membrane nephropathy. *J Am Soc Nephrol,* 24**,** 364-75.

SAYYED, S. G., RYU, M., KULKARNI, O. P., SCHMID, H., LICHTNEKERT, J., GRUNER, S., GREEN, L., MATTEI, P., HARTMANN, G. & ANDERS, H. J. 2011. An orally active chemokine receptor CCR2 antagonist prevents glomerulosclerosis and renal failure in type 2 diabetes. *Kidney Int.* 80, 68-78

SCHACHTER, J., MOTTA, A. P., DE SOUZA ZAMORANO, A., DA SILVA-SOUZA, H. A., GUIMARAES, M. Z. & PERSECHINI, P. M. 2008. ATP-induced P2X7-associated uptake of large molecules involves distinct mechanisms for cations and anions in macrophages. *J Cell Sci,* 121**,** 3261-70.

SCHENK, U., FRASCOLI, M., PROIETTI, M., GEFFERS, R., TRAGGIAI, E., BUER, J., RICORDI, C., WESTENDORF, A. M. & GRASSI, F. 2011. ATP inhibits the generation and function of regulatory T cells through the activation of purinergic P2X receptors. *Sci Signal,* 4**,** 12.

SCHULZE-LOHOFF, E., ZANNER, S., OGILVIE, A. & STERZEL, R. B. 1992. Extracellular ATP stimulates proliferation of cultured mesangial cells via P2-purinergic receptors. *Am J Physiol,* 263**,** 374-83.

SCHULZE-LOHOFF, E., HUGO, C., ROST, S., ARNOLD, S., GRUBER, A., BRUNE, B. & STERZEL, R. B. 1998. Extracellular ATP causes apoptosis and necrosis of cultured mesangial cells via P2Z/P2X7 receptors. *Am J Physiol,* 275**,** 962-71.

SCHWIEBERT, E. M., WALLACE, D. P., BRAUNSTEIN, G. M., KING, S. R., PETI-PETERDI, J., HANAOKA, K., GUGGINO, W. B., GUAY-WOODFORD, L. M., BELL, P. D., SULLIVAN, L. P., GRANTHAM, J. J. & TAYLOR, A. L. 2002. Autocrine extracellular purinergic signaling in epithelial cells derived from polycystic kidneys. *Am J Physiol Renal Physiol,* 282**,** 763-75.

SEMAN, M., ADRIOUCH, S., SCHEUPLEIN, F., KREBS, C., FREESE, D., GLOWACKI, G., DETERRE, P., HAAG, F. & KOCH-NOLTE, F. 2003. NAD-induced T cell death: ADP-ribosylation of cell surface proteins by ART2 activates the cytolytic P2X7 purinoceptor. *Immunity.* 19, 571-82

SERON, D., CAMERON, J. S. & HASKARD, D. O. 1991. Expression of VCAM-1 in the normal and diseased kidney. *Nephrol Dial Transplant,* 6**,** 917-22.

SHARMA, K., MCCUE, P. & DUNN, S. R. 2003. Diabetic kidney disease in the db/db mouse. *Am J Physiol Renal Physiol.* 284, 1138-44

SHARP, A. J., POLAK, P. E., SIMONINI, V., LIN, S. X., RICHARDSON, J. C., BONGARZONE, E. R. & FEINSTEIN, D. L. 2008. P2x7 deficiency suppresses development of experimental autoimmune encephalomyelitis. *J Neuroinflammation,* 5**,** 33.

SHI, S. R., KEY, M. E. & KALRA, K. L. 1991. Antigen retrieval in formalin-fixed, paraffin-embedded tissues: an enhancement method for immunohistochemical staining based on microwave oven heating of tissue sections. *J Histochem Cytochem,* 39**,** 741-8.

SHIKANO, M., SOBAJIMA, H., YOSHIKAWA, H., TOBA, T., KUSHIMOTO, H., KATSUMATA, H., TOMITA, M. & KAWASHIMA, S. 2000. Usefulness of a highly sensitive urinary and serum IL-6 assay in patients with diabetic nephropathy. *Nephron.* 85, 81-5.

SHIRLEY, D. G., VEKARIA, R. M. & SEVIGNY, J. 2009. Ectonucleotidases in the kidney. *Purinergic Signal,* 5**,** 501-11.

SICA, A. & MANTOVANI, A. 2012. Macrophage plasticity and polarization: in vivo veritas. *J Clin Invest,* 122**,** 787-95.

SIM, J. A., YOUNG, M. T., SUNG, H. Y., NORTH, R. A. & SURPRENANT, A. 2004. Reanalysis of P2X7 receptor expression in rodent brain. *The Journal of neuroscience : the official journal of the Society for Neuroscience,* 24**,** 6307-14.

SIPOS, A., VARGAS, S. & PETI-PETERDI, J. 2010. Direct demonstration of tubular fluid flow sensing by macula densa cells. *Am J Physiol Renal Physiol,* 299**,** 1087-93.

SIU, B., SAHA, J., SMOYER, W. E., SULLIVAN, K. A. & BROSIUS, F. C., 3RD 2006. Reduction in podocyte density as a pathologic feature in early diabetic nephropathy in rodents: prevention by lipoic acid treatment. *BMC Nephrol,* 7**,** 6.

SLUYTER, R., SHEMON, A. N. & WILEY, J. S. 2004. Glu496 to Ala polymorphism in the P2X7 receptor impairs ATP-induced IL-1 beta release from human monocytes. *J Immunol,* 172**,** 3399-405.

SLUYTER, R. & STOKES, L. 2011. Significance of P2X7 receptor variants to human health and disease. *Recent Pat DNA Gene Seq,* 5**,** 41-54.

SOLINI, A., CHIOZZI, P., FALZONI, S., MORELLI, A., FELLIN, R. & DI VIRGILIO, F. 2000. High glucose modulates P2X7 receptor-mediated function in human primary fibroblasts. *Diabetologia,* 43**,** 1248-56.

SOLINI, A., CHIOZZI, P., MORELLI, A., ADINOLFI, E., RIZZO, R., BARICORDI, O. R. & DI VIRGILIO, F. 2004. Enhanced P2X7 activity in human fibroblasts from diabetic patients: a possible pathogenetic mechanism for vascular damage in diabetes. *Arterioscler Thromb Vasc Biol,* 24**,** 1240-5.

SOLINI, A., IACOBINI, C., RICCI, C., CHIOZZI, P., AMADIO, L., PRICCI, F., DI MARIO, U., DI VIRGILIO, F. & PUGLIESE, G. 2005. Purinergic modulation of mesangial extracellular matrix production: role in diabetic and other glomerular diseases. *Kidney Int.* 67, 875-85

SOLINI, A., SANTINI, E., CHIMENTI, D., CHIOZZI, P., PRATESI, F., CUCCATO, S., FALZONI, S., LUPI, R., FERRANNINI, E., PUGLIESE, G. & DI VIRGILIO, F. 2007. Multiple P2X receptors are involved in the modulation of apoptosis in human mesangial cells: evidence for a role of P2X4. *Am J Physiol Renal Physiol.* 292, 1537-47

SOLINI, A., MENINI, S., ROSSI, C., RICCI, C., SANTINI, E., BLASETTI FANTAUZZI, C., IACOBINI, C. & PUGLIESE, G. 2013. The purinergic 2X7 receptor participates in renal inflammation and injury induced by high fat diet: possible role of NLRP3 inflammasome activation. *J Pathol*, 231, 342-53

SOLLE, M., LABASI, J., PERREGAUX, D. G., STAM, E., PETRUSHOVA, N., KOLLER, B. H., GRIFFITHS, R. J. & GABEL, C. A. 2001. Altered cytokine production in mice lacking P2X(7) receptors. *J Biol Chem,* 276**,** 125-32.

SRAER, J. D., DELARUE, F., HAGEGE, J., FEUNTEUN, J., PINET, F., NGUYEN, G. & RONDEAU, E. 1996. Stable cell lines of T-SV40 immortalized human glomerular mesangial cells. *Kidney Int,* 49**,** 267-70.

STUYT, R. J., NETEA, M. G., GEIJTENBEEK, T. B., KULLBERG, B. J., DINARELLO, C. A. & VAN DER MEER, J. W. 2003. Selective regulation of intercellular adhesion molecule-1 expression by interleukin-18 and interleukin-12 on human monocytes. *Immunology.* 110, 329-34

SUGIMOTO, H., SHIKATA, K., HIRATA, K., AKIYAMA, K., MATSUDA, M., KUSHIRO, M., SHIKATA, Y., MIYATAKE, N., MIYASAKA, M. & MAKINO, H. 1997. Increased expression of intercellular adhesion molecule-1 (ICAM-1) in diabetic rat glomeruli: glomerular hyperfiltration is a potential mechanism of ICAM-1 upregulation. *Diabetes,* 46**,** 2075-81.

SURPRENANT, A., RASSENDREN, F., KAWASHIMA, E., NORTH, R. A. & BUELL, G. 1996. The cytolytic P2Z receptor for extracellular ATP identified as a P2X receptor (P2X7). *Science,* 272**,** 735-8.

SURWIT, R. S., KUHN, C. M., COCHRANE, C., MCCUBBIN, J. A. & FEINGLOS, M. N. 1988. Diet-induced type II diabetes in C57BL/6J mice. *Diabetes,* 37**,** 1163-7.

SUZUKI, D., MIYAZAKI, M., NAKA, R., KOJI, T., YAGAME, M., JINDE, K., ENDOH, M., NOMOTO, Y. & SAKAI, H. 1995. In situ hybridization of interleukin 6 in diabetic nephropathy. *Diabetes,* 44**,** 1233-8.

SZKUDELSKI, T. 2001. The mechanism of alloxan and streptozotocin action in B cells of the rat pancreas. *Physiol Res,* 50**,** 537-46.

TAK, E., RIDYARD, D., KIM, J. H., ZIMMERMAN, M., WERNER, T., WANG, X. X., SHABEKA, U., SEO, S. W., CHRISTIANS, U., KLAWITTER, J., MOLDOVAN, R., GARCIA, G., LEVI, M., HAASE, V., RAVID, K., ELTZSCHIG, H. K. & GRENZ, A. 2013. CD73-Dependent Generation of Adenosine and Endothelial Adora2b Signaling Attenuate Diabetic Nephropathy. *J Am Soc Nephrol*. Epub ahead of print, doi: 10.1681/ASN.2012101014

TAM, F. W. 2006. Current pharmacotherapy for the treatment of crescentic glomerulonephritis. *Expert Opin Investig Drugs,* 15**,** 1353-69.

TAM, F. W., RISER, B. L., MEERAN, K., RAMBOW, J., PUSEY, C. D. & FRANKEL, A. H. 2009. Urinary monocyte chemoattractant protein-1 (MCP-1) and connective tissue growth factor (CCN2) as prognostic markers for progression of diabetic nephropathy. *Cytokine.* 47, 37-42

TAN, C., SALEHI, A., SVENSSON, S., OLDE, B. & ERLINGE, D. 2010. ADP receptor P2Y(13) induce apoptosis in pancreatic beta-cells. *Cell Mol Life Sci,* 67**,** 445-53.

TAY, Y. C., WANG, Y., KAIRAITIS, L., RANGAN, G. K., ZHANG, C. & HARRIS, D. C. 2005. Can murine diabetic nephropathy be separated from superimposed acute renal failure? *Kidney Int.* 68, 391-8.

TAYLOR, S. R., TURNER, C. M., ELLIOTT, J. I., MCDAID, J., HEWITT, R., SMITH, J., PICKERING, M. C., WHITEHOUSE, D. L., COOK, H. T., BURNSTOCK, G., PUSEY, C. D., UNWIN, R. J. & TAM, F. W. 2009. P2X7 deficiency attenuates renal injury in experimental glomerulonephritis. *J Am Soc Nephrol,* 20**,** 1275-81.

TERVAERT, T. W., MOOYAART, A. L., AMANN, K., COHEN, A. H., COOK, H. T., DRACHENBERG, C. B., FERRARIO, F., FOGO, A. B., HAAS, M., DE HEER, E., JOH, K., NOEL, L. H., RADHAKRISHNAN, J., SESHAN, S. V., BAJEMA, I. M. & BRUIJN, J. A. 2010. Pathologic classification of diabetic nephropathy. *J Am Soc Nephrol.* 21, 556-63.

TESCH, G. H., YANG, N., YU, H., LAN, H. Y., FOTI, R., CHADBAN, S. J., ATKINS, R. C. & NIKOLIC-PATERSON, D. J. 1997. Intrinsic renal cells are the major source of interleukin-1 beta synthesis in normal and diseased rat kidney. *Nephrol Dial Transplant,* 12**,** 1109-15.

TESCH, G. H. & ALLEN, T. J. 2007. Rodent models of streptozotocin-induced diabetic nephropathy. *Nephrology (Carlton),* 12**,** 261-6.

TESCH, G. H. & LIM, A. K. 2011. Recent insights into diabetic renal injury from the db/db mouse model of type 2 diabetic nephropathy. *Am J Physiol Renal Physiol.* 300, 301-10.

THAYER, T. C., WILSON, S. B. & MATHEWS, C. E. 2010. Use of nonobese diabetic mice to understand human type 1 diabetes. *Endocrinol Metab Clin North Am.* 39, 541-61.

TOMA, I., BANSAL, E., MEER, E. J., KANG, J. J., VARGAS, S. L. & PETI-PETERDI, J. 2008. Connexin 40 and ATP-dependent intercellular calcium wave in renal glomerular endothelial cells. *Am J Physiol Regul Integr Comp Physiol,* 294**,** 1769-76.

TORRES, V. E. & HARRIS, P. C. 2009. Autosomal dominant polycystic kidney disease: the last 3 years. *Kidney Int,* 76**,** 149-68.

TSUKADA, T., YOKOYAMA, K., ARAI, T., TAKEMOTO, F., HARA, S., YAMADA, A., KAWAGUCHI, Y., HOSOYA, T. & IGARI, J. 1998. Evidence of association of the ecNOS gene polymorphism with plasma NO metabolite levels in humans. *Biochem Biophys Res Commun.* 245, 190-3.

TURNER, C. M., VONEND, O., CHAN, C., BURNSTOCK, G. & UNWIN, R. J. 2003. The pattern of distribution of selected ATP-sensitive P2 receptor subtypes in normal rat kidney: an immunohistological study. *Cells Tissues Organs,* 175**,** 105-17.

TURNER, C. M., KING, B. F., SRAI, K. S. & UNWIN, R. J. 2007a. Antagonism of endogenous putative P2Y receptors reduces the growth of MDCK-derived cysts cultured in vitro. *Am J Physiol Renal Physiol,* 292**,** 15-25.

TURNER, C. M., TAM, F. W., LAI, P. C., TARZI, R. M., BURNSTOCK, G., PUSEY, C. D., COOK, H. T. & UNWIN, R. J. 2007b. Increased expression of the pro-apoptotic ATP-sensitive P2X7 receptor in experimental and human glomerulonephritis. *Nephrol Dial Transplant,* 22**,** 386-95.

UNWIN, R. J., BAILEY, M. A. & BURNSTOCK, G. 2003. Purinergic signaling along the renal tubule: the current state of play. *News Physiol Sci,* 18**,** 237-41.

URUSOVA, I. A., FARILLA, L., HUI, H., D'AMICO, E. & PERFETTI, R. 2004. GLP-1 inhibition of pancreatic islet cell apoptosis. *Trends Endocrinol Metab,* 15**,** 27-33.

USRDS 2012 Annual Data Report: Atlas of Chronic Kidney Disease and End-Stage Renal Disease in the United States, National Institutes of Health, National Institute of Diabetes and Digestive and Kidney Diseases. Bethesda, MD.

VANDESOMPELE, J., DE PRETER, K., PATTYN, F., POPPE, B., VAN ROY, N., DE PAEPE, A. & SPELEMAN, F. 2002. Accurate normalization of real-time quantitative RT-PCR data by geometric averaging of multiple internal control genes. *Genome Biol,* 3**,** RESEARCH0034.

VEKARIA, R. M., UNWIN, R. J. & SHIRLEY, D. G. 2006. Intraluminal ATP concentrations in rat renal tubules. *J Am Soc Nephrol,* 17**,** 1841-7.

VERGANI, A., FOTINO, C., D'ADDIO, F., TEZZA, S., PODETTA, M., GATTI, F., CHIN, M., BASSI, R., MOLANO, R. D., CORRADI, D., GATTI, R., FERRERO, M. E., SECCHI, A., GRASSI, F., RICORDI, C., SAYEGH, M. H., MAFFI, P., PILEGGI, A. & FIORINA, P. 2013. Effect of the purinergic inhibitor oxidized ATP in a model of islet allograft rejection. *Diabetes,* 62**,** 1665-75.

VIGNE, P., HECHLER, B., GACHET, C., BREITTMAYER, J. P. & FRELIN, C. 1999. Benzoyl ATP is an antagonist of rat and human P2Y1 receptors and of platelet aggregation. *Biochem Biophys Res Commun.* 256, 94-7.

VILAYSANE, A., CHUN, J., SEAMONE, M. E., WANG, W., CHIN, R., HIROTA, S., LI, Y., CLARK, S. A., TSCHOPP, J., TRPKOV, K., HEMMELGARN, B. R., BECK, P. L. & MURUVE, D. A. 2010. The NLRP3 inflammasome promotes renal inflammation and contributes to CKD. *J Am Soc Nephrol,* 21**,** 1732-44.

VONEND, O., TURNER, C. M., CHAN, C. M., LOESCH, A., DELL'ANNA, G. C., SRAI, K. S., BURNSTOCK, G. & UNWIN, R. J. 2004. Glomerular expression of the ATP-sensitive P2X receptor in diabetic and hypertensive rat models. *Kidney Int.* 66, 157-66

VORA, J. P., ZIMSEN, S. M., HOUGHTON, D. C. & ANDERSON, S. 1996. Evolution of metabolic and renal changes in the ZDF/Drt-fa rat model of type II diabetes. *J Am Soc Nephrol,* 7**,** 113-7.

WADA, J. & MAKINO, H. 2013. Inflammation and the pathogenesis of diabetic nephropathy. *Clin Sci (Lond).* 124, 139-52.

WADA, T., FURUICHI, K., SAKAI, N., IWATA, Y., YOSHIMOTO, K., SHIMIZU, M., TAKEDA, S. I., TAKASAWA, K., YOSHIMURA, M., KIDA, H., KOBAYASHI, K. I., MUKAIDA, N., NAITO, T., MATSUSHIMA, K. & YOKOYAMA, H. 2000. Up-regulation of monocyte chemoattractant protein-1 in tubulointerstitial lesions of human diabetic nephropathy. *Kidney Int.* 58, 1492-9.

WAJANT, H., PFIZENMAIER, K. & SCHEURICH, P. 2003. Tumor necrosis factor signaling. *Cell Death Differ.* 10, 45-65

WANG, C. H., LI, F., HILLER, S., KIM, H. S., MAEDA, N., SMITHIES, O. & TAKAHASHI, N. 2011. A modest decrease in endothelial NOS in mice comparable to that associated with human NOS3 variants exacerbates diabetic nephropathy. *Proc Natl Acad Sci U S A.* 108, 2070-5.

WANG, J., TAKEUCHI, T., TANAKA, S., KUBO, S. K., KAYO, T., LU, D., TAKATA, K., KOIZUMI, A. & IZUMI, T. 1999. A mutation in the insulin 2 gene induces diabetes with severe pancreatic beta-cell dysfunction in the Mody mouse. *J Clin Invest,* 103**,** 27-37.

WANG, Z., NAKAYAMA, T., SATO, N., IZUMI, Y., KASAMAKI, Y., OHTA, M., SOMA, M., AOI, N., OZAWA, Y. & MA, Y. 2010. The purinergic receptor P2Y, G-protein coupled, 2 (P2RY2) gene associated with essential hypertension in Japanese men. *J Hum Hypertens,* 24**,** 327-35.

WELCH, B. D., CARLSON, N. G., SHI, H., MYATT, L. & KISHORE, B. K. 2003. P2Y2 receptor-stimulated release of prostaglandin E2 by rat inner medullary collecting duct preparations. *Am J Physiol Renal Physiol,* 285**,** 711-21.

WENZEL, U., SCHNEIDER, A., VALENTE, A. J., ABBOUD, H. E., THAISS, F., HELMCHEN, U. M. & STAHL, R. A. 1997. Monocyte chemoattractant protein-1 mediates monocyte/macrophage influx in anti-thymocyte antibody-induced glomerulonephritis. *Kidney Int,* 51**,** 770-6.

WEST, D. B., BOOZER, C. N., MOODY, D. L. & ATKINSON, R. L. 1992. Dietary obesity in nine inbred mouse strains. *Am J Physiol,* 262**,** 1025-32.

WILDMAN, S. S., UNWIN, R. J. & KING, B. F. 2003. Extended pharmacological profiles of rat P2Y2 and rat P2Y4 receptors and their sensitivity to extracellular H+ and Zn2+ ions. *Br J Pharmacol.* 140, 1177-86

WILDMAN, S. S., MARKS, J., TURNER, C. M., YEW-BOOTH, L., PEPPIATT-WILDMAN, C. M., KING, B. F., SHIRLEY, D. G., WANG, W. & UNWIN, R. J. 2008. Sodium-dependent regulation of renal amiloride-sensitive currents by apical P2 receptors. *J Am Soc Nephrol.* 19**,** 731-42.

WILDMAN, S. S., BOONE, M., PEPPIATT-WILDMAN, C. M., CONTRERAS-SANZ, A., KING, B. F., SHIRLEY, D. G., DEEN, P. M. & UNWIN, R. J. 2009. Nucleotides downregulate aquaporin 2 via activation of apical P2 receptors. *J Am Soc Nephrol,* 20**,** 1480-90.

WILEY, J. S., SLUYTER, R., GU, B. J., STOKES, L. & FULLER, S. J. 2011. The human P2X7 receptor and its role in innate immunity. *Tissue Antigens,* 78**,** 321-32.

WILSON, P. D., HOVATER, J. S., CASEY, C. C., FORTENBERRY, J. A. & SCHWIEBERT, E. M. 1999. ATP release mechanisms in primary cultures of epithelia derived from the cysts of polycystic kidneys. *J Am Soc Nephrol,* 10**,** 218-29.

WOLF, G., CHEN, S. & ZIYADEH, F. N. 2005. From the periphery of the glomerular capillary wall toward the center of disease: podocyte injury comes of age in diabetic nephropathy. *Diabetes,* 54**,** 1626-34.

WU, C. C., SYTWU, H. K., LU, K. C. & LIN, Y. F. 2011. Role of T cells in type 2 diabetic nephropathy. *Exp Diabetes Res,* 2011**,** 514738.

WU, J., ZHANG, R., TORREGGIANI, M., TING, A., XIONG, H., STRIKER, G. E., VLASSARA, H. & ZHENG, F. 2010a. Induction of diabetes in aged C57B6 mice results in severe nephropathy: an association with oxidative stress, endoplasmic reticulum stress, and inflammation. *Am J Pathol.* 176, 2163-76

WU, J. P., ZHANG, W., WU, F., ZHAO, Y., CHENG, L. F., XIE, J. J. & YAO, H. P. 2010b. Honokiol: an effective inhibitor of high-glucose-induced upregulation of inflammatory cytokine production in human renal mesangial cells. *Inflamm Res,* 59**,** 1073-9.

XU, C., SHMUKLER, B. E., NISHIMURA, K., KACZMAREK, E., ROSSETTI, S., HARRIS, P. C., WANDINGER-NESS, A., BACALLAO, R. L. & ALPER, S. L. 2009. Attenuated, flow-induced ATP release contributes to absence of flow-sensitive, purinergic Cai2+ signaling in human ADPKD cyst epithelial cells. *Am J Physiol Renal Physiol,* 296**,** 1464-76.

XU, J., HUANG, Y., LI, F., ZHENG, S. & EPSTEIN, P. N. 2010. FVB mouse genotype confers susceptibility to OVE26 diabetic albuminuria. *Am J Physiol Renal Physiol,* 299**,** F487-94.

XU, X. J., BOUMECHACHE, M., ROBINSON, L. E., MARSCHALL, V., GORECKI, D. C., MASIN, M. & MURRELL-LAGNADO, R. D. 2012. Splice variants of the P2X7 receptor reveal differential agonist dependence and functional coupling with pannexin-1. *J Cell Sci,* 125**,** 3776-89.

YAGI, K., KIM, S., WANIBUCHI, H., YAMASHITA, T., YAMAMURA, Y. & IWAO, H. 1997. Characteristics of diabetes, blood pressure, and cardiac and renal complications in Otsuka Long-Evans Tokushima Fatty rats. *Hypertension,* 29**,** 728-35.

YAMAMOTO, K., SOKABE, T., MATSUMOTO, T., YOSHIMURA, K., SHIBATA, M., OHURA, N., FUKUDA, T., SATO, T., SEKINE, K., KATO, S., ISSHIKI, M., FUJITA, T., KOBAYASHI, M., KAWAMURA, K., MASUDA, H., KAMIYA, A. & ANDO, J. 2006. Impaired flow-dependent control of vascular tone and remodeling in P2X4-deficient mice. *Nature med,* 12**,** 133-7.

YAN, Z., KHADRA, A., LI, S., TOMIC, M., SHERMAN, A. & STOJILKOVIC, S. S. 2010. Experimental characterization and mathematical modeling of P2X7 receptor channel gating. *J Neurosci,* 30**,** 14213-24.

YODER, B. K. 2007. Role of primary cilia in the pathogenesis of polycystic kidney disease. *J Am Soc Nephrol,* 18**,** 1381-8.

YONEMOTO, S., MACHIGUCHI, T., NOMURA, K., MINAKATA, T., NANNO, M. & YOSHIDA, H. 2006. Correlations of tissue macrophages and cytoskeletal protein expression with renal fibrosis in patients with diabetes mellitus. *Clin Exp Nephrol,* 10**,** 186-92.

YOSHIOKA, M., KAYO, T., IKEDA, T. & KOIZUMI, A. 1997. A novel locus, Mody4, distal to D7Mit189 on chromosome 7 determines early-onset NIDDM in nonobese C57BL/6 (Akita) mutant mice. *Diabetes,* 46**,** 887-94.

YOUNG, B. A., JOHNSON, R. J., ALPERS, C. E., ENG, E., GORDON, K., FLOEGE, J., COUSER, W. G. & SEIDEL, K. 1995. Cellular events in the evolution of experimental diabetic nephropathy. *Kidney Int,* 47**,** 935-44.

YUEN, D. A., STEAD, B. E., ZHANG, Y., WHITE, K. E., KABIR, M. G., THAI, K., ADVANI, S. L., CONNELLY, K. A., TAKANO, T., ZHU, L., COX, A. J., KELLY, D. J., GIBSON, I. W., TAKAHASHI, T., HARRIS, R. C. & ADVANI, A. 2012. eNOS deficiency predisposes podocytes to injury in diabetes. *J Am Soc Nephrol.* 23, 1810-23

YUSUF, S., ZHAO, F., MEHTA, S. R., CHROLAVICIUS, S., TOGNONI, G. & FOX, K. K. 2001. Effects of clopidogrel in addition to aspirin in patients with acute coronary syndromes without ST-segment elevation. *N Engl J Med,* 345**,** 494-502.

ZANCHI, A., MOCZULSKI, D. K., HANNA, L. S., WANTMAN, M., WARRAM, J. H. & KROLEWSKI, A. S. 2000. Risk of advanced diabetic nephropathy in type 1 diabetes is associated with endothelial nitric oxide synthase gene polymorphism. *Kidney Int.* United States. 57, 405-13

ZHANG, Y., SANDS, J. M., KOHAN, D. E., NELSON, R. D., MARTIN, C. F., CARLSON, N. G., KAMERATH, C. D., GE, Y., KLEIN, J. D. & KISHORE, B. K. 2008. Potential role of purinergic signaling in urinary concentration in inner medulla: insights from P2Y2 receptor gene knockout mice. *Am J Physiol Renal Physiol,* 295**,** 1715-24.

ZHANG, Y., NELSON, R. D., CARLSON, N. G., KAMERATH, C. D., KOHAN, D. E. & KISHORE, B. K. 2009. Potential role of purinergic signaling in lithium-induced nephrogenic diabetes insipidus. *Am J Physiol Renal Physiol,* 296**,** 1194-201.

ZHANG, Y., KOHAN, D. E., NELSON, R. D., CARLSON, N. G. & KISHORE, B. K. 2010. Potential involvement of P2Y2 receptor in diuresis of postobstructive uropathy in rats. *Am J Physiol Renal Physiol,* 298**,** 634-42.

ZHAO, H. J., WANG, S., CHENG, H., ZHANG, M. Z., TAKAHASHI, T., FOGO, A. B., BREYER, M. D. & HARRIS, R. C. 2006. Endothelial nitric oxide synthase deficiency produces accelerated nephropathy in diabetic mice. *J Am Soc Nephrol.* 17, 2664-9

ZHENG, D., WANG, Y., CAO, Q., LEE, V. W., ZHENG, G., SUN, Y., TAN, T. K., ALEXANDER, S. I. & HARRIS, D. C. 2011. Transfused macrophages ameliorate pancreatic and renal injury in murine diabetes mellitus. *Nephron Exp Nephrol.* 118, e87-99

ZHENG, F., STRIKER, G. E., ESPOSITO, C., LUPIA, E. & STRIKER, L. J. 1998. Strain differences rather than hyperglycemia determine the severity of glomerulosclerosis in mice. *Kidney Int,* 54**,** 1999-2007.

ZHENG, F., HE, C., CAI, W., HATTORI, M., STEFFES, M. & VLASSARA, H. 2002. Prevention of diabetic nephropathy in mice by a diet low in glycoxidation products. *Diabetes Metab Res Rev,* 18**,** 224-37.

ZHENG, F., PLATI, A. R., POTIER, M., SCHULMAN, Y., BERHO, M., BANERJEE, A., LECLERCQ, B., ZISMAN, A., STRIKER, L. J. & STRIKER, G. E. 2003. Resistance to glomerulosclerosis in B6 mice disappears after menopause. *Am J Pathol.* 162, 1339-48

ZHENG, S., NOONAN, W. T., METREVELI, N. S., COVENTRY, S., KRALIK, P. M., CARLSON, E. C. & EPSTEIN, P. N. 2004. Development of late-stage diabetic nephropathy in OVE26 diabetic mice. *Diabetes,* 53**,** 3248-57.